ISSN 2542-2049

Saint-Petersburg State University

17 International School-Conference

Magnetic resonance and its applications

proceedings

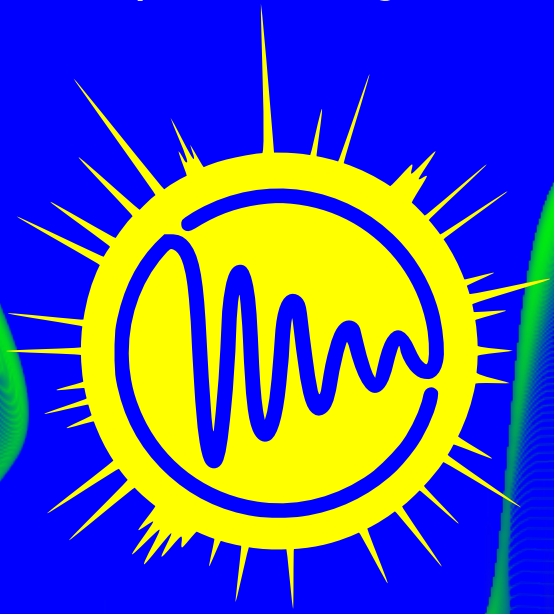

Spinus

29 March — 3 April 2020

Saint-Petersburg, Russia

SAINT PETERSBURG STATE UNIVERSITY
Department of Nuclear Physics Research Methods

17th International School-Conference

MAGNETIC RESONANCE AND ITS APPLICATIONS

Proceedings

an AMPERE event

March 29 — April 3, 2020
Saint Petersburg, Russia

Magnetic Resonance and its Applications. Spinus-2020.
Proceedings. Saint Petersburg State University, 2020. 308 pp.
ISSN 2542-2049

Schola Spinus

17th International School-Conference

MAGNETIC RESONANCE AND ITS APPLICATIONS
SPINUS-2020

ORGANIZING COMMITTEE

Chairman	Dr. Sci. Denis Markelov, professor, SPSU
Vice-chairman	M. Sc. Alexander Ievlev, researcher, SPSU
Committee members	Dr. Andrey Egorov, associate professor, SPSU Dr. Andrey Komolkin, associate professor, SPbU Dr. Marina Shelyapina, associate professor, SPSU Dr. Pavel Kupriyanov, assistant, SPSU Dr. Konstantin Tyutyukin, senior teacher, SPSU M. Sc. Timofey Popov, SPSU M. Sc. Sergei Bystrov, SPbU
Layout of proceedings	Aleksandr Levantovskii

CONTACTS

1, Ulyanovskay st., Peterhof, 198504, St. Petersburg, Russia
Department of Nuclear Physics Research Methods
St. Petersburg State University

Tel.	+7-953-350-0640
Fax	+7-812-428-7240
E-mail	spinus@spinus.spb.ru
Website	spinus.spb.ru

PROGRAM COMMITTEE

SCIENTIFIC ADVISER OF THE SCHOOL-CONFERENCE

Vladimir Chizhik	Honored scientist of Russia, Professor SPSU

ADVISORY BOARD

Balevicius V.	Professor, Vilnius, Lithuania
Cabal C.	Professor, Havana University, Cuba
Chizhik V. I.	Professor, St. Petersburg State University, Russia
Dvinskikh S. V.	Professor, Royal Institute of Technology, Stockholm, Sweden
Fraissard J.	Professor, University Pierre and Marie Curie, Paris, France
Grunin L. Yu.	Associate Professor, CEO, Resonance Systems, Russia
Lahderanta E.	Professor, Lappeenranta Technical University, Finland
Michel D.	Professor, Leipzig University, Germany
Rameev B.	Professor, Gebze Technical University, Turkey
Skrynnikov N. R.	Professor, St. Petersburg University, Russia, Purdue University, USA
Tagirov M. S.	Professor, Kazan Federal University, Russia
Varela L. M.	Professor, University Santiago de Compostela, Spain
Vasiliev S.	Professor, University of Turku, Finland

Spinus

Saint Petersburg State University
spbu.ru

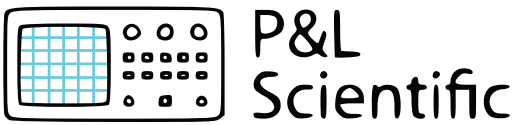

plscientific.se

Magicplot Systems, LLC
magicplot.com

MRRC "Spinus" SPbU, LLC
magres.ru

Contents

THE SCHOOL-CONFERENCE "SPINUS" OF SAINT PETERSBURG STATE UNIVERSIT 23

SECTION 1 25

Yu. M. Bunkov
Spin Superfluidity and its application for quantum computing 26

Carlos Cabal Mirabal
Synopsis of the MRI physical and hardware bases 30

Elena V. Charnaya, Denis Yu. Nefedov, Andrei V. Uskov, Dmitrii Yu. Podorozhkin
NMR studies of phase transitions in confined metals and alloys 32

V. I. Chizhik, S. S. Bystrov, V. V. Matveev, A. V. Egorov, Y. S. Chernyshev, V. A. Konovalov, and V. Balevičius
Molecular mobility in ionic liquids $[bmim]^+A^-$ and their mixtures with water by NMR and molecular dynamics simulation methods 33

Jean-Marie Colet, Manon Delcourt, Vanessa Tagliatti, Anne-Emilie Declèves
Unveiling the importance of succination in the differenciation of adipocytes: A NMR-based approach 35

Jacques Fraissard
The physical state of di-nitrogen in the presence of porous solids probed by ^{15}N spin-lattice relaxation of pure $^{15}N_2$ in the 30 K – 300 K range 36

Viacheslav Frolov, Konstantin Tyutyukin
Specifics of NMR-visualization at ultralow magnetic field 37

Leonid Grunin
Fast techniques for measurements of surface area, pores volume distribution, particle sizes and concentrations in colloidal systems by TD-NMR 38

Arthur Harrison, Max Filkins, Xinpei Wang, Sean P. Rigby, Chengbo Wang, Galina E. Pavlovskaya, Thomas Meersmann
From lungs to car catalysts: A breath taking journey with hyperpolarized noble gas MRI 39

Peter Höfer, Uwe Eichhoff
75 Years of EPR: Milestones in the 62 years Bruker EPR History 41

M. D. Ibragimova, A. B. Khalilov, G. J. Huseynov, S. A. Seidova
Ion-liquid extraction cleaning of oil distillates of various viscosities 44

Jacek Jenczyk, Stefan Jurga
Studies of structure and molecular dynamics in block copolymers by means of NMR and related methods 45

Igor V. Koptyug
Parahydrogen-induced polarization in NMR and MRI: the state of the art 46

Olga B. Lapina, Aleksandr A. Shubin, Evgeniy Papulovskiy, Ilya V. Yakovlev
NMR Crystallography as a tool for characterization of active sites of solid catalysts 48

Vadim L. Matukhin, Andrey N. Gavrilenko, Ecaterina V. Schmidt, Iliya G. Sevastianov, Jiri Navratil, Pavel Novak
$^{63,65}Cu$ NMR study of doped chalcopyrite $Cu_{1-X}Pd_XFeS_2$ compounds 50

Dieter Michel
Nuclear spin relaxation of water and other small molecules sorbed on solid interfaces 52

Yury A. Pirogov
Magnetic nuclear hyperpolarization and alternative approaches for MRI signal amplification 53

Yu. Plotnikova, A. Frolov, D. Kitanin, A. I. Pogoreltsev
The effect of Zn impurity on the rlectric field gradient on La nuclei in the $La_2Cu_{1-x}ZnxO_4$ system 56

B. Rameev
Development of cost-effective approaches for MW and NMR detection of threat liquids in security checkpoints 58

N. Suryaprakash
NMR methodologies, novel chiral auxiliaries and water compatible weak chiral aligning media for enantiomeric discrimination 61

N. Suryaprakash
Orchestrated approaches for combating the challenging problems of NMR spectroscopy 62

M. S. Tagirov
Enhanced nuclear magnetic resonance in magnetically concentrated and dilute solids 63

Peter M. Tolstoy, Valeria V. Mulloyarova, Ivan S. Giba, Alexei S. Ostras', Mikhail A. Kostin, Svetlana A. Pylaeva
Fluxional hydrogen-bonded complexes involving POOH groups: structure and dynamics revealed by ^{1}H and ^{31}P NMR 64

Konstantin Usachev, Alexander Golubev, Bulat Fatkhullin, Azat Gabdulkhakov, Aydar Bikmullin, Dmitriy Blokhin, Liliya Nurullina, Natalia Garaeva, Daut Islamov, Evelina Klochkova, Vladimir Klochkov, Albert Aganov, Iskander Khusainov, Shamil Validov, Marat Yusupov
Structural studies of the translation regulation factors from *Staphylococcus aureus* by NMR spectroscopy 67

Tatiana Zinkevich, Frank Tietz, Sylvio Indris, Helmut Ehrenberg
NMR spectroscopy as a tool to characterize ion dynamics in solid electrolytes 70

SECTION 2 75

E. M. Alakshin, G. A. Dolgorukov, A. V. Klochkov, E. I. Kondratyeva, V. V. Kuzmin, K. R. Safiullin, A. A. Stanislavovas, M. S. Tagirov
The ^{3}He NMR as a probe for nanostructures research 76

Anastasiia O. Antonenko, Elena V. Charnaya, J. Haase, V. V. Marchenkov
^{125}Te longitudinal relaxation in WTe_2 Weyl semimetal 77

Ramadan Atta, Anastasia V. Penkova, Maria E. Dmitrenko, Andrey A. Zolotarev
Polyphenylene isophthalamide pervaporation and ultrafiltration membranes modified by Pluronic F127 79

Georgii A. Bochkin, Edward B. Fel'dman, Sergey G. Vasil'ev
Free induction decay in quasi-one-dimensional spin chains in fluorapatite under the action of pulse sequence used in multiple quantum NMR experiments 80

Sergei S. Bystrov, A. V. Egorov, Prof. Dr. V. I. Chizhik
Analysis of Structural and Dynamical Properties of Mixtures of Imidazolium-based Ionic Liquids with Water by Molecular Dynamics Simulations 83

Mariia E. Dmitrenko, Vladislav P. Liamin, Anna I. Kuzminova, Anastasia V. Penkova
Investigation and characterization of mixed matrix membranes based on composite sodium alginate - fullerene derivative 85

Yuriy B. Grunin, Leonid Yu. Grunin, Daria S. Masas, Maria S. Ivanova
Determination the thermodynamic parameters of cellulose-water system by Time-Domain NMR.....86

M. Lores Guevara, R. N. Muller, S. Lauren, J. García Naranjo, V. I. Chizhik, C. Cabal Mirabal
Possible explanation of magnetic relaxation mechanism during the HbS aggregation process in Sickle Cell Disease 88

A. Ievlev, A. Koroleva, K. Tyutyukin, V. Matveev, O. Cabeza, L. Varela
NMR and X-ray photoelectron spectroscopy possibilities for study complex ionic liquids 89

Örs Istok
1D Moisture transport in thin cement paste samples measured with GARFIeld MRI evidencing dynamic porosity 92

Naira R. Khusnutdinova, Denis A. Markelov
Modeling the system of the carbosilane dendrimer of various generations 93

Remi Kogon, Anastasiia Nagmutdinova, Leonardo Brizi, Villiam Bortolotti, David Faux, Peter McDonald
3 Tau Model: Interpretation of FFC-NMR profiles 96

Tatiana P. Kulagina, Grigorii E. Karnaukh, Irina Yu. Golubeva
Free induction decay and primary echo in linear flexible polymers 100

Pavel Kupriyanov, Vladimir Chizhik
Registration of weak spectral lines in NMR-spectra of organic liquids in Earth magnetic field 103

Galina Kupriyanova, Sultonazar Mamadazizov, George Mozzhukhin
^{14}N NQR relaxation study of tetrazole derivatives 106

V. Kuzmin, K. Safiullin, A. Stanislavovas, M. Tagirov
Self-diffusion and relaxation of gaseous ^{3}He in oriented aerogels..... 108

A. I. Kuzminova, A. V. Penkova, M. E. Dmitrenko, A. A. Zolotarev, S. S. Ermakov
Development of novel membranes based of PA with MOFs for pervaporation separation of methanol/toluene mixture..... 110

D. Majhi, M. Cifelli, S. V. Dvinskikh
Translational diffusion in thermotropic ionic liquid crystals 111

Debashis Majhi, Jing Dai, Andrei V. Komolkin, Sergey V. Dvinskikh
Cation dynamics in hydrated ionic liquid crystals 113

G. V. Mozzhukhin, G. S. Kupriyanova, S. Mamadazizov, B. Z. Rameev
The studies of temperature-dependent ^{14}N NMR relaxation 115

G. V. Mozzhukhin, G. S. Kupriyanova, A. Maraşlı, S. Mamadazizov, M. Vafadar, B. Z. Rameev
^{1}H NMR detection of liquids in bottles with use of surface coils.....117

Valeriya Mulloyarova, Peter Tolstoy
Vicinal H/D isotopic effects on δ^{1}H in NMR spectra of hydrogen-bonded cyclic hererocomplexes formed by phosphinic and phosphoric acids.....120

Anastasiia Nagmutdinova, Remi Kogon, Leonardo Brizi and Villiam Bortolotti
Fast Field Cycling. Overview.....122

Evgeniy Papulovskiy, Sergei D. Kirik, Dzhalil F. Khabibulin, Aleksandr A. Shubin, Valentina M. Bondareva, Aleksandr S. Samoilo, Olga B. Lapina
Condensation of ammonium niobium oxalate studied by NMR crystallography and X-ray powder diffraction.....125

A. F. Privalov, Elena Galitskaya, Vitaly Sinitsyn, Michael Vogel
NMR diffusometry study of ^{1}H-^{2}D isotope effect in nafion polymer electrolite 127

Sevastyan O. Rabdano, Sergei S. Bystrov, Carlos Cabal, Vladimir I. Chizhik
The NMR relaxation of solvent nuclei for monitoring protein aggregation 130

Sharifi A. M. Saleh, Afarideh Hoseyn, Ghergherehchi Mitra, Chai Jong Seo
New approach in ANC-based noise reduction of Remote Sensing NQR analysis.....131

S. Vasiliev, J. Ahokas, J. Järvinen, S. Sheludiakov, V. V. Khmelenko and D. M. Lee
Magnetic resonance studies of atomic hydrogen in porous Ne at ultra-low temperatures 134

S. G. Vasil'ev, A. V. Chernyak, I. A. Avilova, K. L. Boldyrev, E. V. Selezneva, E. A. Tatarinova, A. M. Muzafarov
The self-diffusion of polymethylsilsequioxane dendrimers in dilute solutions and melts.....135

Aleksandr S. Voronin, Andrei V. Komolkin, Denis A. Markelov
Ordering of water-soluble derivatives of fullerenes in water from the molecular dynamics simulation 138

Sergei V. Zhurenko, Alexey V. Tkachev, Natalia E. Gervits, Anton V. Gunbin, Dina I. Fazlizhanova, Chia Nung Kuo, Chin Shan Lue, Andrei A. Gippius
Investigation of intermetallic thermoelectric compound $RuGa_3$ by NQR spectroscopy 140

SECTION 3 145

Svetlana Ya. Alexandrova, Alina A. Pichugina, Larisa V. Tsyro
Essentuki Mineral Water Analysis..... 147

N. A. Antonova, A. V. Komolkin
Computer simulation of 1B03 and 1D2D proteins 150

Valeriy V. Bezrodniy, Emil Fatullaev, Oleg V. Shavykin, Igor M. Neelov
Molecular dynamics simulation of global and local dynamics in lysine-based dendrimers with double arginine and double histidine... 152

Valeriy V. Bezrodniy, Sofia E. Miktaniuk, Oleg V. Shavykin, Igor M. Neelov
The orientational dynamics in the dipeptides: the role of type of the side chains 155

Inna G. Borodkina, Gennady S. Borodkin, Alexandra A. Kolodina, Nadezhda S. Trofimova, Vladimir T. Abaev, Pavel B. Chepurnoy, Natalya V. Stankevich
Structural studies of 2-(2-(2-azido-5-chlorophenyl)-2-(5-methylfuran-2-yl)ethylidene)-1,1-dimethylhydrazine by heteronuclear two-dimensional NMR spectroscopy 158

Ann Butyugina, Andrei V. Komolkin
Mini-protein denaturation at high temperatures..... 161

Nikita M. Chernov, Igor P. Yakovlev, Stanislav I. Selivanov
NOE application for ratio estimation of conformer populations in chromone-fused allylmorpholines 164

Nina Djapic
Porphyrins: proton spectra 167

Anaïs Draguet, Corentin Schepkens, Vanessa Tagliatti, Jean-Marie Colet
^{1}H-NMR evaluation of the LDH-A inhibitor Oxamate on the metastatic breast cancer cell lines MDA-MB-231 and MCF-7..... 169

E. V. Edinach
Application of high-frequency EPR spectroscopy for the identification and separation positions of electrically active impurities of nitrogen, boron and vanadium in silicon carbide crystals and heterostructures 170

Alexandra A. Efimova
Methylpyrazole as a molecular probe for the investigation of the acid-base properties of silica surface: computational ^{15}N NMR study .. 173

Maria I. Egorova, Andrei V. Egorov, Vladimir I. Chizhik, A. Laaksonen
Peculiarities of water arrangement around nitrate-anion in aqueous solution. A computer simulation study 176

Sophie Fourez, Matthieu Dallons, Vanessa Tagliatti
Nicotinamide riboside as a potential cardioprotective agent for counteracting doxorubicin-induced cardiotoxicity in H9C2 cells 177

Stanislav O. Garkavyi, Ecaterina V. Schmidt, Vadim L. Matukhin, Georgy V. Mozzhukhin
Nuclear spin-lattice relaxation in antiferromagnetic thermoelectric $CuFeS_2$ 179

Natalia E. Gervits, Alexey V. Tkachev, Sergey V. Zhurenko, Anton V. Gunbin, Andrey A. Gippius, Vjacheslav S. Pokatilov
Proposal for the method for measuring ^{57}Fe NMR spectra of compounds based on $BiFeO_3$ unification 182

Irina Yu. Golubeva, Grigorii E. Karnaukh, Tatiana P. Kulagina
Investigation of the primary echo signal in polymers with three-spin groups..... 183

Roman V. Haponchik, Alexey B. Ustinov
Numerical simulation of the nonlinear frequency shift of a ferromagnetic film resonator 185

M. D. Ibragimova, S. A. Seidova
Ionic liquid of N-methylpyrrolidoneacetate as an extract agent in the process of selective cleaning of oil fractions 188

Magdalena Janota, Peter J. McDonald, David A. Faux, Agata Gajewicz-Jaromin
Upscaling towards applications – water transport in C-S-H agglomerates studied by MRI measurements 190

Jérôme Jeandriens
Application of ^{1}H-NMR spectroscopy to highlight the metabolic plasticity of human melanoma cells upon glutamine depletion and glutaminase inhibition 191

Grigorii E. Karnaukh
Absence of the signal after solid-echo pulse sequence in the system of three spins..... 192

V. A. Konovalov, A. V. Egorov, V. I. Chizhik
Reorientational motion of water molecules in mixtures of imidazolium-based ionic liquids with water. A molecular dynamic simulation study..... 195

Mikhail Kostin, Peter Tolstoy, Sona Melikova
The study of intermolecular interactions involving models of modern volatile anesthetics by quantum-chemistry calculations 196

Ekaterina A. Krylova, Marina G. Shelyapina
Influence of the Si/AL ratio to the local structure of H-Mordenites 198

Aleksandra Sergeevna Kudashkina,
Vladimir Maksimovich Cheremisin, Konstantin Vadimovich Paveletz, Dmitriy Sergeevich Rusanov, Viktoria Vladimirovna Pritz
The significance of 3D modeling in assessment resectability of cancer of the pancreatic head 200

Anna I. Kuzminova, Anastasia V. Penkova
Development and study of novel green membranes based on sodium alginate modified by MOFs..... 201

A. I. Kuzminova, V. A. Surkova, A. V. Penkova, M. E. Dmitrenko, S. S. Ermakov
Development of novel membranes based of PVA with MOFs for pervaporation separation of water/isopropanol mixture 202

Nikolai A. Kuznetsov, Erkki Lähderanta, Alexey B. Ustinov
Numerical simulation of the nonlinear spin-wave phase shift in magnetic films 203

N. V. Latyshev, O. V. Kryukova, R. N. Yaroslavtsev, V. F. Pyankov, S. V. Stolyar
Electronic paramagnetic resonance of Ehrlich ascites carcinoma cells cultured with magnetic nanoparticles 206

Anna Y. Lavrova, M. A. Zubkov, V. M. Cheremisin
Introduction to diffusion tensor imaging and tractography: basic physics, anatomy and ROI-based reconstruction of the major white matter bundles 210

Vladislav P. Liamin, Mariia E. Dmitrenko, Anastasia V. Penkova, Sergey S. Ermakov
Development and study of novel pervaporation membranes based on sodium alginate modified by fullerene derivatives.....213

Vladislav P. Liamin, Mariia E. Dmitrenko, Andrey A. Zolotarev, Anastasia V. Penkova
Development and characterization of novel pervaporation membranes based on polyphenylene isophtalamide modified by various fullerene derivatives.....214

Kenan Mammadhasanov, Minaver D. Ibragimova, Sabina A. Seidova, Andrei V. Komolkin
Computer model and experimental investigation of ionic liquid-diesel fuel systems.....215

S. E. Miktaniuk, V. V. Bezrodniy, E. I. Fatullaev, I. M. Neelov
Computer simulation of interaction of lysine dendrimer with molecules of Gly-Glu-Asp peptide 217

Sofia E. Miktaniuk, Valerii V. Bezrodniy, Oleg V. Shavykin, Igor M. Neelov
Computer simulation of orientational dynamics in the peptide dendrimers with different excluded volume interactions.....221

Zh. T. Mukan, A. B. Ruhin, T. A. Seredavina, N. S. Suchkova, Zh. Beksultanov, I. V. Danko, N. V. Gluchshenko
Experimental application of alanine detectors for control of technological irradiations at the accelerator ILU-10 at INP RK 224

D. A. Narenkova, V. M. Cheremisin, I. G. Kamyshanskaya, P. I. Simeshchenko, V. V. Prits
Posterior reversible encephalopathy syndrome (PRES) in patients in the postpartum period.....225

A. V. Nikitina, Yu. V. Bogachev, Ya. Yu. Marchenko, B. P. Nikolaev
Investigations and modeling of MRI contrast enhancement in the presence of magnetic nanoparticles 227

V. V. Pelipko, R. I. Baichurin, S. V. Makarenko
Study of the structure of spiro-linked nitrocyclopropanecarboxylates by 1D and 2D NMR spectroscopy 230

Alina A. Pichugina, Larisa V. Tsyro
The study of urinary stones by the method of electron paramagnetic resonance.....232

Daria Poltorabatko, Vitalii Salnikov, Kuprian Beliychenko, Ivan Mershiev, Galina S. Kupriyanova
Using composite excitation pulses for T2 relaxation measurements with the inverse integral transformation 235

Maria V. Popova, Viktoria V. Vasinovich, Elizaveta A. Andronova
^{1}H and ^{13}C NMR investigation of SLAS in mixtures and SiO_2 dispersions 236

Mikhail G. Rudavets
Correlations of internal magnetic field due to grains in microfluids 239

A. M. Ryzhkov, A. V. Komolkin
Model of ions in concentrated solutions of ionic surfactants for the molecular dynamics method 242

A. A. Selivanov, A. V. Ievlev
Molecular dynamics modeling of ionic liquid [BMIM][SCN] 244

Julia R. Shakirova, Sergey P. Tunik, Stanislav I. Selivanov
Precise proton-proton distance estimation on base eNOE-data in Ir(III) complex at slow (in NMR time scale) exchange condition 247

S. A. Shubin, V. V. Frolov, K. V. Tyutyukin
Obtaining MR images of nuclei other than a hydrogen nucleus by an indirect method using double nuclear magnetic resonance 251

Irina A. Silanteva, Veronika V. Mamontova, Andrei V. Komolkin
Interaction of DNA with azobenzene-containing surfactant..... 254

Anastasia Sklyarova, Vadim I. Popkov, Ivan V. Pleshakov, Vladimir V. Matveev
Possible spatial spin modulation in europium orthoferrites 257

Mark Smirnov, Ivan Mershiev, Alexsander Musaenko, Galina Kupriyanova
1H NMR study of soybean oils 258

Artyom S. Tarasov, Ilfat Z. Rakhmatullin, Dmitry S. Blokhin, Vladimir V. Klochkov
Spectral characteristics of metal complexes of tetrapeptide with metal ions in solutions determined by NMR spectroscopy 261

Aleksei V. Tkachev, Andrei A. Gippius, Sergei V. Zhurenko, Norbert Büttgen, Martina Schädler, Igor V. Morozov, Ivan O. Chernyavskii, Alexander S. Moskvin
Evolution of the magnetic structure of a binary helimagnet FeP in an external field by ^{31}P NMR 263

Violet Traxel, Konstantin Tyutyukin, Yury Chernyshev, Viacheslav Frolov
NMR-visualization of the structure of plants 265

Larisa V. Tsyro, Alina A. Pichugina, Felix G. Unger
Features of the study of bitumen compositions by electron paramagnetic resonance.....267

Sophie Tumson, Manon Delcourt, Jean-Marie Colet
Optimization of polar metabolite extraction from White Adipose Tissue for 1H-NMR spectroscopy. Comparison with HR-MAS NMR on tissue section 270

Anna S. Tyurtyaeva, Marina G. Shelyapina, Denis Y. Nefedov, Anastasya O. Antonenko, Yurii S. Chernyshev
^{1}H NMR study of water in pillared mordenite and ZSM-5 zeolites.....271

Milosh Ubovich, Vsevolod V. Beshanov, Andrei V. Egorov
Rotational motion of ions in alkylammonium nitrate ionic liquids. A molecular dynamics simulation study 273

Sirvan Sultan Uguz, Emin Burcin Ozvural, Mecit Halil Oztop
Physicochemical characterisation of bovine and porcine gelatin based soft candies by Time Domain (TD) NMR Relaxometry 274

N. I. Uskova, E. V. Charnaya, D. Yu. Podorozhkin, S. V. Baryshnikov
NMR studies of diisopropylammonium iodide embedded into opal 275

Daria O. Ustimchuk, Valeriia V. Mulloyarova, Peter M. Tolstoy
Hydrogen bond and proton transfer in homo-conjugated anions of phosphorous-containing acids. Effects in ^{1}H and ^{31}P NMR spectra.....277

Florent Valcke, Aude Devalckeneer
NMR-based metabolomic evaluation of the toxicity threshold of 1,2-dichloroethane in an invertebrate model 280

Andrei K. Whaley, Vladimir G. Luzhanin, Stanislav I. Selivanov
Flavonoid C-glycoside rotameric conformational analysis using NMR-spectroscopy 282

A. Yagfarova, I. Yatsyk, J. Deeva, I. Gilmutdinov, N. Lyadov, T. Chupakhina, R. Eremina, T. Gavrilova
Magnetic proximity effects in nanostructured $(SrFe_{12}O_{19})_x(CaCu_3Ti_4O_{12})_{1-x}$ composites 285

Irina Yefimova, Andrei V. Egorov, Enisa Selimović, Tanja Soldatović, Andrei V. Komolkin
Structure and dynamics of [$CuCl_n$(1,2-diaminoethane)] complexes in aqueous solution by Quantum Chemistry and Molecular Dynamics methods 288

Dmitry S. Zasukhin, Yury G. Kolyagin, Ivan A. Kasyanov
Characterization of acid sites in zeolite Y by ^{31}P MAS NMR spectroscopy 290

K. V. Zinkevich, V. M. Cheremisin, I. G. Kamyshanskaya
A magnetic resonance spectroscopy in complex differential diagnosis of nodular lesions of the thyroid gland 293

POEMS ABOUT SCHOOL 295

AUTHOR INDEX 303

Spinus

The School-Conference "Spinus" of Saint Petersburg State University

The St. Petersburg State University (SPbSU) holds International School-Conference "Magnetic resonance and its application" (Spinus) since 2004. "Spinus" is organized in according to the subjects of researches and Master Programs, which are developed and implemented in the SPbSU. In modern physics, the term "magnetic resonance" refers to a set of phenomena accompanied with the emission or absorption of electromagnetic waves of the radiofrequency diapason by quantum systems (nuclei, electrons, atoms, molecules, etc.). These phenomena, the physical nature of which is of independent interest, provided the basis of radiospectroscopic methods for studying the structure of matter and physical-chemical processes in it. They are also used for the creation of quantum generators, amplifiers, and magnetometers. For the development of ideas and applications of magnetic resonance six Nobel Prizes were awarded in the areas of physics, chemistry, biology, physiology and medicine (the latter was in 2003).

Primarily, magnetic resonance methods are:

- Nuclear Magnetic Resonance (NMR)
- Electron Paramagnetic Resonance (EPR)
- Nuclear Quadrupole Resonance (NQR)

These methods, being contactless, do not destroy an object under a study, that makes them unique and in demand not only in physics and chemistry, but also in medicine, geology, biology, archeology. Now, any medical center with high reputation has a magnetic resonance imaging (MRI). In Russia, NMR is used in oil well logging, laboratory analysis of the productivity of oil-bearing reservoirs, analysis of oil content and moisture of seeds; EPR technique is used for geological research, non-destructive control of precious stones, as well as for the dating of paleontological artifacts; there are NQR applications for remote detection of solid explosives and narcotics. Magnetometry methods based on magnetic resonance are indispensable for carrying out archaeological researches.

Earlier the school organizers worked at the Department of quantum magnetic phenomena (QMPh) of the St. Petersburg State University, which was founded in 1993 on the initiative of Professor V. I. Chizhik on the basis of the laboratory, created in the 50s of the last century by F. I. Skripov at the Department of Radio Physics (the branch "Quantum Radiophysics"). On January 1, 2014, the Department of QMPh joined the united Department of nuclear-physics research methods (Head of the Department is Corresponding Member of the Russian Academy of Sciences, Professor Mikhail Kovalchuk). The QMPh collective has a number of priority works in the field of nuclear magnetic resonance. One of the most significant achievements was the first in the world implementation (in 1958) of the Fourier transform of a free induction signal in order to obtain a NMR spectrum. Concurrently with the research activity, the staff of the department are actively involved in the development of practical applications of magnetic resonance. The department graduates work not only in Russia and the CIS, but also in Sweden, USA, New Zealand, England, Cuba, Germany, France, Italy, occupying positions from a highly advanced operator of radiospectrometers to a professor.

The main research areas developing in the team of quantum magnetic phenomena:

- Nuclear magnetic relaxation in liquids;
- Nuclear magnetic resonance in solids, including magnetically ordered materials;
- NMR in liquid crystals;
- NMR in heterogeneous systems;
- MRI in weak magnetic fields;
- Electron paramagnetic resonance;

- Nuclear magnetic resonance in the magnetic field of the Earth;
- The quantum magnetometry in archeology.

It is evident from the above that the scope of our research interests is quite wide. We are always open for the collaboration with researchers from various fields of science.

Our team has published a series of monographs, textbooks and training manuals on Magnetic Resonance. For example:

1. Vladimir I. Chizhik, Yuri S. Chernyshev, Alexey V. Donets, Viatcheslav Frolov, Andrei Komolkin, Marina G. Shelyapina. Magnetic Resonance and Its Applications. 2014, Springer-Verlag. 782 pp. *(Now more than 30000 chapter downloads).*
2. Квантовая радиофизика: магнитный резонанс и его приложения. Учеб. пособие. 2-е изд., перераб. Под ред. В. И. Чижика. – СПб.: Изд-во С.-Петерб. ун-та, 2009. 700 с.
3. В. И. Чижик. Ядерная магнитная релаксация. Учеб. пособие. 3-е изд. – СПб.: Изд-во С.-Петерб. ун-та, 2004. 388 с.
4. Практикум по магнитному резонансу. Учебное пособие. Под ред. В. И. Чижика. – СПб.: Изд-во С.-Петерб. ун-та, 2003. 184 с.

Due to the COVID-19 coronavirus pandemic and the prohibition to hold any public events, the Organizing Committee of "Spinus-2020" have decided not to implement the School-Conference in a face-to-face format (as there are no definite prospects with the transfer), but to publish the materials sent, that will allow participants to familiarize themselves with current research. We hope that the next "Spinus-2021" will be held in the usual format! We hope to see you at "Spinus-2021"! Welcome!

Dr. Sci., Professor, SPbSU, Denis A. Markelov
Chairman of Organizing committee of the 17th School-conference
"Magnetic resonance and its applications" Spinus-2020

Section 1

Spin Superfluidity and its application for quantum computing

Yu. M. Bunkov

Russian Quantum Center, Skolkovo, 143025 Moscow, Russia.
E-mail: y.bunkov@rqc.ru

The conventional magnon Bose-Einstein condensation (BEC of magnons with k = 0) has been observed in magnetically ordered materials with repulsive interaction between magnons. In particularly it was observed in Yttrium Iron Garnet (YIG) film, magnetized perpendicular to the surface. For YIG film the critical density of non-equilibrium magnons for BEC condensation is $N_{BEC} \simeq M - M_z = M\,(1-\cos\beta)$, and corresponds to a deflection of precessing magnetization on an angle $\beta \simeq 3^\circ$ [1]. Here M is the magnetization and M_z its projection on the magnetic field. In these conditions the eigen state of magnon BEC determines by its frequency and does not depend on the exciting RF power (Fig. 1) [2].

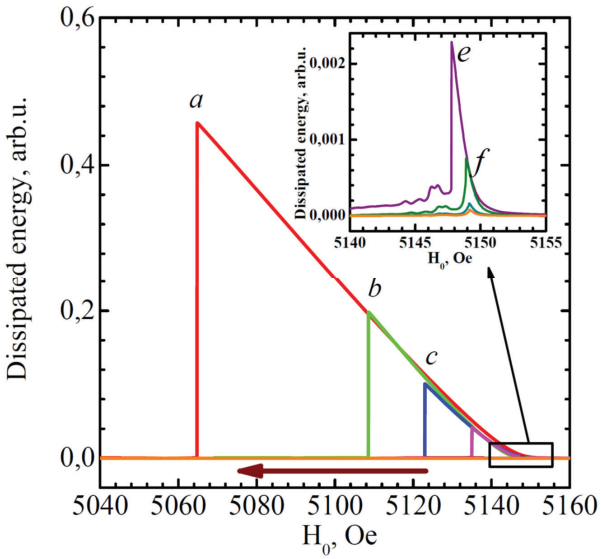

Figure 1. The energy dissipated by a magnon spin system at a magnetic field sweep at a different level of exciting RF power. The energy was calculated as a product of absorption signal on the amplitude of magnetic field. The dissipated energy depends on a frequency shift from the resonance and does not depend on the RF power! The enlarged scale is shown in the inset

The BEC state persists permanently at the conditions, when the losses (evaporation) of quasiparticles are replenished by an excitation of new quasiparticles. This is the first permanent superfluid state, which exist at room temperature. The energy gap of magnon superfluid state can be adjusted by RF pumping frequency. Our discovery open the way for observation of coherent quantum transport phenomena at a room temperature, like magnetic Josephson effect, long distance spin transport, phase slippage, Goldstone modes (analog of second sound in superfluid ^{4}He) and others. This discovery may be applied for quantum computing. It may combine the spin type Q-bit and Josephson superfluid Q-bit at a combined systems.

Particularly, the qubit magnetic systems, analogous to a well-known superconducting qubits, can be considered: charge qubit (a), flux qubit (b) and phase qubit (c).

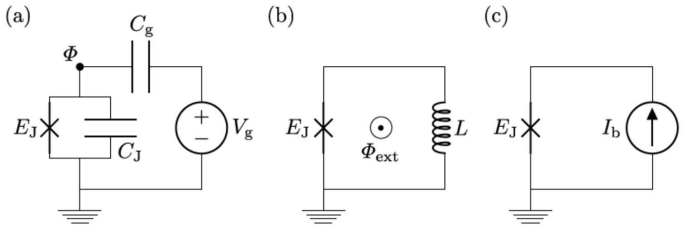

Figure 2. The types of circuits of Josephson junction superconducting qubit

Roughly speaking, the charge qubit is a box for charge, controlled by an external voltage V_g; the flux qubit is a loop controlled by an external magnetic flux F_{ext}; and the phase qubit is a Josephson junction biased by a current I_b. Using the analogy between electric superconductivity and spin superfluidity, we can suggest the next constructions of magnonic qubits. The charge qubit based on the repulsive interaction between magons, which realized by a frequency shift of the resonance frequency from the number of non-equilibrium magnons. For YIG film it reads:

$$\omega - \omega_0 = \gamma 4\pi M_S(1 - \cos\beta),$$

In the units of number of magnons n it roughly reads:

$$\Delta\omega(n) = \omega_0(1 + n/3N),$$

The pumping RF frequency plays a role of voltage for magnonic superfluid state. By choosing the frequency between the n and n + 1 state we can make a magnonic analog of charge qubit. The atomic density in the ferromagnetic sublattice of the YIG is of the order of $N = 10^{22}$ per cm^3. If a sample of a YIG film has dimensions of the order of 10^{-15} cm^3, each new non-equilibrium magnon shifts the resonance frequency on about 30 kHz at RF frequency about 10 GHz. By connect the sample with the source of magnons with a given chemical potential by a Josephson junction, we will be able to recognize the quantum states with n and n+1 magnon.

The analogy with a phase qubit is more complicate. The superconducting phase qubit based on Aharonov-Bohm effect. The phase of charged particle, moving along a path *L* changes by a:

$$\Delta\alpha_{AB} = -e\int_L \vec{A}\cdot d\vec{r}.$$

For the close path it leads to a quantization of a phase on 2nπ. The similar effect exist for a manetic particles (or quasiparticles) and names Aharonov- Casher effect:

$$\theta_{\text{A-C}} = \frac{g\mu_B}{\hbar c^2}\oint \mathrm{d}\mathbf{l}\cdot(\mathbf{E}\times\mathbf{e}_z)$$

It leads to a similar effect of phase quantization for spin supercurrent. In this way, the phase difference at the Josephson junction can be controlled by passing electric current through a closed loop. Furthermore, this phase can oscillate by application of AC electric voltage. This possibility makes a new way for dealing with phase qubit. As concerning the flax qubit, the situation is more complicate, since the magnetic flax does not quantized in a close magnonic loop. Indeed, the real superconducting qubits are the superposition of a big number of a small samples connected by the Josephson junctions [3].

The similar system can be fabricated with the small samples of YIG films, as shown in Fig. 3. The magnonic superconducting system may have many advantages. First of all, they exist at room temperature, since the temperature of ferromagnetic transition in YIG is about 600K. Secondary, the magnonic precession interacts directly with the RF field. This simplifies the programing and read out the results of calculations. Furthermore, the dimensions of Josephson junction can be much large, then for a supercunducting quantum circuits. It can be adjusted by locally applying the magnetic field (3) or electric current (2) (See Fig. 3). The problem of relaxation of magnons can be solved by a permanent source of a new magnons with a controllable chemical potential throw the peripheral YIG strips (1). The read out of the information from each element can be performed by RF resonator (4) or Spin-Hall effect (5), as well by optical methods (6). The very important circumstance is the possibility of print circuits fabrication and scaling the construction. The last question is the temperature of real processor. It's, possibly, necessary to cool down the processor to a sub-kelvin region of temperature for to avoid the thermal fluctuations of qubits. Indeed, question of noise of Bose condensate magnon gas is not so clear. Definitely, the magnon processor will be less sensitive to an external noise, since there is not an electric charged particle. In conclusion, the idea to use the magnonic superfluidity for quantum calculations is very new and has a great potential of its development. For review of spin superfluidity please see [4].

In conclusion it is useful to mention, that the spin superfluid phenomena is the result of repulsive interaction between non-equilibrium magnons in out of plain magnetized YIG film. There were published many experiments with in-plane magnetized film. The long distance spin waves propagating were demonstrated. The magnon BEC formation was also announced. Indeed, in these systems the magnonic interaction is attractive and, consequently, the critical superfluid velocity is zero and effect of magnon superfluidity does not exist. For review of spin superfluidity please see [4].

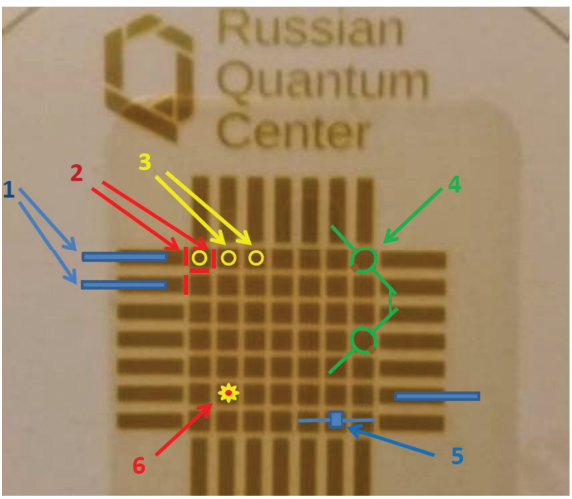

Figure 3. The prototype of magnonic quantum processor

Financial support by the Russian Science Foundation within the Grant 19-12-00397 "Spin Superfluids" is gratefully acknowledged.

References

1. Yu. M. Bunkov and V. L. Safonov, J. Magnetism Magnetic Materials, **452**, 30–34 (2018).
2. Yu. M. Bunkov et al., https://arxiv.org/abs/1810.08051; https://arxiv.org/abs/1911.03708
3. F. Arute, et al., Nature, 574, 505 (2019).
4. Yu. M. Bunkov and G. E. Volovik, “Spin Superuidity and Magnon BEC" in Novel Superuids Ch.4, eds. Bennemann, K. H. & Ketterson, J. B. Oxford Univ. Press, Oxford, (2013), arXiv:1003.4889v3.

Synopsis of the MRI physical and hardware bases

Carlos Cabal Mirabal

Physics Faculty Havana University, Cuba
E-mail: carlos.cabal@fisica.uh.cu

A didactic general overview of the Magnetic Resonance Imaging (MRI) is presented. The role of different electromagnetic fields in the image's formation is deliberated. Similarly, the relationship between these fields are discussed [1-8]:

- Intensity, stability and homogeneous of external homogeneous Magnetic field (Bo),
- The pulse shape, stability and intensity of Gradient of the Magnetic Field
- The intensity, modulation's law and pulse duration of Radiofrequency field (RFB1)

The requirements and characteristics of these fields in order to make possible the MR imaging are emphasizing. Phase and frequency codification as a base of the Fourier images are presented. The Phase space are defined. The 2D and 3D Spin Echo (SE) and Gradient Echo (GE) pulse sequences are deliberated [1-8].

The connection between the Gradients characteristics, Field of View (FOV), Spatial and Spectral resolutions, the matrix dimension and Images Time is considerate.

The Phase space characteristics for different pulse sequences and its connection with the image's characteristics are discussed. The relationship between the Images Contrast, Contrast Noise ratio, Signal Noise ratio and Images Time of the images are briefly evaluated. Similarly, the image's distortions and artifacts are appraised [1-8].

The possibilities and challenges of the MRI focusing in the physical and technological opportunities and restrictions, are presented. Undesirable situations related to fields interactions and eddy currents are examined. Some methods to overcome these unwanted conditions are deliberated.

Different alternatives to decrease the Images Time keeping and even improving the images characteristics are exposed: diverse pulse sequences, the array of RF coils and the parallel imaging including the use of localized gradients by no linear gradients [3-9]

The original, simple and useful case of the Single-side NMR is concisely commented [10]. Likewise, the fashions of Nonlinear gradient is presented.

Cuban´s experiences concerning to the calculation, design, construction and validation Magnetic Resonance (MR) technology and introduction in the clinical practice are mention. Cuban MR Technology includes MR relaxometer, Magnetometers and MRI whole body machines.

Acknowledgements

The author express gratitude to Prof. Dr. V.I. Chizhik and to the collective of Medical Biophysics Centre of University of Oriente, Cuba.

References

1. R.W. Brown, Yu-Chung N. Cheng, E. Mark Haacke, M. R. Thomson, R. Venkatesan, "*Magnetic Resonance Imaging Physical Principles and Sequence Design"* Second edition, Willey Blackwell, 2014.
2. C.N Chen and D.I. Hoult "*Biomedical Magnetic Resonance Technology".* Adam Hilger, NY, 1989.
3. M. A. Berstein, K.F. King X.J. Zhou*, "Handbook of MRI Pulse sequences".* Elsevier, Academic Press, 2004.
4. J. T. Vaughan, J. R. Griffiths "RF Coils for MRI" John Willey and Sons, 2012.

5. J. Mispelier, M. Lapu, A. Briguet "NMR Probe heads for Biophysical and Biomedical Experiments. Theoretical Principles and Practical Guidelines" Imperial Collage Press, 2009.
6. A. G. Webb *"Magnetic Resonance Technology» Hardware and System component design"* The Royal Society of Chemistry, 2016.
7. J. Jin, *Electromagnetic Analysis and Design in MRI» CRC Press, 1999.*
8. Zhi Pei Liang, P: Lauterburg *"Principles of Magnetic Resonance Imaging. A signal Processing Perspective",* IEEE Press, NY 2000.
9. G. Shultz, *"Magnetic Resonance Imaging with Nonlinear Gradient Fields. Signal encoding and Images Reconstruction"* Springer Spectrum, 2013.
10. F. Casanova, J. Perlo, B. Blümich *"Single -Sided NMR"* Springer, 2011.
11. Schultz G. (2013) Overview of PatLoc Imaging and Presentation of Initial Hardware Designs. In: Magnetic Resonance Imaging with Nonlinear Gradient Fields. Springer Spektrum, Wiesbaden https://doi.org/10.1007/978-3-658-01134-5_3

NMR studies of phase transitions in confined metals and alloys

Elena V. Charnaya, Denis Yu. Nefedov, Andrei V. Uskov, Dmitrii Yu. Podorozhkin

St. Peterburg State University, St. Peterburg 198504 Russia
E-mail: charnaya@mail.ru

Introduction

A concise review of the use of NMR as a probe for studying different kinds of phase transitions in liquid and solid metals and alloys embedded into nanoporous silica matrices is presented. The attention is focused on last studies of the liquid-liquid phase transitions in confined melts and structural modifications under nanoconfinement while the melting and freezing transitions are also discussed.

Liquid-liquid phase transitions under nanoconfinement

Structural transformations in liquids pose severe challenges to condensed matter physics. The nature of LLPT is poorly understood and even its occurrence in many substances is in doubt. It was suggested that LLPT at ambient pressure takes place under strong supercooling. Therefore, LLPT in bulk is disguised by crystallization or vitrification processes. In contrast, liquids confined to nanoporous matrices are easy to supercool to temperatures much lower than the melting temperatures. This raises expectations that LLPT can be found in liquids under nanoconfinement. For metallic substances NMR acts as a powerful experimental technique which gives valuable information about the internal structure of liquids through measurements of the Knight shift caused by coupling with conduction electrons. Here we review NMR measurements of the Knight shift, which were carried out to study LLPT in the nanostructured Ga and Ga-In-Sn and Ga-In alloys in the supercooled state. NMR studies revealed a step-like splitting of the gallium resonance line upon cooling. At warming the gradual change of the Knight shift was observed which could happen when the confined melts pass over the critical point of the LLPT line on the phase diagram.

Structural transformations under nanoconfinement

NMR was applied to studies of polymorphism in confined metals and alloys. It was shown that for metallic sodium within fine pores of porous glasses the temperature of the structural phase transition, which occurs in bulk below 40 K, rises remarkably up to more than 200 K. The emergence and stabilization of a solid phase with the structure of β-Ga was observed for gallium alloy confined to silica opal matrices. The temperature ranges of this phase occurrence and quadrupole constant temperature dependences were obtained.

Melting and freezing in confined nanoparticles

The melting and crystallization phase transitions for metallic components of nanocomposites were noticeably moved to lower temperatures and strongly diffused. For some metals as mercury and tin the occurrence of the liquid skin upon melting was suggested. The pronounced hysteresis between melting and freezing was ascribed to heterogeneous nucleation under confinement. The step-like freezing and melting of gallium within pores was found to occur due to the emergence of different crystalline phases.

Acknowledgements

This work is supported by RFBR (grant 19-07-00028). Part of measurements was done in SPbGU using the equipment of "Centre for Diagnostics of Functional Materials for Medicine, Pharmacology and Nanoelectronics".

Molecular mobility in ionic liquids $[bmim]^+A^-$ and their mixtures with water by NMR and molecular dynamics simulation methods

V. I. Chizhik[1], S. S. Bystrov[1], V. V. Matveev[1], A. V. Egorov[1], Y. S. Chernyshev[1], V. A. Konovalov[1], and V. Balevičius[2]

[1] Saint Peterburg State University, Saint Peterburg, 198504, Russia
[2]Vilnius University, Vilnius, Lithuania
E-mail: v.chizhik@spbu.ru

Unique physical and chemical properties of ionic liquids, ILs, (neat and in solutions) such as high thermal stability, low vapor pressure, high boiling point, and the ability to dissolve a wide range of chemical species, determine numerous applications in "green" chemistry and material science. Aqueous solutions of ILs play a large role in various practical applications.

The results of detailed investigation of the local and translational mobility in a set of imidazolium-based ionic liquids (1-butyl-3-methylimidazolium) in a wide temperature range and varying anions (BF_4^-, I^-, Cl^-, Br^-, NO_3^-, TfO^-) are presented. The measurements of temperature dependencies of the spin-lattice relaxation times of ^1H and ^{13}C nuclei are motivated, in particular, by the need to obtain a fundamental characterization of molecular mobility in the substances under study, namely, to estimate the correlation times for the motion of individual molecular groups. The approach based on the investigation of the NMR relaxation allows the estimation of the mobility of selected molecular groups from independent information. It follows from our results that the mobility of the hydrocarbon "tail" is higher than the one of the imidazole ring, especially at low temperatures. It is worth noting that this expected effect is quantified.

The study of translational diffusion is very important for deeper understanding the peculiarities of molecular motion of the components in objects under investigation, since it constitutes to the basic form of "transport" which reflects molecular interactions of molecules or ions with their environment. The correlation between local and translational mobility in pure ionic liquids of the [bmim][A] type was investigated using the data on NMR-relaxation rates and diffusion coefficients. It has been found that a sufficiently clear correlation is realized only in the case of ILs with relatively low viscosity and only at temperatures above room temperature, that is, rapid reorientations of molecular groups of the hydrocarbon "tail" almost does not affect the translational mobility of the cation as a whole. The mutual sequence of the values of diffusion coefficients (D) for different ILs corresponds qualitatively to the data on their viscosity η, namely: the minimum D value has been observed for ILs with the highest viscosity ([bmim] Cl), and the maximum D ones have been registered for ILs with lowest viscosity ([bmim] TfO and [bmim] BF_4). However, it is shown here that for the $[bmim]^+$ cation the temperature dependencies of the product $D\eta$ do not follow the Stokes-Einstein relation for most systems studied, i.e. there realized so-called "diffusion-viscosity decoupling".

In terms of practical application, it is important to have an idea how the IL structure changes with the addition of water. There are a few points of view on this issue. In the past few years, the hypothesis about the existence of so-called "water pockets" in mixtures of water with a number of ionic liquids has been discussed in the literature. The concept of "water pockets" was introduced by a group (groups) of Japanese researchers. The hypothesis is based on a certain set of experimental data (obtained by various methods: SANS/SAXS, Raman, NMR, ... etc.) about the heterogeneous structure of such mixtures at a nanometer level [1-4]. In the report the critical review of existing models of the microstructure of mixtures "IL – water" and the justification of a new hypothesis about the structure of systems such as "[bmim]A – H_2O" are given [5, 6]. In addition to the data available in the literature, we carried out the measurements

of self-diffusion coefficients and computer simulations of molecular dynamics for various components of mixtures.

Acknowledgements

The NMR measurements have been carried out in the Center for Magnetic Resonance of Research park of Saint Petersburg State University.

This work was supported by Russian Foundation for Basic Research (RFBR) grant #17-03-00057a.

References

1. Abe, H.; Hatano, N.; Ima, Y.; Ohta, S.; Shimizu, A.; Yoshimura, Y. Peculiar Concentration Dependence of H/D Exchange Reaction in 1-Butyl-3-Methylimidazolium Tetrafluoroborate-D2O Mixtures. Open J. Phys. Chem. 2011, 01 (03), 70. https://doi.org/10.4236/ojpc.2011.13010.
2. Abe, H.; Takekiyo, T.; Shigemi, M.; Yoshimura, Y.; Tsuge, S.; Hanasaki, T.; Ohishi, K.; Takata, S.; Suzuki, J. Direct Evidence of Confined Water in Room-Temperature Ionic Liquids by Complementary Use of Small-Angle X-Ray and Neutron Scattering. J. Phys. Chem. Lett. 2014, 5 (7), 1175–1180. https://doi.org/10.1021/jz500299z.
3. Saihara, K.; Yoshimura, Y.; Ohta, S.; Shimizu, A. Properties of Water Confined in Ionic Liquids. Sci. Rep. 2015, 5, 10619. https://doi.org/10.1038/srep10619.
4. Abe, H.; Takekiyo, T.; Yoshimura, Y.; Saihara, K.; Shimizu, A. Anomalous Freezing of Nano-Confined Water in Room-Temperature Ionic Liquid 1-Butyl-3-Methylimidazolium Nitrate. ChemPhysChem 2016, 17 (8), 1136–1142. https://doi.org/10.1002/cphc.201501199.
5. Bystrov S. S., V. V. Matveev, Y. S. Chernyshev, V. Balevičius, V. I. Chizhik. Molecular Mobility in a Set of Imidazolium-Based Ionic Liquids [bmim] + A - by the NMR-Relaxation Method. Journal of Physical Chemistry B. 123, 10, 2362-2372. Doi: 10.1021/acs.jpcb.8b11250.
6. Bystrov S. S., Vladimir V. Matveev, Andrei V. Egorov, Yurii S. Chernyshev, Vladislav A. Konovalov, Vytautas Balevičius, and Vladimir I. Chizhik. Translational Diffusion in a Set of Imidazolium-Based Ionic Liquids [bmim]+A- and Their Mixtures with Water. J. Phys. Chem. B DOI: 10.1021/acs.jpcb.9b06802.

Unvealing the importance of succination in the differenciation of adipocytes: A NMR-based approach

Jean-Marie Colet, Manon Delcourt, Vanessa Tagliatti, Anne-Emilie Declèves

Department of Human Biology and toxicology at the university of Mons

The thiol groups carried by different biological structures such as cysteine are known to react spontaneously and easily with the fumarate produced by the mitochondria, resulting in the formation of S-(2-succino) stable derivatives by a process called "succination".

Thiol succination increases in some tumors, particularly following a deficiency of fumarate hydratase, the enzyme responsible for the conversion of fumarate to malate. Thus, the accumulated fumarate serves as a proto-oncometabolite which, by binding to glutathione to form 2- (S-glutathionyl) -succinate, results in the accumulation of reactive oxygen species (ROS). An increased rate of succination has also been reported in situations of glucotoxicity. For example, both fumarate and protein succination are increased in adipocytes cultured in a glucose-rich medium.

Adiponectin is a major target for the succination of adipocytes and adipose tissue. Cysteine at position 39, which is involved in the crosslinking of adiponectin monomers to form trimers, has been identified as a preferred site for the adiponectin succination in adipocytes. Among the "succinoma" proteins, there is also insulin.

As evidenced by the growing number of associated publications, the phenomenon of succination is of increasing interest to the biomedical world and represents the central element of the project that will be presented at the SPINUS 2020 meeting. In particular, we developed and applied NMR-based approaches to study the potential impact of succination of key proteins of adipocyte differentiation in a context of obesity. Preliminary results will be exposed at the meeting.

The physical state of di-nitrogen in the presence of porous solids probed by ^{15}N spin-lattice relaxation of pure $^{15}N_2$ in the 30 K – 300 K range

Jacques Fraissard

University Pierre and Marie Curie, Paris
Ecole supérieure de Physique et Chimie Industrielle de Paris, France

^{15}N NMR spin−lattice relaxation times of pure $^{15}N_2$ in the presence of mesoporous SBA-80 and selected zeolites (Y, OMEGA, MORDENITE, ZSM-5, ZSM-11, AlPO-5, RHO) have been measured at 30 MHz and at temperatures ranging from 300K to about 30 K. The interpretation of these experimental data rests on two relaxation mechanisms: spin-rotation (mainly active when N_2 molecules reorient rapidly) and dipolar interaction with surface centers (depending essentially on the N_2 translational diffusion mobility). Both mechanisms have to be taken into account for all samples except SBA-80 (for which the interpretation of experimental data requires two different spin-rotation interactions), and RHO (for which two different dipolar interactions are required). For all zeolites investigated here it has been indispensable to define a cutoff temperature below which spin-rotation is no longer active, indicating the quasi-disappearance of the gaseous state to the benefit of a condensed state. This cutoff temperature is 77 K for Y, OMEGA, and possibly MORDENITE, whereas it is higher for those zeolites with pore diameters approaching the dinitrogen molecular length. It is thus concluded that these NMR relaxation measurements are able to reveal the physical state of dinitrogen in the presence of SBA-80 and zeolites possessing very different structures.

What can be deduced from $^{15}N_2$ adsorption results for the characterization of porous and, more particularly, microporous solids? ^{15}N NMR relaxation confirms, partly, the validity of the BET model in the case of solid SBA-80. This was expected, since SBA is a mesoporous solid. As postulated in the BET model, there must be a difference in the adsorption energy between the first molecules in contact with the solid surface and those in the subsequent layers. However, the NMR results show that at 77 K (at adsorption equilibrium) there is a fast exchange not only between the molecules of the upper layers of the adsorbate and those of the gas phase, but also between those of all the adsorbed layers.

The case of zeolites is much more complex. The fact that there is necessarily a steric limitation to the thickness of the multilayer would not be important if the adsorption was homogeneous with unrestricted diffusion inside the pores. However, not only the pore diameter but also the complexity of the pore structure controls the relaxation and the motion of N_2. The existence of a cutoff temperature is a clear indication of this complexity. It must, however, be noted that it is close (if not identical) to the dinitrogen boiling point (77 K) for some zeolites (Y, OMEGA), i.e. the larger-pore zeolites. In this case the BET model for adsorption is not still valid but, thanks to the more or less easy diffusion of nitrogen in the pores, the isotherms of dinitrogen adsorption at 77 K can be used to calculate the porosity, if we use techniques which distinguish between the amount of dinitrogen located in the pores and at the external surface of the crystallites.

In contrast, for the other zeolites investigated here, where the principal adsorption zones are connected by smaller pores, the cutoff temperature is higher (or even much higher) than 77 K, indicating that N_2 adsorption occurs in small pores well above 77 K. This adsorbate has a very restricted mobility at 77 K and its distribution can be heterogeneous, sometimes with a nearly rigid fraction, as it is the case with ZSM-5. Moreover, even at relatively high temperature, the variation of the relaxation rate with temperature can be rather complicated, as in the case of MORDENITE and, above all, for the RHO zeolite. The chemical nature also plays an important role, even if the surface is in principle homogeneous, as in the case of the AlPO-5 zeolite.

Specifics of NMR-visualization at ultralow magnetic field

Viacheslav Frolov, Konstantin Tyutyukin

St. Petersburg State University,1, Ulyanovskaya str.,
St. Petersburg, 198504, Russian Federation
E-mail: vfrolovv@bk.ru

In the last decade, there has been a renewed interest in nuclear magnetic resonance (NMR) research in very weak magnetic fields (units mT and below) compared to those used in proprietary instruments [1, 2]. Interest in such research extends to magnetic resonance imaging. This is due, on the one hand, to the extremely high cost of equipment operating in strong magnetic fields and using liquid helium or rare earth-based magnetic materials. On the other hand, as the authors of [3] note, it is not always advisable to use a very strong magnetic field: 80% of diagnostic examinations can be performed in a much weaker field.

It should be noted that in addition to the high cost, there are other negative factors in MRI in the very strong magnetic field caused by the use of high radio frequencies (hundreds of MHz). Since the living organism is a conductive medium, the risk of tissue overheating and exceeding the permissible level of absorbed power (SAR) increases with increasing frequency. In addition, the conductive medium becomes an additional source of noise [4], which reduces the effect of improving the signal-to-noise ratio as the field level increases. One of the negative factors is also the reduction of relaxation contrast due to the phenomenon of frequency dispersion of relaxation times [2]. In addition, strong magnetic field and high frequency cause difficulties in examining certain groups of patients. It is impossible to examine patients with metal implants and cardiostimulator, there are difficulties with individuals suffering from claustrophobia, some poorly tolerate the noise produced by the gradient system.

The presented lecture deals with examples of magnetic resonance imaging in ultralow magnetic field.

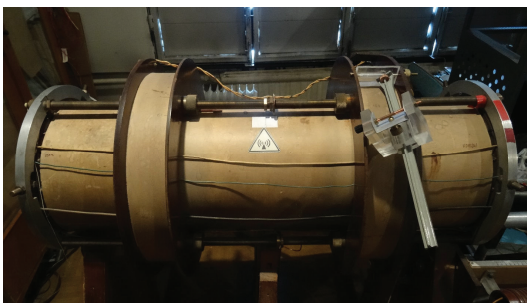

Figure 1. Magnetic resonance imager for small objects in field 7 mT designed at St. Petersburg University

References

1. Ю. В. Богачев, М. Н. Князев, Я. Ю. Марченко, А. Н. Наумова, К. В. Тютюкин, В. А. Фокин, В. В. Фролов, Ю. С. Черненко. Диагностический магнитный резонанс. СПб: Изд-во СПбГЭТУ "ЛЭТИ", 2013. 212 с.
2. Андреев Н.К. Методы и приборы низкочастотной релаксационной ЯМР-интроскопии. Казань: Казан. гос. энерг. ун-т, 2003. ISBN 5-89873-078-8.
3. Coffey A.M., Truong M., Chekmenev E.Y. // J. Magn. Reson. 2013. V. 237. P. 169.
4. Edelstein W, Glover G, Hardy C, Redington R. // Magnetic Resonance in Medicine. 1986. V. 3. P. 604.

Fast techniques for measurements of surface area, pores volume distribution, particle sizes and concentrations in colloidal systems by TD-NMR

Leonid Grunin

Resonance systems GmbH

Capacitors, resistors, semiconductors, inks and dyes as well as pills, cosmetics, environmental adsorbents and many other things in industry and in daily life represent heterogeneous colloidal substances. To characterize them there are several very important values like Surface Area, Particles Dimensions, Colloid Concentration (solid particles mass or volume fraction in liquid solution). Surely there exists a number of classical methods to measure these values like light scattering, diffraction, electron microscopy, viscosimentry, centrifuging etc. Time Domain NMR (TD-NMR) is one of the most promising approach of all existing ones that is extremely cost effective, easy and accurate.

Using a dispersion medium (DM, normally liquid) for probing the surface properties of dispersed phase being investigated (DP, normally solid) is based on the mobility variation of molecules of a liquid that depends on how a DP molecule is experiencing interactions with active adsorption centers of DP surfaces. In some cases, experimentally observed NMR Relaxation curve shows up a non-exponential behavior and allows deconvolution of the signal into components that can be referred to bounded and relatively free volumes of a DM, so the contribution of DP surface is being measured nearly directly. In other cases, the fast magnetizations exchange between bulk and surface liquids brings the exponential NMR relaxation decay, so the properties of a DP are revealed by calibrating of the relaxation rate value against known concentration of a solid material.

Relatively easy calculations are masking the real complexity in obtaining of stable, accurate and reproducible values of a DP surface chemistry parameters due to multiple side effects. In the presentation the application of NMR relaxometery to analysis of different adsorbents, fillers and porous solids for needs of electronic components, batteries, inks as well as pharmaceutical industries are considered in details.

From lungs to car catalysts: A breath taking journey with hyperpolarized noble gas MRI

Arthur Harrison[1], Max Filkins[1], Xinpei Wang[1,3], Sean P. Rigby[2], Chengbo Wang[3], Galina E. Pavlovskaya[1], Thomas Meersmann[1,3]

[1]Sir Peter Mansfield Imaging Centre, Division of Respiratory Medicine, School of Medicine, University of Nottingham, Nottingham, NG7 2RD, United Kingdom
[2]Department of Chemical and Environmental Engineering, University of Nottingham NG7 2RD, United Kingdom
[3]Department of Electrical and Electronic Engineering, University of Nottingham, Ningbo, PR China

Introduction

The technological revolutions made at the physics – biomedical sciences interface with hyperpolarized (HP) noble gas MRI have produced one of the most significant advances in pulmonary diagnostics in decades. Hyperpolarization improves the gas phase MR signal by 4 – 5 orders of magnitude and thus enables lung functional MRI. Using spin exchange optical pumping (SEOP), this laser-based technology can produce hp ^{129}Xe as MRI contrast agent for the gas phase. Xenon's tissue solubility, large chemical shift range, and interaction with specific sensor molecules allows for a variety of biomedical hyperpolarized ^{129}Xe application [1].

Hyperpolarized ^{83}Kr

Our group has previously shown that quadrupolar T_1 relaxation of the hyperpolarized noble gas isotope ^{83}Kr (nuclear spin I = 9/2) can utilized to probe surfaces that are in contact with the noble gas. For example, surface quadrupolar relaxation (SQUARE) T_1 maps of ^{83}Kr are indicative of an emphysema model in excised rodent lungs [2]. MRI at the very low resonance frequency ^{83}Kr (i.e. 11.5 MHz at 7 T) requires hyperpolarization through spin exchange optical pumping (SEOP) similar to that for the hp ^{129}Xe production. However, as a consequence of quadrupolar relaxation, hp ^{83}Kr cannot be concentrated from buffer gases of the laser pumping process through cryogenic separation or through membranes without depolarization. Therefore, a new production methodology was developed that uses molecular hydrogen as buffer gas during SEOP and its subsequent removal through catalytic combustion [3]. Currently, novel instrumentation is being developed to make this approach feasible for clinical applications (Fig. 1).

In situ ^{129}Xe applications

Similar to ^{83}Kr MRI SQUARE contrast, paramagnetic relaxation of hp ^{129}Xe can be applied to study surfaces, in particular for chemical engineering and materials science applications. Generally, MRI of fluid flow can probe the structure-transport relationship [3], and we use hp ^{129}Xe to study gas transport and reactive zones in diesel catalysts that consist of materials with hierarchical pore structure. The combustion and high temperature resistance of the hyperpolarized spin state allows usage of these novel contrast agents for in situ MRI of chemical reactors. The accessibility of catalytic and paramagnetic centers can be probed through ^{129}Xe relaxation measurements provide insights into catalytic activity in these systems [4].

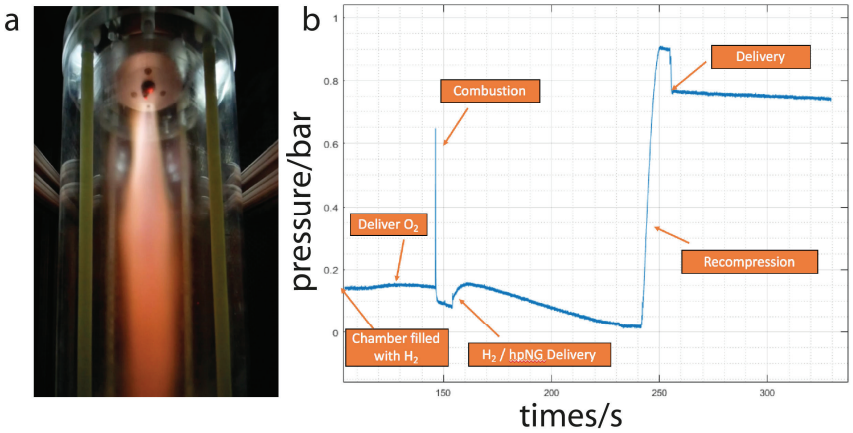

Figure 1. Combustion system to concentrate hyperpolarized noble gases. a) Combustion chamber with 4 L volume to remove H_2 through catalytically triggered combustion. The SEOP gas mixture only contains about 5% xenon or krypton for the laser pumping process and molecular hydrogen (95%) is used as buffer gas for the laser pumping process. b) Pressure curve of the purification process. Initially, the chamber is filled with pure hydrogen and O_2 is added to trigger the initial Knallgas reaction at about 150s. After this time the SEOP gas mixture is added to react the H_2 away (H_2O will condense out of the gas phase). After completed reaction, a pneumatically operated piston will pressurizer the remaining noble gas to for delivery to a breathing apparatus

Bibliography

1. David M.L. Lilburn, Galina E. Pavlovskaya, and Thomas Meersmann, J. Magn. Res, **229**, (2013), 173-186.;
2. D. M. L. Lilburn, C. Lésbats, J. S. Six, E. Dubuis, L. Yew-Booth, D. Shaw, M. G. Belvisi, M. A. Birrell, G. E. Pavlovskaya, T. Meersmann, *J. R. Soc. Interface* **2015**, *12*.;
3. GN. J. Rogers, F. Hill-Casey, K. F. Stupic, J. S. Six, C. Lesbats, S. P. Rigby, J. Fraissard, G. E. Pavlovskaya, T. Meersmann, *P Natl Acad Sci USA* **2016**, *113*, 3164-3168;
4. D.B. Burueva, E.V. Pokochueva, X. Wang, M. Filkins, A.I. Svyatova, S.P. Rigby, C. Wang, G.E. Pavlovskaya, K.V. Kovtunov,* T. Meersmann,* and I.V. Koptyug, ACS Catalysis Letter, 10.1021/acscatal.9b05000;

75 Years of EPR: Milestones in the 62 years Bruker EPR History

Peter Höfer[1], Uwe Eichhoff[2]

[1]Bruker BioSpin GmbH, D 76287 Rheinstetten, Germany, Silberstreifen 4
[2]Bruker BioSpin GmbH retired; D 76571 Gaggenau, Germany, Max Hildebrandt-Str.40
E-mail: Peter.Hoefer@bruker.com, barbara.uwe@t-online.de

In the first years of EPR cw-spectrometers were home built. They usually were designed for an optimal performance for a special application. But in contrary to home built instruments commercial instruments must be universal and offer optimal sensitivity and resolution for all methods and applications.. Additionally they should be easily adaptable to other frequency bands. These requirements for cw-EPR have been fulfilled over the years with the development of a signal channel with 24 bit resolution and fast conversion time resulting in a dynamic range of up to 106db resolving 256.000 points on the y-axis with a minimal conversion time of 320μsec. An extremely stable magnetic field controller allows sweep of 256.000 points. Even an exceptional sweep range with 180.000 points for 14kG can be realized resulting in 80mG resolution. With the high dynamic range over an extremely broad magnetic field range no available signal should be missed. New resonators with a better conversion factor have been developed for effective utilization of the microwave power enabling more accurate saturation experiments as well as for measurements in a wide temperature range.

The sensitivity of the EPR has increased in consecutive steps. In the early 1970 a S/N on the weak pitch of 200:1 was a good value. Improved klystrons led to a twofold increase in our new ESP 300. Then klystrons got worse and became almost unavailable. Bruker had to look for a new microwave source and developed a Gunn diode locked to a cavity, which gave together with a new super high Q cavity (SHQE) an improvement in S/N of more than one order of magnitude. So far all the main requirements for a universal cw-EPR spectrometer for scientific applications have been met successfully.

Another point was the introduction of EPR as a routine analyser in industry. These table top instruments should be dedicated to a special application and easy to use for employees not familiar with EPR. A spin counting software has been implemented to allow direct readout of the absolute number of spins. Shelf life time of beer and dosimetry as well as reactive oxygen and reactive nitrogen species in biomedical investigations were important applications.

Working hard on continous improvement of the cw-EPR instrumentation, Bruker was aware of the various pulse EPR spectrometers built by excellent scientists in the USA, Soviet Union, Netherlands and other countries. Even with all experience in pulse- and FT-NMR Bruker hesitated a long time to start the development of Pulse EPR. On the way we had long discussions institute about a low power version. But we came to the conclusion, that the only commercially satisfied development would be a universal high power pulse/FT-EPR spectrometer enabling the use of all known pulse methods and even flexible enough to incorporate new methods unknown at that moment. Most of our partners believed this to be impossible. Nevertheless we tried and in 1987 with the ESP380 the first commercial pulse EPR spectrometer was introduced. This was no more an improvement of the previous EPR, this was a revolution in EPR instrumentation. Some necessary microwave-components were not available on the market and had to be developed and produced by the company itself. To cope with the extremely short relaxation times, necessitating high bandwidths, a new range of resonators had to be developed.

In 1996 the new universal ELEXSYS spectrometer optimized for cw (E500, E 600) and pulse/FT-mode E580,E680) was introduced with a time resolution of 4 nanoseconds. The patternJet II creates the pulse sequences and the transient recorder SpecJet II is responsible for

the registration of the fast transient signal with a digitization speed of 1GHz, resulting in a sweep range of 500MHz. Both units take care of the basic digital signal processing such as base line correction, window function, fast Fourier transform and phase cycling for selectively enhancing the wanted signal and suppressing the unwanted transient responses. The pulse sequence can be adjusted directly looking at the signal. Special pulse sequences allow to selectively excite one of the many contributions to the Hamiltonian. To overcome the problem of limited bandwidth an arbitrary wave form generator SpinJet-AWG was developed allowing to edit any pulse form with any phase, frequency and modulation. These shaped pulses have a broader bandwidth at a lower power level and significantly increase to possibilities of all Pulse EPR experiments.

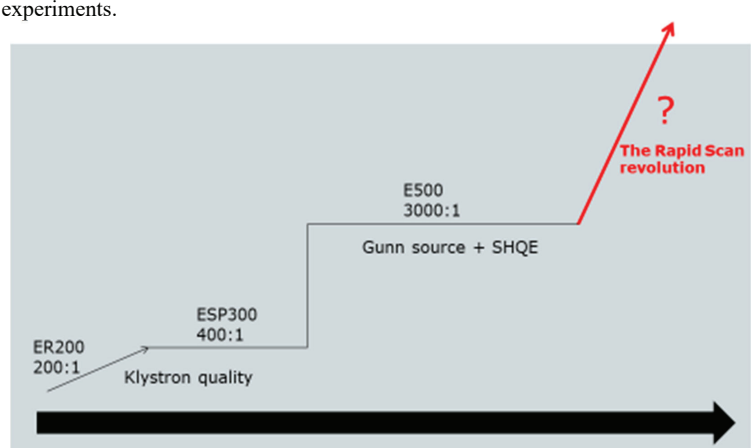

Figure 1. cw-EPR signal-to-noise history

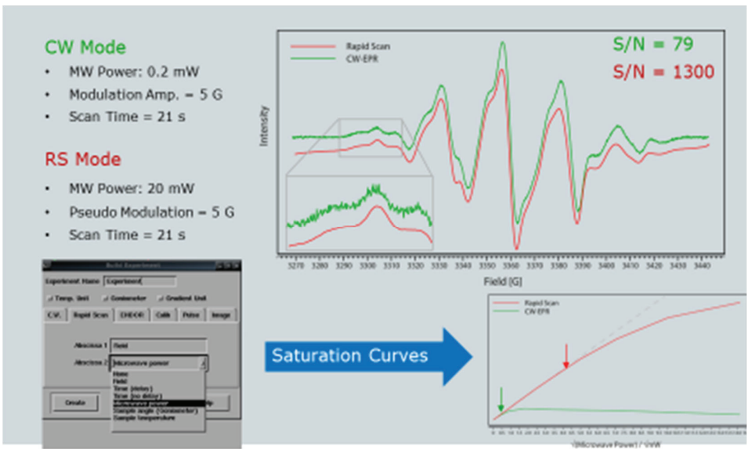

Figure 2. Alanine 0.3 kGy S/N comparison cw vs. rapid scan

In contrary to NMR the short EPR-relaxation-times in the nsec range allow a S/N-increase in FT-EPR as compared to cw-EPR only for a very few samples. The merit of Pulse EPR is the access to new information about the spin system but not a gain in sensitivity. During

the last years Sandra and Gareth Eaton have developed rapid scan EPR. An extremely fast, sinusoidal or triangular sweep is applied to the sample in a rapid passage [1,2]. The resonance condition is hit in a time short compared to the relaxation time and in this way saturation is avoided. Compared to standard signal/noise gain of 2 orders of magnitude seems to be possible. In cooperation with the Eaton-group Bruker has introduced a rapid scan accessory for the ELEXSYS spectrometers.

Biomedical (S- and L.band) and material EPR imaging (X-band) so far have found only limited applications, because cw-EPR imaging is extremely time-consuming and the fast Fourier.imaging methods, standard in MRI, cannot be applied because of the short EPR-relaxation times. Rapid scan EPR may change this situation and open new possibilities for biomedical EPR imaging in the much less sensitive S- and L-bands [3].

References

1. D.G.Mitchell,R.W.Quine,M.Tseitlin,A.A.Eaton,G.R.Eaton JMR **214** (2012) 221-226
2. D.G-Mitchell, G.M.Rosen, M.Tseitlin, B.Symmes, S.S.Eaton,G.R.Eaton Biophysical Journ. **105** (2013) 338-342
3. J.R.Biller,M.Tseitlin,R.Quine,G.A.Rinard,H.A.Weismiller, H.Elajaili, G.M.Rosen, J.P.Y.Kao, S.S.Eaton, G.R.Eaton JMR **242** (2014) 162-168

Ion-liquid extraction cleaning of oil distillates of various viscosities

M. D. Ibragimova, A. B. Khalilov, G. J. Huseynov, S. A. Seidova

Y. H. Mammadaliyev Institute of Petrochemical Processes of Azerbaijan National Academy of Sciences, AZ 1025, Baku, 30 Khojaly ave.
E-mail: minaver-ibrahimova@rambler.ru, sabina.seidova.ai@mail.ru
Keywords: selective purification, ionic liquid, extractant, raffinate, extract

With the expansion of the scope and volue of application of lubricating oils for various purposes, the requirements for their quality indicators are becoming more stringent. To obtain high-quality base oils, one of the technological stages of oil production is selective purification, in particular extraction purification of petroleum fractions with selective solvents.

With the aggravation of environmental problems, the creation of extraction methods for oil fractions using the so-called “green chemistry” reagents — ionic liquids — is an urgent oil refining problem.

Systematic studies conducted at the Institute of Petrochemical Processes of the National Academy of Sciences of Azerbaijan showed the possibility of ion-liquid extraction purification of various oil fractions, in particular oil fractions with a viscosity of 6.89 mm^2/s, 8.5 mm^2/s and an oil fraction distillate from a mixture of low-paraffin oils with a viscosity of 18.0 mm^2/s at 100°C, distillate of transformer oil, with a boiling limit of 250-405°C, distillate of hydraulic fluid AMG-10 and etc. [1-5]. The optimal conditions for ion-liquid extraction purification of the above oil distillates of various viscosities are determined.

The IR and NMR spectral analysis was used to determine the group hydrocarbon composition obtained in the process of extraction purification of raffinates.

In our studies, were used as an extractant ionic liquids synthesized based on formic and acetic acids using morpholine, aniline, di-, triethylamine, N-methylpyrrolidon, etc. as the amine component.

The conducted research cycle showed the prospects and effectiveness of ion-liquid extraction purification with obtaining base oils of improved quality, in particular, characterized by an increased viscosity index, improved color, viscosity-temperature indices, and low aromatic hydrocarbon content.

References

1. Azərbaycan Patenti, № a 20070183, 2008.
2. Azərbaycan Patenti. № və 20080044, 12.03. 2008.
3. В.М. Аббасов С.Г. Алиева А.Б.Халилов Г.Д.Гусейнов В.А. Нагиев С.А.Сеидова А.Э.Ализаде Селективная очистка нефтяных фракций с использованием в качестве экстрагента ионной жидкости на основе N-метил-пирролидонацетата Процессы нефтехимии и нефтепереработки, 2018, № 3, с. 302-314.
4. В.А. Нагиев, Г.Дж. Гусейнов, А.Б. Халилов, Р.З. Гасанова, Х.А. Абдуллаева Ионная жидкость N-метилпирролидонацетат в качестве экстрагента в процессах избирательной очистки дистиллята трансформаторного масла Нефтепереработка и Нефтехимия, 2019.
5. А.Б.ХалиловМ.Д. Ибрагимова Г.Дж.Гусейнов В.А.Нагиев С.Г.Алиева и др. Структурно-групповой состав рафината от процесса селективной очистки нефтяной фракции, выделенного из нефти балаханского месторождения. Мир нефтепродуктов. Вестник нефтяных компаний", 2019, № 4, с. 4-9.

Studies of structure and molecular dynamics in block copolymers by means of NMR and related methods

Jacek Jenczyk, Stefan Jurga

NanoBioMedical Centre, Adam Mickiewicz University, Wszechnicy Piastowskiej 3, 61-614 Poznań, Poland
E-mail: cnbm@amu.edu.pl

Block copolymers due to their unique self-assembling properties represent important group among synthetic materials [1-5]. It is well known that below certain critical temperature TODT (order-disorder transition temperature) two or three dissimilar polymer subchains (blocks) become immiscible and tend to separate one from another gathering with similar chemical species accordingly forming domain-like structures. The potential application of various BCPs domains requires a thorough understanding of the system including information concerning e.g. polymer dynamics versus domain architecture, confined crystallization processes, reorientations present within rigid amorphous phase fraction and domain interface thickness. These features were examined using NMR and dielectric spectroscopy techniques as well as other techniques. We combined AFM with NMR spin diffusion experiment to painstakingly monitor BCPs domain architecture together with interfacial space thickness, which is a parameter of greatest importance for nanolithographic design purposes. Moreover, we have shown that fabricated BCPs nanotemplates can be effectively employed in the process of directed nanoparticles assembly. Our results revealed both NPs nanowires formation on top of BCP films and selectively embedded NPs into BCP matrix. We confirm that Directed Self Assembly (DSA) strategy, can successfully rely on thermally reconstructed sapphire substrates, providing a unique platform for BCP's long range assembly. Furthermore, our data reveal the importance of annealing conditions and their impact on BCPs film quality. It has been shown that inappropriate thermal treatment can lead to quasi 2D crystalline forms growth.

References

1. J. Jenczyk, E. Coy, S. Jurga Eur Polym J., 75, 234 (2016).
2. J. Jenczyk, M. Woźniak-Budych, M. Jarek, M. Grzeszkowiak, G. Nowaczyk, S. Jurga., Appl Surf Sci 406, 235 (2017).
3. J. Jenczyk, M. Woźniak-Budych, M. Jarek, S. Jurga.,Eur Polym J 98, 384 (2018).
4. M. Dobies, M. Makrocka-Rydzyk, J. Jenczyk, M. Jarek, R. J. Spontak, S. Jurga., Langmuir 33, 8856 (2017).
5. J. Jenczyk, M. Woźniak-Budych, M. Jancelewicz, M. Jarek, S. Jurga., Polymer 167, 130 (2019).

Parahydrogen-induced polarization in NMR and MRI: the state of the art

Igor V. Koptyug

International Tomography Center SB RAS. Institutskaya 3A, Novosibirsk. 630090, Russia
E-mail: koptyug@tomo.nsc.ru
http://www.tomo.nsc.ru/en/structure/lab/lmrm/

Introduction

Parahydrogen-induced polarization (PHIP), including its most recent variants such as SABRE, is arguably the simplest and technically least demanding hyperpolarization technique which in recent years attracts significant attention of the magnetic resonance community. Since the first unambiguous demonstration of PHIP in 1987 and until 2007, observation of PHIP effects was associated exclusively with homogeneous processes in solution, such as H_2 activation and catalytic hydrogenation of unsaturated compounds by dissolved transition metal complexes. However, during the past decade PHIP (and recently SABRE) effects in liquid and gas phase hydrogenations of alkenes and alkynes have been also demonstrated with numerous heterogeneous hydrogenation catalysts, thus opening the way for the utilization of parahydrogen-based hyperpolarization for the exploration of this broad and important class of functional porous materials. The studies performed to date [1-3] deal with transition metal complexes immobilized on porous solid supports, supported metals, metal oxides, metal sulfides, etc. Further extension to other catalyst types such as single-metal-atom, single-site and/or molecularly defined heterogeneous hydrogenation catalysts was also demonstrated.

Current trends and developments

The ability to produce and observe PHIP effects in heterogeneous catalytic processes (HET-PHIP) significantly expands the range of potential applications of PHIP-derived signal enhancement in NMR and MRI. One of the directions in HET-PHIP research that we currently pursue encompasses mechanistic studies of heterogeneous catalytic transformations of industrial importance which involve H_2 as the key reactant. In addition to heterogeneous hydrogenations, recent demonstrations include catalytic oligomerization and desulfurization processes. Furthermore, utilization of PHIP-derived signal enhancement in MRI can provide new valuable knowledge about the dynamic processes taking place within the pores and voids of the packed catalyst beds in operating reactors. Thus, combining the unique chemical specificity of NMR spectroscopy and the non-invasive nature of MRI with the strong parahydrogen-based signal enhancement can be beneficial for catalytic and chemical engineering applications of magnetic resonance. Representative recent examples of such studies will be discussed.

One very important issue for the use of hyperpolarized NMR and MRI is a relatively fast decay of enhanced signals due to nuclear spin relaxation in hyperpolarized molecular species. This issue becomes even more important when these techniques are used to address porous media, since nuclear spin relaxation times of fluids enclosed in the pore space are normally significantly reduced compared to those of bulk fluids. In addition to the transfer of hydrogen hyperpolarization to heteronuclei, another promising approach relies on the use of the so-called long-lived spin states, e.g., a spin-zero state formed by two spin-1/2 nuclei in a molecule. Such states are produced naturally upon pairwise hydrogenation of a suitable unsaturated substrate with parahydrogen, providing a way to significantly extend the observation time windows while studying porous media using parahydrogen-based hyperpolarization. Combined with the ability of HET-PHIP to produce continuous streams of hyperpolarized liquids and gases, a significant prolongation of hyperpolarization lifetime makes a broader range of porous materials and processes within them accessible using this approach.

Examples of the production and observation of long-lived hyperpolarized spin states generated in HET-PHIP processes will be presented.

Acknowledgements

This work was supported by the grants from RFBR (17-54-33037 and 19-53-12013).

References

1. D. B. Burueva, I. V. Skovpin, V. V. Zhivonitko, O. G. Salnikov, A. S. Romanov, K. V. Kovtunov, I. V. Koptyug. – *Russ. Chem. Bull.,* **66**, 273-281 (2017).
2. K. V. Kovtunov, O. G. Salnikov, V. V. Zhivonitko, I. V. Skovpin, V. I. Bukhtiyarov, I. V. Koptyug. – *Topics in Catalysis*, 5**9**, 1686-1699 (2016).
3. D. B. Burueva, K. V. Kovtunov, A. V. Bukhtiyarov, D. A. Barskiy, I. P. Prosvirin, I. S. Mashkovsky, G. N. Baeva, V. I. Bukhtiyarov, A. Y. Stakheev, I. V. Koptyug. – *Chem. Eur. J.*, **24**, 2547-2553 (2018).

NMR Crystallography as a tool for characterization of active sites of solid catalysts

Olga B. Lapina[a,b], Aleksandr A. Shubin[a,b], Evgeniy Papulovskiy[a], Ilya V. Yakovlev[a,b]

[a]Boreskov Institute of Catalysis, pr. Lavrentieva 5, 630090, Novosibirsk, Russia
[b]Novosibirsk State University, Pirogova 2, 630090, Novosibirsk, Russia
E-mail: olga@catalysis.ru

NMR crystallography combines state-of-the-art high-resolution solid-state NMR experiments with state-of-the-art quantum chemistry calculations thus allowing determining structural and dynamic characteristics in a variety of systems. In this work, we are going to demonstrate different steps of NMR crystallography approaches with an example of supported oxide catalysts. The recent advances in NMR of oxide-based systems are primarily associated with the achievements in NMR spectroscopy of quadrupolar nuclei since the majority of NMR-observable isotopes of elements composing oxide systems possess quadrupole moments. Ultra-high magnetic fields (up to 23.5 T), ultra-high sample spinning (~ 100 kHz), as well as modern electronic components and devices together with *a number of software programs* allowing researchers to extract parameters of chemical shift and nuclear quadrupole interaction tensors, as well as their mutual orientation.

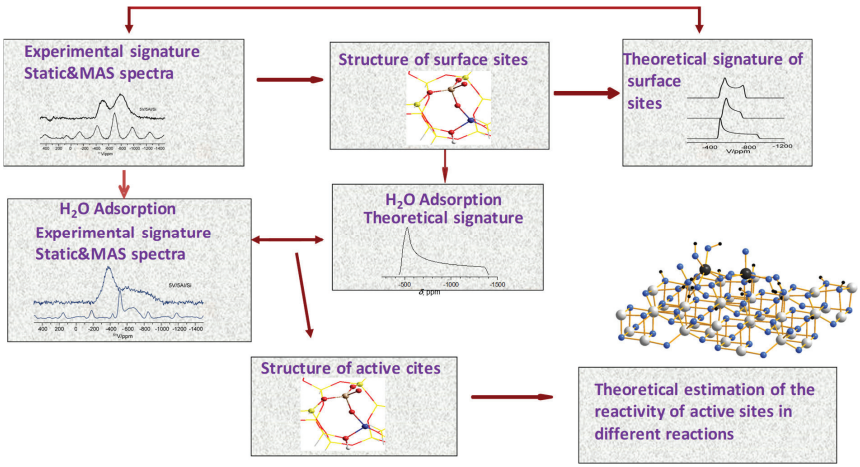

Figure 1. Scheme of NMR crystallography approach for characterization of active sites of solid catalysts

The first step of the study is to test NMR crystallography approach on individual compounds. On the next step, experimental NMR parameters of real catalysts should be determined (experimental signature on Scheme 1). Based on the values obtained in experimental part, several sets of models could be proposed, then for suggested models, NMR parameters should be calculated by DFT (on the Scheme: Theoretical signature of the surface sites). When a good matching between experimental and calculated NMR parameters will be achieved, it possible to conclude that the 3D structure of surface sites is identified (on the Scheme: Structure of surface sites).

It is very important that NMR crystallography in application to catalysts could serve not only for characterization of structure of surface sites, but also for characterization of their

catalytic activity, for this we have to check catalytic activity of different sites by probe molecules both experimentally and theoretically. Thus, the next step sould be connected with adsorption of test molecules (H_2O, CO_2, CH_3OH, etc.) on real catalysts (on the Scheme: Adsorption, Experimental signature) and on model surface sites (on the Scheme: Adsorption, Theoretical signature). At this stage, it is reasonable to use additional experimental techniques (for instance, FTIR). In case of good agreement between experimantal and theoretical parameters, it is possible to determine 3D structures of active sites.

Acknowledgements

The authors thank for partial financial support RFBR17-53-150018 and budget project for Boreskov Institute of Catalysis. The Siberian Supercomputer Centre is gratefully acknowledged for providing supercomputer facilities.

^{63,65}Cu NMR study of doped chalcopyrite $Cu_{1-X}Pd_XFeS_2$ compounds

Vadim L. Matukhin[1], Andrey N. Gavrilenko[1], Ecaterina V. Schmidt[1], Iliya G. Sevastianov[1], Jiri Navratil[2], Pavel Novak[2]

[1]Kazan State Power Engineering University, Krasnoselskaya, 51, Kazan 420066, Russian Federation
[2]Institute of Physics of the Czech Academy of Sciences Cukrovarnicka 10/112, 16200, Praha 6, Czech Republic
E-mail: ang_2000@mail.ru

Introduction

Highly efficient thermoelectric materials have been attracting much attention because of their potential applications, especially for energy harvesting by waste heat. Recently, it has been proposed to use magnetic semiconductors as effective thermoelectrics [1]. One characteristic feature of magnetic semiconductors is the strong coupling between carriers and the spins of magnetic ions. This strong interactions may to a large effective mass of carriers, which can enhance the Seebeck coefficient with good carrier conduction. One of the representatives of this class of compounds is the well-known semiconductor mineral chalcopyrite $CuFeS_2$.

Recent first-principle studies suggested a possible enhancement of thermoelectric properties of this compound, especially by a dilute doping [2, 3]. Therefore, a detailed understanding is necessary for the achievement of highly efficient thermoelectric compounds.

In this work, we present a study of a series of $Cu_{1-X}Pd_XFeS_2$ (x=0-0.02) compounds by ^{63,65}Cu NMR in local field method. Previously, the thermoelectric and transport properties of hot-pressed $Cu_{1-X}Pd_XFeS_2$ (x=0-0.1) sample pellets were studied in [4].

Experiment

Polycrystalline samples with the nominal composition of $Cu_{1-X}Pd_XFeS_2$ (x=0, 0.01, 0.02) were synthesized from a mixture of pure elements obtained from Sigma-Aldrich, including Cu (4 N shots), Pd (4 N powder), Fe (4 N granular) and S (5 powder). The synthesis of the samples is described in Ref. [4].

The spectral parameters of $^{63.65}$Cu NMR in a local field in $CuFeS_2$ were measured on a Tecmag Redstone multi-pulse NQR/NMR spectrometer. Measurement of the NMR line shape was performed using quadrature detection by recording spin echo signals with step-by-step passage of the frequency range and signal accumulation.

Results and discussion

A detailed study of the shape of the resonance lines revealed their asymmetric nature with a more gentle decay in the high-frequency region.

The experimental Cu NMR spectrum of the compounds at 77 K can be considered as a superposition of two Cu NMR spectra: the first spectrum consisting of low-frequency resonance lines assigned to the main phase (blue lines l_1, l_1', c_1, c_1', h_1, h_1' in fig. 1) and the second spectrum consisting of high-frequency lines due to resonance centers located in defective areas of crystalline structure (red lines l_2, l_2', c_2, c_2', h_2, h_2' in fig. 1).

A broadening of the resonance lines may be the result of an increase in the number of defects in the crystal lattice of the compound, leading to a larger spread of EFG on the resonant copper nuclei. The formation of such defects (Fe_{Cu}^{2+} antisite (AS) defects as proposed in [4]) is caused by the formation of the PdS phase in the chalcopyrite matrix, with increasing nominal content of Pd. The frequency shift of the resonance lines can be explained by the Ruderman-Kittel-Kasuya-Yosida (RKKY) interaction [5]. This is supported by the increased conductivity observed for $Cu_{0.98}Pd_{0.02}FeS_2$ sample [4].

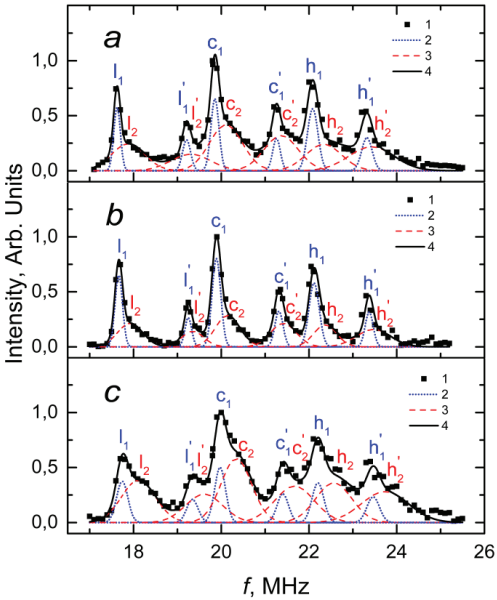

Figure 1. Measured NMR spectra of ^{63,65}Cu in local field at a temperature 77 K of $CuFeS_2$ (a), $Cu_{0.99}Pd_{0.01}FeS_2$ (b) and $Cu_{0.98}Pd_{0.02}FeS_2$ (c) samples. 1 – experimental data, 2 – narrow line (l_1, l_1', c_1, c_1', h_1, h_1'), 3 – wide line (l_2, l_2', c_2, c_2', h_2, h_2'), 4 – cumulative line. The doted (2) and dashed (3) curves indicating the splitting of the each resonance lines (1 or 4) on two pairs of lines are present

Conclusions

The broadening of the NMR resonance lines may be the result of an increase in the number of defects in the crystal lattice of the compound, leading to a larger spread of EFG on the resonant copper nuclei. Such defects can be Fe_{Cu}^{2+} antisite (AS) defects. The formation of such defects is caused by the formation of the PdS phase in the chalcopyrite matrix, with increasing nominal content of Pd. Thus, it was shown that the Cu NMR method in a local field can be used to assess the defectiveness of polycrystals of $Cu_{1-X}Pd_XFeS_2$ (x=0-0.02) compounds.

Acknowledgements

We are grateful for the financial support from the Czech Science Foundation, Project No18-12761S.

References

1. N. Tsujii. – *J. Electron. Mater.,* **42**, 1974 (2013).
2. H. Takaki, K. Kobayashi, M. Shimono, N. Kobayashi, K. Hirose, N. Tsujii, and T. Mori. – *Mater. Today Phys*., **3**, 85 (2017).
3. H. Takaki, K. Kobayashi, M. Shimono, N. Kobayashi, K. Hirose, N. Tsujii, and T. Mori. – *Appl. Phys. Lett*., **110**, 072107 (2017).
4. J. Navratil, J. Kasparova, T. Plechacek, L. Benes, Z. Olmrova-Zmrhalova, V. Kucek, and C. Drasar. – *J. Electron. Mater*., **48,** (2019).
5. T. Koyama, M. Matsumoto, S. Wada, Y. Muro and M. Ishikawa. – *J. Phys. Soc. Jap.,* **70**, 3667 (2001).

Nuclear spin relaxation of water and other small molecules sorbed on solid interfaces

Dieter Michel

Leipzig University, Faculty of Physics and Geosciences, Linnéstrasse 5, D-04103 Leipzig

The lecture mainly deals in the beginning with proton spin relaxation studies on water molecules sorbed on the surfaces of highly porous very pure silica gel and in well-structured materials of zeolites and metal organic frameworks (MOFs). The work is based on previous studies which have enabled an unambiguous interpretation of the complex proton relaxation behaviour. The problem was to separate the (sometimes dominant) influence of interactions with paramagnetic species (e.g. present as impurities). The aim of this contribution is to present a clear experimental evidence for the time scales of the local motions of the adsorbed water molecules. The NMR studies includes the influence of confinement, the dynamic behaviour of protons in structural hydroxyl groups and the exchange of the protons between neighbouring adsorbed water molecules. The proton spin relaxation rates are studied over a wide range of temperatures. The studies enabled a differentiation of various types of adsorbed water molecules with different mobilities. The measurements allow to characterize the exchange between them and the role of slower dynamic processes like proton exchange processes with structural hydroxyl groups. Moreover, infrared measurements of fundamental and higher harmonic vibrations are presented to differentiate between water molecules and structural hydroxyl groups. It will be shown that water molecules sorbed in MOFs are so strongly adsorbed within the pores that the exchange dynamics can no more be observed in the NMR measurements which were run in a wide range of temperature.

Moreover, extensive nitrogen-15 NMR studies of NO and carbon-13 NMR studies of CO and CO_2 sorbed in MOFs are carried out over a wide temperature range. In these measurements the nitrogen oxides NO and the carbon ones CO_x are highly enriched with nitrogen-15 and/or carbon-13 isotopes to ensure a sufficient signal-to-noise ratio. It will be pointed out the results of NMR studies (and also the EPR studies) of adsorbed NO molecules very strongly differ from those in the gaseous phase. Because nitric oxide molecules are of particular interest due to their broad biological-medical applications, a deeper understanding of the different behavior is necessary. From the physical point of view, NO molecules in the gaseous phase reveal interesting coupling phenomena between the electron spin, the orbital angular momentum, and the angular momentum. These particular properties are related to the free rotation of the NO molecules. Moreover, NO molecules are very interesting because they possess an unpaired electron. Studies by means of EPR are very suitable in this range. In the liquid phase the NO molecules show the tendency to form NO-NO dimers which are diamagnetic and thus detectable by means of nitrogen-15 NMR. Thus, studies of the interesting physical properties of NO molecules are accessible both on the basis of EPR und NMR studies. By means of EPR detailed studies of the behaviour of NO molecules in the gaseous phase, above the boiling point at 120 K, may be carried out. In this temperature range the EPR the spectra allow a detailed study of the coupling phenomena between the angular momentum due to the free rotation of the molecules and the spin and orbital momenta. Hence, by means of EPR the adsorption-desorption equilibrium of NO molecules can be studied in detail. 15N NMR measurements on NO molecules in the temperature range above the boiling temperature molecules are not possible because of the presence of the strong magnetic paramagnetic momenta of NO. Thus it becomes obvious that ^{15}N NMR measurements of highly ^{15}N enriched NO molecules can be only carried out in a certain temperature region of the liquid phase of NO and for solid NO. In summary, the extensive EPR and NMR studies performed will lead to a deeper understanding on the behaviour of the interesting NO species.

Magnetic nuclear hyperpolarization and alternative approaches for MRI signal amplification

Yury A. Pirogov

Faculty of Phyics, M. V. Lomonosov Moscow State University, Moscow, Russian Federation
E-mail: yupi937@gmail.com

Introduction

Magnetic resonance imaging in its current form was invented only 40 years ago and in 2003 was acknowledged by the Nobel Prize in medicine awarded to Paul Lauterbur (Stony Brook University, New-York, USA) and Peter Mansfield (Nottingham University, UK). In fact, the first proposal to use NMR for magnetic resonance visualization was made by a young officer of the Soviet Army Vladislav Ivanov 13 years before them. Unfortunately, the Moscow Patent Institute declined his patent at that time and only approved it in 1986, when MRI scanners were already in use in many clinics all over the world. Currently, no diagnosis of a serious health problem can be done without MRI diagnostics. The technology is very informative, especially when applied to the soft tissues of living organism (humans and animals). However a level of NMR signals forming the MRI image is quite low, and to increase the signal-to-noise ratio special methods of NMR response accumulation and digital processing of the images are used. As a consequence, acquiring a good quality image can take long time. The signal magnitude depends on the difference in population of the main level and of the excited level, where the nuclei of the magnetized ensemble are located after being excited by the radio-frequency radiation.

MRI hyperpolarization

At room temperature, mentioned difference in population is very low, hence the low level of polarization in the ensemble. However, with the help of special hyper-polarization approaches, the polarization, along with the NMR signal, can be increased 5-6 orders of magnitude (up to a million times). This would dramatically improve the characteristics of the MRI signal, namely shorten the analysis time, improve spatial resolution and enhance image contrast. This methodology was first developed at the Sir Peter Mansfield MRI Centre of the Nottingham University, UK. It allowed to accomplish a very important task of visualizing the respiratory organs and internal structure of the lungs, that was not possible before due to low quantity of protons in lungs that are tracked by regular medical MRI scanners. The group implemented the laser polarization of nuclei of noble gases (xenon, krypton, helium), the inhalation of which produces a substantial response, when MRI scanner is tuned to the Larmor frequency of the hyperpolarized gas [1].

Multinuclear investigations

Later, the need arose to detect the areas of localization of medications injected into the body and containing, for instance, carbon C13 atoms or silicon Si29 atoms [2, 3]. For that, a method of dynamic nuclear polarization (DNP) at super-low (sub-helium) temperatures was developed combined with microwave pumping of electron assembly at the EPR frequency with subsequent transfer of electron magnetization to the polarized nuclei. It is extremely expensive procedure characterized by a very fast loss of hyperpolarized state of the substance during its unfreezing and injection into the body. Nevertheless, because the signal from partially depolarized nuclei is still much stronger than from regular nuclei, the bright and distinct images of tissues containing hyperpolarized substances can be obtained very fast, during tens of seconds. Thus, the difficulties of the PND method of creating hyperpolarized state are justifiable, when such hyperpolarized substances allow for visualization that cannot be achieved by regular means.

Hyperpolarization of Si29 micro-particles

This method is still under development and recently has demonstrated a truly breakthrough result: polymer-coated silicon-29 micro-particles that underwent the DNP procedure were able to keep their hyperpolarized state at room temperature for up to half an hour [4]. Now, the use of hyperpolarized Si29 particles as an independent medication or as a bio-container allows visualizing reliably their location within the body. The delayed relaxation of hyper-polarized Si29 particles is based on the multi-step process of the magnetized state diffusion from the surface layers of the micro-particle to its inner parts during magnetization and on the similar reverse multi-step diffusion of depolarization after de-freezing of the particles. There are three main steps in this process. After placing micro-particles into 1-2 T magnetic field and irradiating them with microwaves at 80-90 GHz frequencies, quasi-free electrons on the surface defects of silicon under polymer coating are being polarized due to EPR phenomenon and then transfer their magnetization to upper layers of the Si29 nuclei through the electron-nuclear Overhauser effect. In their turn, magnetization of hyper-polarized surface layers of Si29 is transferred to deeper layers through the nuclear-nuclear Overhauser effect and so on, until full hyperpolarized state is reached. This process of magnetization diffusion from the outer layers of silicon particles to their innermost parts takes 10-20 hours, whereas the reverse diffusion of de-magnetization from external layers to the center goes much faster – during half an hour, which is quite enough for medical procedures. Hyper-polarization approaches allow for express-visualization of newly formed pathological growths with targeted delivery of hyperpolarized substance into the area of pathology and for creation of sharp MRI images even with very low magnetic fields.

Visualization with F19 MRI

However hyperpolarized technologies are very expensive and labor-intensive, requiring special cryogenic infrastructure in combination with microwave and laser systems. Therefore, there is a need for alternative approaches to the enhancement of MRI visualization, without the use of hyperpolarized procedures. One of them is application of fluorine-containing substances that produce a high-intensity signal at the Larmor frequency of fluorine-19 (F19). The operation of MRI scanner at the fluorine frequency is functionally close to proton MRI visualization, because the Larmor frequency of fluorine nuclei differs only by 5% from the one of protons. This fact allows for tuning of standard reception-transmission coils of medical MRI scanners to the frequency of fluorine-19, the natural content of which is 100%, i.e. even better than for hydrogen. Special advantage of the medical diagnostics based on fluorine nuclei is almost complete absence of such nuclei in animal and human tissues: the NMR signal from the injected F19 nuclei will be seen on zero background from tissues free from the substance. This advantage of fluorine-based methods compared to hyperpolarization techniques is most prominent in visualizing hollow body structures such as lungs or gastrointestinal tract [5, 6]. Filling lungs with fluorine gas provides sharp image of internal structure of respiratory organs and allows for detection of pathological morphology on the lungs walls. Injection of specially synthesized fluorine-containing fluids can also significantly enhance the contrast of MRI images.

Acknowledgements

Mentioned works with F19 MRI visualization were performed on the equipment of the MSU collective-use center and unique complex of devices "Biospectrotomography" with support of RFBR grant No. 19-29-10015.

References

1. Super-MRI // Presentations of the Russian-British Workshop on MRI hyperpolarization / Ed. Yu. Pirogov and A. Makurenkov.- M.: MSU, 2018, 117. http://hp-mri-workshop.com/.

2. Yu. A. Pirogov *Physics procedia* 2016, **82**, 3. doi: 10.1016/j.phpro.2016.05.002.
3. N. V. Anisimov, *et al*. *Biomed. Radio Electron.* 2019, No.2, 38. doi: 10.18127/j15604136-201902-04.
4. M. Cassidy, *et al. Nature Nanotechnology* 2013. **8**. 363-8. doi:10.1038/nnano.2013.65.
5. O. S. Pavlova, *et al. Radio Electron. J.* 2018, No.11. doi 10.30898/1684-1719.2018.11.16.
6. D. V. Volkov, *et al. // Appl. Magn. Res.* 2018, 49, No.1. 71-75. doi: 10.1007/s00723-017-0934-5.

The effect of Zn impurity on the rlectric field gradient on La nuclei in the $La_2Cu_{1-x}ZnxO_4$ system

Yu. Plotnikova, A. Frolov, D. Kitanin, A. I. Pogoreltsev

Kazan State Power Engineering University, Kazan, Russia
E-mails: kozyr_j@list.ru, kitanin7235@gmail.com, darkmay34@gmail.com

Introduction

Zinc is one of the active dopants, despite the fact that its ions have a $3d^{10}$ configuration, i.e. non-magnetic. It was experimentally established that the doping of the La_2CuO_4 system with zinc causes a noticeable decrease in the Néel temperature [1, 2]. A study of the $La_2Cu_{1-x}ZnxO_4$ system by NQR on ^{139}La nuclei revealed a noticeable broadening of the spectral lines, as well as a definite tendency toward an increase in the quadrupole frequency in comparison with the "pure" La_2CuO_4.

Research results

In this work, we studied the electron density distribution in the $La_2Cu_{1-x}ZnxO_4$ system. The frequency of the onset of the phase transition for the $La_2Cu_{0.9}Zn_{0.1}O_4$ system, which is 12.7 MHz, was used as a "support". The parameters of the electric field gradient (EFG) on the La core were estimated using the cluster method - we used the $La_{10}Cu_4ZnO_{29}^n$ cluster (n is the cluster charge that needs to be selected) - Figure 1.

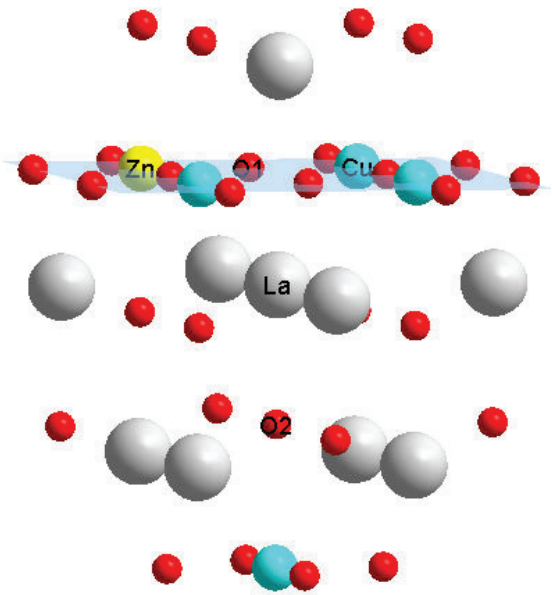

Figure 1. Cluster $La_{10}Cu_4ZnO_{29}^n$

The Zn atom replaced the Cu atom in the copper-oxygen plane (see Fig. 1). The EFG estimates on ^{139}La nuclei were performed within the framework of the self-consistent open-shell Hartree – Fock method (SCF-LCAO-ROHF) (the Firefly program was used [3]).

The cluster charge varied in the range from -10 to 10. The frequencies for the 5/2 - 3/2 transition were obtained by solving the corresponding secular equation. The best agreement with experiment was obtained for n = 4 (ROHF MIDI basis). In this case, the quadrupole frequency is ν_Q = 12.7072 MHz, and the asymmetry parameter is η = 0.0049. It was also found that for all n frequencies ν_Q of the doped Zn compound is slightly higher than for pure La_2CuO_4. For the $La_{10}Cu_4ZnO_{29}^4$ cluster, the electron density distribution was constructed using the theory of R. Bader [4]. Based on the analysis of the electron density distribution maps, it can be assumed that, when doping lanthanum cuprate with Zn atoms, a noticeable redistribution of electron density occurs due to the pulling of electrons along the Zn-O bond line, which, ultimately, leads to the observed change in the electric field EFG on lanthanum nuclei.

References

1. Nowik I.,Lichti R.L.,Cooke D.W.,Boekema C. // Sol.St.Comm., 1990,v.74,p.957
2. Pogoreltsev A.I., Anashkin V.N., Matukhin V.L., Kukovitsky E.F., Safin I.A. // Letters to ZhETF, 1995, v.62, p.552Granovsky A. A. Firefly version 8.2.
3. http://classic.chem.msu.su/gran/firefly/index.html
4. R.F.W. Bader, Atoms in Molecules - A Quantum Theory, Oxford University Press, Oxford, 1990. ISBN: 0198558651.

Development of cost-effective approaches for MW and NMR detection of threat liquids in security checkpoints

B. Rameev

[1]*Department of Physics, Gebze Technical University, 41400, Gebze-Kocaeli, Turkey*
[2]*Zavoisky Physical-Technical Institute, FRC Kazan Scientific Center of RAS, 420029 Kazan/Tatarstan, Russian Federation*
E-mail: rameev@gyte.edu.tr

Introduction

Fast and effective discrimination between various threat and benign liquids is an issue of extreme importance for public safety in objects of transportation and other infrastructure [1-4]. An ideal security scanner device is expected to be based on the reliable and low-cost detection techniques in a typical scenario of the airport security checkpoint, which means a need to discriminate between a rather large cluster of *threat* liquids and a huge group of *benign* liquids. In this work, we discuss the concept for the technical implementation of a scanning device based on the combined use of two techniques: 1) time-domain nuclear magnetic resonance (TD NMR) technique and 2) probing of dielectric permittivity of liquids in the microwave range of frequencies. The first efforts on application of TD NMR for the detection of dangerous liquids have been done almost 30 years ago [1, 5]. Typically, the spin-lattice relaxation time (T_1) and the spin-spin relaxation time (T_2) are used to separate between various groups of liquids (see, e.g. [1-6]). In some cases, the diffusion constant (D) is also measured [7-9] as additional discrimination parameter. Unfortunately, classical methods of TD NMR, usually applied for T_1 or D measurements, cannot be directly used in the scanning devices due to unacceptably long times of these measurements (from several minutes to hours, typically). For successful implementation of TD NMR in a practical device the total time of measurements should be at most several seconds. On the other hand, microwave (MW) technique, based on measurements of parameters related to the complex dielectric permittivity, has an important advantage to be very fast technique, which potentially can be also easily integrated with the TD NMR in a combined detection device [10]. In our work, some aspects of the practical application of ^{1}H TD NMR for fast scanning of liquids have been presented. Approaches for the technical realization of MW technique with the use of resonance sensors tuned at various probing frequencies as well as the possibilities for the combination of the MW approach with TD NMR in a single device have also been discussed.

Experimental procedures

In our experiments with TD NMR, a model setup, consisting of *Magritek KEA-2* NMR console, a home-made permanent magnet system with the distance between the poles of 65 mm and a gradiometric RF probe have been used. For the details of the magnet and the RF probe, see another work presented at this Spinus-2020 conference [11]. The magnetic field of the magnet was about 206 mT that corresponds to ^{1}H resonance frequency of about 8.7 MHz. Carr-Purcell-Meiboom-Gill (CPMG) pulse sequence was applied to obtain T_2 relaxation times, while inversion/saturation recovery protocol was used to measure T_1 relaxation time.

For the demonstration of possibilities of the MW detection technique, low-cost electronic components have been used to minimize the cost of the whole device and to promote its commercial implementation. These are: Signal Hound scalar network analyzer and tracking generator boards, Minicurcuits relay switches, Arduino UNO Microcontroller and home-made microstrip resonators (see the details in work [12]). A user-interface software for signal acquisition and processing have also been developed and tested with the use of PET bottles with various liquids. Both in NMR and MW detection measurements the 0.25 L PET bottles filled with various liquids have been used.

TD NMR for detection of threat liquids

During our previous studies on NMR for detection of liquids, we measured a large number of various dangerous and benign liquids [7-9]. Approximately 10 potentially dangerous liquids (precursors for explosives or flammable solvents) have been measured. It has been concluded that NMR measurements of three parameters ($T_1 - T_2 - D$) instead of one or two parameters increase much the reliability of liquid discrimination in security scans.

However, there is an important issue with respect to the classical NMR sequences: too long time needed to measure the T_1 relaxation time or the diffusion constant. Therefore, shortening the total measurement time is a critical issue in TD NMR detection. One of the possible ways is the application of ^{14}N NMR because the acquisition time of the ^{14}N NMR signal is much shorter [13]. An important advantage of the nitrogen NMR is that the mere fact of detection of ^{14}N NMR signal indicates the threat! It should be noted, however, that in any case the ^{1}H TD NMR technique should be used in parallel to ^{14}N to detect some precursors (e.g. hydrogen peroxide). Therefore, it is clear that the smart protocol of identification should start from measuring of only one (^{1}H T_2) or two parameters (e.g. ^{1}H T_2 + ^{14}N T_2 or ^{1}H T_2 + dielectric permittivity) and proceed with measurements of other variables (diffusion constant, ^{1}H T_1 relaxation time, etc.) if needed. From the practical point of view, there is an important problem that the magnetic field profile of the permanent magnet system of the bottle scanner is not uniform over a volume of a scanned bottle (several hundreds of ppm for a sphere with an outer diameter of 1-2 cm is a typical value in the TD NMR). Therefore, TD NMR device should not aim to measure accurate values of T_1 and T_2 relaxation constants but to probe some effective values instead. The TD NMR scanner should also rely on “open” design giving a possibility of attaching additional MW sensors and easy access from various directions. Besides, the planar RF probes for the distant detection only a (small) part of bottle volume have to be used.

MW technique for detection of threat liquids

MW technique, which probes the complex dielectric permittivity, has a potential advantage of easy integration with the TD NMR in a single detection device. We successfully constructed a prototype of a standalone table-top MW detection device (without NMR scanning) to scan bottle with liquids [12]. The device is based on an approach, which involves a combination of several sensors for various frequencies to measure the MW parameters as a function of probing distance. In this manner, the measured parameters are not affected by variations in the distance between a sensor and a scanned bottle. Various hardware components have been tested and finally, the most optimal configuration has been used to assemble the device prototype. Special accent has been made on the use of low-cost MW electronic components and units in order to develop a cost-effective solution for commercial implementation. A set of three home-made microstrip sensors for frequencies between 1–4GHz have been used to probe the permittivities of the same set of liquids as probed in NMR. User-interface software has been developed for both signal acquisition and effective approximation of the frequency-dependent transmittance curves of the resonance probes. Furthermore, a special algorithm for MW signal processing which obtains the Q factor as well as the resonance frequency of the resonance probes has been designed. An automatic algorithm of classification of the tested liquids by MW technique has been tested as well. Further work is planned for combining of the TD NMR and MW technique in a single bottle scanning device.

Conclusions

In this work, we discussed some possible approaches for the technical realization of time-domain NMR as well as of microwave detection technique for fast scanning of liquids. Possible protocols of the fast TD ^{1}H NMR measurements and combined use of ^{1}H together ^{14}N NMR have been proposed. A low-cost model device for MW detection of liquids with the use of resonance sensors tuned at various frequencies between 1 and 4 GHz has been developed.

Acknowledgements

The work was supported by NATO Science for Peace and Security Programme (NATO SPS grant No. 985005 [G5005]). The author acknowledges all participants of the project and expresses special thanks to S.Tarapov, İ. Ünal, B.Çolak, G.Mozzhukhin, M.Vafadar, S.Polevoy, A.Maraşlı, S.Mamadazizov.

References

1. L. J. Burnett, Liquid explosives detection, SPIE Vol. 2092 Substance Detection Systems (1993) 208-216.
2. Fraissard J., Lapina O., eds.: Explosives Detection using Magnetic and Nuclear Resonance Techniques, NATO Science for Peace and Security Series B: Physics and Biophysics. Dordrecht, Netherlands: Springer, 2009.
3. Rameev B.Z., Mozzhukhin G.V., Aktas B., eds.: Magnetic Resonance Detection of Explosives and Illicit Materials, Appl. Magn. Reson. 43, no. 4, 463-467 (2012).
4. Apih T., Rameev B., Mozzhukhin G., Barras J., eds.: Explosives Detection using Magnetic and Nuclear Resonance Techniques, NATO Science for Peace and Security Series B: Physics and Biophysics, Dordrecht, Netherlands: Springer, 2014.
5. S. Kumar, W.C.McMichael, Y.-W. Kim, A.G. Sheldon, E. E. Magnuson, L. Ficke, T. K. Chhoa, C. R. Moeller, G. A. Barrall, L. J. Burnett, P.V. Czipott, J. S. Pence, D. C. Skvoretz, Screening sealed bottles for liquid explosives, Proceedings of SPIE Vol. 2934 (1997)126-137.
6. J. Mauler, E. Danieli, F. Casanova, B. Blimich, In: Explosives Detection using Magnetic and Nuclear Resonance Techniques. NATO Science for Peace and Security Series B: Physics and Biophysics. J. Fraissard; O.Lapina,(Eds.). Pp.193-203 (2009)
7. B. Rameev, G.V. Mozzhukhin, R.Khusnutdinov, B.Aktas, A. Konov, N.A. Krylatyh, Ya.V. Fattakhov, D.D. Gabidullin, K.M. Salikhov, SPIE Proceeding. DSS12 - SPIE Defense, Security, and Sensing, 8357 - 33 V. 1, 83570Z (2012).
8. A.B. Konov, K.M. Salikhov, E.L. Vavilova, B.Z. Rameev, Multiparameter NMR Identification of Liquid Substances, in NATO book “Magnetic Resonance Detection of Explosives and Illicit Materials", NATO Science for Peace and Security Series - B: Physics and Biophysics, Eds: Tomaz Apih, Bulat Rameev, Georgy Mozzhukhin, and Jamie Barras Springer, 2013, pp.111-122.
9. N.A. Krylatykh,Y.V. Fattakhov, A.R. Fakhrutdinov, V.N. Anashkin, V.A. Shagalov, R.Sh. Khabipov, Detection of Explosive Precursors Using Low-Field Magnetic Resonance Imaging, Appl. Magn. Reson., 47, 8, 2016 pp. 915-924.
10. B. Rameev, Magnetic Resonance and Microwave Techniques for Security Applications, 2019 PhotonIcs & Electromagnetics Research Symposium-Spring (PIERS-Spring, 17-20 June, 2019, Roma, Italy), IEEE, 2019, pp. 3997-4000; DOI: 10.1109/PIERS-Spring46901.2019.9017563.
11. G. V. Mozzhukhin, G. S. Kupriyanova, S. Mamadazizov, A. Maraşlı, B. Z. Rameev. 1H NMR detection of liquids in bottles with use of surface coils. Proceedings of 17th International School-Conference: Magnetic resonance and its applications (Spinus 2020), St. Petersburg, Russia, March 29 - April 3, 2020.
12. M. Vafadar Yengejeh, S. Mamadazizov, B. Çolak, B. Rameev. Development of Multifrequency MW Detection Device to Scan Liquids in Security Checkpoints. 2019 PhotonIcs & Electromagnetics Research Symposium-Spring (PIERS-Spring, 17-20 June, 2019, Roma, Italy), IEEE, 2019, pp. 3974-3977; DOI: 10.1109/PIERS-Spring46901.2019.9017237.
13. G.V. Mozzhukhin, G.V. Kupriyanova, S.Sh. Mamadazizov, A. Maraşlı, B.Z. Rameev, Low-field 14N nuclear magnetic resonance for detection of dangerous liquids, Chem. Phys. 513 (2018) 129-134. https://doi.org/10.1016/j.chemphys.2018.07.032

NMR methodologies, novel chiral auxiliaries and water compatible weak chiral aligning media for enantiomeric discrimination

N. Suryaprakash

NMR Research Centre, Indian Institute of Science, Bangalore 560012, India
Tel: +91 9845124802; +9180 23607344; Fax: +9180 23601550
E-mail: nsp@sif.iisc.ernet.in
http://nrc.iisc.ernet.in/nsp/

NMR spectroscopy is intrinsically blind to distinguish enantiomers in achiral media and demands the conversion of substrates to diastereomers utilizing the chiral auxiliaries, which are functional group specific. Instead of utilizing the chemical shift as the only NMR parameter for discrimination, aligning the chiral molecules in the weakly ordered liquid crystalline medium provides access to number of order parameter dependent anisotropic parameters, enabling the discrimination of enantiomers and the measurement of their composition. The ^{1}H NMR spectra of doped molecules exhibit complex multiplicity pattern due to number of pairwise interaction of dipolar coupled spins, small chemical shift dispersion and the superposition of spectra of different enantiomers. These inherent challenges have been addressed by the discovery of water compatible weakly ordered chiral aligning medium, with physical parameter dependent tunability of its degree of order, sustainability of the mesophase over a broad range of temperature and the concentration of ingredients. In addition the appropriate new NMR techniques have also been developed to simplify the spectral complexity, unravel the spectra of enantiomers and facile extraction of spectral parameters.

Orchestrated approaches for combating the challenging problems of NMR spectroscopy

N. Suryaprakash

NMR Research Centre, Indian Institute of Science, Bangalore 560012, India
Tel: +918022933300, +918023607344, +919845124802
E-mail: nsp@sif.iisc.ernet.in
http://nrc.iisc.ernet.in/nsp/

We have developed fast data acquisition experiments to enhance the sensitivity of detection of NMR signals and for the extraction of structurally important NMR parameters from the complex NMR spectra in an orchestrated manner. The techniques cited as CLEAN-G-SERF and PS-CLEAN-G-SERF circumvents the problem of evolution of zero frequency peaks and prevents evolution of unwanted couplings. For enhancing the sensitivity of NMR signals in the gradient based slice selective experiments the polarization sharing technique is utilized to transfer polarization from unutilized protons to selectively excited protons. This facilitates rapid data acquisition without any customary inter-scan relaxation delay, resulting in nearly 2-fold sensitivity enhancement per unit time. For deriving the homonuclear scalar couplings, a one dimensional experiment cited QG-SERF has been designed which provides multiple scalar couplings information from a single experiment. In another developed 1D NMR technique, HF-QG-SERF, based on real time spin edition, the significant simplification of the spectrum is derived which permits straightforward determination of all the possible $^{n}J_{HF}$ values of a chosen fluorine. The sequence removes all J_{HF} and J_{HH} while retaining only $^{n}J_{HF}$ of a chosen fluorine thereby permitting the easy extraction of the coupling information. The results of our new methodological developments will be discussed.

Enhanced nuclear magnetic resonance in magnetically concentrated and dilute solids

M. S. Tagirov

Kazan Federal University, 420008, Kazan, Russian Federation

Van Vleck (VV) or polarization paramagnets comprise a rather wide class of solid-state magnets that has been studied for a long time since the pioneering work of M. M. Zaripov in 1955. Van Vleck paramagnetism is as universal a magnetic property of solids as diamagnetism. It is caused by the elastic deformation of the electron shell of an atom or ion by an external magnetic field, giving rise to an induced magnetic moment. Thus, unlike orientational paramagnetism, where already-formed magnetic moments of atoms or ion sure ordered in a magnetic field, Van Vleck paramagnetism is of a polarization nature. The static magnetic susceptibility of these magnets obeys a Curie law at high temperatures and becomes constant at low temperatures. The quantum-mechanical theory developed by Van Vleck explains this behavior of the magnetic susceptibility by the absence of a magnetic moment in the ground state of the ion the electronic ground state is either a singlet or a nonmagnetic doublet and the appearance of a contribution to the susceptibility due to virtual transitions induced by the Zeeman interaction with the external magnetic field between the ground and excited states of the ion. The Van Vleck paramagnetism most often occurs in crystals containing non-Kramer's rare-earth (RE) ions, i.e., RE ions with an even number of electrons in the unfilled 4-*f* shells (e.g., Pr^{3+}, Eu^{3+}, Tb^{3+}, Ho^{3+}, Tm^{3+}), where the crystalline electric field lifts the degeneracy of the ground multiplet, leading to typical splitting of the Stark structure of the order of 10-100 cm^{-1}.

All magnetically concentrated dielectric Van Vleck paramagnets was intensively investigated by using enhanced nuclear magnetic resonance during more than 65 years mainly in Kazan University as well as in Oxford University. Main problem of spectroscopy and spin kinetics were already solved. At the same time in dilute compounds such experiments was not reliable because of weak signal. Only in last days due to the digital self made experimental set up it became possible to observe and investigate magnetically diluted VV paramagnets. At report it will present a new result in such compound and its will compared with magnetically concentrated VV paramagnets.

This work was financially supported by the Russian Science Foundation (grant RFBR 18-42-160012).

Fluxional hydrogen-bonded complexes involving POOH groups: structure and dynamics revealed by ^{1}H and ^{31}P NMR

Peter M. Tolstoy[1], Valeria V. Mulloyarova[1], Ivan S. Giba[1], Alexei S. Ostras[1], Mikhail A. Kostin[2], Svetlana A. Pylaeva[3]

[1]Institute of Chemistry, St. Petersburg State University, St. Petersburg, Russia
[2]Department of Physics, St. Petersburg State University, St. Petersburg, Russia
[3]Department of Chemistry, Padeborn Uniersity, Padeborn, Germany
E-mail: peter.tolstoy@spbu.ru

Introduction

Phosphorous acids – phosphinic R_2POOH, phosphoric $(RO)_2POOH$ and phosphonic $RPO(OH)_2$ ones – have both proton-donating group POH and proton-accepting group P=O, thus being able to form various hydrogen-bonded self-associates. While the complexation motifs are relatively well studied in the gas phase and in crystals, where exclusively cyclic dimers and infinite chains are formed (Fig. 1) [1, 2], the case of self-association in aprotic solutions (and soft matter in general) turned out to be quite challenging.

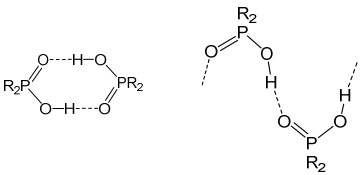

Figure 1. Schematic structure of cyclic dimers and infinite chains formed by R_2POOH acids

Fortunately, in the case of POOH-containing acids, apart of the bridging proton itself, there is always another sensitive NMR nucleus in the proximity of the hydrogen bridge, namely, ^{31}P, thus making such systems well suited for an NMR investigation. In this presentation we showcase the usage of low-temperature ^{1}H and ^{31}P NMR for the elucidation of the complexes' structure and dynamics.

Model systems and the main goal

Over the last two years we have investigated self-associates and mixed complexes formed by a number of phosphinic (Fig. 2a), phosphoric (Fig. 2b) and, recently, phosphonic acids (Fig. 2c) [3, 4].

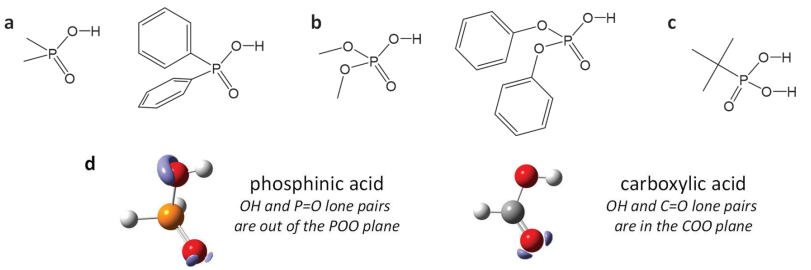

Figure 2. (a)-(c) Schematic structures of POOH-containing acids studied in this work; (d) comparison of orientations of OH groups and lone pairs in sp^2 hybridized oxygen atoms in model phosphinic and carboxylic acid

The structures of associates formed by the abovementioned molecules in aprotic media are strongly influenced by the orientation of OH groups and oxygen's lone pairs in P=O groups with respect to the POO plane, as shown in Fig. 2d for model acid H_2POOH in comparison with a model carboxylic acid HCOOH.

The main goal of this work is to study the conformational manifold of self-associates and mixed complexes which could be formed between the molecules such as shown in Fig. 2a-c. Our main questions deal with the solution of the reverse spectroscopic problem: could the stoichiometry and the structure of a complex be derived from the experimental ^{1}H and ^{31}P NMR spectra? Which conformational motions are still present in the complex even at low temperatures? How these motions manifest themselves in NMR spectra? What limits the diagnostic value of ^{31}P NMR spectroscopy of such systems?

Methodology

The observation of intrinsic (not averaged) NMR parameters of complexes having different stoichiometry and isotopic composition requires the proton and molecular exchanges to be slow in the NMR time scale. The increase of the complex's life time in solution is usually achieved by lowering down the temperature of the sample. For the investigation of self-association of POOH-containing acids we have used the mixture of liquefied freonic gases CDF_3/CDF_2Cl as a solvent, which allowed us to record ^{1}H and ^{31}P NMR spectra at temperatures as low as 100 K. Such solvent exhibits relatively good solubility of organic compounds and remain non-viscous practically down to its freezing temperature. In Fig. 3 as an example we show ^{1}H, ^{13}C and ^{19}F NMR spectra of the solvent, recorded at 140 K.

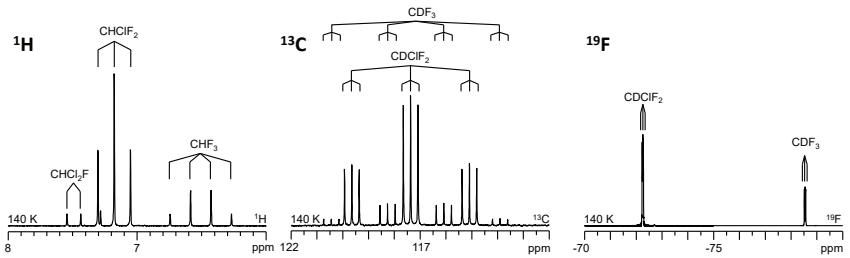

Figure 3. ^{1}H, ^{13}C and ^{19}F NMR spectra of the low-freezing solvent mixture used in this work

Another important stratagem used for this investigation is the usage of partial H/D substitution in mobile proton sites. For the majority of hydrogen bonds, when the bridging proton is substituted by a deuteron, the bond lengthens, *i.e.* the heavy atom distance increases. For complexes with several mutually influencing hydrogen bonds this means that when one of the hydrogen bonds is deuterated the geometry of the remaining (not deuterated) hydrogen bonds changes as well, which is observed as a change in corresponding ^{1}H NMR chemical shifts, the phenomenon which is called "vicinal H/D isotope effects". The two coupling schemes – cooperative or anti-cooperative coupling – manifest themselves by opposite signs of vicinal isotope effects, thus allowing one to elucidate the coupling scheme within a complex.

Example of the results

To demonstrate the complexity of the complexation equilibria present in the solution as well as the complexity of hydrogen bond interactions within each complex, in Fig. 4 we show as an example the low-field part of ^{1}H NMR spectrum of the sample containing approximately equal amounts of partially deuterated acids $(PhO)_2POOL$ and $(MeO)_2POOL$ (L = H, D). Signals of complexes with different stoichiometry could be seen, each split into several signals

stemming from individual isotopologs of the corresponding complex. By analyzing such spectra we have established the co-existence of cyclic dimers, cyclic trimers and in some cases even cyclic tetramers of POOH-containing acids in solution, as well as the presence of several conformational motions: puckering motion within each hydrogen bond cycle and double(triple) proton transfers.

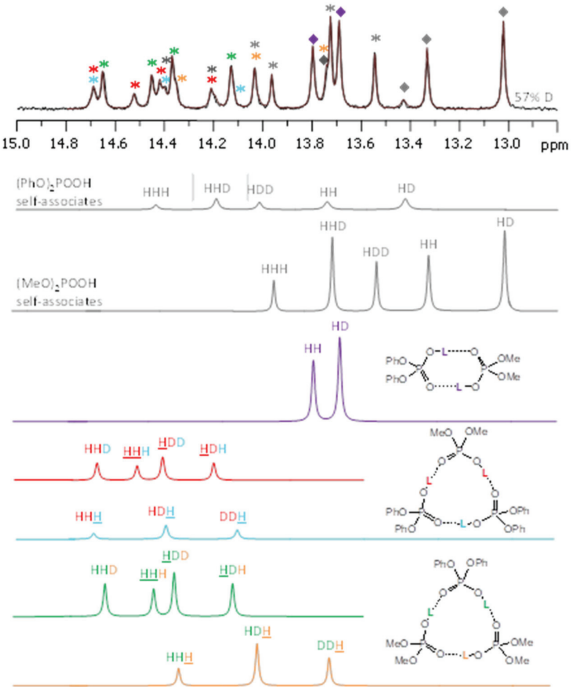

Figure 4. the low-field part of ^{1}H NMR spectrum of the sample containing approximately equal amounts of partially deuterated acids $(PhO)_2POOL$ and $(MeO)_2POOH$ (L = H, D)

Acknowledgements

This work is supported by the RSF grant 18-13-00050. The NMR spectra were recorded at the Center for Magnetic Resonance of SPbU Research Park. The quantum-chemical calculations were performed at the Computing Center of SPbU Research Park.

References

1. R. E. Asfin, G. S. Denisov, D. N. Poplevchenkov, K. G. Tokhadze, T. V. Velikanova, *Pol. J. Chem.* **2002**, *76*, 1223−1231.
2. (a) M. E. Druyan, A. H. Reis Jr, E. Gebert, S. W. Peterson, G. W. Mason, D. F. Peppard, *J. Am. Chem. Soc.* **1976**, *98*, 4801−4805. (b) F. Giorando, A. Ripamonti, *Acta Crystallogr.* **1967**, *22*, 678−682.
3. V. V. Mulloyarova, I. S. Giba, M. A. Kostin, G. S. Denisov, I. G. Shenderovich, P. M. Tolstoy, *Phys. Chem. Chem. Phys.* **2018**, *20*, 4901-4910.
4. V. V. Mulloyarova, I. S. Giba, G. S. Denisov, P. M. Tolstoy, *J. Phys. Chem A* **2019**, *123*, 6761−6771.

Structural studies of the translation regulation factors from *Staphylococcus aureus* by NMR spectroscopy

Konstantin Usachev[1], Alexander Golubev[1,2], Bulat Fatkhullin[1,3], Azat Gabdulkhakov[3], Aydar Bikmullin[1], Dmitriy Blokhin[1,4], Liliya Nurullina[1], Natalia Garaeva[1], Daut Islamov[1], Evelina Klochkova[1], Vladimir Klochkov[4], Albert Aganov[4], Iskander Khusainov[1,2,&], Shamil Validov[1], Marat Yusupov[1,2]

[1]*Laboratory of Structural Biology, Institute of Fundamental Medicine and Biology, Kazan Federal University, 18 Kremlyovskaya, Kazan 420008, Russian Federation; E-mail: k.usachev@kpfu.ru*
[2]*Département de Biologie et de Génomique Structurales, Institut de Génétique et de Biologie Moléculaire et Cellulaire, CNRS UMR7104, INSERM U964, Université de Strasbourg, 1 rue Laurent Fries, F-67400 Illkirch, France; marat.yusupov@igbmc.fr*
[3]*Institute of Protein Research, Russian Academy of Sciences, Institutskaya 4, 142290 Puschino, Moscow Region, Russian Federation; azat@vega.protres.ru*
[4]*NMR Laboratory, Medical Physics Department, Institute of Physics, Kazan Federal University, 18 Kremlyovskaya, Kazan 420008, Russian Federation; Vladimir.Klochkov@kpfu.ru*
[&]*Present address: Department of Molecular Sociology, Max Planck Institute of Biophysics, Max-von-Laue-Straße 3, 60438 Frankfurt am Main*

Introduction

For the sake of energy preservation bacteria, upon transition to stationary phase or under stress conditions, bacteria abate their metabolism, largely by re-programming their protein synthesis apparatus through the interactions with a number of small proteins. Recent structural studies by high-resolution NMR spectroscopy, X-ray and cryo-EM methods revealed the mechanisms of action of some of these ribosome-bound proteins, such as ribosome hibernation promoting factor (HPF), ribosome modulation factor (RMF), ribosome-associated inhibitor A (RaiA/YfiA), ribosome splitting factor HflX, ribosome binding factor A (RbfA), ribosome silencing factor (RsfS), Elongation factor P (EF-P). The understanding of the detailed landscape of translation regulation factors – ribosome interactions shed new light on the mechanism of ribosome shutdown in the pathogens such as *Staphylococcus aureus* and opens the road for the structure-based drug design of possible antibiotics that is of a great significance due to growing antibiotic resistance.

Hibernation promoting factor (HPF)

Staphylococcus aureus hibernation promoting factor (SaHPF) is responsible for the formation of 100S ribosome dimers (disomes), which in turn help this pathogen to reduce energy spent under unfavorable conditions [1]. By cryo-electron microscopy we solved at near-atomic resolution the structure of disomes from *Staphylococcus aureus* containing a long variant of the HPF, and by high-resolution NMR spectroscopy and X-ray analysis we solved the structure of the N- and C-terminal domains of SaHPF and shown that SaHPF-CTD present as a homodimer dimer in solution [2, 3]. Our reconstructions of cryo-EM data reveal that the CTD protrudes out of each ribosome to mediate dimerization, with secondary interactions provided by helix 26 of the 16S ribosomal RNA. Disomes form whether ribosomes adopt unrotated or rotated conformations, suggesting translation can be paused by SaHPF at any stage. Residues Phe160, Val162, Thr171, Ile173, Tyr175, Ile185 andThr187 in the dimer interface of SaHPF protein were mutated and the effects were analyzed for the formation of 100S disomes of ribosomes isolated from *S.aureus*. It was shown that substitution of any of single residues Phe160, Val162, Ile173, Tyr175 and Ile185 in the SaHPF homodimer interface abolished the ribosome dimerization *in vitro* [4]. Overall, our work illustrates that the dimerization mode

of bacterial ribosomes is species-specific, a finding that may help improve the selectivity of antimicrobials.

Elongation Factor P (EF-P)

Elongation Factor P (EF-P) is a 20.5 kDa protein that provides specialized translation of special stalling amino acid motifs. Proteins with stalling motifs are often involved in various processes, including stress resistance and virulence. Thus it has been shown that the virulent properties of microorganisms can be significantly reduced if the work of EF-P is disrupted. By high-resolution NMR spectroscopy and X-ray analysis, we solved the structure of EF-P from *S.aureus* and have compared it with other known EF-P's structures [5]. By EPR spectroscopy we investigated a spin-labeled *Sa*EF-P. Addition of MTSL ((*S*-(1-oxyl-2,2,5,5-tetramethyl-2,5-dihydro-1*H*-pyrrol-3-yl)methyl methanesulfonothioate)) label covalently bound to 32Cys in the highly conservative part of EF-P loop in the domain I of the EF-P allows us to analyze protein dynamics by EPR spectroscopy of the high mobility region which was not observed in NMR spectra due to fast proton exchange leading to the absence of the corresponding amide NMR resonances [6]. Thr obtained structure of EF-P by NMR and X-ray diffraction analysis, as well as the structure of the ribosome complex by cryo-electron microscopy, will allow further screening of highly selective inhibitors of the translation of the pathogenic bacterium *S. aureus* [7].

Ribosome binding factor A (RbfA)

Ribosome binding factor A (RbfA) is a 14.9 kDa adaptive protein of cold shock, which is important for bacterial growth at low temperatures. RbfA can bind to the free 30S ribosomal subunit and interacts with the 5′-terminal helix (helix I) of 16S rRNA. RbfA is important for the efficient processing of 16S rRNA and the maturation (assembly) of 30S ribosomal subunits. By high-resolution NMR spectroscopy and X-ray diffraction analysis we solved the RbfA structure from S.aureus and shown that secondary structure of RbfA have KH-domain fold topology with βααβ subunit which is characterized by a helix-kink-helix motif in which the GxxG sequence is replaced by a conserved AxG sequence, where an Ala residue at position 70 forming an interhelical kink [8]. The obtained structure of this protein factor and its complex with the ribosome cryo-electron microscopy will allow further development of highly selective substances for slowing or completely stopping the translation of the pathogenic bacterium *S. aureus*, which will interfere with the synthesis and isolation of its pathogenicity factors.

Acknowledgments

This work was supported by the Russian Science Foundation (Grant 17-74-20009).

References

1. I. Khusainov, Q. Vicens, R. Ayupov, K. Usachev, A. Myasnikov, A. Simonetti, Sh. Validov, B. Kieffer, G. Yusupova, M. Yusupov, Y. Hashem. – *The EMBO journal*, **36**, 2073-2087 (2017).
2. K.S. Usachev, R.Kh Ayupov, Sh. Z. Validov, I. Sh. Khusainov, M.M. Yusupov. – *Biomolecular NMR Assignment*, **12**, 85-89 (2018).
3. K.S. Usachev, S.Z. Validov , I.Sh. Khusainov, V.V. Klochkov, A.V. Aganov, M.M. Yusupov. – *Journal of Biomolecular NMR*, **73(5)**, 223-227 (2019).
4. K.S. Usachev, B.F. Fatkhullin, E.A. Klochkova, A.K. Miftakhov, A.S. Golubev, A.G. Bikmullin, L.I. Nurullina, N.S. Garaeva, D.R. Islamov, A.G. Gabdulkhakov, N.V. Lekontseva, S.V. Tishchenko, V.A. Balobanov, I.Sh. Khusainov, M.M. Yusupov, Sh.Z. Validov. – *Journal of Structural Biology*, in press (2019).
5. K.S. Usachev, A.A. Golubev, Sh.Z. Validov, V.V. Klochkov, A.A. Aganov, I. Sh. Khusainov, M.M. Yusupov. – *Biomolecular NMR Assignment*, **12**, 351-355 (2018).

6. K.S. Usachev, E.A. Klochkova, A.A. Golubev, S.Z. Validov , F.F. Murzakhanov, M.R. Gafurov, V.V. Klochkov, A.V. Aganov, I.Sh. Khusainov, M.M. Yusupov. – *Springer Nature Applied Science*, **1**, article 442 (2019).
7. A.A. Golubev, Sh.Z. Validov, K.S. Usachev, M.M. Yusupov. – *Molecular biology*, **53(4)**, 501-512 (2019).
8. D.S. Blokhin, A.G. Bikmullin, L.I. Nurullina, N.S. Garaeva, Sh.Z. Validov, V.V. Klochkov, A.V. Aganov, I.Sh. Khusainov, M.M. Yusupov, K.S. Usachev. – *Biomolecular NMR Assignment*, **13(1)**, 27-30 (2019).

NMR spectroscopy as a tool to characterize ion dynamics in solid electrolytes

Tatiana Zinkevich[1,2], Frank Tietz[3], Sylvio Indris[1,2], Helmut Ehrenberg[1,2]

[1]Institute for Applied Materials – Energy Storage Systems, Karlsruhe Institute of Technology, Karlsruhe, Germany
[2]Research group Methods - Helmholtz Institute Ulm, Germany
[3]Institute of Energy and Climate Research, Material Synthesis and Processing (IEK-1), Forschungszentrum Jülich, Germany
E-mail: tatiana.zinkevich@kit.edu

Introduction

During the last decades the availability mobile electronic devices and recently also of electric cars drastically increased. Only twenty years ago you would be considered as a mad, if you told that you need to charge your cigarette or a book. Nowadays, it's completely understandable.

All these applications need high-power or high-energy long-lasting energy sources – batteries. The efficiency, light weight and low price are the prerequisites for modern batteries. Due to environmental concenrs, safety issues in battery production attracted specific interest recently. It has been shown that all-solid-state batteries (ASSB), in which the liquid electrolyte is replaced by solid materials, might possess an increased stability and could be less harmful for our environment. One of the key challenges in ASSB design is the development of solid electrolytes, which could compete with liquid materials in terms of ionic conductivity. Most of the solids possess a low diffusivity of the charge carriers; however, there are few families of structures which represent so-called superionic behavior. The diffusion rate of the ions in such materials reaches the one of the liquid electrolytes.

In order to enable the rational improvement of potential solid electrolytes, one needs prior knowledge of the mechanism of ionic transport in superionic solids on the microscopic scale. The crystal structure determines the available sites for ionic jumps and energy landscapes along which transport occurs. The rate of the jumps in most cases determines the bulk conductivity. Only the combined studies of the structure and dynamics in a wide frequency range can provide sufficient information for the elucidation of the transport mechanism. Solid-state NMR spectroscopy provides a variety of techniques to capture peculiarities of the material. In the current work we combine different NMR methods for investigation of structure and ion dynamics in solid electrolytes.

High-field magic-angle spinning (MAS) NMR

NMR spectroscopy is making use of nuclear spin which experience different interactions with the local environment. These spins are surrounded by other spins in the matter. All spins mutually influence each other, and this influence drastically depends on the distance between spins and is reflected in the NMR spectrum as a shift of the signal towards higher or lower frequencies as a result of shielding/deshielding. Therefore, even small changes and rearrangements of the overall structure can be traced with solid state MAS spectroscopy.

NMR spectroscopy can be measured on different nuclei which are evenly distributed over the material, and, thus, we can accurately follow any perturbations which affect chemically and elementally inequivalent groups.

Figure 1 shows exemplarily how the effect of the sintering temperature on the crystal structure can be detected with MAS NMR spectroscopy. The series of $Li_{1.5}Al_{0.5}Ti_{1.5}(PO_4)_3$ samples [1] were measured with multi-nuclear solid-state NMR spectroscopy. The first sample of the series is a non-calcined sample, whereas the other samples are sintered at different temperatures.

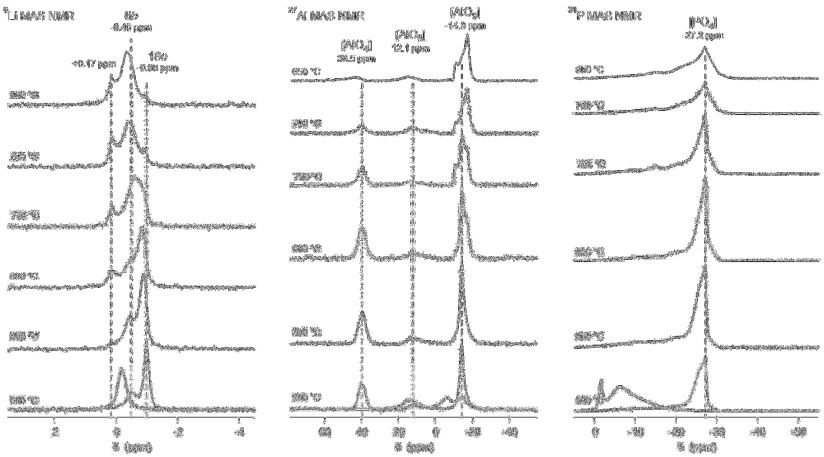

Figure 1. ^{6}Li, ^{27}Al and ^{31}P solid-state NMR spectra of the series of LATP samples sintered at different temperatures. The black bold line shows spectra of the original material

From the figure one can see how the final structure of LATP evolves. ^{6}Li NMR spectra show that the spectrum of the initial sample consists of a single broad line at -0.33 ppm which gradually evolves into peaks at -0.48 and -0.98 ppm under the thermal treatment. In the samples treated at 850° C and 900° C, one can identify Li ions occupying two different sites in the structure, and the occupation of both sites is approximately equal. Overall, the ^{6}Li NMR data are consistent with the results of structural investigations by XRD.

In ^{27}Al NMR spectra one can distinguish between different local structural units – AlO_4, AlO_5 and AlO_6. We can attribute the AlO_4 units to an $AlPO_4$ impurity, whereas AlO_6 units belong to the main LATP phase. As evident from the figure, with increasing sintering temperature the lines become gradually narrower. This effect can be attributed to the formation of a more ordered structure with less defects in good agreement with the result of X-ray diffraction.

Line narrowing, T_1 and $T_{1\rho}$ studies

The position of the signal in an NMR spectrum is very sensitive to the local structure around the specific nucleus. However, there are also other NMR observables that can shed light on the motions at different frequencies – relaxation times. The main time constants which bear the dynamical information are spin-lattice relaxation time T_1, spin-spin relaxation time T_2 and relaxation time in rotating frame $T_{1\rho}$. All of them depend on different combinations of the spectral density functions, which are Fourier-transforms of the correlation function of the motion. The main contribution to T_1 stems from the spectral density function at the Larmor frequency $J(\omega_L)$, thus, it is sensitive to fast dynamics in the nanosecond range. T_2 depends on $J(0)$ and is a measure of slow mobility. $T_{1\rho}$ detects motions in the frequency range of some kHz. The schematic representation of all three can be found in Figure 2a.[2] Here, one can distinguish between the maximum of the sensitivity of each experiment.

Temperature dependences of the relaxation times in combination with analytical approach reveal the number, rates and activation energies of the dynamical processes. Sometimes the shape of the temperature dependence of $T_1/T_{1\rho}$ curves hints at the geometry of motion as indicated in Figure 2b.

The correlation time and the activation energy can be convert into the diffusion coefficients and conductivity values: [3, 4]

$$D = \frac{l^2}{2d} K_{exchange}, \sigma = \frac{DNq^2}{k_B T}.$$

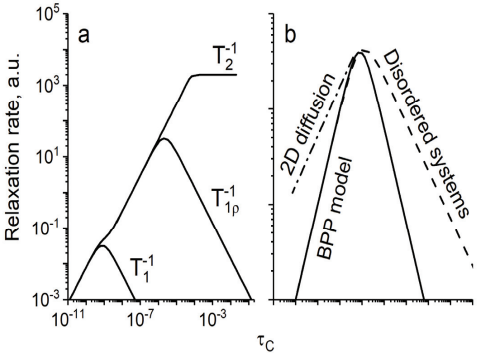

Figure 2. Schematic representation of a) relaxation rates $1/T_1$, $1/T_2$ and $1/T_{1\rho}$ for 3D diffusion and b) $1/T_1$ in disordered systems and for the motions with lower dimensionality

Self-diffusion coefficient measurements

Relaxation time experiments provide dynamical information on very short time scales. The long-range transport which is especially important for dc conductivity cannot be measured directly. PFG-NMR experiments allow direct evaluation of the ionic transport occurring over micrometer distances. This type of experiments can be performed in two modes – pulsed-field gradient mode and with static gradients. Both of the possibilities have their own advantages and disadvantages [5] and yield the rate of the diffusivity and, if measured as a function of temperature, activation energies. Figure 3 exemplarily shows the diffusion-induced damping of the echo signal measured at different temperatures and the temperature dependence of the diffusion coefficient. With this experiment it is possible to reveal high ionic mobility of Li nuclei in $Li_7P_3S_{11}$.

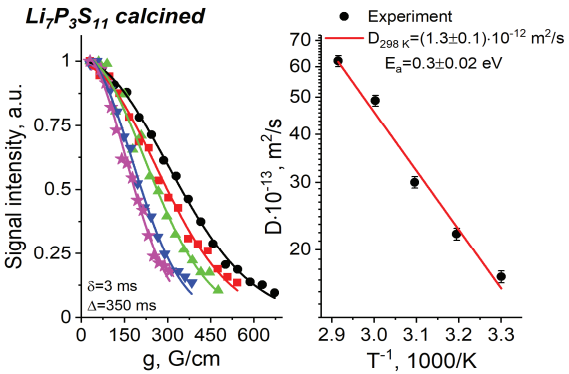

Figure 3. The results of PFG-NMR experiments with $Li_7P_3S_{11}$

In summary, it is worth noting that the listed experiments are just a small part of the possible techniques which can be and are applied to gain insights into the multiple dynamical processes and structural rearrangements occurring in solid electrolytes. However, even these show that solid-state NMR is a very suitable tool for research on battery materials.

References

1. B. Davaasuren, F. Tietz. Impact of sintering temperature on phase formation, microstructure, crystallinity and ionic conductivity of Li1.5Al0.5Ti1.5(PO4)3. – Solid State Ionics 338 (2019) 144-152.
2. P. Heitjans, A. Schirmer, S. Indris. NMR and β-NMR studies of diffusion in interface-dominated and disordered solids. – "Diffusion in Condensed Matter – Methods, Materials, Models", Berlin 2005.
3. A. Einstein. Über die von der molekularkinetischen Theorie der Wärme geforderte Bewegung von in ruhenden Flüssigkeiten suspendierten Teilchen. – Ann. Phys. 322 (1905) 549-560.
4. M. von Smoluchowski. Zur kinetischen Theorie der Brownschen Molekularbewegung und der Suspensionen. Ann. Phys. 326 (1906) 756-780.
5. D. Fischer, et al. Tracer diffusion measurements in solid lithium: a test for the comparison between NMR in static and pulsed magnetic field gradients after upgrading a standard solid state NMR spectrometer. SSNMR 26 (2004) 74-83.

Section 2

The ^{3}He NMR as a probe for nanostructures research

E. M. Alakshin[1], G. A. Dolgorukov[1], A. V. Klochkov[1], E. I. Kondratyeva[1], V. V. Kuzmin[1], K. R. Safiullin[1,2], A. A. Stanislavovas[1], M. S. Tagirov[1,2]

[1]Kazan Federal University, 420008, Kazan, Russian Federation
[2]Institute of Applied Research, 420111, TAS, Kazan, Russian Federation
E-mail: alakshin@gmail.com

The study of the spin kinetics of helium-3 in contact with nanostructures will be presented.

Aerogels

Our group systematically studied the nuclear magnetic relaxation of ^{3}He in contact with silicate aerogels. The determining role of the adsorbed layer in relaxation processes of gaseous and liquid ^{3}He was confrmed. It is known that aerogel acts as an impurity and affects phases of superfluid ^{3}He. Nowadays, it is of interest to study superfluid ^{3}He in contact with anisotropic aerogels (group of prof. Dmitriev V.V., Moscow). An additional mechanism of the ^{3}He relaxation in aerogels is found and it is shown that this relaxation mechanism is not associated with the adsorbed layer. A hypothesis about the influence of intrinsic paramagnetic centers on the relaxation of gaseous ^{3}He is proposed.

Nanoparticles

The spin kinetics data of ^{3}He in contact with varios trifluoride nanosized powders will be presented. Results for LaF_3 nanopowder demonstrated that the nuclear magnetic relaxation of the absorbed ^{3}He occurs due to the modulation of dipole-dipole interaction by the quantum motion in the adsorbed two-dimensional film. The analysis of obtained data for PrF_3 nanoparticles testifies in favor of cross-relaxation presence in the nuclear spin–lattice relaxation data, which takes place between ^{3}He and ^{141}Pr nuclei. The magnetic phase transition in DyF_3 is accompanied by a considerable change in the character of fluctuations of the magnetic moments of dysprosium ions, which affect the spin kinetics of ^{3}He in contact with the substrate. Significant changes in the relaxations rates of the longitudinal and transverse magnetizations of liquid ^{3}He have been discovered in the region of magnetic ordering of the solid matrix.

Nanodimonds

In recent years nanodiamonds have become a widely investigated material for quantum engineering, biological and electronic applications. The spin-lattice (T_1) and spin-spin (T_2) relaxation times of ^{3}He were measured in adsorbed, gas and liquid phases in a detonation nanodiamond sample at the frequency range of 5–18 MHz and at T = 1.6 K temperature. The observed T_1 and T_2 are much shorter in comparison with ^{3}He in similar experiments for samples with restricted geometry, thus we assume a strong impact of paramagnetic centers on nuclear magnetic relaxation. Experiments with nanodiamond surface preplated with N_2 or ^{4}He layers will be presented. The model of ^{3}He relaxation in contact with detonation nanodiamonds that describes our experimental results will be proposed.

This work was supported by the Russian Science Foundation (project no. 19-72-10061).

^{125}Te longitudinal relaxation in WTe_2 Weyl semimetal

Anastasiia O. Antonenko[1], Elena V. Charnaya[1], J. Haase[2], V. V. Marchenkov[3,4]

[1]St. Petersburg State University, St. Petersburg, 198504 Russia
[2]University of Leipzig, Leipzig, 04103 Germany
[3]Mikheev Institute of Metal Physics, Ural Branch of the Russian Academy of Sciences, Yekaterinburg, 620108 Russia
[4]Ural Federal University, Yekaterinburg, 620002 Russia
E-mail: a.antonenko@spbu.ru

Introduction

Last few years a great attention in the scientific world is focused on topological materials which possess a non-trivial topology of the electronic band structure. Topological materials demonstrate unique physical properties. The recent discoveries of such topological systems had a huge and deep impact on the science community and were a trigger for active experimental studies of these materials. Weyl semimetals (WSMs) are representatives of materials with non-trivial topology. WSMs were theoretically predicted and then experimentally found only few years ago [1, 2] and since then numerous experimental studies have started. These days, WSMs are turning out to be a rapidly evolving field in condensed matter, since they are good candidates for using in a plethora of spintronic or valleytronic applications. Moreover, the high mobility of Weyl fermions in WSMs may find use in electronics and computing.

There are two types of WSMs. Type-I WSMs respect Lorentz symmetry [3, 4] and those of type-II do not [1, 5]. The latter family includes the transition metal dichalcogenide tungsten ditelluride, WTe_2. Eight Weyl points in WTe_2 occur in the Brillouin zone in the presence of spin orbit coupling (SOC) as a consequence of the crossover of electron and hole pockets [1]. The charge carriers have unusual properties near the Weyl points. Nuclear magnetic resonance (NMR) is a good local probe of the density of states of the conduction electrons. Due to the hyperfine coupling between the electrons and nuclear spins there is a nuclear resonance frequency shift and a contribution to spin-lattice relaxation, which describes the dynamics of nuclear spins. Therefore, it is reasonable to use NMR to investigate the influence of Weyl points on the electron subsystem in WSMs. Nevertheless, despite a large number of different experimental works on WSMs there is only one publication presenting our first NMR results on WTe_2 WSMs [6].

Sample and experiment

In this work the ^{125}Te spin-lattice relaxation behavior in the layered single crystalline WTe_2 was studied in the temperature range from ~28 K to the room temperature using the wide line static probe with the cryostat. Temperature stabilization was better than 2 K. Measurements were performed on a Bruker Avance 500 NMR pulse spectrometer with the magnetic field 11.75 T. The saturation recovery technique was applied to measure the spin-lattice relaxation times. In the all cases the magnetization recovery described well by a single exponential law. The orientation and the phase homogeneity of the single crystal were tested using the X-ray diffraction. The NMR data were obtained for the single crystal in two orientations: $\vec{c} \parallel \vec{B}_0$ and $\vec{c} \perp \vec{B}_0$, where $\vec{c}$ is the WTe_2 crystallographic axis, which is perpendicular to its atomic layers.

Results

It was shown that ^{125}Te NMR spectra for both orientations consisted of several lines which corresponded to non-equivalent positions of the tellurium atoms in WTe_2 [6]. For the each line in the ^{125}Te NMR spectra there was found the temperature dependence of the spin-lattice relaxation rate; the data were obtained for the both crystal orientations in magnetic field. An example of such dependence is given on Figure 1. It is clear that the dependence $1/T_1(T)$

obtained is not typical for conventional metals or semiconductors. We have found that for all lines in the NMR spectra for the both orientations there was a temperature range ΔT where the crossover appeared between two different kinds of the temperature dependences. Such relaxation behavior is quite similar to that observed experimentally other topological systems such as Dirac and Weyl semimetals [7, 8] but is not entirely consistent with theoretical calculations for WSMs [9].

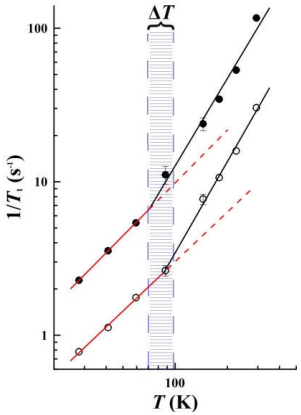

Figure 1. The temperature dependence of the ^{125}Te relaxation rate ($1/T_1$) for the WTe_2 single crystal in the orientation $\vec{c} \parallel \vec{B}_0$. At ΔT the crossover between two different regimes of relaxation is seen. Below ΔT the Korringa law is valid

Acknowledgements

This work is supported by the Russian Foundation for Basic Research (grant No. 19-57-52001). The X-ray analysis and part of NMR measurements were done in the Research park of St. Petersburg State University using the equipment of "Centre for X-ray Diffraction Studies" and "Centre for Diagnostics of Functional Materials for Medicine, Pharmacology and Nanoelectronics".

References

1. A.A. Soluyanov, D. Gresch, Z. Wang, Q. Wu, M. Troyer, X. Dai, B.A. Bernevig. – *Nature*, 527, 495-498 (2015).
2. L. Peng, Y. Yuan, G. Li, X. Yang, J.-J. Xian, C.-J. Yi, Y.-G. Shi, Y.-S. Fu. – *Nat. Commun*., 8, 659 (2017).
3. L.X. Yang, Z.K. Liu, Y. Sun, H. Peng, H.F. Yang, T. Zhang, B. Zhou, Y. Zhang, Y.F. Guo, M. Rahn, D. Prabhakaran, Z. Hussain, S.-K. Mo, C. Felser, B. Yan, Y.L. Chen. – *Nat. Phys*., 11, 728-732 (2015).
4. Z.K. Liu, L.X. Yang, Y. Sun, H. Peng, H.F. Yang, C. Chen, Y. Zhang, Y.F. Guo, D. Prabhakaran, M. Schmidt, Z. Hussain, S.K. Mo, C. Felser, B. Yan, Y.L. Chen. – *Nat. Mater*., 15, 27-31 (2016).
5. Y. Sun, S.-C. Wu, M.N. Ali, C. Felser, B. Yan. – *Phys. Rev. B*, 92, 161107 (2015).
6. A.O. Antonenko, E.V. Charnaya, M.K. Lee, L.J. Chang, J. Haase, S.V. Naumov, A.N. Domozhirova, V.V. Marchenko. – *Phys. Solid State*, 61, 1979-1984 (2019).
7. D. Koumoulis, R.E. Taylor, J. McCormick, Y.N. Ertas, L. Pan, X. Che, K.L. Wang, L.-S. Bouchard. – *J. Chem. Phys*., 147, 084706 (2017).
8. H. Yasuoka, T. Kubo, Y. Kishimoto, D. Kasinathan, M. Schmidt, B. Yan, Y. Zhang, H. Tou, C. Felser, A.P. Mackenzie, M. Baenitz. – *Phys. Rev. Lett.*, 118, 236403 (2017).
9. Z. Okvátovity, F. Simon, B. Dóra. – *Phys. Rev. B*, 94, 245141 (2016).

Polyphenylene isophthalamide pervaporation and ultrafiltration membranes modified by Pluronic F127

Ramadan Atta[1,2], Anastasia V. Penkova[1], Mariia E. Dmitrenko[1], Andrey A. Zolotarev[1]

[1]St. Petersburg State University, 7/9 Universitetskaya nab., St. Petersburg 199034, Russia
[2]Damietta University, Damietta, Egypt
E-mail: ramadanatta75@du.edu.eg

Introduction

Membrane processes has become an effective and attractive separation technology over the past decade. Membrane technology operates without the addition of chemicals, with a relatively low energy consumption and well-arranged process conductions. The search for new membranes with perfect transport properties is needed. Polymers are the most widely used materials in membrane technologies. Poly (phenylene isophthalamide) (PA) is a commercial polymer, which is used for the preparation of porous membranes, employed in ultrafiltration and for the creation of nonporous membranes for the pervaporation processes due to its chemical resistance and good mechanical properties. However, PA have shown to be vulnerable to fouling for the application in ultrafiltration and low permeation flux and separation factor for the pervaporation. To improve the membrane quality, PA was modified by incorporation of Pluronic F127 into membrane matrix. Pluronic F127 is amphiphilic synthetic tri-block copolymers of poly(ethylene oxide) poly(propylene oxide)-poly(ethylene oxide) (PEO-PPO-PEO), and it is using as a pore forming agent and to increase the hydrophilicity of the membrane surface. Addition of pluronic F127 into polymer membrane matrices controls the hydrophilicity and roughness of the membrane selective layer surface, pore size, porosity and size of macrovoids in the membrane substructure.

In this study, novel pervaporation and ultrafiltration membranes based on polyphenylene isophthalamide (PA) modified by Pluronic F127 were developed. The effect of the Pluronic F127 on physicochemical, transport membrane and membrane structure of PA was investigated by IR-spectroscopy, nuclear magnetic resonance, scanning electron microscopy, sorption experiments, porosimetry, and contact angle measurements. The transport properties of the dense membranes were analyzed in separation of azeotropic methanol/toluene (72/28 wt%) mixture by pervaporation, while the porous membranes were examined in ultrafiltration of pure water and bovine serum albumin (BSA) solution.

Acknowledgements

The experimental work was facilitated by equipment from Resource Centers: for Nano technology, Magnetic Resonance Research Centre, X-ray Diffraction Methods, Thermal Analysis and Calorimetry, Centre for Diagnostics of Functional Materials for Medicine, Pharmacology and Nanoelectronics, Chemical Analysis and Materials Research Centre and GEOMODEL at St. Petersburg State University.

Free induction decay in quasi-one-dimensional spin chains in fluorapatite under the action of pulse sequence used in multiple quantum NMR experiments

Georgii A. Bochkin, Edward B. Fel'dman, Sergey G. Vasil'ev

Institute of Problems of Chemical Physics of RAS
E-mail: bochkin.g@yandex.ru

Introduction

Extraction of information about structure from the free induction decay (FID) and theoretical calculation of the FID are important classes of problems in NMR. Among the experimental methods of NMR, multiple quantum (MQ) NMR experiments are an interesting way of obtaining information about the distribution of spins, allowing, for example, to count the nuclei in a molecule (in a dilute solution) or estimate the effective dimensionality of the spin system (in a solid) [1]

Here, we consider the free induction decay in one-dimensional spin chains under the action of a pulse sequence used in a MQ NMR experiment [1] (see Fig.1). For a comparison with experimental data, the FID obtained on fluorine nuclei chains in a single crystal of fluorapatite was used. The distance between chains is 2.7 times the distance between neighboring nuclei in the same chain, which means that the nearest neighbor dipolar coupling constant is at least 40 times greater than the coupling constant between spins in adjacent chains, if the chains of nuclei are parallel to the external magnetic field. Thus, the interaction between the chains can be neglected.

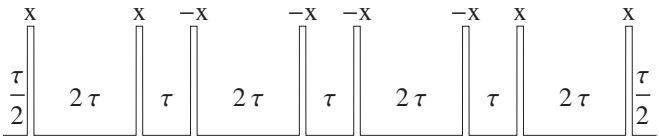

Figure 1. One period of the RF pulse sequence used in the experiment

Calculation of the FID in the high temperature case

The evolution of the system

In the multiple-quantum experiment, the behavior of the system can be described [1] by the average Hamiltonian

$$H_{MQ} = -\frac{D}{2}\sum_{i}^{N-1}\left(I_i^+ I_{i+1}^+ + I_i^- I_{i+1}^-\right),$$

where D is the dipolar coupling constant between adjacent spins, I_i^+ and I_i^- are, respectively, the raising and lowering spin angular momentum operators acting on spin i,.and N is the number of spins in the chain.

For the case of long spin chains, the evolution of the system under the pulse sequence shown in Fig.1 has been calculated in [2]. The density matrix of the system at time instant t can be written as

$$\rho = \rho_0 + \rho_2 + \rho_{-2},$$

where the term ρ_i represents multiple quantum coherence of order i. For long chains ($N >> 1$), the ρ_0 term can be written [3] as

$$\rho_0 = \sum_{\substack{l=1,3,...N-1 \\ l'=1,3,...N-1}} 2^{l+l'-2}\left[J_{l-l'}(2Dt)+J_{l+l'}(2Dt)\right] I_1^z I_2^z ... I_{l-1}^z I_l^+ I_1^z I_2^z ... I_{l'-1}^z I_{l'}^- -$$

$$- \sum_{\substack{l=2,4,...N \\ l'=2,4,...N}} 2^{l+l'-2}\left[J_{l-l'}(2Dt)+J_{l+l'}(2Dt)\right] I_1^z I_2^z ... I_{l-1}^z I_l^- I_1^z I_2^z ... I_{l'-1}^z I_{l'}^+,$$

where J_k is the Bessel function fo the first kind of order k.
The FID can be calculated as

$$G(t) = \mathrm{Tr}(\rho(t) I_z) = \mathrm{Tr}(\rho_0(t) I_z),$$

After substituting the ρ_0 in the previous equation and simplifying, we obtain

$$G(t) = (2N+1)2^{N-3} J_0(2Dt) - 2^{N-3}\cos 2Dt,$$

and, taking into account that $N >> 1$ and normalizing so that $G(0) = 1$, we get

$$G(t) = J_0(2Dt). \quad (1)$$

Comparison with the experimental data

The experiments were performed on a Bruker Avance III spectrometer on a single crystal of calcium fluorapatite with static magnetic field of 9.4 T (the corresponding frequency on ^{19}F nuclear spins is 376.6 MHz). From Fig.2, it can be seen that there is qualitative agreement of the theoretical calculation with the experimental data. The possible reasons for the discrepancy include neglecting the interaction of the fluorine nuclei which are not nearest neighbors (the heteronuclear interaction is averaged to zero by the RF pulse sequence).

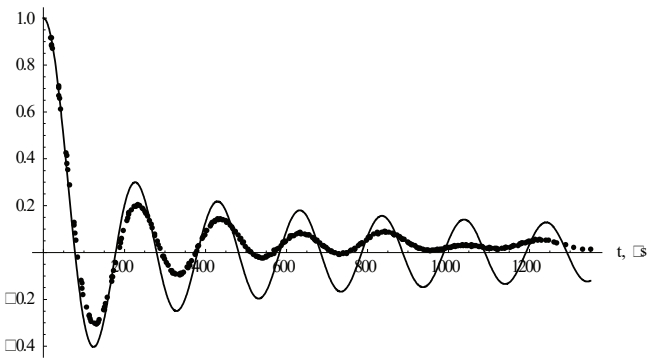

Figure 2. The theoretical FID (the solid line, the equation (1) with dipolar coupling constant $D=15.5\times10^3$ s^{-1}) and the experimental data

Acknowledgements

This work was performed as part of the state task, state registration No. 0089-2019-0002. This work was performed using the equipment of the Center of Shared Analytical Facilities of IPCP RAS. This work is supported by RFBR (project № 19-32-80004) and Presidium of RAS program № 5 "Photonic technologies in probing inhomogeneous media and biological objects".

References

1. J. Baum, M. Munowitz, A.N. Garroway, A. Pines. Multiple-quantum dynamics in solid state NMR, *J. Chem. Phys.*, 83, 2015-2025 (1985).

2. S. I. Doronin, I. I. Maksimov, E. B. Fel'dman. Multiple-quantum dynamics of one-dimensional nuclear spin systems in solids. – *J. Exp. Theor. Phys.,* 91, 597-609 (2000).
3. G. A. Bochkin, E. B. Fel'dman, S. G. Vasil'ev. The exact solution for the free induction decay in a quasi-one-dimensional system in a multi-pulse NMR experiment. – *Physics Letters A,* 383, 2993-2996 **(**2019)

Analysis of Structural and Dynamical Properties of Mixtures of Imidazolium-based Ionic Liquids with Water by Molecular Dynamics Simulations

Sergei S. Bystrov, A. V. Egorov, Prof. Dr. V. I. Chizhik

Department of Nuclear-Physics Research Methods, Faculty of Physics, Saint-Petersburg State University
E-mail: barigapunk@gmail.com

Ionic liquids (ILs)/room temperature ionic liquids (RTILs), by the most widely accepted definition, are compounds consisting entirely of ions, but in contrast to ordinary salts they remain liquid at the room temperature or at temperatures close to it. The ILs have been suggested as non-aqueous electrolytes for electrochemical applications, energy storage and conversion, super- or ultra-capacitors, light-emitting and dye-sensitized solar cells. Beside physical and chemical properties, their biological activity, antimicrobial and cytotoxic properties and, thus, potential application in pharmaceutics and medicine have been attracting significant interest of scientists working in the fields of life science, biochemistry, drug synthesis, etc.

Molecular dynamics (MD) simulations are widely used for studying structure, thermodynamic and transport properties of liquid systems, in particular mixtures of water with imidazolium-based ionic liquids (see, for instance, works [1-5] and references wherein). It is advisable to use MD data to interpret various experimental results. Aqueous solutions of 1-butyl-3-methylimidazolium tetrafluoroborate are among the most studied systems, and many simulations were focused on the structural characteristics such as radial and spatial distribution functions.

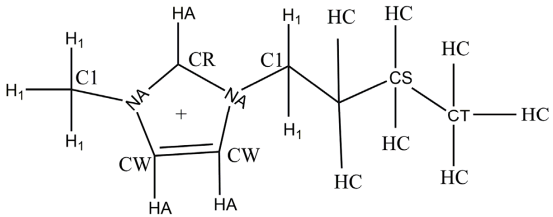

Figure 1. Ionic liquid of the [BMIM] type with labeling of the atoms within the molecule

In the work [1] authors analyzed the effect of replacing BF_4^- with NO_3^- and other anions on mixture structuring. However, in spite of considerable efforts, many problems are still unsolved. For example, the available MD data, obtained using different models and simulation protocols, do not allow one to describe all details of water molecules and ions structural arrangements in the whole concentration range from pure water to pure IL. The cumulative effect of water content on nanostructural organization (formation of ionic and water clusters, existence of microheterogeneity, etc.) still remains unclear.

Figure 2 shows the self-diffusion coefficients concentration dependencies calculated for some systems under the study using the TIP5P water model. In this study we consider the relationship between the structural organization and various parameters of the system under study (concentration, water model, etc.), and also try to compare these datasets with experimental results obtained earlier [6].

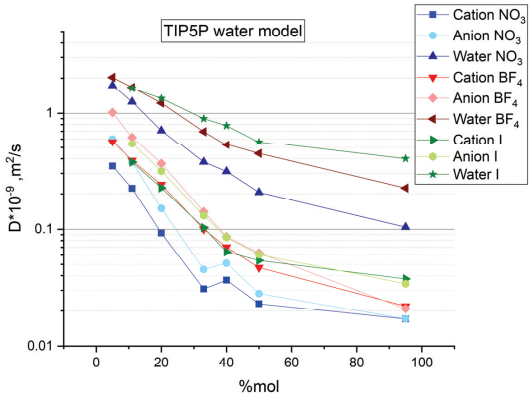

Figure 2. The concentration dependencies of the self-diffusion coefficients for the various functional parts of the solution under simulation

Acknowledgements

The work is supported by the RFFI grant 17-03-00057.

References

1. Koishi, T. Molecular Dynamics Study of the Effect of Water on Hydrophilic and Hydrophobic Ionic Liquids. *J. Phys. Chem. B* **2018**, *122* (51), 12342–12350. https://doi.org/10.1021/acs.jpcb.8b07774.
2. Nickerson, S. D.; Nofen, E. M.; Chen, H.; Ngan, M.; Shindel, B.; Yu, H.; Dai, L. L. A Combined Experimental and Molecular Dynamics Study of Iodide-Based Ionic Liquid and Water Mixtures. *J. Phys. Chem. B* **2015**, *119* (28), 8764–8772. https://doi.org/10.1021/acs.jpcb.5b04020.
3. Jiang, W.; Wang, Y.; Voth, G. A. Molecular Dynamics Simulation of Nanostructural Organization in Ionic Liquid/Water Mixtures †. *J. Phys. Chem. B* **2007**, *111* (18), 4812–4818. https://doi.org/10.1021/jp067142l.
4. Schröder, C.; Rudas, T.; Neumayr, G.; Benkner, S.; Steinhauser, O. On the Collective Network of Ionic Liquid/Water Mixtures. I. Orientational Structure. *J. Chem. Phys.* **2007**, *127* (23), 234503. https://doi.org/10.1063/1.2805074.
5. Moreno, M.; Castiglione, F.; Mele, A.; Pasqui, C.; Raos, G. Interaction of Water with the Model Ionic Liquid [Bmim][BF_4]: Molecular Dynamics Simulations and Comparison with NMR Data. *J. Phys. Chem. B* **2008**, *112* (26), 7826–7836. https://doi.org/10.1021/jp800383g.
6. Bystrov, S. S.; Matveev, V. V.; Egorov, A. V.; Chernyshev, Y. S.; Konovalov, V. A.; Balevičius, V.; Chizhik, V. I. Translational Diffusion in a Set of Imidazolium-Based Ionic Liquids [Bmim]$^+$ A^- and Their Mixtures with Water. *J. Phys. Chem. B* **2019**, *123* (43), 9187–9197. https://doi.org/10.1021/acs.jpcb.9b06802.

Investigation and characterization of mixed matrix membranes based on composite sodium alginate - fullerene derivative

Mariia E. Dmitrenko, Vladislav P. Liamin, Anna I. Kuzminova, Anastasia V. Penkova

St. Petersburg State University, 7/9 Universitetskaya nab., 199034 St. Petersburg, Russia
E-mail: m.dmitrienko@spbu.ru

Introduction

Membrane separation technologies belong to the most important and perspective field of sustainable processes due to the fact that these methods are environmentally friendly, resource and energy saving. One of the perspective membrane technologies for separation is pervaporation, which is widely and effectively used for separation of azeotropic and isomers mixtures, close-boiling and thermally unstable substances in various industrial fields. This method also is especially important for the dehydration purposes. Due to the rapid development of pervaporation and the requirements for increased process efficiency the search for new highly effective materials and the development of green membranes based on it with tailored transport properties are needed. One of the most promising ways to improve the properties of polymeric membranes is the preparation of mixed matrix structures, namely, the introduction of carbon nanoparticles into polymeric matrix to combine the advantages of both polymer and inorganic structures. In the present work water soluble fullerene derivatives (polyhydroxylated fullerene and fullerene derivative with L-arginine) were used as modifiers and cross-linking agents for sodium alginate.

Membrane investigation

The aim were to develop green mixed matrix membranes based on sodium alginate modified by fullerene derivatives (polyhydroxylated fullerene (fullerenol) or fullerene derivative with L-arginine) with improved transport characteristics for pervaporation dehydration and to characterize them by various methods of investigation. The structure of obtained composites and membranes based on them was studied by NMR and FTIR spectroscopies, SEM and AFM microscopies. Contact angle measurements and sorption experiments were carried out to evaluate the changes in surface and physicochemical properties of membranes. The transport properties of membranes were investigated by pervaporation for separation of water-isopropanol mixture in the wide concentration range.

Conclusion

It was shown that the application of fullerene derivative particles as modifiers for sodium alginate led to the significant change and the improvement of membrane properties due to the changes in the inner structure and morphology.

Acknowledgements

This work was supported by Russian Science Foundation [project No 19-73-00105]. The experimental work was facilitated by equipment from Resource Centres for Nanotechnology, Magnetic Resonance, X-ray Diffraction Studies, Thermogravimetric and Calorimetric Research Centre, Chemical Analysis and Materials Research Centre and Centre "Nanofabrication of Photoactive Materials (Nanophotonics)" at St. Petersburg State University.

Determination the thermodynamic parameters of cellulose-water system by Time-Domain NMR

Yuriy B. Grunin, Leonid Yu. Grunin, Daria S. Masas, Maria S. Ivanova

Volga State University of Technology, Lenin sq. 3, Yoshkar-Ola, Russian Federation
E-mail: manyunya1107@gmail.com

Cellulose is the most common biopolymer of plant and animal origin [1]. This biodegradable polymer can be used to produce materials with desired characteristics.

The aim of this research is to develop a mechanism for the adsorption of water molecules on the active surface of cellulose and methods for determining the thermodynamic parameters of their interaction using Time-Domain NMR.

The objects of study were samples of I_β-cellulose from cotton fiber (GOST 595-79). NMR measurements were performed on the "Spin Track" NMR-relaxometer [2] with an operating frequency of 20 MHz. Spin-spin relaxation times of cotton cellulose samples were determined by Free Induction Decay (FID) and Carr–Pursell–Meiboom–Gill (CPMG) pulse sequences [3].

Adsorption isotherms of water vapor on cellulose samples were obtained using the isopiestic series method [1]. Samples previously dried in an oven at 105 °C for 12 hours were kept in desiccators with preset values of the relative pressure of water vapor to a constant mass at 20 °C.

We give a brief description of the process of water adsorption on the active surface of cellulose. In our opinion, the water molecule can be adsorbed on the glucopyranose rings of the surface chains of cellulose in two ways. If a $–CH_2OH$ group acts as a surface active center it is more convenient for the water molecule to adsorb on it through an oxygen atom. In this case, the hydrogen atom of the water molecule can form an additional hydrogen bond with O_4 or with O5 or with glycosidic oxygen, depending on the conformation of the $–CH_2OH$ group. In the neighboring glucopyranose ring of the cellulose chain, which experiences a 180° conformational revolution, the adsorption centers are O_2 and O_3 atoms, with which water molecules form two hydrogen bonds [4].

The ^1H NMR-relaxation methods together with sorption measurements can solve a number of issues related to the structural organization of cellulose and the nature of its interaction with adsorbed water.

The change in Gibbs free energy is associated with the net heat of adsorption and the entropy term by the expression [1]:

$$\Delta G^0 = \Delta H^0 - L + T\Delta S^0, \quad (1)$$

where ΔH^0 is the standard enthalpy of adsorption interaction; L is the heat of condensation of the adsorptive; ΔS^0 is the standard entropy of the adsorbate; T is the absolute temperature.

The change in Gibbs free energy is also related with the adsorption equilibrium constant by the Van't-Hoff equation:

$$\Delta G^0 = -RT\ln C, \quad (2)$$

where R is the universal gas constant; C is the adsorption equilibrium constant.

The adsorption equilibrium constant C is determined by solving the Brunauer-Emmett-Teller (BET) equation as applied to the isotherm of water adsorption on cotton cellulose [4].

The net heat of adsorption is determined by the formula:

$$\Delta H^0 - L = RT\ln\frac{T_2^2}{T_2^1}, \quad (3)$$

where T_2^1, T_2^2 are the true spin-spin relaxation times of the first (monolayer) and the second layers of adsorbed water, respectively.

After substituting (2) and (3) in (1), the change in entropy of the adsorbate is determined by the equation [4]:

$$R\ln(C\frac{T_2^1}{T_2^2}) = \Delta S^0. \quad (4)$$

We have obtained the following values of thermodynamic parameters for bilayer adsorption:

ΔG^0=7.94 kJ/mol, ΔH^0-L=4.87 kJ/mol, ΔS^0=10.24 J/(K·mol), C=24.

Thus, the mechanism for the adsorption of water molecules on the active surface of cellulose and the approach for calculating the thermodynamic parameters as applied to bilayer water adsorption on cotton cellulose are presented.

References

1. Yu.B. Grunin, L.Yu. Grunin, D.S. Masas et al. – *Russ. J. Phys. Chem. A.*, V.90, Iss.11, 2249-2253 (2016).
2. http://www.nmr-design.com/
3. A.A. Abragam. The principles of nuclear magnetism. – Clarendon Press, 1961.
4. Yu.B. Grunin, M.S. Ivanova, D.S. Masas, L.Yu. Grunin – *Russ. J. Phys. Chem. A.*, V.94, Iss.4, 704-708 (2020).

Possible explanation of magnetic relaxation mechanism during the HbS aggregation process in Sickle Cell Disease

M. Lores Guevara[1], R. N. Muller[2], S. Lauren[3], J. García Naranjo[1], V. I. Chizhik[3], C. Cabal Mirabal[1,4]*

[1]Centro de Biofísica Médica. Universidad de Oriente. Patricio Lumumba S/N. CP: 90500. Santiago de Cuba, Cuba
[2]Laboratoire de RMN et d'Imagerie Moléculaire. Département de Chimie Générale, Organique et Biomédicale. Faculté de Médecine et de Pharmacie. Université de Mons. Belgique
[3]San Petersburg State University
[4]Facultad de Física, Universidad de la Habana, Cuba
E-mail: carlos.cabal@fisica.uh.cu
**Corresponding Author*

Sickle Cell Disease (SCD), is a serious and genetic blood disorder [1-3] caused by the polymerization of the hemoglobin S (HbS) under deoxygenation conditions. Due to the polymerization of HbS, the erythrocytes are affected, changing their shape, flexibility and the permeability of membrane, which gives place to vaso-occlusion at the capillary blood vessels and hemolytic anemia.

The behavior of the proton magnetic relaxation times (T1 and T2) has been very useful to study the HbS polymerization process, describing its 3 characteristic stages [1-3]. It has been assumed that these behaviors can be explained considering an increasing in the Rotational Correlation time of the water bound to the hemoglobin [1-3]. Nevertheless, the experimental dependences of the T1 and T2 relaxations times at the field strength need to be understand in these news experimental conditions.

In this work an assessment of the possible relaxation mechanism taking place during the aggregation process as a consequence of the increase of the Rotational correlation time [1-3]. The change of the speed of the molecular exchange between the free and the bounded water simultaneously with the various new molecular stages (monomers, dimers, tubules and polymers) multistage exchange are discuses. The existence of the Spin Curie relaxation mechanism is introduced as hypothesis. The quantitative contribution of this mechanism is evaluated. Feasibly, the contribution of the Spin Curie relaxation during the HbS agglutination process can be the first reported experimental evidence of this mechanism.

References

1. Manuel Arsenio Lores Guevara, Juan Carlos García Naranjo, Carlos Alberto Cabal Mirabal. MR relaxation studies of hemoglobin aggregation process in Sickle Cell Disease: applications for diagnostics and therapeutics. Applied Magnetic Resonance, December 2018. DOI 10.1007/s00723-018-1104-0.
2. Lores M., Cabal C. Proton Magnetic Relaxation Process during the polymerization of Hemoglobin S. Applied Magnetic Resonance. Volumen: 28. Number: 1. 79-84. 2005.
3. Lores M., Cabal C., Nascimento O., Gennaro. EPR study of the hemoglobin rotational correlation time and microviscosity during the polymerization of hemoglobin S. Applied Magnetic Resonance. Volumen:30. Number: 1. 121-128. 2006.

NMR and X-ray photoelectron spectroscopy possibilities for study complex ionic liquids

A. Ievlev[1], A. Koroleva[2], K. Tyutyukin[1], V. Matveev[1], O. Cabeza[3], L. Varela[4]

[1]Department of Nuclear Physics Research Methods, Saint Petersburg State University, 199034, 7/9 Universitetskaya nab., Saint Petersburg, Russia
[2]Resource Center "Physical methods of surface investigation", Saint Petersburg University, 199034, 7/9 Universitetskaya nab., Saint Petersburg, Russia
[3]Departamento de Física y Ciencias de la Tierra, Facultade de Ciencias, Universidade da Coruña, Campus de A Zapateira s/n, E-15071 A Coruña, Spain
[4]Grupo de Nanomateriais, Fotónica e Materia Branda, Departamentos de Física de Partículas e de Física Aplicada, Universidade de Santiago de Compostela, Campus Vida s/n Santiago de Compostela, E-15782, Spain
E-mail: a.ievlev@spbu.ru

Introduction

Interest in the study of ionic liquids (hereinafter IL) has not decreased over the past few decades. First of all, this is due to the increasing variety of applications of this class of substances, which, in turn, necessitates the synthesis of new compounds based on partially or fully studied cations and anions. In this work, in particular, we analyzed the composition and structure of a series of recently synthesized IL based on the well-known cation 1-butyl, 3-methyl imidosolium ($Bmim^+$) and complex anions of the form $(M\text{-}SCN_x)^{y-}$, where M = Al^{+3}, Fe^{+3}, Cr^{+3}, Mn^{+2}, Ni^{+2}, Hg^{+2}, Zn^{+2}, Co^{+2}, Cd^{+2} and Cu^{+}[1]. Often after the synthesis of such complex anions, it is necessary to confirm the structure of the complex. NMR spectroscopy can best cope with this task. For example, by the ratio of the integrals in the ^{13}C NMR spectrum, one can uniquely determine the quantitative ratio of carbon in the anion and cation. On the other hand, for some samples from the test set, NMR spectroscopy methods cannot be used. This mainly concerns complex anions with paramagnetic metals, such as Fe, Cr, Ni, Mn, Co. However, in this case, a solution can be found using x-ray photoelectron spectroscopy (XPS).

Experimental section

NMR studies were carried out on a Bruker 500 MHz Avance III spectrometer at the Resource Center MRMI of St. Petersburg State University. As can be seen in Figure 1, the ratio of the integrated intensities of the carbon lines in the anion and cation for the IL [Bmim](SCN) is one to one. This is true provided that the spectrum is recorded without polarization transfer from protons to carbon (without NOE), since the carbon core in the anion is not associated with any proton. The figure shows a detailed assignment of lines for our main IL and shows all the relative integrated line intensities, and in table 1 you can see the results of correlation for diamagnetic systems.

Table 1. Anion/cation relationship obtained from ^{13}C NMR [1]

Compound	Anion/cation	Expected
$[Bmim]_2\ Zn(SCN)_4$	1.94 ± 0.02	2
$[Bmim]_3\ Cu(SCN)_4$	1.31 ± 0.02	1.33
$[Bmim]_3\ Al(SCN)_6$	2.03 ± 0.02	2
[Bmim] (SCN)	0.95 ± 0.02	1

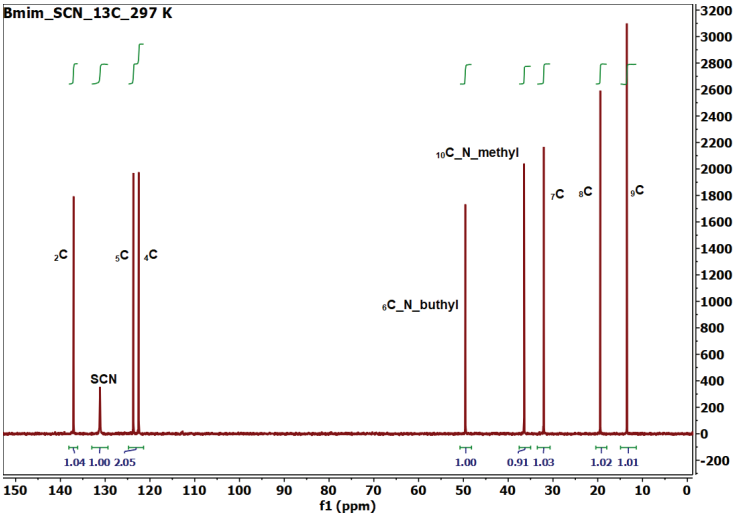

Figure 1. ^{13}C NMR spectrum of [Bmim](SCN)

The XPS analysis of the samples was carried out on an Escalab 250Xi instrument at the PMSI resource center of St. Petersburg State University. Note that the study is carried out in a deep vacuum (pressure in the analytical chamber is 2×10^{-9} mbar), and the measurement data is possible only due to the zero vapor pressure of ionic liquids, one of the main properties of this class of substances. Figure 2 shows the overview spectrum of a sample of pure [Bmim](SCN). As a result of processing the obtained data, the ratio of the chemical elements of the test substance was obtained (see Table 2).

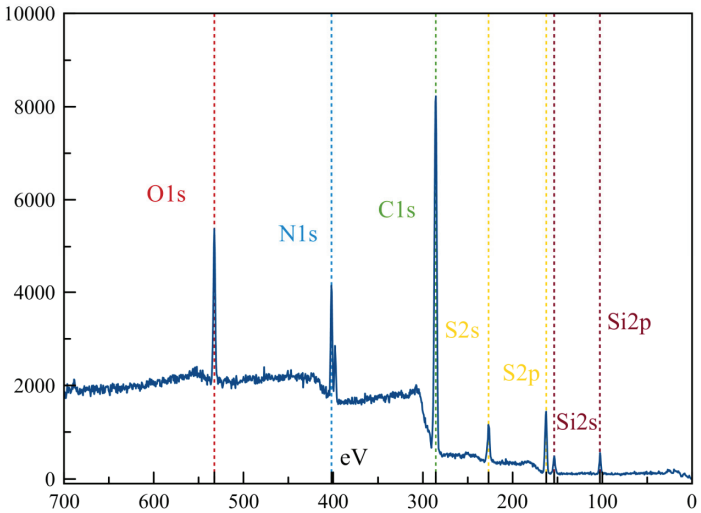

Figure 2. XPS spectrum of [Bmim](SCN)

Table 2. The ratio of elements in [Bmim](SCN), obtained by the results of XPS

Name of atom	Atomic %	Normalized	Expected
C	72,52	9,99	9
N	20,23	2,79	3
S	7,26	1	1

The obtained ratio is very close to the calculated ratio of elements in the studied ionic liquid, they are in satisfactory agreement with ^{13}C NMR data and, thus, confirm the expected composition of IL. Therefore, this makes it possible to use the XPS method to study other similar systems, including those containing paramagnetic metal ions. As a result, we were able to determine the number of anions and cations that make up each IL, and thereby verify the estimated valency and coordination number of the metal ion in the anion complex. For most of the investigated IL, the results obtained coincided with the expected compositions.

Acknowledgements

Investigations were carried out in the framework of the project INI_2019 (ID: 48469317), SPbSU. Scientific researches were performed at the «Magnetic Resonance Research Centre» and «Centre for Physical Methods of Surface Investigation» of Research park of St. Petersburg State University.

References

1. O. Cabeza *et al*, Synthesis, Microstructure and Volumetry of Novel Metal Thiocyanate Ionic Liquids with BMIM Cation. J. Mol. Liq. 283 (2019) 638-651.

1D Moisture transport in thin cement paste samples measured with GARFIeld MRI evidencing dynamic porosity

Örs Istok

University of Surrey
Keywords: cement, anomalous, transport, MRI

This study presents one-dimensional wetting and drying experiments on thin cement paste samples measured with GARField MRI. GARField MRI is an ideal system to measure *1D* moisture transport in cementitious materials, giving spatio-temporally resolved information about the moisture filled-microstructure. The experiments evidence dynamic microstructure. The time dependent microstructure is believed to cause anomalous transport, which deviates from the square root of time dependency. GARField MRI is an unconventional MRI system, based on the stray field imaging technique. The system incorporates a strong static magnetic gradient of 9.16 T m^{-1} that allows high-spatial resolution in a 160 µm thick slice below drying/wetting surface. Quadrature echo trains are acquired at multiple depths, typically 600 and 900 µm from the wetted/drying surface. The data is normalized to a uniform rubber standard, the signal from crystalline solid is subtracted and the data then fit to a 3-component exponential decay to give the time dependence of the moisture filled pore size distribution. Data will be presented for a range of experimental scenarios and fitted to a new transport model.

Modeling the system of the carbosilane dendrimer of various generations

Naira R. Khusnutdinova, Denis A. Markelov

St Petersburg University, 7-9 Universitetskaya Emb., St Petersburg 199034, Russia
E-mail: nai.khus@yandex.ru

Introduction

Dendrimers are highly branched synthetic polymers, usually organized according to three structural building blocks: the core block as the origin of branching points; repeating blocks and the functional groups as the ending structure. The study of structural properties of dendrimers is very important for understanding their physical behavior and interactions with the environment and with other compounds. These studies are also important in the design of structures and in the discovery of new applications.

Diffusion properties can be studied by the following methods: NMR, fluorescence, UV−vis, AFM [1], but NMR is preferable due to the possibility of measurements and a well-established technique. Also, diffusion properties can be theoretically studied using molecular dynamics (MD) simulations and it is most natural to compare the translational mobility data from MD with the results of diffusion measurements in an NMR experiment.

One important application, where translational mobility data can be utilized, is nanoparticle synthesis [2]. For example, it is shown in Ref. [3], that the translational mobility with / without nano particles inside the dendrimer is different.

However, the study of the diffusion properties of dendrimers in solutions or in a melt by molecular dynamics methods encounters various problems that can be caused by both modeling artifacts and by a rather long subdiffusion regime. For instance, several works have such problems [4, 5]. The aim of this work is to study problem of translational mobility in MD simulation. For this, a polybutyl carbosilane dendrimer of various generations (G2-G4) in a solution of chloroform was used.

Computer modelling

In order that the initial configuration of the system does not affect the results, a mixing procedure is carried out. A necessary condition for good mixing is the displacement of the macromolecule by 2Rg, for which an initial simulation of the solution with a dendrimer was carried out, which allowed the root mean square displacement (MSD) to significantly exceed the value of $(2Rg)^2$.

To establish the fact of reaching the diffusion mode, the following criterion was used: the slope of the function MSD (t) versus the offset time t in the double logarithmic scale should be equal to 1.

$$MSD = 6\pi D t^{\alpha} \quad (1)$$

Studied molecule was modeled with GROMACs package in chloroform solution. For each case with different generation and cell size was made an energy minimization and equilibration conducted in two phases – NVT and NPT. After, the MD simulations for 0.1–2 μs, depending on the generation was run.

It was found that the translational mobility of the dendrimer under consideration (CSD G = 2) in solution can be described by two modes: ballistic and diffusion modes. The absence of a subdiffusion regime was also confirmed when considering autocorrelation functions for the velocity of the center of mass of the dendrimer. The absence of a subdiffusion regime in CSD in solution allowed us to develop a methodology for studying the diffusion properties of a macromolecule.

When averaging over the entire trajectory (1 μs), the diffusion regime for MSD depending on the displacement time t' was observed from t' = 0.4 ns to 30 ns. To study the influence of the path length on the diffusion coefficient calculations, we constructed the MSD function for various lengths of the final path (Fig. 1). As can be seen from Figure 1, the interval of the correct trajectory substantially narrows with decreasing average length of the trajectory. This is due to the fact that averaging statistics for the MSD function are not enough at long times. According to the results of modeling dendrimers of various generations, it can be argued that to study the diffusion properties of dendrimers in a solution, it is necessary to use an interval of no more than 5% of the entire trajectory.

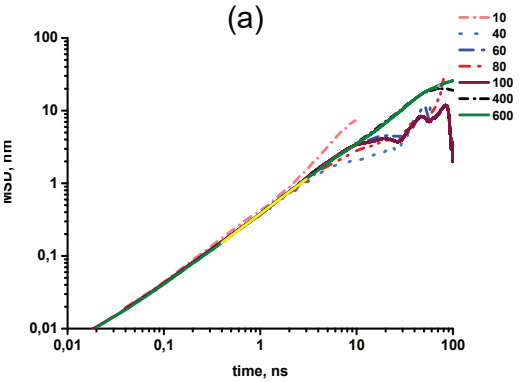

Figure 1. The root mean square displacement (MSD) as function of time averaged over different lengths of the time path (see legend) in a double logarithmic scale for a cell of 6.5 nm. The range of the diffusion regime is marked in yellow

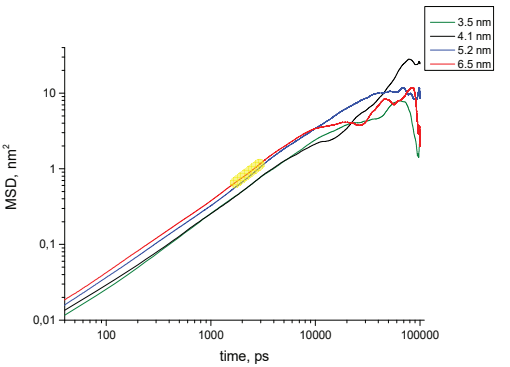

Figure 2. MSD as a function of time, for different sizes of cubic cells (see legend) in a double logarithmic scale. The range of the diffusion regime is marked in yellow

In fact, the condition was also verified that cell sizes should not affect the diffusion of the macromolecule. To verify this condition, cells with different amounts of solvent were modeled (Fig. 2). The size of the simulation ranged from 4 Rg to 10 Rg. The minimum cell sizes

were established, which are necessary for realistic translation mobility and the correct calculation of the diffusion coefficient.

Fig. 3 shows the MSD function for generations G2-G4. As can be seen from the figure, the range of the diffusion regime shifts by an order to large times region with an increase in the number of dendrimer generations from 2 to 4. This fact significantly complicates obtaining the correct data of translational mobility for high generations dendrimers, because the simulation trajectory have to be increased proportionally.

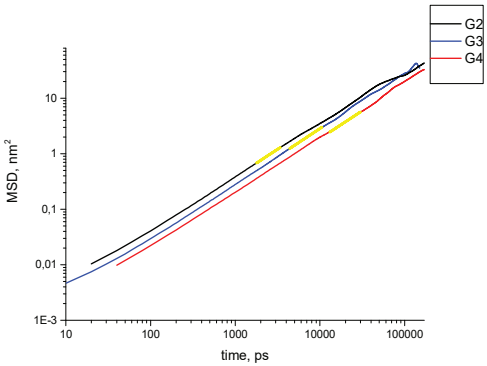

Figure 3. MSD as a function of time for various generations. The range of the diffusion regime for each generation is marked in yellow

Acknowledgements

Helpful discussions with Dr. Maxim Dolgushev are gratefully acknowledged. MD simulations were carried out in the computing resource center of St. Petersburg State University. This work is supported by Russian Science Foundation (grant № 19-13-00087).

References

1. Ramos M.C., Horta V.A.C., Horta B.A.C. Molecular Dynamics Simulations of PAMAM and PPI Dendrimers Using the GROMOS-Compatible 2016H66 Force Field. - *J. Chem. Inf. Model* (2019).
2. Yamamoto K. et al. New Horizon of Nanoparticle and Cluster Catalysis with Dendrimers. - *Chemical Reviews* (2020).
3. Yang P.Y. et al. Molecular dynamics simulations of PAMAM dendrimer-encapsulated Au nanoparticles of different sizes under different pH conditions. - *Comput. Mater. Sci.* (2017).
4. Molina N. et al. Dendrimeric antigens for drug allergy diagnosis: A new approach for basophil activation tests. - *Molecules* (2018).
5. Barra P.A. et al. Drug-dendrimer supramolecular complexation studied from molecular dynamics simulations and NMR spectroscopy. - *Struct. Chem.* (2014).

3 Tau Model: Interpretation of FFC-NMR profiles

Remi Kogon[1], Anastasiia Nagmutdinova[2], Leonardo Brizi[1], Villiam Bortolotti[2], David Faux[3], Peter McDonald[3]

[1]Department of Physics and Astronomy, University of Bologna, Italy
[2]Department of Civil, Chemical, Environmental and Materials Engineering, University of Bologna, Italy
[3]Department of Physics, University of Surrey, Guildford, Surrey, GU2 7XH, UK
E-mail: remialbert.kogon2@unibo.it

Introduction

Fast Field Cycling (FFC), a robust non-destructive technique, allows us the possibility to get the spin-lattice relaxation rates T_1^{-1} as a function of different NMR working frequencies (dispersion profile curves), from kHz to MHz [1]. The interpretation of this data is very challenging, especially when the dispersion curves concern the motion of spin-bearing molecules confined in pores of porous media such as cement paste, oil rocks, etc... The shape and magnitude of the dispersion curve is driven by the spin dynamics and the motion timescale is large - from picoseconds to microseconds. In order to extract the time parameters of the spin motion, models which can predict the dynamics of spins have been created [2, 3]. The 3 Tau model from Faux *et al*. describes the motion of spins, it evolves from Korb's model and defines and uses 3 correlation times to describe the molecular dynamics [4]. This model can fit the experimental dispersion curves from porous media with or without paramagnetic impurities. In this work we will focus on a system which contains paramagnetic impurities. A GUI Matlab script, called 3TM, permits a friendly use of the 3 Tau Model in order to achieve excellent fits of the experimental relaxation rates over the full frequency range and to obtain good values for the three different correlation times [5]. With these parameters it is possible to get additional information. The underpinning science behind the 3τ model will be described, and the analysis of the software will be demonstrated with synthetic data.

1. The 3Tau Model

1.1. The 3Tau Model and physics

The physical principles of the 3 Tau model are grounded in molecular dynamics simulations, and a sketch of the physics of the 3 Tau model is shown in Fig.1 [6-8]. Parallel to the surface, the proton from the surface of the pore moves according a diffusion time constant τ_l, representing the diffusion correlation time for spins within the layer surface. The proton contained in bulk water or remaining water is characterized by a diffusion time constant τ_b, representing the diffusion correlation time for spins within the bulk water. Its order of magnitude is around few picoseconds. The final time constant is τ_d, representing the surface residency time, the characteristic time it takes a spins to desorb from the surface layer to the bulk water.

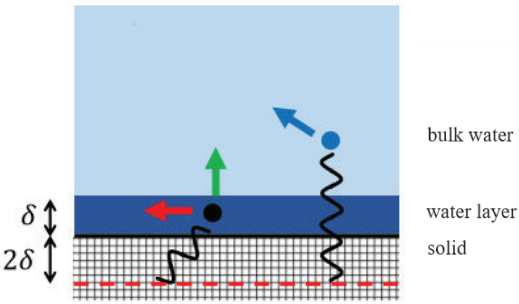

Figure 1. The arrows represent the layer spin diffusion (red), desorption (green) and bulk diffusion (blue). T_1^{-1} *is influenced by the interaction of fixed paramagnetic impurities. Its density is represented by a monolayer (dashed line) which is at 2δ (δ=0.27 Å) below the surface*

1.2. The spin-lattice relaxation rate dispersion $T_{1,Th}^{-1}$

In order to define the 3 Tau model some steps are necessary. The first step is to determine the probability spin density function; this can be done as computing a solution of the diffusion equation for the geometry related to the problem. The second step is to determine the time-dependent dipolar correlation function G(t is to apply the Fourier transform to the G(t) function in order to get the spectral densities J(ω). Then, the spectral densities are used to calculate the relaxation rate $T_{1,\sigma Y}^{-1}$ of fluids within porous media [9]:

$$T_{1,\sigma Y}^{-1}=\frac{1}{3}\beta_{\sigma I}[7J_{\sigma Y}(\omega_\sigma)+3J_{\sigma Y}(\omega_I)]$$

Where the subscript "Y" refers to either surface layer (l) or bulk (b), where $\beta_{\sigma I}=(\mu_0/4\pi)^2\gamma^2{}_I\gamma^2{}_\sigma\hbar^2S(S+1)$, I refers to the proton spin (I=1/2) and γ_σ is the gyromagnetic ratio for the paramagnetic impurity with S=5/2 for Fe^{3+}. ω_I is the angular Larmor frequency for proton and that for the impurity is ω_σ=658.21ω_I.

The spectral densities $J_{\sigma b}$ are associated with the specific parameter τ_b. Whereas, the spectral densities $J_{\sigma l}$ are associated according different τ_d, which are also dependant of τ_l i.e. given by the τ_l value, the range of τ_d is different and so different spectral densities $J_{\sigma l}$ are correlated.

Then, the complete expression for the relaxation rate $T_{1,Th}^{-1}$ is defined as [4]:

$$T_{1,Th}^{-1}=N_v\left[xT_{1,\sigma l}^{-1}+(1-x)T_{1,\sigma b}^{-1}\right]$$

Where x is the fraction of the total number of spins in the surface volume and the density N_v is the number of paramagnetic impurity/nm^3.

2. 3TM interface

2.1. Fitting process

The interface package 3TM permits an easy use of the 3 Tau Model to fit to the FFC-NMR experimental dispersion curves data. This package has been written under GUI Matlab. It allows the user to import their experimental FFC-NMR profiles and to select the options to run the fitting process.

The fitting process is obtained by the Gauss-Newton minimization method. It is explained in the Fig.2. To test the goodness of the 3TM fitting package, its efficiency has been

demonstrated on synthetic profile referring to a sample with paramagnetic impurities. The best fit is found by getting the minimum χ^2 fit error. The fit parameters are τ_d, τ_l, τ_b, N_v, x and the range of the T_1/T_2 ratio.

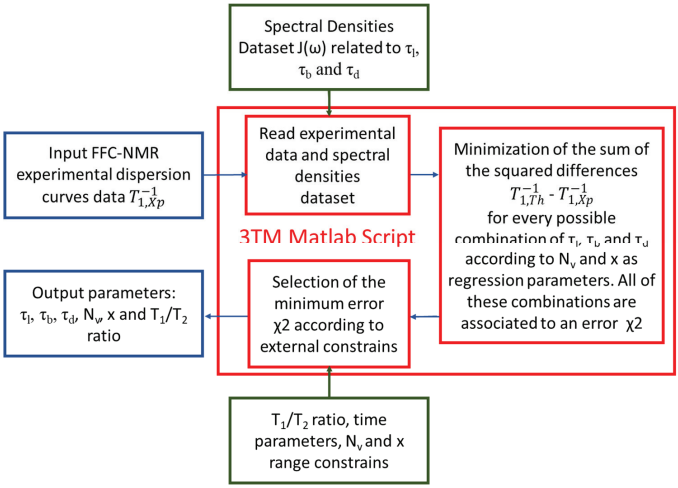

Figure 2. The flow diagram gives a friendly illustration of the functionalities of the 3TM interface package

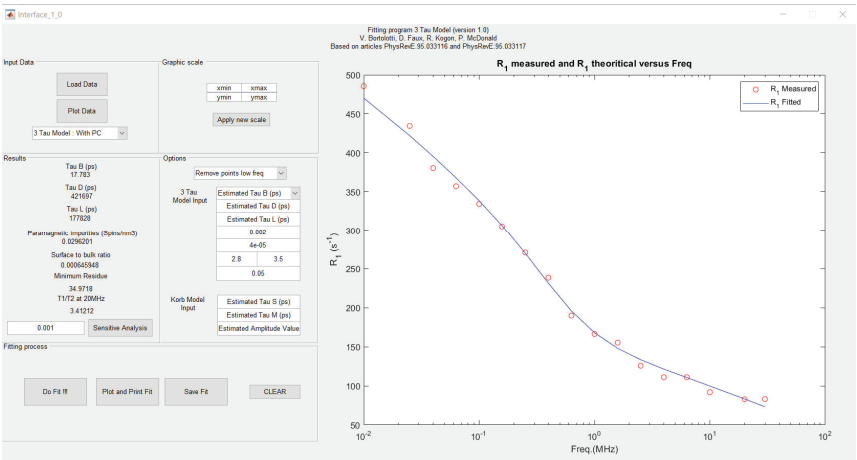

Figure 3. 3TM interface post fitting is shown. Synthetic data has been fitted

2.2. Using of the 3TM interface

The Fig. 3 shows the 3TM interface with which it is possible to set, among other things, the initial values of the different time parameters, and also the range of the T_1 and T_2 ratio at 20MHz (a useful constrain to drive the minimization process). As regression parameters for the fitting minimization process, N_v and x parameters can be also changed. It is possible to perform a sensitive analysis according to a specific percentage of the χ^2 minimum error. The percentage

can be chosen by the user, if not a default value is used. The fitting process is realized according to a tolerance parameter, the finer the more accurate fitting. Output data can be saved on a text file, which will include the fitted best value of parameters τ_d, τ_l, τ_b, N_v, x and T_1/T_2 ratio, and the range of these parameters according to the sensitive analysis. The Korb Model has been also implemented in order to compare results computed by the 3 Tau Model.

To validate and verify the 3TM script, synthetic dispersion profiles have been created using the spectral densities dataset and adding a Gaussian noise. The plot in fig. 3 and the data in table 1 demonstrate the excellent performance of the 3TM script.

Table 1. Comparison between the experimental/synthetic data and the theoretical data found by the 3 Tau Model fitting process

Fitted relaxation rate data (ms^{-1})	***Experimental/Synthetic relaxation rate data (ms^{-1})***	***Fitted relaxation rate data (ms^{-1})***	***Experimental/Synthetic relaxation rate data (ms^{-1})***
470.19	485.56	121.57	110.99
422.06	434.52	110.65	111.07
395.17	380.36	99.83	91.89
367.95	357.01	83.25	82.89
338.39	334.16	73.28	83.18
306.26	305.12	***Fitted Parameters***	***Experimental/Synthetic Parameters***
270.05	270.93	N_V=0.02962 spins/nm^3	N_V=0.03 spins/nm^3
231.56	238.65	x=0.000646	X=0.0007
195.92	190.08	t_B=17.78 ps	t_B=17.78 ps
168.10	166.49	t_D= 0.42 µs	t_D= 0.31 µs
148.11	155.42	t_L= 0.17 µs	t_L= 0.15 µs
133.56	125.92	T_1/T_2 = 3.14	T_1/T_2 = 3

Acknowledgements

This work is supported by Horizon 2020 – Marie Skłodowska-Curie – Innovative Training Network (ITN) – 2017 Actions. Grant Agreement no. 764691.

References

1. R. Steele, G. Ferrante. Fast Field Cycling NMR Relaxometry - from molecular dynamics to practical applications. – Fast field cycling NMR relaxometry project, 2018.
2. J.-P. Korb et al. Translational diffusion of liquids at surfaces of microporous materials: Theoretical analysis of field-cycling magnetic relaxation measurements. – Magnetic Resonance Imaging, 1998.
3. S. Stapf et al. Proton and Deuteron Field-Cycling NMR Relaxometry of Liquids in Porous Glasses: Evidence for Levy-Walk Statistics. – Physical Review Letters, 1995.
4. D. A. Faux, P. J. McDonald, Phys. Rev. E., 95, 033117 (2017).
5. D.A. Faux. Advances in the interpretation of frequency-dependent nuclear-magnetic resonance measurements from porous material. – Molecules, V. 24, 2019
6. Faux, D.A.; McDonald, P.J.; Howlett, N.C.; Bhatt, J.S.; Churakov, S.V. Phys. Rev. E 2013, 87, 062309.344.
7. Bhatt, J.S.; McDonald, P.J.; Faux, D.A.; Howlett, N.C.; Churakov, S.V. Int. J. Quant. Chem. 2014, 114, 1220.345.
8. Faux, D.A.; Cachia, S.H.P.; McDonald, P.J.; Bhatt, J.S.; Howlett, N.C.; Churakov, S.V. Phys. Rev. E 2015,346 91, 032311.
9. Abragam, A. Principles of nuclear magnetism; Clarendon Press, Oxford, 1961.

Free induction decay and primary echo in linear flexible polymers

Tatiana P. Kulagina[1], Grigorii E. Karnaukh[1], Irina Yu. Golubeva[1,2]

[1]Institute of Problems of Chemical Physics RAS, Semenov prospec 1t, Chernogolovka, Moscow region, 142432, Russia
[2]Moscow State University, Moscow
E-mail: tan@icp.ac.ru

Introduction

For carrying out operated synthesis and application of linear flexible polymers (FP) data on their structure, molecular mobility and diffusion are necessary. The data are defined by different methods of NMR [1]. The method of NMR relaxation allows define topological structure and molecular mobility in FP [2, 3].

In linear FP the topological structure depends on mean molecular weight M_w: at $M_w < 10^4$ chains in a sample are the chains with free ends, at M_w increases the physical network of entanglements starts being formed [2]. Earlier the theory of free induction decay (FID) and solid-echo (SE) in the three-spin system with arbitrary constants of dipole-dipole interaction (DDI) was suggested [4]. A general approach to deriving formulas for calculating the of spin echoes decay signal was developed and applied to obtaining data on random processes in linear and crosslinked polymers with different topological structures [3].

In this work the theory of FID and SE in linear polymers containing three spin groups is suggested.

The theory of free induction decay in linear polymers with the group of three-spin

The experimental dependence of the spin–spin relaxation time T_2 on the average molecular weight M_w and temperature for linearpolymers shows that T_2 decreases with an increase in M_w and that the high_temperature range has two clearly pronounced breaks [1]. For any chemical structure of a polymer, the first break is observed at $M_w > 10^4$ and the second one, at $M_w > 10^5$; with a further increase is M_w, T_2 remains unaltered. The observed $T_2(M_w)$ dependence has been qualitatively explained in [1] and connected with the appearance of entanglements with an increase in Mw. To explain these experimental data, a theory has been developed that allows modeling the dependence of spin–spin relaxation on the average length of polymer chains and temperature [2, 3].

We assumed that a short-chain polymer can be envisioned as a chain with free ends. An increase in M_w leads to the appearance of physical nodes (entanglements), and, once a certain M_w value has been achieved, there is formed an entanglement quasi-network, which is most pronounced in the high temperature range. In this model, the free polarization decay in linear polymers is represented as the sum of the FIDs of chains with free ends ($G_0(t)$) and chains with fixed ends ($G_c(t)$):

$$G(t) = (1 - p)G_0(t) + pG_c(t), \quad (1)$$

where p is the fraction of chains connected by physical nodes.

The FIDs for chains with free ends $G_0(t)$ are calculated using the Anderson–Weiss model with the molecular motions correlation function $k_0(\tau)$:

$$k_0(\tau) = (1 - \alpha)k_1(\tau) + \alpha k_2(\tau), \quad (2)$$

where the correlation functions $k_1(\tau)$ and $k_2(\tau)$ are the correlation functions of Bloembergen-Persell-Pound and Kargin-Slonimskii-Rouse, accordingly. To study the effect of the average

molecular weight on the topological structure of linear polymers, the FID was simulated at different average lengths of polymer chains in a wide temperature range. Comparison with experimental data [1] was performed (Fig. 1) and showed qualitatively consistent with the experimental data.

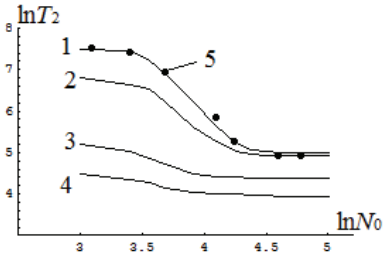

Figure 1. The dependence of time spin-spin relaxation T2 on molecular weight [2]: τ_c: $5 \cdot 10^{-4}$ (1), 10^{-3} (2), 10^{-2} (3), $5 \cdot 10^{-3}$ (4), points – data [1]

Proposed above theory can describe FID and the line shape in linear polymer which contains dedicated three-spin groups. Expression of FID for the whole spin system is as follows:

$$G(t) = G_3(t)G_r(t), \tag{2}$$

where $G_r(t)$ is the signal of a linear polymer, $G_3(t)$ is the signal of three-spin group [4]. The line shape F(ω) is calculated by means of Fourier's transformation (2).

Primary-echo in linear polymers

According to the theory of spin echo with magnetic field gradient [3], the amplitude of the *i*th echo signal A_{id} ($1 \le i \le 5$) is related to the mean square of the random phase shift $\langle \delta^2 \varphi_i \rangle$ due to a change in the local magnetic field on the nucleus spin [3]. I On the base of general approach to deriving formulas for calculating the of spin echoes decay signal in view of the additivity of the displacements $s(t_i, t_j)$ over the time interval $[t_i, t_j]$, for each realization of the random process, the following equality holds: For the correlation of the displacements the next expression is valid:

$$\langle r(t_1,t_2)r(t_3,t_4)\rangle = \frac{1}{2}\left(\langle r^2(t_1,t_4)\rangle + \langle r^2(t_2,t_3)\rangle - \langle r^2(t_1,t_3)\rangle - \langle r^2(t_2,t_4)\rangle\right) \tag{3}$$

For steady-state process we obtain:

$$\langle r^2(t_1,t_2)\rangle = \langle r^2(0,t_2-t_1)\rangle = \langle r^2(t_2-t_1)\rangle. \tag{4}$$

Using formula (3), (4), we obtained expressions for the mean squares of displacements for echoes 1 (primary echo), 4, and 5, the following expression was derived:

$$\left\langle \left(r(0,\tau)-r(\tau,2\tau)\right)^2 \right\rangle = 4\langle r^2(\tau)\rangle - \langle r^2(2\tau)\rangle, \tag{5}$$

where τ is a time between pulses.

Primary echo signal was expressed as:

$$A_r(t,\tau) = \frac{G^2(t)G^2(\tau)}{G(t+\tau)}. \tag{6}$$

Expression of primary echo after the second pulse in linear polymers with group of three-spin is the next:

$$A(t) = A_3(t)A_r(t), \tag{7}$$

where A_3(t) is the spin echo of three spin group with arbitrary constant DDI [4].

In Fig. 2 the signal of Fourier's transformation of primary echo in linear polymers with the equal constants DDI is given.

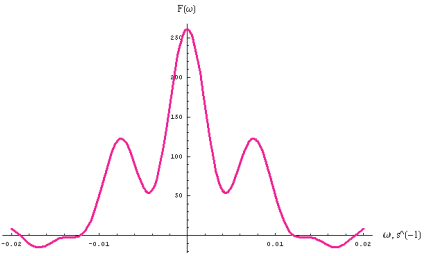

Figure 2. Fourier's transformation of primary echo signal, calculated by formulas (7)

A theory of the line shape in linear polymers with three-spin groups is proposed. Computer simulation of the signals showed the influence of $G_3(t)$ on FID and primary echo signals. That allows getting more information about the structure and mobility of polymer chains.

Acknowledgements

This work was performed in accordance with the state task, state registration No. 0089-2019-0002

References

1. M. Kehr,. N. Fatkullin, R. Kimmich, *J. Chem. Phys.*, **126**, 094903-094910 (2007).
2. T.P. Kulagina, V.A. Varakina, A.N. Kuzina, *Doklady Phys. Chem.* **444,** 79-82 (2012).
3. T.P. Kulagina, G.E. Karnaukh, A.N. Kuzina, L.P. Smirnov, *Russian Journal of Phys. Chem. B.* **7,** 170-176 (2013).
4. T. P. Kulagina, G. E. Karnaukh, I. Yu. Golubeva. *J. Applied Magnetic Resonance* **51**, 155-163 (2019).

Registration of weak spectral lines in NMR-spectra of organic liquids in Earth magnetic field

Pavel Kupriyanov, Vladimir Chizhik

St. Petersburg State University, St. Petersburg, 199034 Russia
E-mail: p.kupriyanov@spbu.ru
http://magres.ru

For the first glance, the absence of chemical shifts in proton NMR-spectra in the Earth magnetic field makes this method unattractive to researchers. However, the measurements of ^{13}C-^{1}H coupling constants would compensate this disadvantage. Unfortunately, the natural content of the ^{13}C isotope is very low and requires signal accumulations that is very difficult due to fluctuations of Earth magnetic field, which are especially strong under laboratory conditions. The original algorithm applied to a series of NMR-signals allows the neutralization of the influence of field fluctuations. The main condition for the realization of this method is the presence of a single strong line in a NMR-specrum of a sample under investigation. In the spectra of most organic substances, such a line is observed from hydrogen nuclei bound to the ^{13}C carbon isotope.

The NMR in Earth magnetic field technique has a number of advantages: (i) there are no permanent electro- or superconducting magnets that significantly decreases the cost of equipment, (ii) the high mobility of devices, (iii) the highest absolute resolution of spectral lines can be reached, (iv) it is possible to examine liquids in sealed containers of large volume.

The original algorithm was realized in the equipment created in the Saint Petersburg State University [1, 2]. The volume of samples is about 100 ml (it can be changed in a wide diapason if necessary), the current of prepolarization is 1,5 A. The experiment duration did not exceed 10 min.

The NMR-spectra in Earth magnetic field of some organic liquids were registered (see Fig. 1-4). The spectra reliably reflect the lines due to the interaction of protons with ^{13}C nuclei of natural content.

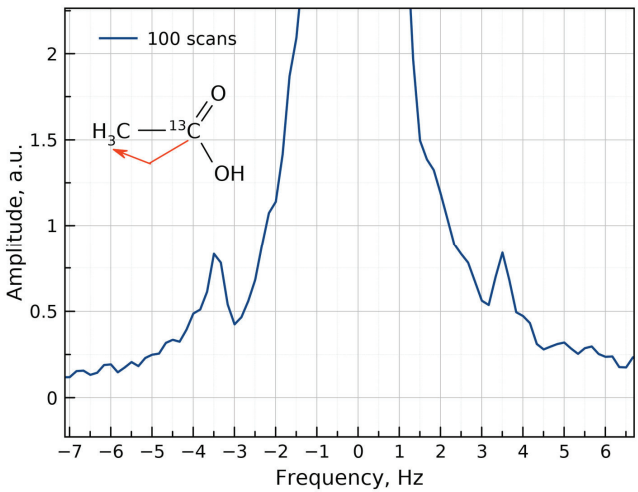

Figure 1. NMREF-spectrum of Acetic acid, 100 scans

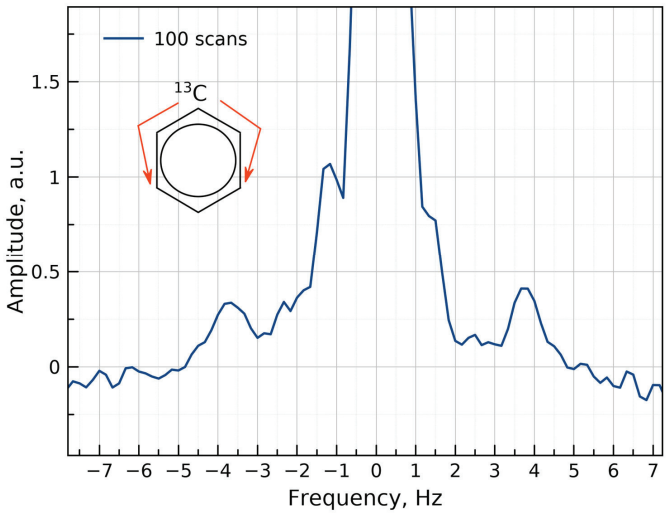

Figure 2. NMREF-spectrum of benzene, 100 scans

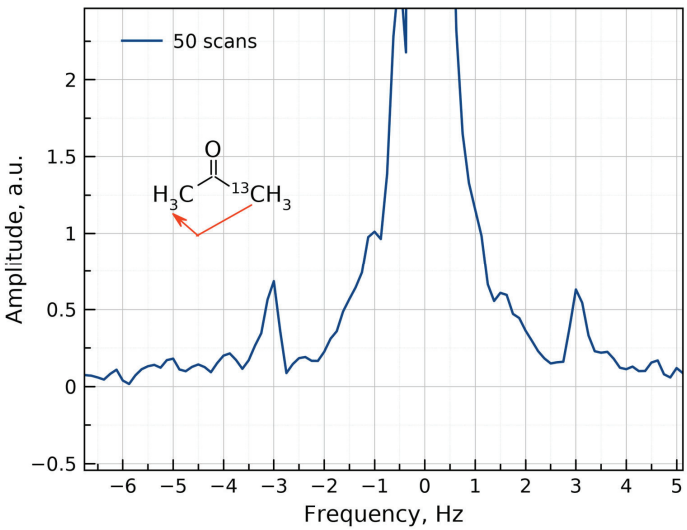

Figure 3. NMREF-spectrum of acetone, 50 scans

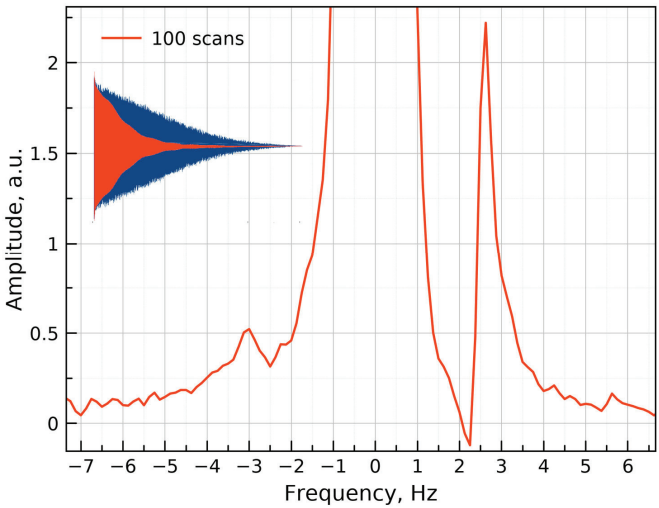

Figure 4. NMREF-spectrum of acetone without algorithm, 100 scans, signal FID (top left) one scans (blue) and accumulated (red)

References

1. Kupriyanov P.A., Dmitriev K.A., Chizhik A.V. "On some improvements in the registration of nuclear magnetic resonance in the earth's field" Bulletin of St. Petersburg University. Series 4: Physics, Chemistry, 2016.V. 3 (61), no. 1, p. 60-70 (in Russian)
2. Chizhik V.I., Kupriyanov P.A. “Neutralization of fluctuations in resonance conditions during registration of NMR spectra in the Earth's magnetic field” Spinus. Magn. res. app. Abstracts. 2018. p. 198-199

^{14}N NQR relaxation study of tetrazole derivatives

Galina Kupriyanova[1], Sultonazar Mamadazizov[2], George Mozzhukhin[2]

[1]I. Kant Baltic Federal University, Kaliningrad 236041, Russian Federation,
[2]Department of Physics, Gebze Technical University, Gebze/Kocaeli 41400, Turkey
E-mails: sultonazar.mamadazizov@mail.ru, mgeorge@yandex.ru, galkupr@yandex.ru

Tetrazole family is a class of nitrogen compounds that recently attracted much attention due to a broad range of potential applications, such as powerful explosives, solid rocket propellant fuels as well as novel biologically active substances. ^{14}N NQR is a unique method for studying the molecular structure and dynamics of highly nitrogenous compounds such tetrazole derivatives, since it allows one to obtain detailed information both on the movement of ring nitrogen and on the dynamic processes associated with the formation of hydrogen bonds N-H in monohydrates [1, 2]. It should be noted the important advantages of the ^{14}N NQR method in the study of tetrazole derivatives. The ^{14}N NQR method allows the detection of signals from all nonequivalent quadrupole nuclear in a wide frequency range from 400 to 4000 kHz. The symmetry of solid crystals uniquely determines the positions of the ^{14}N quadrupole nucleus and the number of lines for nonequivalent nuclei. Therefore, NQR provides chemically specific information for nitrogen compounds comparable to fingerprints [3].

Theoretical studies have been conducted previously to provide ^{14}N NQR data calculated by the means of DFT for 1-Phenyl-1H-tetrazole-thiol, 5-aminotetrazole (Fig.1), 1H-tetrazole and analysis of ^{14}N spectra shifts due to intermolecular and intramolecular distances changes. Additional attention was paid to study influence of phenyl and amino groups on corresponding nitrogen ^{14}N NQR data and its neighbors in tetrazole ring. Information on correct assignment, hydrogen bond formation and bonding of tetrazole ring with different radical was obtained. Interconnected transitions (that is the transitions belonging to the same type of centers) were established by conducting two-frequency ^{14}N NQR experiments [3, 4].

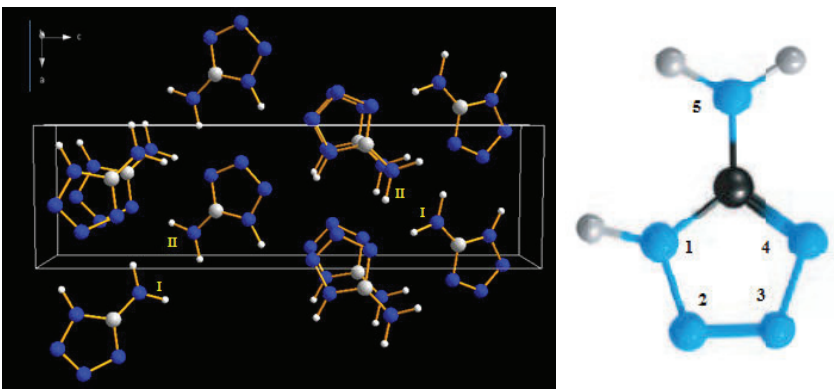

a) *b)*

Figure 1. Unit cell in [0 1 0] viewing directions (a) of 5-aminotetrazole (b)

^{14}N NQR relaxation experiments were carried out at the frequencies of ring nitrogen and NH_2 nitrogen in order to study dynamic processes. Carr-Purcell-Meiboom-Gill (CPMG) and the inversion-recovery sequences were used to measure the T_2, T_1 relaxation times in 5-aminotetrazole monohydrate [6, 7]. The modified RILT script executed in the MatLab environment was applied to process the experimental data. The distribution functions of

relaxation times f (Ti) for N2 and N3 (Fig.1 (b)) which are the inverse integral Laplace transform of the experimental data ^{14}N are two-component. The relaxation process is satisfactorily described in the framework of the model of vibrational molecular motion developed by Bayer and Osokin [8, 9]. It was found that the high-temperature approximation satisfactorily describes the spin-lattice relaxation process for N 2 and 3. However, this model does not explain the absence of a temperature dependence at the frequency (v-). In addition, this model does not adequately describe the relaxation process of N1, N 4 nuclei involved in the hydrogen bond and NH of the nearest protons. In this paper, a new approach is proposed to describe the dynamics of these nuclei, taking into account a number of factors.

1. The effect of hydrogen bonds N1..N .. N 4 is taken into account the dipole – dipole interaction with the nearest protons, the distance to which varies, as well as increasing the degree of boundedness of the vibrational motion. 2. The process of cross-relaxation between two nitrogen nuclei in the NH2 group of neighboring molecules located antisymmetrically, belonging to types I and II (Fig. 1). These nuclei have the same ^{14}N NQR frequencies, and the directions of the axes of their electric field gradient tensors are different. The following relaxation equations are used :

$$\frac{dn^{(I)}}{dt} = -R(I)n^{(I)} + rn^{(I)} \qquad n^{(I,II)} = \begin{pmatrix} N_1 - N_{01} \\ N_2 - N_{02} \\ N_3 - N_{03} \end{pmatrix}$$
$$\frac{dn^{(II)}}{dt} = -R(II)n^{(II)} + rn^{(II)}$$

Here, n is the population difference matrix Ni - Ni0 of the nuclear level ^{14}N, R (I, II) relaxation matrix for I and II types (Fig.1 (a)), r is the cross-relaxation rate between the excited states. A comparison of the results with experimental data showed that the proposed approach can be used to explain the specific features of the dynamics of the ^{14}N nuclei in the NH and NH_2 groups.

References

1. E. Balchin *et al.*, “Potential of nuclear quadrupole resonance in pharmaceutical analysis,” *Anal. Chem.*, vol. 77, no. 13, pp. 3925–3930, 2005.
2. J. Barras, K. Althoefer, M. D. Rowe, I. J. Poplett, and J. A. S. Smith, “The Emerging Field of Medicines Authentication by Nuclear Quadrupole Resonance Spectroscopy,” *Appl. Magn. Reson.*, vol. 43, no. 4, pp. 511–529, 2012.
3. S. Mamadazizov, M. G. Shelyapina, G. S. Kupriyanova, and G. V. Mozzhukhin, “New assignment of14N NQR spectral lines for tetrazoles derivatives,” *Chem. Phys.*, 2018.
4. G. V. Mozzhukhin, B. Z. Rameev, N. Doğan, and B. Aktaş, “The Application of the Two Frequency Composite Pulses for NQR Detection of Nitrogen-Based Compounds,” *J. Supercond. Nov. Magn.*, vol. 24, no. 1–2, pp. 653–658, Jan. 2011.
5. G. V. Mozzhukhin, J. Barras, G. Kupriyanova, and B. Rameev, “Two-Frequency Nuclear Quadrupole Resonance for Line Identification,” *Appl. Magn. Reson.*, vol. 46, no. 2, pp. 161–179, Feb. 2015.
6. J. Pirnat *et al.*, “14N NQR in the tetrazole family,” *Chem. Phys.*, vol. 364, no. 1–3, pp. 98–104, 2009.
7. G. S. Kupriyanova, G. Mozzhukhin, S. Mamadazizov. ^{14}N NQR relaxation in 5 aminotetrazole. Spinus. Saint- Petersburg, Russia. 1- 6 April 2018, p.212
8. A.Safin, D.Ya. Osokin. Nuclear quadrupole resonance in nitrogen compounds. Moscow. 1977
9. H.Bayer, Z. fur Phys. 130, 227 (1951).

Self-diffusion and relaxation of gaseous ^{3}He in oriented aerogels

V. Kuzmin[1], K. Safiullin[1], A. Stanislavovas[1], M. Tagirov[1,2]

[1]Kazan Federal University, 420008, Kremlevskaya 18, Kazan, Russian Federation
[2]Institute of Applied Research, Tatarstan Academy of Sciences, Kazan, 420111, Russian Federation

Introduction

Aerogels are objects of many recent scientific studies. Due to their high porosity and low thermal conductivity they are widely used in space technology, for example as a thermal insulator and a Cherenkov radiation detectors [1]. Aerogels are materials with very low dielectric constant which allows to use them in microelectronics for reducing the stray capacitance. It is known that a dielectric constant of aerogels depends on porosity [1]. ^{3}He is a one of the best probe for studies of the magnetic properties of nanosized porous samples at low temperatures due to sufficiently long relaxation times and the absence of a nuclear quadrupole moment [2-5]. It is found that chaotic and oriented aerogels have significant effects on certain properties of ^{3}He NMR in superfluid phases and normal states at very low temperatures [6-9].

Experimental

The study of ^{3}He gas self-diffusion and spin-lattice relaxation in five types of ordered Al_2O_3 aerogels with different density (82, 125, 180, 597 and 920 mg/cm^3) was performed. The samples with higher densities (597 and 920 mg/cm^3) were fabricated from 82 and 125 mg/cm^3 samples, respectively, by technique described in [10]. It included the soaking of aerogel in the water for 20 minutes and drying at the room temperature for 48 hours.

A series of gas pressure dependencies *versus* amount of ^{3}He in the samples with different types of surfaces (raw and modified by N_2 or ^{4}He) are measured at 4.2 K. It is known that ^{3}He atoms build a monolayer on substrate surface at a temperature of 4.2 K and changes negligibly at pressures higher than 50 mbar amount of adsorbed ^{3}He not depends on gas pressure.

The ^{3}He gas diffusion and relaxation study was carried out using pulsed NMR methods at temperature of T = 4.2 K (and 1.5 K for relaxation experiments) at frequency of f_0 = 16 MHz (H_0 = 490 mT) and in constant magnetic field gradient of G = 2.2 mT/cm (only for diffusion experiments).

Results

^{3}He gas self-diffusion

The ^{3}He gas density observed from isotherms is higher than expected for free gas.

The measured diffusion coefficient of ^{3}He atoms in aerogels are significantly suppressed by the immobile adsorbed layer of ^{3}He (the estimated diffusion coefficient in the adsorbed layer lies between 10^{-9} and 10^{-8} cm^{2}s^{-1} depending on the layer coverage [11, 12]). This is confirmed by two facts: 1) the diffusion coefficient anomalously drops at low pressures compared to expected for free gas diffusion; 2) the covering of the aerogel surface with monolayer of ^{4}He significantly increases the measured gaseous ^{3}He diffusion coefficient at low pressures.

Following refs. [13] and [14] the apparent diffusion in aerogels is just weighted diffusion between that in the adsorbed layer and that in the gas phase. As diffusion in the gas phase is much faster than in the adsorbed layer the apparent diffusion in the aerogel is assumed to be governed by a “fast exchange” process. The model of two-phases “fast-exchange” process is correct if the lifetime of ^{3}He atom in each phase is much shorter than measured time. This condition is always obeyed in present work, as the estimated typical lifetime of ^{3}He atom in

adsorbed layer is 1 ns and in gas phase is 10 ns. Both values are much shorter than typical measured time.

It was found that value of diffusion coefficient of ^{3}He atoms in gas phase D_{gas}^{aero} is less than expected for ideal gas at low pressure range, where the fraction of adsorbed atoms is large. In addition, the computed values of D_{gas}^{aero} does not depend on type of sample surface (raw or covered by N_2 or ^{4}He). Therefore, the observed effect of slow gas diffusion cannot be explained by the influence of surface diffusion. Unfortunately, the simplest Knudsen model cannot describe the decreasing of the ^{3}He diffusion coefficient at low temperature. This fact can be ascribed to the influence of the Van der Waals forces created by the fibers, which is indirectly confirmed by ^{3}He gas densification.

More details will be presented in oral report.

^{3}He gas spin-lattice relaxation

The observed linear increase of T_1 with ^{3}He gas amount indicates on the surface relaxation involved in the total ^{3}He relaxation process. After excluding of ^{3}He adsorption by ^{4}He pre-plating an increase of T_1 by order of magnitude was observed. In that case the influence of surface relaxation through ^{3}He adsorbed layer should be negligible and other rather weak remained relaxation mechanisms should dominate. Among them we discuss the spin-lattice relaxation due to atoms motion in gas in inhomogeneous magnetic fields created by fibers for different diffusion motion regimes in aerogels. In addition, we consider a possible sources of inhomogeneity: a paramagnetic centers in the aerogel, the diamagnetic susceptibility of the fibers and a possible existence of “dirty” aerogel fibers surrounded by rather clean fibers. In the latter case the nuclear magnetic relaxation should be governed by the time needed for atoms to diffuse to “dirty” walls (fibers). The bulk ^{3}He spin-lattice relaxation time is known to be extremely long. The mechanism a of dipole-dipole relaxation of ^{3}He gas in restricted geometry considered in [16] is omitted as being negligible for large pores and open pore geometry in aerogels.

More details will be presented in oral report.

This work was financially supported by the Russian Science Foundation (grant RSF 20-42-09023).

References

1. Yu. K. Akimov, Instrum. Exp. Tech., 46, 287 (2003).
2. E. M. Alakshin et. al., JETP Lett., 107, 2, 111 (2018).
3. L. J. Friedman et. al., Phys. Rev. Lett., 47, 1078 (1981).
4. L. J. Friedman et. al., J. Low Temp. Phys., 55, 83 (1984).
5. V. Kuzmin et. al., Phys. Chem. Chem. Phys., 20, 1476 (2018).
6. V. V. Dmitriev et. al., Phys. Rev. Lett., 115, 165304 (2015).
7. D. Candela and N. Kalechofsky, J. Low Temp. Phys., 113, 3/4, 351 (1998).
8. V. V. Dmitriev et.al., JETP Lett., 101, 12, 808 (2015).
9. N. Zhelev. et. al., Nat. Commun., 7, 12975 (2016).
10. V. V. Volkov et. al., Instrum. Exp. Tech., 60, 737 (2017).
11. B. P. Cowan et. al., Phys. Rev. Lett., 38, 165 (1977).
12. B. Cowan et. al., Phys. B, 165, 707 (1990).
13. R. Valiullin et. al., J. Phys. Chem. B, 109, 5746 (2005).
14. J. A. Lee et. al., Phys. Rev. B: Condens. Matter Mater. Phys., 90, 174501 (2014).
15. E. Collin et. al., Phys. Rev. B: Condens. Matter Mater. Phys., 80, 094422 (2009).
16. J.-P. Korb, Shu Xu, and J. Jonas, J. Chem. Phys., 98, 2411 (1993).

Development of novel membranes based of PA with MOFs for pervaporation separation of methanol/toluene mixture

A. I. Kuzminova, A. V. Penkova, M. E. Dmitrenko, A. A. Zolotarev, S. S. Ermakov

St. Petersburg State University, St. Petersburg, 199034 Russia
E-mail: ai.kuzminova@mail.ru

Introduction

Pervaporation is a promising method for the separation of liquids in the bioprocessing, petrochemical and pharmaceutical industries. This method allows to separate closely boiling and thermally unstable components, as well as azeotropic mixtures and mixtures of isomers. Pervaporation is an environmentally-friendly method of separation, for its implementation does not require expensive equipment and high energy consumption. The rapid development of pervaporation requires the search for new high-performance membrane materials with desired properties.

In the present work the influence of bulk modification on transport properties of novel membranes based on polyphenylene isophthalamide (PA) was studied. Bulk modification was carried out by incorporation of the metal-organic framework UiO-66(NH_2)-EDTA into membrane matrix. The porous structure of the metal-organic frameworks leads to the improvement of the transport properties of PA membranes. The study of structural and physicochemical properties of the membranes was carried out by NMR spectroscopy, scanning electron microscopy, IR spectroscopy, contact angle and swelling degree measurements. The transport properties of the developed membranes were studied by pervaporation separation of the azeotropic methanol – toluene mixture (72 wt.% of methanol). All developed membranes were highly selective for methanol. The introduction of UiO-66(NH_2)-EDTA into the PA matrix leads to significant changes in both the physicochemical and transport properties of polyphenylene isophthalamide membranes.

Acknowledgements

This work was supported by Russian Science Foundation [grant No. 17-73-20060]. The experimental work was facilitated by equipments from Interdisciplinary Resource Centre for Nanotechnology, Magnetic Resonance Research Centre, Thermogravimetric and Calorimetric Research Centre, Centre for X-ray Diffraction Studies, Chemical Analysis and Materials Research Centre, Nanophotonics Centre and Centre for Geo-Environmental Research and Modelling at St. Petersburg State University.

Translational diffusion in thermotropic ionic liquid crystals

D. Majhi[1], M. Cifelli[2], S. V. Dvinskikh[1,3]

[1]Department of Chemistry, KTH Royal Institute of Technology, Stockholm, 10044, Sweden,
[2]Dipartimento di Chimica e Chimica Industriale, Universita di Pisa, 56124 Pisa, Italy
[3]Laboratory of Bio-NMR, St. Petersburg State University, St. Petersburg, 199034, Russia
E-mail: sergeid@kth.se

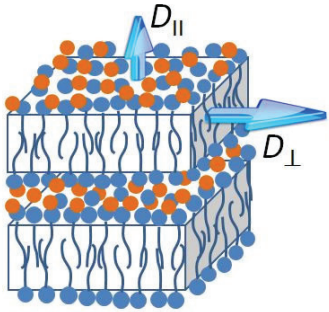

Organic salts with melting points below 100°C are classified as ionic liquids (ILs). Ionic liquids capable of self-assembling into thermodynamically stable liquid-crystalline phases, on cooling from the isotropic state, are referred to as ionic liquid crystals (ILCs) [1]. Thermotropic mesogenic materials, consisting solely of cations and anions, have the typical properties of ionic liquids, as well as nano-scale structures of liquid crystals, where high degrees of molecular translational and rotational mobilities are combined with partial orientational and positional orders. This synergy leads to new dynamic properties exploited, for example, in the development of functional materials for low dimensional transport of electrons, ions, and molecules in electrochemical energy conversion and storage technologies [2]. For these applications, understanding the molecular/ion transport and dynamics is essential.

The translational diffusion coefficients of molecules/ions in ILCs can be accurately measured by pulsed-field-gradient NMR [3, 4]. Diffusion anisotropy is most easily accessed if a mesophase sample is macroscopically aligned. The anisotropic diamagnetic susceptibility of mesogenic functional groups induces a macroscopic molecular alignment in the presence of a strong magnetic field of NMR spectrometer. This provides access to the diffusion anisotropy by applying gradients in orthogonal directions.

Anisotropic diffusion was observed in the smectic and columnar ionic phases [4-6]. Diffusion was found to be faster within the aggregates, layers or columns, compared to the diffusion across the aggregates. The anisotropy varied with the type of anion: a relatively small anisotropy was found for the decreased interactions (electrostatic attraction, hydrogen bonding) between the cation and anion. A strong hydration effect on the diffusion anisotropy, which was related to the water contribution to the hydrogen-bonding network in the ionic sublayers, was observed. The diffusion coefficients near the phase transition were of the same order of magnitude with the relationship: $D_{within} > D_{iso} > D_{across}$. This general behaviour is consistent with the results of molecular dynamics computational analysis of diffusion in the ionic smectic phase.

Diffusion coefficients deliver direct molecular level information on translation mobility, and thus contribute to the fundamental understanding of the complex ion dynamics in ionic liquid-crystalline materials. The obtained diffusion data have provided support for structural models in ILCs. Ion diffusion coefficients depend on the extent of ionic association, and thus

reflect ionic activity. Advances in understanding molecular/ion diffusion processes assisted the molecular-level explanation of the macroscopic conductivity behaviour in an anisotropic low-dimensional environment.

This work was supported by the Swedish Research Council and by the RFBR grant 17-03-00057.

References

1. Goossens K, Lava K, Bielawski CW, et al. Ionic Liquid Crystals: Versatile Materials. Chem Rev. 2016;116:4643-4807.
2. Kato T, Yoshio M, Ichikawa T, et al. Transport of ions and electrons in nanostructured liquid crystals. Nat Rev Mater. 2017;2:17001.
3. Dvinskikh SV, Furó I. Nuclear magnetic resonance studies of translational diffusion in thermotropic liquid crystals. Russ Chem Rev. 2006;75:497-506.
4. Dvinskikh SV. Nuclear magnetic resonance studies of translational diffusion in thermotropic ionic liquid crystals. Liq Cryst. 2019.
5. Cifelli M, Domenici V, Kharkov BB, et al. Study of Translational Diffusion Anisotropy of Ionic Smectogens by NMR Diffusometry. Mol Cryst Liq Cryst. 2015;614:30-38.
6. Frise AE, Dvinskikh SV, Ohno H, et al. Ion Channels and Anisotropic Ion Mobility in a Liquid-Crystalline Columnar Phase As Observed by Multinuclear NMR Diffusometry. J Phys Chem B. 2010;114:15477-15482.

Cation dynamics in hydrated ionic liquid crystals

Debashis Majhi[1], Jing Dai[1], Andrei V. Komolkin[3], Sergey V. Dvinskikh[1,2]

[1]Department of Chemistry, KTH Royal Institute of Technology, SE-10044 Stockholm, Sweden
[2]Laboratory of Biomolecular NMR, Saint Petersburg State University, Saint Petersburg 199034, Russia
[3]Faculty of Physics, Saint Petersburg State University, Saint Petersburg 199034, Russia
Email: majhi@kth.se

Introduction

Ionic liquid crystals (ILCs) are composed solely of cations and anions and feature the remarkable properties of liquid crystals such as optical anisotropy, ordered microstructure, and high ionic conductivity [1,2]. Recently, ILCs have emerged as promising materials in numerous chemicals and industrial applications which includes electrochemistry, catalysis, synthesis, photovoltaics, and lubrication [3]. Therefore, there has been a growing body of research targeting to design the ILCs with an increasingly larger temperature range of mesophase stability. It has been observed that the long alkyl chain (n≥12) imidazolium-based ionic liquids exhibit liquid-crystalline state. Electrostatic and hydrogen bonding interaction among the cation and anion are the two main driving forces in ILCs, responsible for their liquid-crystalline behavior. The mesophase stability increases with increasing the strength of H-bonding interaction among anions and cations in imidazolium based ILCs. Previously, some studies have suggested that the presence of a trace amount of water in ILC samples increases the mesophase stability in a wider range of temperature [1]. Water molecules form hydrogen bond with the anions and weaken the hydrogen bond between cation and anion. Hydration increases the mesophase stability in ILCs by formation of hydrogen bond network in the ionic layers. Presence of water molecule in ILCs not only modifies the hydrogen bonds but also affects the dynamics and cation conformation in the mesophase. However, no experimental evidence is available to support this scenario. To the best of our knowledge, there has been no study on the change of the cation dynamics at a molecular level upon hydration. In our work, we investigate the coupling between molecular ordering and the hydrogen-bonding interaction contributing to phase stabilization.

Results and discussion

We have studied ionic dynamics by measuring local and molecular orientational order parameters in anhydrous and monohydrated 1-dodecyl 3-methyl imidazolium bromide (C_{12}mimBr) and 1-dodecyl 3-methyl imidazolium chloride (C_{12}mimCl) by using advanced solid-state NMR methods. Translational dynamics in mesophase was also explored. Theoretical DFT optimized molecular geometry studies have been carried out to support the experimental results.

The mesophase stability range in anhydrous and hydrated samples of both the ionic liquid crystals were examined by checking the phase transition temperatures. The mesophase of hydrated samples is stabilized in a larger temperature range as compared to that in anhydrous materials. The C-H bond order parameters S_{CH} and order parameters S for cations of both C_{12}mimBr and C_{12}mimCl samples in anhydrous and hydrated form are estimated by performing ^{13}C-^{1}H dipolar NMR spectroscopic measurements [4]. The order parameters for both the alkyl chain carbons and imidazolium ring carbons are calculated. Remarkably, lower order parameters are found in hydrated as compared to anhydrous materials. Different temperature dependence behavior of the order parameter of alkyl chain carbon has been observed in hydrated samples as compared to the data with the anhydrous samples. For hydrated salts, the order parameter shows relatively weak temperature dependence and goes a plateau with decreasing temperature for both the ILCs.

The translational diffusion coefficients of the ILCs in hydrated and anhydrous samples are measured by using pulse field gradient NMR technique combined with spin-decoupling. In mesophase, the diffusion coefficients are calculated along ($D_{\parallel}$) and perpendicular ($D_{\perp}$) to the director. Relatively larger diffusion anisotropy $D_{\perp}/D_{\parallel}$ is found in the hydrated samples as compared to anhydrous materials. The results indicate that upon hydration, the translational mobility within the layers accelerates to a greater extent compared to that across the layers. The observed effects on ionic mobility of ILCs are important for the understanding of the specific roles of various intermolecular interactions that give rise to the dynamic properties of ionic liquid crystals.

Acknowledgements

Authors thank Swedish Research Council VR and the Russian Foundation for Basic Research grant 17-03-00057 for providing the funding.

References

1. K. Goossens, K. Lava, C.W. Bielawski, K. Binnemans, *Chem. Rev.* **2016**, *116*, 4643-4807.
2. A. A. Fernandez, P.H.J. Kouwer, *Int. J. Mol. Sci.* **2016**, *17*, 731.
3. T. Kato, M. Yoshio, T. Ichikawa, B. Soberats, H. Ohno, M. Funahashi, *Nat. Rev. Mater.* **2017**, *2*, 17001.
4. J. Dai, D. Majhi, B. B. Kharkov, S. V. Dvinskikh, *Crystals* **2019**, *9*, 495.

The studies of temperature-dependent ^{14}N NMR relaxation

G. V. Mozzhukhin[1], G. S. Kupriyanova[2], S. Mamadazizov[2], B. Z. Rameev[1,3]

[1]Gebze Technical University, 41400 Gebze/Kocaeli, Turkey
[2]Baltic Federal University by Immanuel Kant, 236041 Kaliningrad, Russian Federation
[3]Zavoisky Physical-Technical Institute, FRC Kazan Scientific Center of RAS, 420029 Kazan, Tatarstan, Russian Federation
Email: mgeorge@yandex.ru

^{14}N NMR measurements of the relaxation parameters of liquids may be utilized for the detection of dangerous or illicit substances [2] by low field (< 1 T) NMR device. ^{14}N NMR can be also applied in the measurements of quadrupole constants of nitrogen in various liquids [2]. The quadrupole constants may be calculated from the ^{14}N NMR relaxation parameters T_1 and T_2. Following the paper [3], the similar approximations were used: i) narrowing limit $(\omega_0\tau_c)^2<<1$; ii) substances have isotropic molecular reorientations. In this approach, we can use the following expression for the quadrupole contribution to the relaxation rate. In this approximation the relaxation times of the transverse and longitudinal relaxation are equal:

$$\left(\frac{1}{T_1}\right)_Q = \left(\frac{1}{T_2}\right)_Q = \frac{3}{8}\left(1+\frac{\eta^2}{3}\right)\left(\frac{e^2Qq_{zz}}{\hbar}\right)^2\tau_c . \quad (1)$$

Studies of quadrupole relaxation allow us to estimate the quadrupole coupling constant e^2Qq_{zz}, if the correlation time of molecular motion and asymmetry parameter η are known.

With used the Stokes-Einstein-Debye model [4] for the correlation time of rotational motion of spheroid molecules in a solution in the diffusion limit. In this case, it is defined by molecular volume V, viscosity and temperature of a solution:

$$\tau_C = \frac{4\pi a^3}{3kT}\sigma, \quad (2)$$

where a is the radius of a molecule with the volume of V, σ is a viscosity, k is a Boltzmann constant, T is the absolute temperature.

The relaxation data were used to estimate quadrupole coupling constants in [5-7]. However, this approach does not produce data which enough to determine quadrupole constants unambiguously, because based on a linear approximation to the data borrowed from the measurements in solid and gaseous states.

To avoid this limitation, we designed time-domain NMR measurement system to perform the ^{14}N NMR relaxation measurements in the temperature range from 1°C to 30 °C. The setup for these experiments consists of a permanent magnet with a magnetic field of 0.575 T and a home-made RF probe with a resonance frequency of about 1.770 MHz. *Tecmag Apollo* NMR console and 500 W *Tomco* power amplifier were used in the NMR experiments. The temperature probe was made using a *Julabo* refrigerated - heating circulator. In this work we present the results of the measurements in a solution of nitric acid (65% of HNO_3, Riedel-de Haen AG) and acetonitrile (CH_3CN, 99.8% Merck).

References

1. G.V. Mozzhukhin, G.V. Kupriyanova, S.Sh. Mamadazizov, A. Maraşlı, B.Z. Rameev, Low-field 14N nuclear magnetic resonance for detection of dangerous liquids, Chem. Phys. 513 (2018) 129-134.
2. A.N.Troganis, C.Tsanaktsidis, and I.P.Gerothanassis, 14N NMR relaxation times of several protein amino acids in aqueous solution- comparison wit 17O NMR data and

estimation of the relative hydration numbers in cationic and zwitterionic forms, J. Magn.Reson. 164 (2003) 294-303.
3. M. Witanovski, Nitrogen N.M.R. Spectroscopy, Pure Appl. Chem. 37 (1-2) (1974) 225-233.
4. A. Abragam, The Principles of Nuclear Magnetism, The Clarendon Press, Oxford, 1961, p. 314.
5. G.J.Jenks, NMR Investigation of the Nitrogen Quadrupole Coupling Constant in Liquid Samples, J. Chem. Phys. 54 (2) (1971) 658-663.
6. A.Loewentein. Nuclear quadrupole coupling constants in the liquid phase. Adv.in Nuclear Quadrupole Resonance. Ed.: J.A.S. Smith, Vol. 5, 1983, p. 53-82.
7. W. B. Moniz and H. S. Gutowsky, Nuclear Relaxation of N14 by Quadrupole Interactions in Molecular Liquids, J. Chem. Phys. 38 (1963) 1155-1162.

^{1}H NMR detection of liquids in bottles with use of surface coils

G. V. Mozzhukhin[1], G. S. Kupriyanova[2], A. Maraşlı[1], S. Mamadazizov[2], M. Vafadar[1], B. Z. Rameev[1,3]

[1]Gebze Technical University, 41400 Gebze/Kocaeli, Turkey
[2]Baltic Federal University by Immanuel Kant, 236041 Kaliningrad, Russian Federation
[3]Zavoisky Kazan Physical-Technical Institute, 420029 Kazan, Russian Federation
E-mail: mgeorge@yandex.ru

The nuclear magnetic resonance (NMR) is a well-known method for analysis of liquids. The method includes the spectral and relaxation analysis of substances. In the case of mobile devices for analysis and identification of liquids, the NMR measurements of relaxation parameters can be applied. The application of this approach is described in [1]. Time-domain NMR (TD-NMR) measurements up to three parameters (T_1, T_2, D) may be used by TD NMR device to detect the type of chemical substance. We studied the NMR detection of the bottle using gradiometric surface coils in partially shielded probe

In low-field TD NMR application the quality of probe-head and permanent magnet have an important role. The probe-head of NMR TD devices is usually made of the parallel or serial resonance LC circuit. The current in the resonance L coil creates the radiofrequency radiation for the signal excitation in the sample. The commonly used coils in commercially available TD NMR spectrometers are the solenoidal and saddle ones, while planar coils are needed for a distant detection of the signal. The planar coils, however, have much less RF field homogeneity in comparison with the solenoidal and saddle coils. Planar coils are advantageous for use when the object of observation is bigger than the coil. In this case, it is not possible to use an RF shield to enclose the detection probe. Thus, two important requirements for the probe-head used in the distant detection should be satisfied: i) the probe should be designed in a way to mitigate outside noise, because the shielding in real devices may be done only partially; ii) in the small and mobile bottle scanner devices, the bottles and plastic containers may be larger than the RF probe. We have also a problem with homogeneity of the permanent magnet for the containers such as plastic soft drink bottles. One of the possible solutions for attenuation of interference is to use of gradiometric coils [2, 3]. We used a planar gradiometric coil [3] with the attenuation value of far interference of at least 20 dB.

The system was assembled with use of *Magritek KEA-2* NMR console and homemade probe with a flat coil of the diameter of 3 cm. We also used permanent homemade magnet tuned to 8.860 MHz of NMR proton resonance. The distance between magnet poles was 6.5 cm. The surface coil consists of two concentrical parts. These parts of the planar coils were connected in such a manner that a current flowing in these parts creates the magnetic fields in their centers with directions opposite to each other, producing the closed loops of the RF magnetic field in near zone. The NMR signal can be excited and detected at most for the distances of about one radius of a circular part of this probe. On the other hand, noise signals due to far distance sources produce the currents compensating each other in these two parts of gradiometer. The gradiometric coil has a size of 3x6 cm (Fig.1). We used three types of coils: two printed boards coils with circular (the diameter of 3 cm) and rectangular (3x3 cm) parts and the coil consisting of two rectangular coils (3x3 cm) wounded from a litz wire.

We also studied the distribution of magnetic field inside our permanent magnet. One of these plots is presented in Fig.2. We see that only small region (approximately 10x10 mm) in the center of the magnet has enough homogeneity with the magnetic field value of 208 mT.

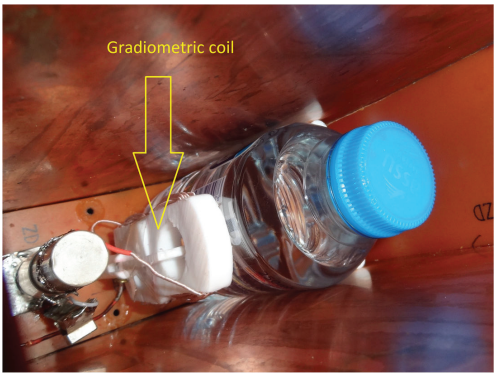

Figure 1. Probe for NMR measurements relaxation parameters in bottles

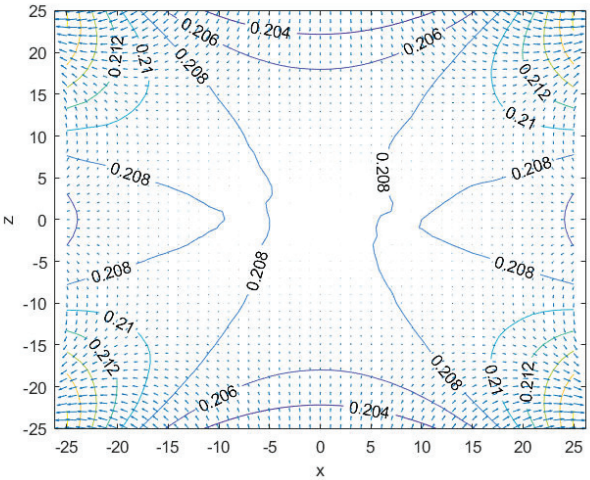

Figure 2. The distribution of the induction of the magnetic field in the permanent magnet system

There is a vast number of various methods for measurements of T_1 and T_2. The most frequently used methods of the measurements are the following ones: free induction decay (FID), saturation recovery sequence, spin-echo multipulse sequence and Carr-Purcell-Meyboom-Gill sequence (CPMG). We carried out the test measurements using sunflower oil and pure water. We defined some conditions that allow reaching the results close to the measurements with the use of a usual solenoidal coil.

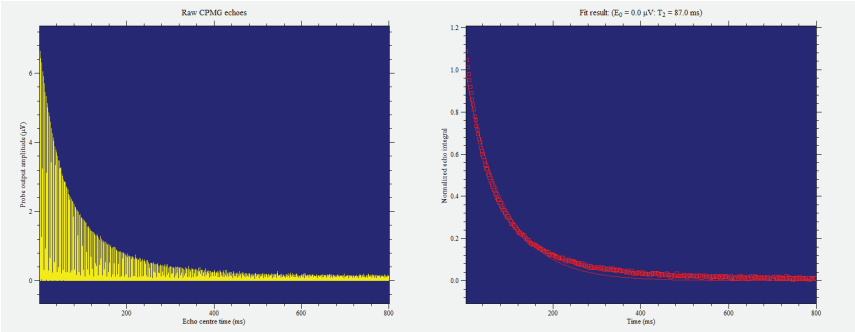

Figure 3. The results of the measurement of sunflower oil with the use of the planar coil

Conclusion

We designed magnet and probe head for the measurements of T_1 and T_2 parameters of liquids in the bottles. The measurement shows that the use of surface coils and a magnet with a large distance between poles allows obtaining good results in the measurements of T_1 and T_2 relaxation parameters for the detection of liquids

References

1. L.Burnett, J.Mauler, E. Danieli, F. Casanova, B. Blümich, “Identification of liquids encountered in carr-on-luggage by mobile NMR”, In: Explosives Detection using Magnetic and Nuclear Resonance Techniques, NATO Science for Peace and Security Series B: Physics and Biophysics.] ed. By J.Fraissard, O. Lapina, Springer, 193-203 (2009).
2. B.H.Suits,et.el., Solid State Magnet.Reson., 24, 123-136(2003).
3. G. V. Mozzhukhin, A. V. Efremov, A. V. Bodnya and V. V. Fedotov, A Two-Spiral Flat Coil for Detecting 14N NQR Signals, Russian Physics Journal, 2005, Volume 48, Number 9, Pages 978-983

Vicinal H/D isotopic effects on δ^1H in NMR spectra of hydrogen-bonded cyclic hererocomplexes formed by phosphinic and phosphoric acids

Valeria Mulloyarova, Peter Tolstoy

Saint Petersburg State University, Saint Petersburg, Russia
E-mail: mylllerka20071993@gmail.com

Introduction

Phosphinic and phosphoric acids can form various hydrogen-bonded complexes. The types of self-association are different in the gas phase (cyclic dimers), crystals (cyclic dimers or infinity chains) and solutions. Thus, in aprotic solution all acids form cyclic dimers and trimers [1]. The equilibrium conditions are shifted towards the formation of cyclic trimers. In these complexes both (for the dimer) and three (for the trimer) hydrogen bonds are coupled cooperatively and all H/D isotopic effects on ^{1}H NMR chemical shifts are negative. The self-associates of phosphinic and phosphoric acids are formed by strong hydrogen bonds. The DFT calculations (B3LYP/6-311++G(d,p)) are shown that the hydrogen bond energies is ~ 11 and 13 kcal/mol per bond for dimers and trimers, respectively [2].

Heterocomplexes of phosphinic and phosphoric acids

In aprotic solution ($CDClF_2/CDF_3$) in a mixture of phosphorus-containing acids not only self-associates "homocomplexes" are formed, but also "heterocomplexes" in various combinations. The equilibrium conditions are shifted towards the formation of heterocomplexes. In Figure 1 the structures of cyclic heterodimer and heterotrimer are presented.

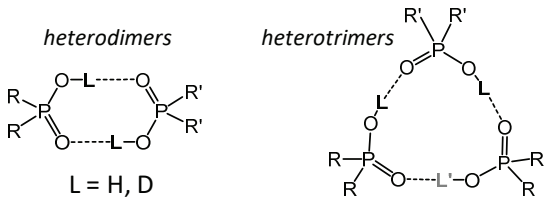

Figure 1. The structures of cyclic heterodimer and heterotrimer

By low-temperature ^{1}H NMR spectroscopy it was established that the chemical shifts of protons involved in the formation of hydrogen bonds in heterocomplexes are in a lower field than the protons in corresponding homodimer and homotrimer. Consequently, these hydrogen bonds are shorter and stronger. Partial deuteration at the hydroxyl position with MeOD was used to determine the stoichiometry of heterocomplexes. As a result of H/D replacement in one of the hydrogen bonds, the strength of neighboring hydrogen bonds is changes and H/D isotopic effects occur on ^{1}H chemical shifts. For example, Figure 2 shows the spectrum of partial deuterated sample (the degree of deuteration is ~ 57%) of $(MeO)_2POOH$ and $(PhO)_2POOH$ mixture. An analyses of these effects showed that, in general, the hydrogen bonds in heterocomplexes couple cooperatively (H/D isotopic effects are negative). However, anticooperativity contributes to the formation of hydrogen bonds in cyclic heterotrimers: with deuteration in one of the three proton positions HHD' the other two bonds are shortened and the H/D isotopic effects are positive in this case, while the deuteration in the other two position leads to negative H/D isotopic effects (cooperativity effect).

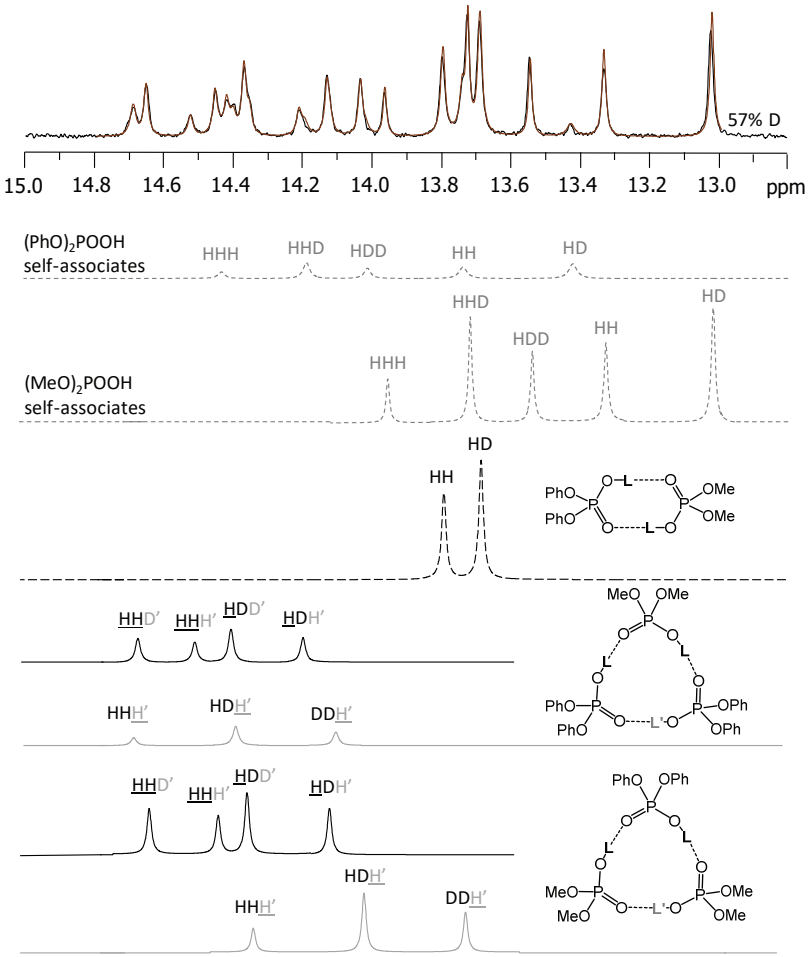

Figure 2. Low-field part of ^{1}H NMR spectrum of mixture of partial deuterated $(PhO)_2POOH$ and $(MeO)_2POOH$ acids in $CDClF_2/CDF_3$ at 100 K. Subspectra of individual complexesare presented in bottom: grey dashed line corresponds to the self-associates, black dashed line– heterodimer, black and grey solid lines – heterotrimers

Acknowledgements

This work has received financial support from the RSF Grant 18-13-00050.

References

1. V. V. Mulloyarova, I. S. Giba, M. A. Kostin, G. S. Denisov, I. G. Shenderovich, P. M. Tolstoy. – *Phys. Chem. Chem. Phys.*, 20, 4901-4910 (2018).
2. V. V. Mulloyarova, I. S. Giba, G. S. Denisov, A. S. Ostras', P. M. Tolstoy. – *J. Phys. Chem. A*, 123, 6761−6771 (2019).

Fast Field Cycling. Overview

Anastasiia Nagmutdinova[1], Remi Kogon[2], Leonardo Brizi[2] and Villiam Bortolotti[1]

[1]Department of Civil, Chemical, Environmental and Materials Engineering, University of Bologna, Italy
[2]Department of Physics and Astronomy, University of Bologna, Italy
E-mail: anastas.nagmutdinov2@unibo.it
https://www.unibo.it/sitoweb/anastas.nagmutdinov2

Introduction

Fast Field Cycling (FFC) Nuclear Magnetic Resonance (NMR) relaxometry allows non-destructive low-field measurements in the range of a few kHz up to around 100 MHz, depending on the instrument [1]. This technique is used for obtaining the longitudinal relaxation time (T_1) or relaxation rate ($R_1=1/T_1$) of magnetic field (or frequency) dependence. In the last case data displayed as Nuclear Magnetic Relaxation Dispersion (NMRD) profile [2], showed at the Fig.1 which is obtained using Stelar s.r.l. apparatus [3].

Application of this technique vary from medical use [4], to porous media and liquids [5].

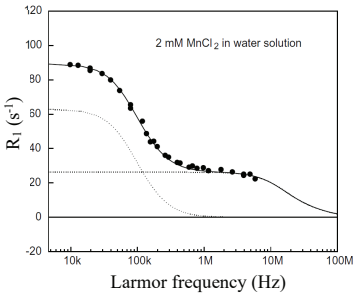

Figure 1. NMRD profile of 2 mM $MnCl_2$ aqueous solution. The fitted curve follows BBP theory [3]

Fast field cycling NMR experiment principle

FFC NMR technique addressed in this abstract refer to ^1H experiments. Thus, it provides data of ^1H-molecular dynamics (motions) in a variety of different environments, but depending on instrument setting any other NMR-sensitive nuclei could be investigated [6].

The typical FFC NMR experiment is showed in Figure 2.

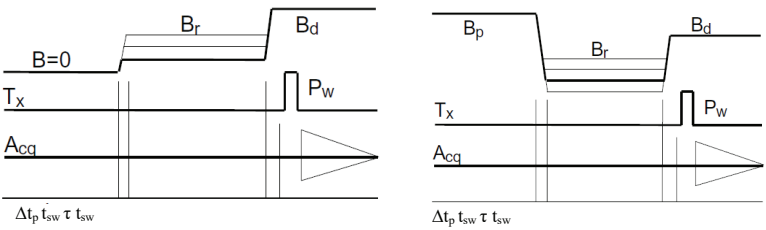

Figure 2. Schematic representation of the main FFC NMR experiments, a) non-polarized (NP), b) pre-polarized (PP) [3]

In the Pre-Polarized experiment, the sample is polarized in the high flux density B_p for a time Δt_p. With a time t_{sw} magnetic field is switched to a lower field B_r (in fig. 2 lines indicate

variable of magnetic field), where relaxation occurs. The goal is to make magnetic field change from B_p to B_r with the quickest possible switching time ($t_{sw} << T_1$). The signal remaining after this relaxation interval B_r is detected in a field of fixed high flux density B_d. Then an recycle delay for the restoration of magnetization follows until the next cycle. The difference in NP sequence is that the magnetization is built up during B_r field and sampled during B_d field [3].

The NMR signal is induced by the 90° RF or a spin echo pulse P_W at the resonance frequency determined by Larmor frequency of NMR nuclei under investigation [7].

Magnetic field cycling NMR technique could be divided into two types by the way of field switching methods: Fast Field Cycling is referred to electronically field switching and Field Cycling or "sample shuttle technique" is referred to mechanically moving the sample between different magnetic fields.

The FFC technique permits measurements over the range of 10^3 Hz < ν_p < 10^9 Hz. Limits at the high frequency are determined by the instrument. At low frequencies different problems could arise, such as: the "local field" from the residual spin couplings may exceed the external flux density in the relaxation interval; the compensation of the other magnetic field may interfere; T_1 at low-field may be too short to permit fast switching; the T_1 may be to short to follow validity condition from Bloch/Wangsness/Redfield theory $T_1 >> \tau_c$ [2].

Theoretical background

The FFC NMR technique is based on Wiener-Khinchin theorem, applicable to time averages of stationary stochastic variables [7]:

$$J(\omega) = \int_{-\infty}^{+\infty} g(\tau) e^{-i\omega\tau} d\tau ,$$

where $J(\omega)$ is a spectral density at the angular frequency ω and is a Fourier transform of autocorrelation function $g(\tau)$, where τ is a time variable conjugate to ω. Functions $J(\omega)$ and $g(\tau)$ provides the main information on molecular dynamic processes, that drive the relaxation.

Transition between energy levels of spin systems in a quantized field B_0 is represented by frequency ω and associated with angular Larmor frequency of the spin. Figure 3 shows the connection between physical background of FFC NMR, raw data from NMRD profile and theoretical model for the investigated system [7].

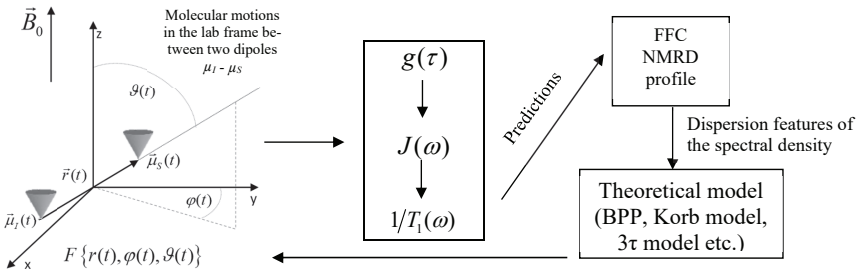

Figure 3. Schematic representation of the molecular dynamics, FFC NMR experiment and theoretical model relation

In terms of molecular orientation and neighbouring distance, the autocorrelation function is defined by a function *F(t)*, which contains thermally fluctuating spherical coordinates *r(t)*, *φ(t)* and *ϑ(t)* (see Figure 3).

The simple example of the autocorrelation function is a mono-exponential decay:

$$g(\tau) = \exp\left(-\frac{|\tau|}{\tau_c}\right),$$

which is a Fourie conjugate of the Lorentzian spectral density [7]:

$$J(\omega) = \frac{2\tau_c}{1+\omega^2\tau_c^2},$$

In this case dynamical process driving the spin fluctuation are characterized by only one correlation time τ_c. This theory is usually referred as Bloembergen-Purcell-Pound (BPP) model, which is applied for bulk liquids [3].

Theoretical model for FFC NMRD profile interpretation

In order to draw some conclusions on molecular dynamic of the investigated system from NMRD profile, theoretical models where developed. One of the first successful approach is BPP model, mentioned above. If the liquid is confined in a porous media and is in interaction with the surface, the theory complexity increases significantly. In such cases Korb model [8] or Kemmich model [9] could be used. Another model is 3τ model, developed by D. Faux and co-workers, characterized by 3 correlation times, is designed for fluid molecules at a flat pore surface, describing water molecules dynamic in two distinct environments [10].

Acknowledgements

This work is supported by Horizon 2020 – Marie Skłodowska-Curie – Innovative Training Network (ITN) – 2017 Actions. Grant Agreement no. 764691.

References

1. R. Steele, G. Ferrante. Fast Field Cycling NMR Relaxometry - from molecular dynamics to practical applications. – Fast field cycling NMR relaxometry project, 2018.
2. R. Kimmich, E. Anoardo. Field-Cycling NMR Relaxometry. – Progress in Nuclear Magnetic Resonance Spectroscopy, V. 44, 2004.
3. E. Anoardo et al. Field-Cycling NMR: Applications and Instrumentations. Stelar s.r.l. – Applied Magnetic Resonance, V. 20, 2001.
4. L.M. Broche et al. A whole-body Fast Field-Cycling scanner for clinical molecular imaging studies. – Scientific report, V. 9, 2019.
5. D. Kruk, A. Hermann, E.A. Rössler. Field-cycling NMR relaxometry of viscous liquids and polymers. – Progress in nuclear magnetic resonance spectroscopy, V. 63, 2012;
6. H.F. Pascal, E. Belorizky. Theory of fast field-cycling NMR relaxometry of liquid systems undergoing chemical exchange. – Molecular Physics, V. 117, 2018.
7. R. Kimmich. Field-cycling NMR Relaxometry. Instrumentation, Model Theories and Applications. Chapter 1, 2018.
8. S. Stapf et al. Proton and Deuteron Field-Cycling NMR Relaxometry of Liquids in Porous Glasses: Evidence for Levy-Walk Statistics. – Physical Review Letters, 1995.
9. J.-P. Korb et al. Translational diffusion of liquids at surfaces of microporous materials: Theoretical analysis of field-cycling magnetic relaxation measurements. – Magnetic Resonance Imaging, V. 16, 1998.
10. D.A. Faux. Advances in the interpretation of frequency-dependent nuclear-magnetic resonance measurements from porous material. – Molecules, V. 24, 2019.

Condensation of ammonium niobium oxalate studied by NMR crystallography and X-ray powder diffraction

Evgeniy Papulovskiy[1], Sergei D. Kirik[2], Dzhalil F. Khabibulin[1,3], Aleksandr A. Shubin[1,3], Valentina M. Bondareva[1], Aleksandr S. Samoilo[2], Olga B. Lapina[1,3]

[1]Boreskov Institute of Catalysis, pr. Lavrentieva 5, 630090, Novosibirsk, Russia
[2]Siberian Federal University, pr. Svobodny 79, 660041, Krasnoyarsk, Russia
[3]Novosibirsk State University, Pirogova 2, 630090, Novosibirsk, Russia
E-mail: fyr@catalysis.ru

Introduction

We found an unusual structure transformation in $NH_4[NbO(C_2O_4)_2(H_2O)_2]\cdot nH_2O$ using NMR crystallography that includes Solid-State NMR spectroscopy, X-ray powder diffraction and DFT calculations. It has been discovered that the mixture of known oxalate phases $NH_4[NbO(C_2O_4)_2(H_2O)_2]\cdot 3H_2O$ (Phase I) and $NH_4[NbO(C_2O_4)_2(H_2O)_2]\cdot 2H_2O$ (Phase II) treated at mild condition (temperature up to 100 °C in vacuo) induces an unknown crystal phase, catena-$NH_4[NbO_{2/2}(C_2O_4)_2(H_2O)]$ (Phase III).

The new orthorhombic phase has polymeric structure consisted of niobium polyhedra of seven vertices $[NbO_{2/2}(C_2O_4)_2(H_2O)]$ connected by oxygen bridges (—Nb—O—Nb—) forming an infinite zigzag chains along the $\vec{c}$ axis. The bridging oxygen atoms are connected to niobium atoms symmetrically with respect to the 2-fold axis. Each of them forms two identical bonds Nb-O of 1.892(6) Å length, indicating their origination from the condensation process. The niobium coordination polyhedron can be crossed by a plane passing through the Nb, O and H_2O positions. Having almost undistorted geometry, the oxalate groups lie in the opposite sides from the plane, making it look like blades of a propeller.

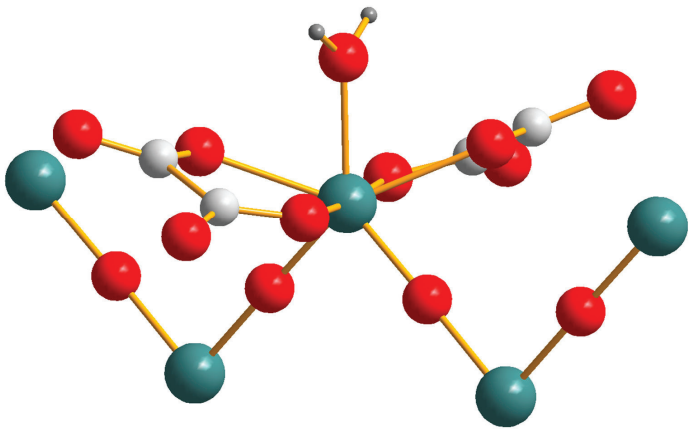

Figure 1. An infinite zigzag chain of —Nb—O—Nb— atoms surrounded by oxalate groups

In the new phase, Phase III, ^{93}Nb has unusually small nuclear quadrupole coupling constant mainly due to developed thermal mobility of the crystal lattice. Variable temperature ^{93}Nb, ^{2}H and ^{13}C NMR experiments together with DFT calculations confirm that the new Phase III has proton and ligand mobility. This mobility of the lattice correlates with the fact that hydrogen bonds present in the structure of Phases I and II virtually disappear in Phase III.

Hydrogen bonds were assumed to restrain the chelate group mobility while water loss removes the restrains, allowing the oxalate groups to move more freely; heating caused hydrogen bonds to disappear.

The main transformation factor at mild conditions *in vacuo* is the removal of water from the system. First, lattice water leaves the substance (Phase I → Phase II), followed by water coordinated to niobium atom (Phase II → Phase III). In this condition, niobium retains its coordination number, causing the bond order of Nb=O to decrease and the bridge structure —Nb—O—Nb— to form. At normal pressure, without evacuation, the substance becomes amorphous and dissolves in the excess of lattice water.

Acknowledgements

The authors thank for partial financial support RFBR17-03-00531 and budget project for Boreskov Institute of Catalysis. Prof. S. D. Kirik and Dr. A. S. Samoilo thank the state program of Ministry of Science and Education RF "Organization of scientific research #1025". The Siberian Supercomputer Center is gratefully acknowledged for providing supercomputer facilities. The authors are grateful to Dr. T. Yu. Kardash and Dr. A. S. Andreev.

NMR diffusometry study of ^{1}H-^{2}D isotope effect in nafion polymer electrolyte

A. F. Privalov[1], Elena Galitskaya[2], Vitaly Sinitsyn[2], Michael Vogel[1]

[1]Institute of Condensed Matter Physics, Technische Universität Darmstadt, Hochschulstr. 6, 64289, Darmstadt, Germany
[2]Institute of Solid State Physics RAS, 2 Academician Ossipyan str. 142432, Chernogolovka, Russia
E-mail: alexei.privalov@physik.tu-darmstadt.de

Introduction

Proton-exchange membraines of Nafion type are known for their fast mass transport, which is close to than in pure water at room temperature [1] while ionic conductivity is several orders of magnitude higher. The present study of the Isotope Effect (IE) aims at contributing to understanding of the mechanisms for mass transport in Nafion. In the literature are two possible diffusion mechanisms proposed: the hopping mechanism of the hydronium ions H_3O^+ (vehicular type) [2] or the Grotthuss mechanism, where the H^+ ions are transferred from one water molecule to another by breaking and forming hydrogen bonds (relay type) [3]. To determine the relevance of these migration mechanisms we investigated IE on diffusion coefficients of membranes loaded with H_2O and D_2O, respectively, because the values depend differently on the mass of the isotope for vehicular-type and relay-type transport. The translational mass transport is proportional to the square-root of the mass ratio [4] $D(m_1)/D(m_2) = \sqrt{m_2/m_1}$, which is around 1.06 for translation of water molecules. Experimentally for pure water a higher ratio of around 1.2 is found. Probable explanation is a contribution of the molecular rotation, where only protons or deuterons are moving while the oxygen is fixed. For such rotation IE must be around $\sqrt{m_D/m_H} \approx 1.4$ for H_2O and for H_3O^+. Thus, the IE in Nafion associated with combined rotation and translation of H_2O or H_3O^+ will be below 1.4. If the Grotthuss mechanism dominates and H^+ or D^+ migrate, IE will lead to a decrease in the translational mobility again by $\sqrt{m_D/m_H} \approx 1.4$. Thus, comparing the diffusion coefficients of protons and deuterons has the potential to provide information about the transport mechanism in Nafion.

Experimental

To measure this effect we exploit that static field gradient (SFG) NMR diffusometry [5]. For our measurements the stimulated echo sequence was used. The echo amplitude *S* decays due to free diffusion and spin relaxation according to:

$$S(t_e, t_m, g) = S_0 \cdot \exp\left(\frac{-t_m}{T_1}\right) \cdot \exp\left(\frac{-2t_e}{T_2}\right) \cdot \exp\left[(\gamma g t_e)^2 \cdot \left(\frac{2}{3}t_e + t_m\right) \cdot D\right] \quad (1)$$

As a typical example, Fig. 1 shows results from ^{2}H SFG NMR measurements at 295 K together with a global fit to the free-diffusion model in Eq. (1).

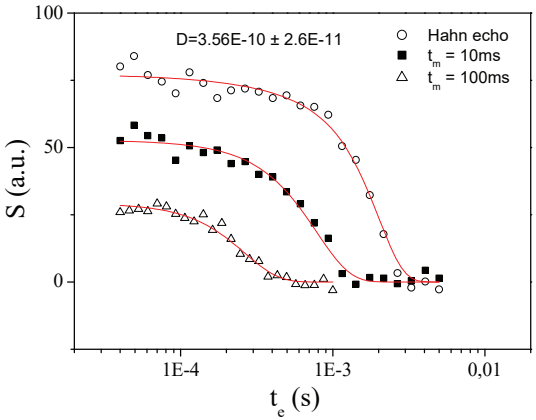

Figure 1. ^{2}H SFG NMR experiments on deuteron diffusion in Nafion 212 membrane at 295 K

Results and Discussion

Figure 2 shows temperature-dependent diffusion coefficients obtained from global fits of ^{1}H and ^{2}H SFG NMR diffusometry data for Nafion 212 membranes saturated at the same conditions with H_2O and D_2O, respectively.

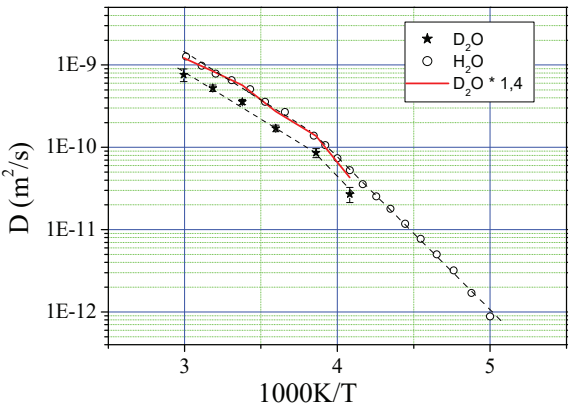

Figure 2. Temperature-dependent diffusion coefficients D measured by ^{1}H and ^{2}H SFG NMR diffusometry for Nafion 212 membranes saturated with H_2O and D_2O ($\lambda \approx 8.5$). The deuteron diffusivities scaled with factor 1.4 are shown as solid line

We see that the Nafion sample containing H_2O shows systematically higher diffusion coefficients with a factor of 1.4 than that containing D_2O, while the temperature dependence of proton and deuteron transport is very similar. The value of 1,4 is in full agreement with the IE expected for the Grotthuss mechanism for proton migration, while it is not compatible with the vehicular transport of hydronium ions. Nevertheless, we cannot exclude that, unlike in the bulk, rotational motion is the relevant process. In this case, the difference in the moments of inertia would dominate, which would also result in a factor of ~1.4. However, previous studies on

confined water did not observe that the relation between the rates of rotational and translational motions is significantly different between bulk and confined waters rendering this explantion for the IE unlikely.

Thus, we can conclude that, in Nafion 212 membranes with high water contents, the Grotthuss mechanism, or relay diffusion of $H^+(D^+)$ ions prevails over the vehicular mechanism, which involves $H(D)_3O^+$ ions, at least in the temperature range from 245 K to 332 K.

References

1. M. Saito, K. Hayamizu, and T. Okada, J. Phys. Chem. B, **109**, 3112 (2005)
2. K.-D. Kreuer, A. Rabenau, W.Weppner, Angew. Chem. Int. Ed:Engl. 21(3), 208 (1982)
3. J. F. Nagle and H. J. Morowitzt, *Molecular Mechanisms for Proton Transport in*
4. R. Mukundan, E. L. Brosha, S. A. Birdsell, A. L. Costello, F. H. Garzon, and R. S. Willms, J. Electrochem. Soc. **146**, 2184 (1999)
5. I. Chang, F. Fujara, B. Geil, G. Hinze, H. Sillescu, and A. Tölle, J. Non. Cryst. Solids. **172**–**174**, 674 (1994)

The NMR relaxation of solvent nuclei for monitoring protein aggregation

Sevastyan O. Rabdano[1], Sergei S. Bystrov[2], Carlos Cabal[3], Vladimir I. Chizhik[2]

[1]Laboratory of Biomolecular NMR, SPbSU, 199034, 7/9 Universitetskaya nab., St. Petersburg
[2]Faculty of Physics, SPbSU, 199034, 1 Ulyanovskaya st, St. Petersburg
[3]Faculty of Physics, Havana University, Havana, Cuba
E-mail: sevastyan@rabdano.ru

The modern arsenal of physico-chemical methods has everything you need to study protein aggregates. However, the method of nuclear magnetic resonance (NMR) stands out especially, since it allows measurements of structure and dynamics in a natural environment for proteins. NMR measurements on the nuclei of protein molecules provide some information, but in most cases, they are impossible for disordered heterogeneous agglomerates of peptide chains that do not have dynamics enough to average the effects of heterogeneity and to observe narrow NMR signals. Nevertheless, a lot of information can be obtained from the signals of residual mobile regions of polypeptide chains in large protein agglomerates [1, 2]. On the other hand, global rearrangements in the structure of protein complexes are reflected in significant changes in the resonance parameters for solvent nuclei, primarily water as the main component [3] and ions of salt in buffer. The sensitivity and non-invasiveness of the NMR relaxation of solvent nuclei make it suitable for studying aggregate particles of proteins.

In present report the NMR relaxation rates of nuclei in buffer (^{1}H, ^{2}H, ^{23}Na and ^{35}Cl) for control and aggregated samples of RRM2 domain of TDP-43 protein are considered as probes for changes in protein conformation and aggregation state. It was found that proton relaxation times are sensitive to protein aggregation at low resonance frequencies in greater extent. The relaxation rates for ions of sodium and chlorine found to be sensible to the presence of protein in solution. The kinetics of RRM2 aggregation was studied using NMR relaxation of ^{1}H nuclei of water. The experimental R_1 and R_2 relaxation rates of solvent nuclei for this system were compared to simulated values obtained in the assumption of three-site exchange.

Acknowledgements

The reported study was funded by RFBR and CITMA according to the research project №18-53-34003.

References

1. Rabdano S.O. et al. Onset of disorder and protein aggregation due to oxidation-induced intermolecular disulfide bonds: case study of RRM2 domain from TDP-43 // Sci. Rep. 2017. Vol. 7, № 1. P. 11161.
2. Christodoulou J. et al. Heteronuclear NMR investigations of dynamic regions of intact Escherichia coli ribosomes // Proc. Natl. Acad. Sci. 2004. Vol. 101, № 30. P. 10949–10954.
3. Taraban M.B. et al. Water Proton NMR: A Tool for Protein Aggregation Characterization // Anal. Chem. 2017. Vol. 89, № 10. P. 5494–5502.

New approach in ANC-based noise reduction of Remote Sensing NQR analysis

Sharifi A. M. Saleh[1], *Afarideh Hoseyn*[1], *Ghergherehchi Mitra*[1,2], *Chai Jong Seo*[2]

[1]*Amirkabir University of technology 424 Hafez Ave, Tehran, Iran*
[2]*Sungkyunkwan University, Suwon, South Korea*
E-mail: eng.ms.sharifi@gmail.com

Introduction

In the Nuclear Quadrupole Resonance or NQR, only the nucleus with spin 1 or greater can be analyzed, because, in addition to a magnetic moment, it can possess an electric quadrupole moment. Unlike Nuclear Magnetic Resonance or NMR, These nuclei do not require an external magnetic field to move the axis and mostly has a natural angle, So, sometimes, this technique is called zero-field NMR. therefore, this technique is more comfortable in remote sensing cases, though the resonance frequency and amplitude of free induction decay or FID signal are less. So the noise is vital [1].

Method

There are several analogs and digital methods to filter the noise but for effective noise cancellation, a new method is needed. According to Fig. 1, the adaptive noise cancelation or ANC includes the two low gain omnidirectional antenna as an Auxiliary antenna, beside a high gain Helical or Spiral antenna as the main antenna, so the weak Noise plus strong FID signal are received by the main antenna, and the strong Noise plus weak FID signal are received by Auxiliary antennas, Although the weak Noise is stronger than strong FID signal [2].

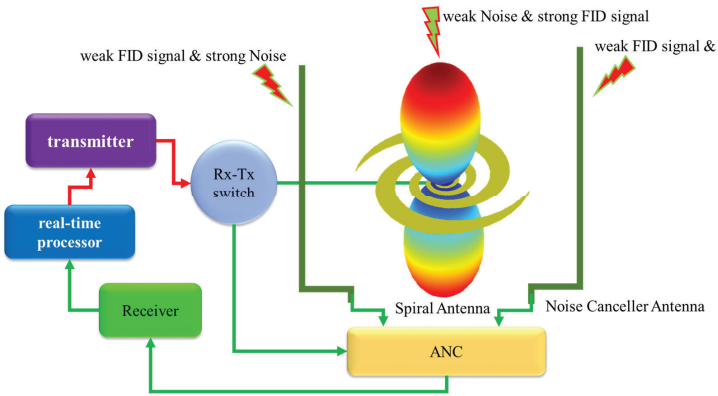

Figure 1. overall schematic

ANC technique

In the ANC unit, the Noise comes from omnidirectional antennas which is amplified in Noise amplifier, the weight of Noise harmonics is adapted to noise of the main antenna by Adaptive filter, the phase of noise 180 degrees changed in Noise phase shifter, simultaneously, the noisy signal SNR is increased by Low Noise Amplifire or LNA. Finally, in Combiner, summing the noisy signal and Noise which is caused to cancel or reduce the noise of the noisy signal (Fig. 2).

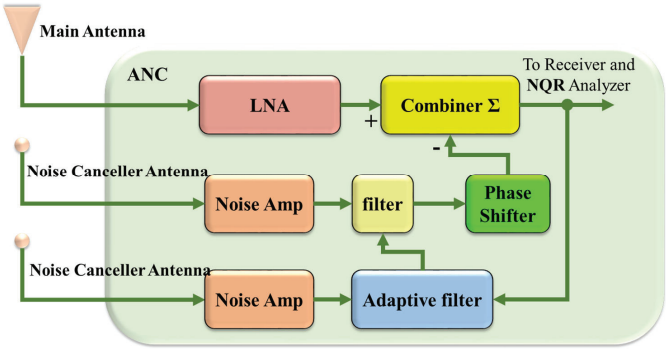

Figure 2. ANC schematic

Results

According to Fig. 3, the effect of ANC on Noise and signal amplitude is shown. Although, the amplitude of the signal is slightly reduced by the ANC, it is increased the signal to noise ratio or SNR.

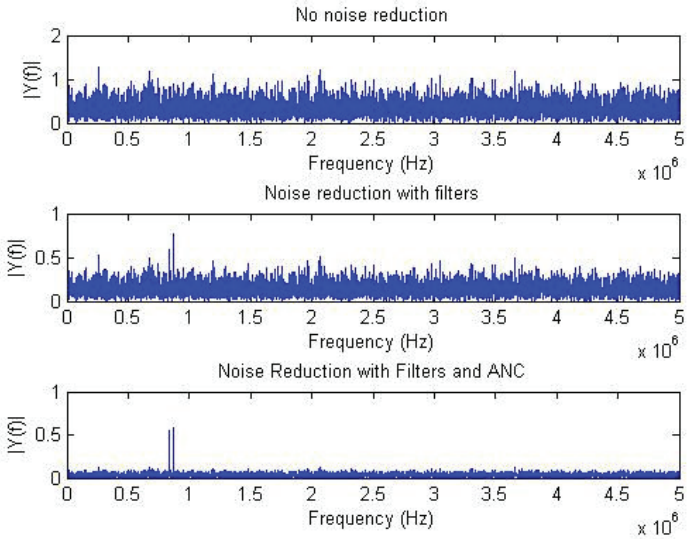

Figure 3. the effect of ANC on noise reduction

Conclusion

By this effective method, the SNR is so enhanced to decrease the measurement time, as a result, the handheld analyzer will be a better practical device.

References

1. Allen N. Garroway, et al. Remote Sensing by Nuclear Quadrupole Resonance. – “IEEE transactions on geoscience and remote sensing”, vol. 39, no. 6, june 2001
2. D. A. Mitchell and J. G. Robertson. Reference antenna techniques for cancelingradio frequency interference due to movingsources. – “Radio Science”, VOL. 40, RS5S11, doi:10.1029/2004RS003152, 2005

Magnetic resonance studies of atomic hydrogen in porous Ne at ultra-low temperatures

S. Vasiliev[1], J. Ahokas[1], J. Järvinen[1], S. Sheludiakov[1], V. V. Khmelenko[2] and D. M. Lee[2]

[1]Department of Physics and Astronomy University of Turku, 20500 Turku, Finland
[2]Department of Physics and Astronomy, Texas A&M University, College Station, TX, 77843, USA
E-mail: servas@utu.fi
http://hturku.utu.fi

The freezing temperature of solid hydrogen may be significantly lowered below bulk value by encapsulating it in a restricted geometry. This can be realized by slow deposition of mixtures of rare gases (Ne, Kr) and molecular hydrogen at sufficiently low temperatures [1]. The films deposited at such conditions exhibit a high degree of porosity with nano-clusters of H_2 inside the pores. Small amounts (<0.1%) of H_2 can be dissolved in the Ne crystalline lattice. From our previous work with mixtures of H isotopes including tritium, we got a tiny amount of T diffused into the metal of the sample cell walls. 5.7 keV electrons resulting from β-decay of tritium escape from the walls and flying through the thickness of the Ne-H_2 films lead to a dissociation of molecular hydrogen into atoms. We utilize ESR at 130 GHz for characterization of the properties of these atoms stabilized inside the Ne-H_2 films in strong magnetic fields of 4.6 T and temperatures below 1 K. We found that H atoms may be trapped in two different substitutional positions in the Ne lattice as well as inside clusters of pure molecular H_2 in the pores of the Ne film. The latter type of atoms was very unstable against recombination at temperatures 0.3-0.6 K. Based on the observed nearly instant decays after rapid small increases of temperature, we evaluate the lower limit of the recombination rate constant $k_r \geq 5 \cdot 10^{-20}$ $cm^3 s^{-1}$ at 0.6 K, five orders of magnitude larger than that previously found in the thin films of pure H_2 at the same temperature. Such behavior assumes a very high mobility of atoms and may indicate a solid-to-liquid transition for H_2 clusters of certain sizes, similar to that observed in experiments with H_2 clusters inside helium droplets [2]. We found that the efficiency of dissociation of H_2 in neon films is enhanced by 2 orders of magnitude compared to that in pure H_2 as a result of strong action of secondary electrons.

References

1. S. Sheludiakov *et. al*., Phys. Rev. B 97, 104108 (2018).
2. Kirill Kuyanov-Prozument and Andrey F. Vilesov, Phys. Rev. Lett 101, 205301 (2008).

The self-diffusion of polymethylsilsequioxane dendrimers in dilute solutions and melts

S. G. Vasil'ev[1], A. V. Chernyak[1], I. A. Avilova[1], K. L. Boldyrev[2], E. V. Selezneva[2], E. A. Tatarinova[2], A. M. Muzafarov[2,3]

[1]Institute of Problems of Chemical Physics of Russian Academy of Sciences, Chernogolovka, Russia
[2]Institute of Synthetic Polymeric Materials of Russian Academy of Sciences, Moscow, Russia
[3]Institute of Organoelement Compounds of Russian Academy of Sciences, Moscow, Russia
E-mail: viesssw@mail.ru

Introduction

Dendrimers are unique class of macromolecules in which the three dimensional structure is formed by the regular branching from a single focal point. Each layer of branching units doubles or triples the number of successive groups. Such structure contains large number of terminal groups comparable to the number of the interior groups which provide wide opportunities to combine useful functions of both. The internal space of dendrimers is often considered attractive for the encapsulation of small molecules and particles. In the present work we investigate the self-diffusion of polymethylsilsequioxanes (PMSSO) dendrimers. The structure of the PMSSO dendrimers includes inorganic backbone formed by the Si-O-Si bonds and the organic methyl side groups. Though the PMSSO dendrimers are among the first dendritic structures discovered [1] the detailed studies were constrained by the absence of the non-functional derivatives until recent times[2]. These macromolecules share common useful features with other silicone polymers, such as high flexibility of the backbone and methyl side groups, high thermal and electrical stability, biological inactivity etc., yet also display unique characteristics inherent to dendrimers. The recent studies of the behavior of dendrimers in melts have revealed some unexpected features. The unprecedentedly high jump in viscosity was observed for carbosilane dendrimers upon the step from 5^{th} to 6^{th} generation, which divide the dendrimers into low-generations exhibiting a Newtonian behavior and high-generations with unusual rheological properties resembling that of the plastic solids[3]. Another manifestation of specific properties of dendrimer melts is the unusual increase of the NMR linewidth with temperature which is commonly associated with the slowing down of the molecular mobility[4]. It has been suggested from both theoretical and experimental data that the presence of the physical entanglements is responsible for such unusual behavior in melts of high generation dendrimers [3-6]. The absence of specific interactions such as hydrogen bonding, electrostatic interactions of polar groups, makes PMSSO dendrimers a good model for studying the effect of regularly branched morphology on the dynamics in solutions and melts. The questions of conformational behavior of dendrimers, their interactions and the role of mutual interpenetration in concentrated solutions and melts remain relevant at the moment. The studies of the self-diffusion by means of PFG NMR are able to shed light on the involved interactions at a molecular level.

Results and discussion

The objects investigated in the present study are trimethylsilyl terminated PMSSO dendrimers of 1-5 generations. The self-diffusion coefficients (SDCs) were measured using spin-echo PFG NMR on a Bruker Avance III spectrometer on ^{1}H nuclei at 400 MHz (9.4 T). Maximum magnetic field gradient amplitude was g=30 T/m. The samples were diluted in toluene and also were studied in bulk. The temperature of measurements was varied between -50 and 80 °C. All dendrimers are above glass temperature in the investigated temperature region[2]. In the ^{1}H spectra of the solutions there were three resolved regions corresponding to aromatics and methyl groups of toluene and methyl groups of dendrimers. The SDCs were

determined separately for these lines. The decay of the spin-echoes was linear in the coordinates of lnA vs g^2.

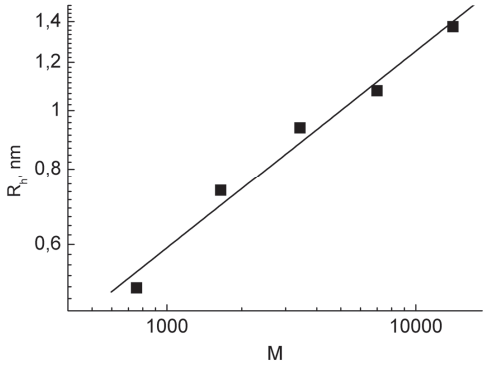

Figure 1. Dependence of the hydrodynamic radii of PMSSO dendrimers with trimethylsilyl terminal groups on molecular mass in diluted solutions of toluene

The SDCs of toluene in dendrimer solutions coincided among different generations and corresponded to the SDC of bulk toluene. The hydrodynamic radii of dendrimers determined using Stock-Einstein equation are shown in fig.1. The dependence was described by a power law relation $R_h \sim M^{\beta}$ with β=0.32±0.02. Such exponent is typical for objects where the mass distribution is almost uniform through the volume. The activation energies determined from the temperature dependence using the Arrhenius equation for different generations of dendrimers in diluted solutions were almost identical (11.5±0.3 kJ/mol). This value is also close to the activation energies of the self-diffusion (~11.0 kJ/mol) of the neat toluene.

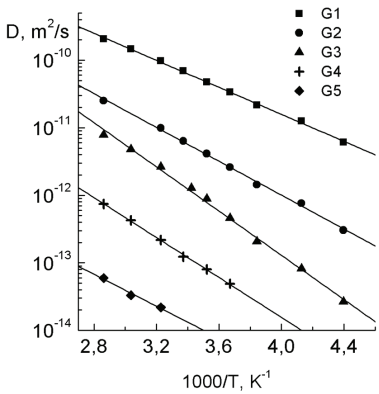

Figure 1. Temperature dependence of SDC for PMSSO dendrimers of 1-5 generations

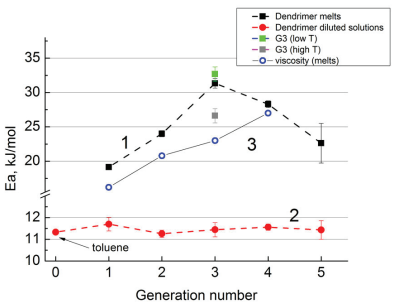

Figure 2. Activation energies of the self-diffusion for PMSSO dendrimers of 1-5 generations in melts (1), diluted solutions (2), activation energies of viscous flow in melts (3)

The changes of the SDCs with temperature in the melts of PMSSO dendrimers are noticeably different (fig. 1). Besides the increase of the activation energy compared to diluted solutions there is a significant dependence on the generation number. The dependence of the activation energy on the generation number appears to have a maximum at the third generation (fig. 3). Such behavior can be attributed to the densification of the structure for higher generations predicted by simulations for PMSSO dendrimers [5]. In addition there is a deviation from a simple Arrhenius dependence for the 3-rd generation. This dependence can be more precisely described by the two different regions in the Arrhenius plot (fig. 3). The activation energies for the high-temperature region of the 3-rd generation and other dendrimers have a good correlation with the activation energy determined from the viscosity measurements [2]. Though the molecular mass dependence of SDCs resembles to that of the objects with dense mass distribution (determined for diluted solutions), the changes of the activation energy for the 3-rd generation indicate some interpenetration of the dendrimer molecules. At high temperatures these entanglements do not result in strong decrease of the translational mobility while at low temperatures the mobility is more restricted.

Molecular dynamics simulations of single PMSSO dendrimers [5] show that for G3 there is a large internal space within the molecule allowing the constituting units to occupy the whole interior owing to relatively long branches. The effect of significant mutual interpenetration of G3 PMSSO molecules may be justified by this large internal space. Lower generation dendrimers are probably too small to exhibit their structural specificity. For higher generation dendrimers mutual interpenetration is hindered by the excluded volume and densification. The effect of interpenetrations for high generations also present and reveal itself in the decrease of SDC but not in the changes of their temperature dependencies.

Acknowledgements

This work is supported by the Russian Foundation for Basic Research (project no. 18-33-20166) The work has been performed using the equipment of the Multi-User Analytical Center of IPCP RAS. This work was performed as part of the state task, state registration No. 0089-2019-0002.

References

1. Rebrov, E.A., A.M. Muzafarov, V.S. Papkov, and A.A. Zhdanov,Space-Network Polyorganosiloxanes, Dokl. Akad. Nauk SSSR, 1989. **309**: p. 376-380.
2. Boldyrev, K., E. Tatarinova, I. Meshkov, N. Vasilenko, M. Buzin, R. Novikov, V. Vasil'ev, E. Shtykova, L. Feigin, A. Bystrova, S. Chvalun, and A. Muzafarov,New approach to the synthesis of polymethylsilsesquioxane dendrimers, Polymer, 2019. **174**: p. 159-169.
3. Vasil'ev, V.G., E.Y. Kramarenko, E.A. Tatarinova, S.A. Milenin, A.A. Kalinina, V.S. Papkov, and A.M. Muzafarov,An unprecedented jump in the viscosity of high-generation carbosilane dendrimer melts, Polymer, 2018. **146**: p. 1-5.
4. Matveev, V.V., D.A. Markelov, S.V. Dvinskikh, A.N. Shishkin, K.V. Tyutyukin, A.V. Penkova, E.A. Tatarinova, G.M. Ignat'eva, and S.A. Milenin,Investigation of Melts of Polybutylcarbosilane Dendrimers by 1H NMR Spectroscopy, Scientific Reports, 2017. **7**(1): p. 13710.
5. Kurbatov, A.O., N.K. Balabaev, M.A. Mazo, and E.Y. Kramarenko,Molecular dynamics simulations of single siloxane dendrimers: Molecular structure and intramolecular mobility of terminal groups, The Journal of Chemical Physics, 2018. **148**(1): p. 014902.
6. Smeijers, A.F., A.J. Markvoort, K. Pieterse, and P.A.J. Hilbers,Coarse-grained simulations of poly(propylene imine) dendrimers in solution, The Journal of Chemical Physics, 2016. **144**(7): p. 074903.

Ordering of water-soluble derivatives of fullerenes in water from the molecular dynamics simulation

Aleksandr S. Voronin, Andrei V. Komolkin, Denis A. Markelov

Faculty of Physics, Saint Petersburg State University, 7-9 Universitetskaya emb., 199034 Saint Petersburg, Russian Federation
E-mail: sahkaxz@gmail.com

Introduction

Water-soluble derivatives of fullerenes are of special importance in medicine due to various functional properties. For instance, hydroxylated fullerenes - fullerenols, may serve as effective antioxidant agents or free radical acceptors in biological systems and reveal high protective properties against radiation and toxic chemicals [1]. As medical usage of fullerenols require a fundamental understanding of their behaviors in aqueous media, both experimental and numerical studies are needed. Lack of knowledge about precise chemical structure of water-soluble fullerenes is another problem to be solved.

Recent studies find out that highly hydroxylated fullerenes $C_{60}(OH)_n$ (n~20-30) are associated into chain-like aggregates (~20 units, few nanometers in size) [2]. The nature of this association can be explained by hydrophobic and hydrophilic interactions of molecules due to arrangements of OH-groups. Quantum chemical calculations of $C_{60}(OH)_{20}$ showed preferred localization of OH-groups at C_{60} spheroids equatorial zone (Fig. 1). This kind of hydroxyls distribution suggests that fullerenols have 2 hydrophobic "poles" and hydrophilic "equator" and molecules can be connected by these zones.

The purpose of current investigation was to determine the characterization of the molecular ordering of fullerenols with the structure described above in water solutions using dynamics simulation.

Model and method

The structure of fullerenols was obtained on B3LYP/6-31G++(d) level of theory and described in previous work [2]. Molecular dynamics simulations were performed in GROMACS package using OPLS-AA force field. Several systems with different concentrations of fullerenols in SPC/E water were simulated. The simulation consisted of the energy minimization by the steepest descent gradient method, equilibration of the system in NVT-ensemble and in NPT-ensemble and productive run in NPT-ensemble. The total simulation time for each system was 200-300 ns depending on the box size. The constant temperature of 300 K was maintained by v-rescale thermostat and pressure of 1 bar was maintained by a Berendsen barostat.

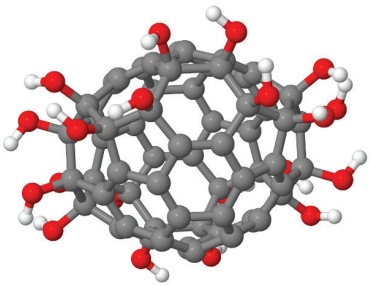

Figure 1. Structure of fullerenols $C_{60}(OH)_{20}$

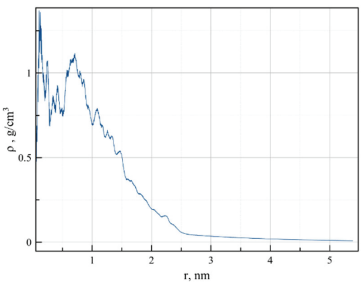

Figure 2. Density profile of 20 fullerenols cluster

Results

In the report, the results of simulations for systems with fullerenols concentrations 1 - 15 wt% will be discussed. For all considered systems molecules of fullerenols are assembling in a cluster during the equilibration. This clusters were stable during the productive run. We studied the structural properties of the clusters. Here we will only present the results for the 20 fullerenols cluster at 2.5 wt%.

The size of a cluster was characterized by the mean-square gyration radius

$$R_g^2 = \frac{1}{M}\sum_i m_i r_i^2,$$

where m_i is the molecular mass of the ith atom and r_i is the distance from the ith atom to a cluster center of mass.

To describe a shape of the fullerenols cluster asphericity was calculated following the definition of Rudnick and Gaspari [3]:

$$\delta = 1 - \frac{3\langle I_2 \rangle}{\langle I_1^2 \rangle},$$

$$I_1 = R_{gx} + R_{gy} + R_{gz},$$

$$I_2 = R_{gx}R_{gy} + R_{gy}R_{gz} + R_{gx}R_{gz},$$

where R_{gx}, R_{gy}, and R_{gz} are gyration radii around axes.

Internal structure of the fullerenols cluster was characterized by density profiles of atoms $\rho(r)$ as

$$\rho(r) = \frac{1}{4\pi r^2}\sum_i^{N_a} m_i \delta(r - r_{com}),$$

where N_a is the fullerenols cluster number of atoms, m_i is the ith atom mass, and r_{com} is distance from the cluster center of mass.

For the 20-fullerenols cluster mentioned above $R_g^2 = 1.5$ nm and $\delta = 0.004$. The value of $\rho(r)$ in the plateau region is about 1 g/cm^3 (Fig. 2) and decreases to the periphery which means that water does not penetrate into a fullerenols cluster.

The mechanism of clustering of fullerenols and will be discussed in the report.

Acknowledgements

This work is supported by the Russian Foundation for Basic Research (No. 19-03-00715). The simulations were performed in Computer Resources Centre of Saint Petersburg State University.

References

1. A.V.Penkova, S.F.A.Acquah, L.B.Piotrovskiy, D.A.Markelov, A.S.Semisalova, H.W.Kroto, Russ. Chem. Rev., 2017, 86 (6) 530 - 566
2. V. T. Lebedev, Yu. V. Kulvelis, A. S. Voronin, A. V. Komolkin, E. A. Kyzyma, T. V. Tropin & V. M. Garamus (2019): Mechanisms of supramolecular ordering of water-soluble derivatives of fullerenes in aqueous media, Fullerenes, Nanotubes and Carbon Nanostructures, DOI: 10.1080/1536383X.2019.1671362
3. J. Rudnick and G. Gaspari 1986, J. Phys. A: Math. Gen. 19 L191

Investigation of intermetallic thermoelectric compound $RuGa_3$ by NQR spectroscopy

Sergei V. Zhurenko[1,2], Alexey V. Tkachev[1], Natalia E. Gervits[1], Anton V. Gunbin[1], Dina I. Fazlizhanova[2], Chia Nung Kuo[3], Chin Shan Lue[3], Andrei A. Gippius[1,2]

[1]Lebedev Physical Institute, Russian Academy of Sciences, 119991, Moscow, Russia
[2]Moscow State University, Faculty of Physics, 119991, Moscow, Russia
[3]Department of Physics, National Cheng Kung University, Tainan 70101, Taiwan
E-mail: Zhurenko.sergey@gmail.com
http://www.researchgate.net/profile/Sergei_Zhurenko

Introduction

The scientific interest in compounds of the structural type $IrIn_3$ (tetragonal, $P4_2/mnm$) arose due to their promising thermoelectric properties. According to the literature [1-3] the thermoelectric activity of $IrIn_3$-type compounds is highly associated with the features of their band structure. In these compounds, a gap near the Fermi level is created by the strong hybridization of the *d*-orbitals of transition metal and the *s*, *p*-orbitals of post-transition element. Since the type of conductivity depends on the concentration of valence electrons, $FeGa_3$, $RuGa_3$, $RuIn_3$ and $OsGa_3$ possessing 17 valence electrons are semiconductors. An increase in number of valence electrons to 18 leads to the metallic properties of $CoGa_3$, $CoIn_3$, $RhIn_3$ and $IrIn_3$ [1]. $RuGa_3$ has a high Seebeck coefficient of 560 μ/ K at 373 K, the Seebeck coefficient of $RuGa_3$ quickly changes from large negative to large positive values around 500 K, and the thermoelectric figure of merit $ZT = (S^2/\rho\kappa)T$ reaches a maximum value of 0,17 at 773 K [2]. However, high electrical resistivity and thermal conductivity reduce the thermoelectric figure of merit.

The purpose of this work is to study $RuGa_3$ by means of nuclear quadrupole resonance (NQR) spectroscopy and to analyze the temperature dependence of the spin-lattice relaxation rate $1/T_1$.

Object of research

In this work, we study the intermetallic compound $RuGa_3$ crystallized in the $P4_2/mnm$ space group. The crystal structure of $RuGa_3$ is shown in Fig. 1, interatomic distances of $RuGa_3$ and $FeGa_3$ are listed in Table 1.

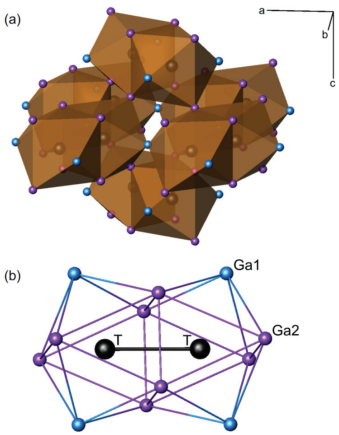

Figure 1. Polyhedral representation of the (a) crystal structure of the $FeGa_3$ and $RuGa_3$, and (b) its building unit—a pair of bicapped trigonal prisms centered by the T – T dumbbell, T=Fe or Ru [3]

Table 1. Interatomic Distances (in A°) calculated with the Lattice Parameters Obtained from X-ray Powder Data of $FeGa_3$ and $RuGa_3$ [4]

$FeGa_3$				$RuGa_3$			
Fe:	2	Ga1	2.365	Ru:	2	Ga1	2.435
	2	Ga2	2.393		2	Ga2	2.459
	4	Ga2	2.500		4	Ga2	2.574
	1	Fe	2.769		1	Ru	2.911
Ga1:	2	Fe	2.365	Ga1:	2	Ru	2.435
	4	Ga2	2.835		4	Ga2	2.916
	4	Ga2	2.924		4	Ga2	3.022
	2	Ga1	3.277		2	Ga1	3.353
Ga2:	1	Fe	2.393	Ga2:	1	Ru	2.459
	2	Fe	2.500		2	Ru	2.574
	1	Ga2	2.756		1	Ga2	2.832
	2	Ga1	2.835		2	Ga1	2.916
	2	Ga1	2.924		2	Ga1	3.022
	1	Ga2	3.120		1	Ga2	3.165
	1	Ga2	3.351		1	Ga2	3.469
	4	Ga2	3.435		4	Ga2	3.541

Experimental results

Ab-initio band structure calculations

The NQR frequencies of $RuGa_3$ were *a-priori* unknown, and we used the *ab-initio* method for calculating the electronic band structure to find their theoretical value. The *ab-initio* calculations of $RuGa_3$ electronic band structure were performed in frames of the density functional theory (DFT) with the local density approximation (LDA) using software VASP [5] and computing resources of MSU Lomonosov supercomputer. The calculated values of the ^{69}Ga NQR frequencies for the Ga1 and Ga2 crystallographic positions of gallium in $RuGa_3$ are 46,75 MHz and 41,01 MHz, respectively.

NQR spectroscopy

The ^{69}Ga NQR measurements were performed at 4,2 K utilizing a home-built phase coherent pulsed NQR spectrometer with direct digital quadrature detection at the carrier frequency. ^{69}Ga NQR spectrum was obtained by Fast Fourier Transform (FFT) of the second half of the Hahn-echo with the RF-probe placed in transport helium dewar.

Nuclear spin-lattice relaxation

The nuclear spin-lattice relaxation rate $1/T_1$ was measured using the ^{69}Ga nuclei for the Ga1 NQR line in a wide temperature range of 4,2–300 K. Spin-lattice relaxation (T_1) was measured by saturation-recovery (SR) method.

It turned out that in the low-temperature part of $1/T_1(T)$ curve (below 40 K) the magnetization recovery curve seems to be non-typical for $RuGa_3$ compounds (see Fig. 2). Indeed, the approximation by the classical Eq.(1) doesn't fit well to the experimental data.

$$M(\tau) = M_0 + A * \left(1 - e^{-\tau/T1}\right) \quad (1)$$

Since there is no doping and hence no disorder in $RuGa_3$, using the stretched exponent (2) as a fitting function seems unjustified.

$$M(\tau) = M_0 + A * (1 - \exp(-(\tau/T1)^n) \quad (2)$$

To obtain reasonable consistency with the experimental recovery curve we used the sum of two exponents:

$$M(\tau) = M_0 + A_1 * \left(1 - e^{-\tau/T1_{slow}}\right) + A_2 * (1 - e^{-\tau/T1_{fast}}) \quad (3)$$

As seen from Fig.2, $RuGa_3$ in this temperature range exhibits two spin-lattice relaxation times: fast and slow. This behavior was previously observed only for some Fe-based superconductors, for example, FeSe [6, 7].

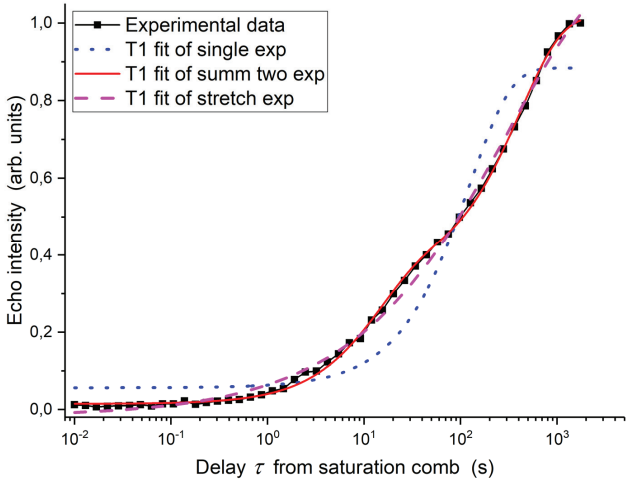

Figure 2. ^{69}Ga magnetization recovery curve for the Ga1 NQR line in the $RuGa_3$ sample at 9 K. Dotted line is the fit to Eq.(1), dashed line is the fit to Eq. (2) and solid line are the best fits to Eq. (3)

Discussion

The physical explanation of the existence of two different times $T1_{slow}$ and $T1_{fast}$ in spin-lattice relaxation with and different temperature dependencies of $1/T1_{slow}(T)$ and $1/T1_{fast}(T)$ in $RuGa_3$ compound still stays unclear and requires further investigation.

Acknowledgements

The work was supported by RFBR according to the research project № 17-52-80036. The research is carried out using the equipment of the shared research facilities of HPC computing resources at Lomonosov Moscow State University.

References

1. M.S. Likhanov, V.Yu. Verchenko, D.I. Nasonova, A.A. Gippius, S.V. Zhurenko, E.I. Demikhov, C.N. Kuo, C.S. Lue, B.L. Young, A.V. Shevelkov. Crystal structure and magnetic properties of intermetallic semiconductor $FeGa_3$ lightly doped by Co and Ni. Journal of Alloys and Compounds, 745, 341–346. (2018)
2. Takagiwa, Y., Kitahara, K., Matsubayashi, Y., & Kimura, K. Thermoelectric properties of $FeGa_3$-type narrow-bandgap intermetallic compounds $Ru(Ga,In)_3$: Experimental and calculational studies. Journal of Applied Physics, 111(12), 123707 (2012)
3. A. A. Gippius, V. Yu. Verchenko, A. V. Tkachev, N. E. Gervits, C. S. Lue, A. A. Tsirlin, N. Büttgen, W. Krätschmer, M. Baenitz, M. Shatruk, and A. V. Shevelkov Interplay between localized and itinerant magnetism in Co-substituted $FeGa_3$ Phys. Rev. B 89, 104426 (2014)

4. Häussermann, U., Boström, M., Viklund, P., Rapp, Ö., & Björnängen, T. $FeGa_3$ and $RuGa_3$: Semiconducting Intermetallic Compounds. Journal of Solid State Chemistry, 165(1), 94–99 (2002)
5. Kresse, G., & Furthmüller, J. Efficient iterative schemes forab initiototal-energy calculations using a plane-wave basis set. Physical Review B, 54(16), 11169–11186 (1996)
6. Kotegawa, H., Masaki, S., Awai, Y., Tou, H., Mizuguchi, Y., & Takano, Y. (2008). Evidence for Unconventional Superconductivity in Arsenic-Free Iron-Based Superconductor FeSe: A ^{77}Se-NMR Study. Journal of the Physical Society of Japan, 77(11), 113703.
7. J Masaki, S., Kotegawa, H., Hara, Y., Tou, H., Murata, K., Mizuguchi, Y., & Takano, Y. (2009). Precise Pressure Dependence of the Superconducting Transition Temperature of FeSe: Resistivity and ^{77}Se-NMR Study. Journal of the Physical Society of Japan, 78(6), 063704.

Section 3

Essentuki Mineral Water Analysis

Svetlana Ya. Alexandrova[1], Alina A. Pichugina[2], Larisa V. Tsyro[2]

[1]Chemical Faculty, National Research Tomsk State University, Lenina avenue, 36, Tomsk, Russian Federation
[2]Institute of Natural and Technical Sciences, Surgut State University, Lenina avenue 1, Surgut, Russian Federation
E-mail: alsya8@yandex.ru
http://www.tsu.ru

Introduction

All waters in nature are mineralized to one degree or another, from snow to brines. All therapeutic properties are determined within the therapeutic action exclusively by the ionic composition, which is given on the label and is very diverse from various sources and manufacturers.

Mineralization determines the amount of substances dissolved in a unit volume of water (without gases) and is expressed in grams per liter. According to this parameter, the commercially available bottled drinking water is divided into canteens (with a mineralization of less than 1 g/l), medicinal and canteen (whose mineralization ranges from 1 to 10 g/l) and medicinal (whose mineralization is 10 – 15 g/l).

Mineral drinking water includes only medicinal-table and medicinal waters, the representatives of which are the mineral waters of Essentuki, which we have chosen as objects of study. The chemical composition of mineral water is given in table 1.

Table 1. The chemical composition of the mineral water of Essentuki, mg/l

	Essentuki-17	Essentuki-4	Essentuki-2	Essentuki-20
Hydrocarbonate HCO_3^-	6300	4500	1400	460
Sulphates SO_4^{2-}	3	1	400	750
Chloride Cl^-	2500	1500	300	90
Calcium Ca^{2+}	140	140	500	200
Magnesium Mg^{2+}	70	50	150	90
Sodium + Potassium Na^+, K^+	3700	2200	700	190
Mineralization	12700	8200	4000	1700

The spin properties of natural waters should affect the vital activity of living organisms, most of the reactions in which are enzymatic in nature, leading to the participation of molecules with unpaired electrons - free radicals.

If dimers of free radicals enter the body with water, then dimers decay under the influence of molecular collisions into doublet pairs with unpaired electrons. These pairs are subject to inhibition and must be localized by the body or inhibitors so as not to interfere with enzymatic reactions.

The aim of this work was to analyze the precipitation of mineral waters by electron spin resonance (ESR) and to study the aggregation processes by photon correlation spectroscopy (PCS).

Research Methods

The electron spin resonance (ESR) method was used to analyze the cores. Preliminary preparation consisted of grinding a core sample in ball mills. The powder thus obtained was

placed in an ampoule made of quartz glass, the ampoule was placed in the resonator of an ESR spectrometer. A spectrometer of the SE/X brand operating in the X-band was used. The device was tuned (the corresponding microwave modulation was selected), the spectrum was recorded. Conditions of spectrum shooting: a) field width 700 mT; b) sweep time 16 min; c) ν 9 GHz; d) the sensitivity was selected depending on the sample. Microwave modulation was selected in such a way that saturation would not occur for the sample.

The PCS method is one of the most informative methods for studying the dynamics of deposition processes in water systems. The experiment was carried out on a UNICOR – SP photon correlation spectrometer in the homodyne detection mode: monochromatic radiation from an He-Ne laser (LG-38, radiation power ~ 50 mW, λ = 632.8 nm), passing through a sample cell, was scattered by particles of the dispersed phase and It was detected by a photodetector operating in a photon counting system (PMT-136, f_{max} = 35 MHz, noise level 10-40 imp/s), the signal from which was fed to a PhotoCor-Sp multi-channel digital correlator built into one of the connectors on the computer motherboard. Information about scattered radiation was processed using the special computer program PhotoCor [1].

Results

In mineral water, which contains a large amount of salts, the formation of natural sediment is allowed. The deposition processes in such systems can be fixed by the PCS method. The experiments performed show that even at room temperature in Essentuki mineral water there are particles of a dispersed phase, the sizes of which vary between 15 – 170 nm (Table 2). With increasing temperature (40 °C), the particle radius increases from 45 to 347 nm. A decrease in the accumulation time on the spectrometer with increasing temperature is observed, which is associated with an increase in the number of particles in the studied system.

Using the ESR method, we undertook a study of the spin properties of sediments obtained from samples of mineral water by natural evaporation.

It was shown by ESR that precipitates from the studied waters have spin properties (the total concentration of spin centers (SC) is of the order of 1020 spin/g according to Table 2).

The data in table 2 show the differences in the mineral water of Essentuki in terms of particle size and the amount of SC in precipitates of the same brand from different manufacturers. For the “Yessentuki No. 2” trademark, these indicators produce a significant difference, which may indicate a different origin of these waters, similarly for “Yessentuki No. 4” and “Yessentuki No. 17”. For the “Yessentuki No. 4” trademark, differences are also observed from different bottling dates, which is a reflection of the technological process for the production of these waters, despite the compliance of these waters with GOST.

For samples of Essentuki mineral water entering the distribution network from different manufacturers, it was shown by PCS and ESR methods that, according to the studied characteristics (particle size and amount of SC), these are waters of different origin.

The joint use of the methods of FCC and ESR makes it possible, by comparing the characteristics of dispersions of natural mineral waters and their trade analogues, to establish their natural or artificial origin, and for waters of the same brand to see the differences in the processes of obtaining water.

Despite the fact that we have investigated mineral waters in glass and plastic packaging, it is impossible to give a definite answer to the question: which container is better? This is determined by the fact that each manufacturer uses his supplier of packaging, which differ in their chemical characteristics. Such an assessment may appear as a result of further research.

References

1. Multifunctional Correlator UNICOR – SP. User's Manual. – 41 p.

Table 2. The results of the analysis of Essentuki mineral water by the methods of PCS and ESR

Trademark	Manufacturer	Tara	t, °C	r, nm	m, g/200 ml	$C_{SC} \cdot 10^{-20}$, spin/g*
Essentuki-2	well No. 1 KMV bis "Aqua-White"	plastic	20	70 ±26	2,79	0,58
			40	120 ±40		
	well No. 1 KMV bis "Wisma"	plastic	20	16 ±3	–	3,37
			40	45 ±5		
Essentuki-20	well 9 "Wimm Bill Dunn"	glass	20	31±10	0,27	2,41
Essentuki-4	well No. 57-RE-bis “Aqua-White”	glass, XX.05.XX year	20	110 ±39	1,21	2,76
			40	198 ±30		
		glass, XX.05.XX year	20	74 ±17	–	13,36
			40	156 ±15		
		plastic	20	49 ±16	1,18	5,85
			40	141 ±23		
	well No. 57-RE-bis “Old Source”	glass	20	73 ±21	–	3,62
			40	126 ±20		
		plastic	20	59 ±25	–	6,43
			40	174 ±27		
	well No. 49 “Essentuki Mineral Water Plant at KMV”	glass	20	77 ±17	–	1,48
			40	227 ±19		
	well Number 71 "Wisma"	plastic	20	73 ±15	–	4,62
			40	118 ±29		
Essentuki-17	well No. 47 “Aqua-White”	glass	20	74 ±22	1,72	12,35
			40	120 ±15		
		plastic	20	60 ±7	1,59	4,32
			40	108 ±8		
	well No. 47 "Old Source"	plastic	20	77±15	1,69	8,83
			40	115±21		
	well No. 46 “Essentuki Mineral Water Plant at KMV”	plastic	20	170 ±62	1,54	6,19
			40	347±73		

t – experience temperature, °C; r – particle radius, nm; τ – accumulation time, s.
*Concentration of spin centers in sediment obtained from a sample of mineral water by natural evaporation (m, g/200 ml)

Computer simulation of 1B03 and 1D2D proteins

N. A. Antonova, A. V. Komolkin

St. Petersburg State University, 7-9 Universitetskaya Emb., 199034, St. Petersburg, Russia
E-mail: st054868@student.spbu.ru

Introduction

Proteins are an important component of all life on Earth. This is one of the reasons why they are of particular interest to researchers. The reason for this study were the researches of the stability of proteins at an unusually high temperature in an ionic liquid solution [1], while in water all is usual.

As known, the most common types of secondary structure of proteins are alpha-helices and beta-sheets. Two proteins with different types of secondary structure were selected for the study. 1D2D [2] (Fig. 1) – ligase, i.e. an enzyme that can catalyze the joining of two large molecules by forming a new chemical bond. Its structure is two alpha-helices. 1D2D contained in the body of *Cricetulus griseus* (Milne-Edwards, 1867), commonly named Chinese hamster. 1B03 [3] (Fig. 2) – viral protein. Its structure is two beta-sheets. 1B03 is a part of Human immunodeficiency virus 1.

The purpose of this work is to compare the behavior of these proteins with increasing temperature in an aqueous solutions.

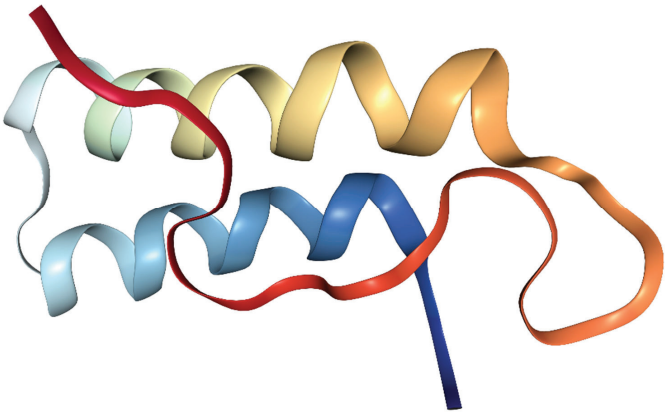

Figure 1. Spatial structure of 1D2D – two alpha-helices

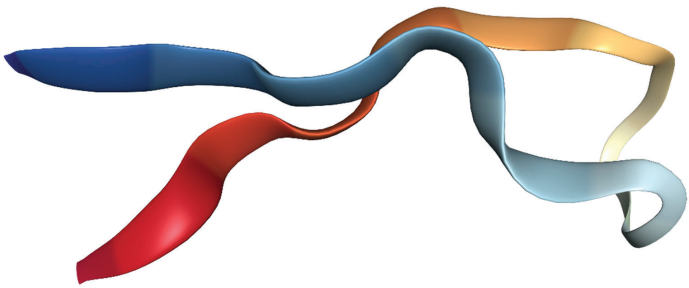

Figure 2. Spatial structure of 1B03 – two beta-sheets

Model systems

Models of proteins were taken from Protein Data Bank [4]. The parameters of simulation were taken from the OPLS-AA [5]. The model of water was chosen SPC/E [6]. Modeling was carried out by the method of molecular dynamics.

The charge of 1D2D protein (Fig. 3) is +2e. Chlorine ions were added to the protein to neutralize the simulation cell. Thus the system of 1D2D consisted of protein molecule, two chlorine ions Cl^- and 15140 water molecules. The density of the solution was 1.0 g/cm^3. At first it was necessary to equilibrate the system. Then the system was warmed to room temperature. After that the system was ready to simulation. Further modeling was carried out in NpT ensemble.

Similar actions were done for another system. The charge of 1B03 protein (Fig. 4) is +5e. The system of 1B03 consisted of protein molecule, five chlorine ions Cl^- and 6649 water molecules. The density of the solution was 1.0 g/cm^3 .

Results analysis

In the report, the temperature stability of the secondary structure of proteins in aqueous solutions will be discussed.

Acknowledgements

Research was carried out using computational resourses provided by Resourse Center "Computer Center of SPbU" (http://cc.spbu.ru).

References

1. G. Chevrot, E. E. Fileti, V. V. Chaban. Protein remains stable at unusually high temperatures when solvated in aqueous mixtures of amino acid based ionic liquids. – *Journal of Molecular Modeling,* **2016**, v. 22, No. 11, article No. 258
2. B. Cahuzac, E. Berthonneau, N. Birlirakis. A recurrent RNA-binding domain is appended to eukaryotic aminoacyl-tRNA synthetases. – *EMBO J.,* **2000**, v. 19, No. 3, 445-452
3. V. Tugarinov, A. Zvi, R. Levy, J. Anglister. A cis proline turn linking two beta-hairpin strands in the solution structure of an antibody-bound HIV-1IIIB V3 peptide. – *Nat. Struct. Mol. Biol.,* **1999**, v. 6, No. 4, 331-335
4. RCSB PDB: Homepage. URL: https://www.rcsb.org/ (accessed 28.02.2020)
5. William L. Jorgensen Research Group — OPLS-AA. URL: http://zarbi.chem.yale.edu/oplsaam.html (accessed 28.02.2020)
6. Berendsen H., Grigera J., Stratsmaa T. The missing term in effective pair potentials. – *J. Phys. Chem.* **1987**, v. 191, No. 24, 6269–6271

Molecular dynamics simulation of global and local dynamics in lysine-based dendrimers with double arginine and double histidine

Valeriy V. Bezrodniy[1,2], Emil Fatullaev[1], Oleg V. Shavykin[1,2], Igor M. Neelov[1,2]

[1]St. Petersburg National Research University of Information Technologies, Mechanics and Optics (ITMO University), Kronverkskiy pr.49, St.Petersburg, 197101, Russia
[2]St.Petersburg State University (SPbSU), 7/9 Universitetskaya nab., St.Petersburg, 199034, Russia
E-mail: kupala-89@mail.ru

Introduction

The peptide dendrimers are interesting object for many biomedical applications including drug and gene delivery. The usual poly-L-lysine dendrimers containing only lysine residues in the repeat units (spacers) were considered in many paperes [1-2]. The insertion of additional charged double aminoacid residues in each spacer between neighboring branching points [3-5] increase dendrimer charge and could lead to better transfection efficiency of dendrimer-DNA or dendrimer RNA complexes. In this paper the molecular dynamics (MD) simulation of orientational mobility of a new dendrimers with double arginine (Lys2Arg) and double histidine (Lys2His) of 2nd generation was performed in water solvent with explicit account of counterions at temperature T=280, 290, 300, 310, 320, 340K and pressure P=1atm using the program package Gromacs-4.5.6 with AMBER99SB-ildn force field. The details of MD simulations were reported earlier for linear [6-18] and branched polymers [19-33].

The local structure

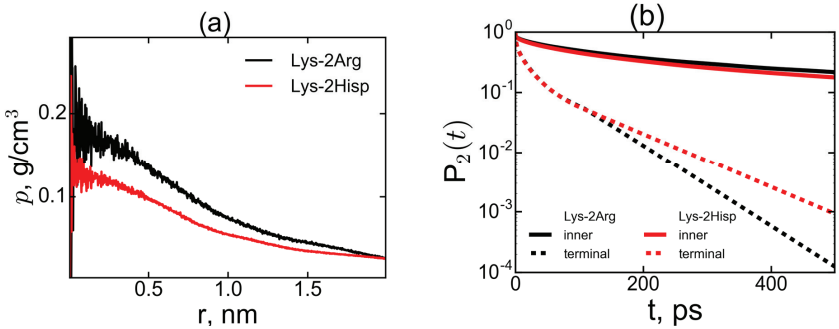

Figure 1. (a)The radial distribution of density of dendrimer's atom and (b) the second order autocorrelation functions (ACFs) for CH_2 of ε-amino group in inner and terminal lysine. Both dendrimers with double arginine (Lys2Arg) and double hystidine (Lys2His) were considered

The radial distribution functions for densitiy $\rho(r)$ is characteristic of local structure of dendrimer and can be obtained from next formulae

$$\rho(r) = \frac{1}{M}\sum_i m_i \delta(r - r_i)$$

where m_i, M – molecular mass of the i-th atom and dendrimer as whole. The radial distribution functions for densities $\rho(r)$ of Lys-2Arg and Lys-2Hisp dendrimers are depicted on Figure 1a. The dendrimer with double arginine more dense in inner region than the dendrimer with double histidine, which is most likely due to the fact that histidine have a massive side groups, that less

compact. The average density less, than in the usual lysine dendrimer [1-2], because the Lys-2Arg and Lys-2His dendrimers have a strong electrostatic repulsion between charged spacer inserted between each pair of neighboring branching points.

The comparison of orientational mobility of inner, side and terminal groups

We estimated also local mobility of the chosen vector ***d*** between two hydrogens in the hydrocarbon at Cε (inner and terminal lysine) carbons using the second order autocorrelation function (ACF) $P_2(t)$

$$P_2(t) = \frac{3}{2}\langle\frac{(\boldsymbol{d}(t),\boldsymbol{d}(0))^2}{|\boldsymbol{d}(t)|^2|\boldsymbol{d}(0)|^2}\rangle - \frac{1}{2}$$

The figure 1b shows the ACFs $P_2(t)$ for both considered dendrimers. It was shown that rotation of terminal groups is faster than of internal ones. For all considered dendrimers mobility weakly depends on the type of dendrimer. This simulation results are in good agreement with the results of our NMR experiment.

Acknowledgements

This work is supported by the Russian Science Foundation (grants No. 19-13-00087). The research is carried out using the equipment of the shared research facilities of HPC computing resources at Lomonosov Moscow State University supported by the project RFMEFI62117X0011.

References

1. S. Falkovich, D. Markelov, I. Neelov, and A. Darinskii. J. Chem. Phys. 2013, 139, 064903.
2. Markelov D.A, Falkovich S.G., Neelov I.M., Ilyash M.Yu, Matveev V.V., Lahderanta E., Ingman P., Darinskii A.A. Physical Chemistry and Chemical Physics. 2015, 17, 3214–3226.
3. Sheveleva N.N., Markelov D.A., Vovk M.A., Mikhailova M.E., Tarasenko I.I., Neelov I.M., Lähderanta E.. Scientific Reports, 2018, 8, 8916.
4. Sheveleva N.N., Markelov D.A., Vovk M.A., Tarasenko I.I, Neelov I.M., E.Lähderanta, 2019, RSC Adv. 9, 18018.
5. Sheveleva N.N., Markelov D.A., Vovk M.A., Tarasenko I.I, Mikhailova M.E., Neelov I.M., 2019, Molecules, 24, 2481.
6. Darinskii A., Gotlib Yu., Lukyanov M., Lyulin A., Neelov I., Progress in Colloid & Polymer Science, 1993, 91, 13.
7. Darinskii A., Gotlib Yu., Lyulin A., Neelov I., Vysokomolek. Soed.. Ser,A 1991, 33, 1211 (translation to English: Polymer Science, 33,1116).
8. Darinskii A., Lyulin A., Neelov I., Makromolekulare Chemie - Theory and Simulations (Macromolecular Theory and Simulations), 1993, 2, 523.
9. Darinsky A., Gotlib Y., Lukyanov M., Lyulin A., Neelov I., Progress in Colloid and Polymer Science, 1993, 91, 13.
10. Ennari J., Neelov I., Sundholm F., Polymer, 2001, 42, 8043.
11. Ennari J., Neelov I., Sundholm F., Polymer, 2000, 41, 4057.
12. Ennari J., Elomaa M., Neelov I., Sundholm F., 2000, Polymer, 41, 985.
13. Ennari J., Neelov I., Sundholm F., Comput Theor Polym Sci, 2000, 10, 403.
14. Ennari J., Neelov I., Sundholm F., Polymer, 2000, 41, 2149.
15. Ennari J., Neelov I., Sundholm F., Polymer, 2004, 45, 4171.
16. Neelov I.M., Adolf D.B., McLeish T.C.B., Paci E., Biophysical Journal, 2006, 91, 3579.

17. Gowdy,J.,Batchelor, M, Neelov, I, Paci, Journal of Physical Chemistry B, 2017, 121, 9518.
18. Neelov I.M., Adolf D.B., Lyulin AV., Davies G.R., J. Chem. Phys., 2002, 117, 4030.
19. Mazo M.A., Shamaev M.Y., Balabaev N.K., Darinskii A.A., Neelov I.M.,Physical Chemistry Chemical Physics, 2004, 1285.
20. Neelov, I. M.; Janaszewska, A.; Klajnert, B, Bryszewska M., Makova N., Hicks D., Pearson N., Vlasov G.P., Ilyash M.Y., Vasilev D.S., Dubrovskaya N.L., Zhuravin I.A., Turner A.J., Nalivaeva N.N., Current Medical Chemistry, 2013, 20, 134.
21. Falkovich S.G., Markelov D., Neelov I., Darinskii A., J. Chem. Phys., 2013, 139, 064903.
22. Neelov, I. M., Markelov D.A, Falkovich S.G., Ilyash M.Y., Okrugin B.M., Darinskii A.A., Polymer Science, 2013, 55, 154.
23. Neelov, I., Markelov D., Falkovich S.G.,, Paci E., Darinskii A., Tenhu H., Molecular Dynamics of Lysine Dendrimers‖ in Computer Simulation and NMR. Dendrimers in Biomedical Applications, (London: RSC) 2013, 99-114
24. Markelov D.A., Falkovich S.G.,, Neelov, I. M.,, Ilyash M.Y., Matveev V.V., Lahderanta E., Ingman, P., Darinskii A.A., Physical Chemistry and Chemical Physics, 2015, 17, 3214.
25. Okrugin B., Ilyash M., Markelov D., Neelov I., Pharmaceutics, 2018, 10, 129.
26. Neelov, I.M., Shavykin, Ilyash M.Y., Bezrodnyi V.V., Mikhtaniuk S.E., Fatullaev E.I., Darinskii A.A., Leermakers F.A.M., Supercomp. Frontiers and Innovations, 2018, 5, 60.
27. Popova E., Khamidova D., Neelov I., Komilov F., Chapter 3. "Lysine Dendrimers and Their Complexes with Therapeutic and Amyloid Peptides: Computer Simulation", in "Dendrimers Fundamentals and Applications"(IntechOpen), 2018, 29-45.
28. Neelov I.M., Adolf D.B., 2003, Macromolecules, 36, 6914.
29. Neelov I.M., Adolf D.B., 2004, J. Phys. Chem. B, 108, 7627.
30. Neelov I.M., Binder K., 1995, Macromolecular Theory and Simulations 4, 1063.
31. Shavykin O.V., Mikhailov I.V., Darinskii A.A., Neelov I.M., Leermakers F.A.M., Polymer, 2018,146, 256.
32. Okrugin B.M., Neelov I.M., Leermakers F.A.M., Borisov O.V., Polymer, 2017, 125, 292.
33. Shavykin O.V., Leermakers F.A.M., Neelov I.M., Darinskii A.A., Langmuir, 2018, 34, 1613.

The orientational dynamics in the dipeptides: the role of type of the side chains

Valeriy V. Bezrodniy, Sofia E. Miktaniuk[1], Oleg V. Shavykin[1,2], Igor M. Neelov[1,2]

[1]St. Petersburg National Research University of Information Technologies, Mechanics and Optics (ITMO University), Kronverkskiy pr.49, St.Petersburg, 197101, Russia
[2]St.Petersburg State University (SPbSU), 7/9 Universitetskaya nab., St.Petersburg, 199034, Russia
E-mail: kupala-89@mail.ru

Introduction

The peptide-based dendrimers are a perspective material for biomedical applications. The repeating linear fragments in this dendrimers are linear chains, i.e. two residues between one inner lysine and other inner or terminal lysine [1-2]. A change in the type of residue within a linear fragment leads to a change in properties. The same lysine as well as glycine, argenin, histidine, etc. can serve as these residues [1-2]. For the last two residues, the pairing effect in the case of terminated (capped) dipeptide chains is known [3]. These molecules consist on ends – Ace, Nme [3] and two linear residues between are lysine, arginine (Arg), charged (Hisp) and uncharged (His) histidines at different pH conditions, In this work the molecular dynamics (MD) simulation of orientational mobility of the same dipeptides (we omit the full notation of the molecules and will only use the peptide pair, for example Arg-Arg instead of Ace-Arg-Arg-Nme) was performed in water solvent with explicit account of counterions at temperature T=300K and pressure P=1atm using the program package Gromacs with AMBER99SB-ildn force field. The details of MD simulations were reported earlier for linear [5-17] and branched polymers [18-32].

The comparison of orientational mobility of side groups

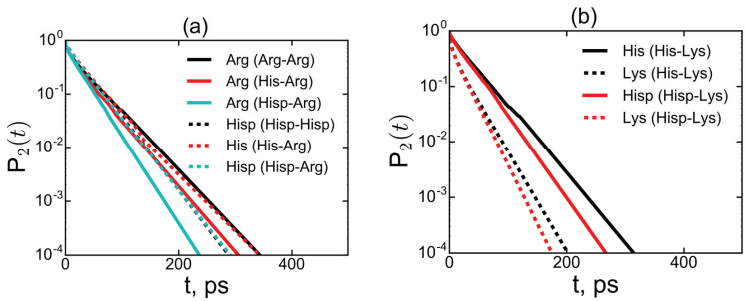

Figure 1. The second order autocorrelation functions (ACFs) for CH_2 of ε,δ and γ-amino groups in side groups of lysine (Lys), arginine (Arg) and histidine (His): (a) Arg, His, Hisp in dipeptides with pairing effects (Arg-Arg, His-Arg, Hisp-Arg; (b) His, Hisp, Lys in dipeptides without pairing effect (His-Lys, Hisp-Lys)

We estimated local mobility of the chosen vector ***d*** between two hydrogens in the hydrocarbon at Cε (side lysine), Cδ (side arginine) and Cγ (side histidine) carbons using the second order autocorrelation function (ACF) $P_2(t)$

$$P_2(t) = \frac{3}{2}\langle\frac{(\boldsymbol{d}(t),\boldsymbol{d}(0))^2}{|\boldsymbol{d}(t)|^2|\boldsymbol{d}(0)|^2}\rangle - \frac{1}{2}$$

Figure 1a presents the ACFs $P_2(t)$ for H-H vectors of side groups in the dipeptides, which capable of the pairing effect, i.e. Arg-Arg, His-Arg, Hisp-Arg, Hisp-Hisp (see, for more information [3]) while Fig.1b for the cases without pairing effect. We obtained that local orientational mobility decreases when pairing effect exists. These results are consistent both with results [3] and with our experimental results for peptide dendrimers [1-2].

Acknowledgements

This work is supported by the Russian Science Foundation (grants No. 19-13-00087). The research is carried out using the equipment of the shared research facilities of HPC computing resources at Lomonosov Moscow State University.

References

1. Sheveleva N.N., Markelov D.A., Vovk M.A., Mikhailova M.E., Tarasenko I.I., Neelov I.M., Lähderanta E.. Scientific Reports, 2018, 8, 8916.
2. Sheveleva N.N., Markelov D.A., Vovk M.A., Tarasenko I.I, Neelov I.M., E.Lähderanta, 2019, RSC Adv. 9, 18018.
3. Sheveleva N.N., Markelov D.A., Vovk M.A., Tarasenko I.I, Mikhailova M.E., Neelov I.M., 2019, Molecules, 24, 2481.
4. J. Heyda, P. E. Mason, and P. Jungwirth. J. Phys. Chem. B, 2010, 114, 8744–8749
5. Darinskii A., Gotlib Yu., Lukyanov M., Lyulin A., Neelov I., Progress in Colloid & Polymer Science, 1993, 91, 13.
6. Darinskii A., Gotlib Yu., Lyulin A., Neelov I., Vysokomolek. Soed.. Ser,A 1991, 33, 1211 (translation to English: Polymer Science, 33,1116).
7. Darinskii A., Lyulin A., Neelov I., Makromolekulare Chemie - Theory and Simulations (Macromolecular Theory and Simulations), 1993, 2, 523.
8. Darinsky A., Gotlib Y., Lukyanov M., Lyulin A., Neelov I., Progress in Colloid and Polymer Science, 1993, 91, 13.
9. Ennari J., Neelov I., Sundholm F., Polymer, 2001, 42, 8043.
10. Ennari J., Neelov I., Sundholm F., Polymer, 2000, 41, 4057.
11. Ennari J., Elomaa M., Neelov I., Sundholm F., 2000, Polymer, 41, 985.
12. Ennari J., Neelov I., Sundholm F., Comput Theor Polym Sci, 2000, 10, 403.
13. Ennari J., Neelov I., Sundholm F., Polymer, 2000, 41, 2149.
14. Ennari J., Neelov I., Sundholm F., Polymer, 2004, 45, 4171.
15. Neelov I.M., Adolf D.B., McLeish T.C.B., Paci E., Biophysical Journal, 2006, 91, 3579/
16. Gowdy,J.,Batchelor, M, Neelov, I, Paci, Journal of Physical Chemistry B, 2017, 121, 9518.
17. Neelov I.M., Adolf D.B., Lyulin AV., Davies G.R., J. Chem. Phys., 2002, 117, 4030.
18. Mazo M.A., Shamaev M.Y., Balabaev N.K., Darinskii A.A., Neelov I.M.,Physical Chemistry Chemical Physics, 2004, 1285.
19. Neelov, I. M.; Janaszewska, A.; Klajnert, B, Bryszewska M., Makova N., Hicks D., Pearson N., Vlasov G.P., Ilyash M.Y., Vasilev D.S., Dubrovskaya N.L., Zhuravin I.A., Turner A.J., Nalivaeva N.N., Current Medical Chemistry, 2013, 20, 134.
20. Falkovich S.G., Markelov D., Neelov I., Darinskii A., J. Chem. Phys., 2013, 139, 064903.
21. Neelov, I. M., Markelov D.A, Falkovich S.G., Ilyash M.Y., Okrugin B.M., Darinskii A.A., Polymer Science, 2013, 55, 154.
22. Neelov, I., Markelov D., Falkovich S.G.,, Paci E., Darinskii A., Tenhu H., Molecular Dynamics of Lysine Dendrimers‖ in Computer Simulation and NMR. Dendrimers in Biomedical Applications, (London: RSC) 2013, 99-114

23. Markelov D.A., Falkovich S.G.,, Neelov, I. M.,, Ilyash M.Y., Matveev V.V., Lahderanta E., Ingman, P., Darinskii A.A., Physical Chemistry and Chemical Physics, 2015, 17, 3214.
24. Okrugin B., Ilyash M., Markelov D., Neelov I., Pharmaceutics, 2018, 10, 129.
25. Neelov, I.M., Shavykin, Ilyash M.Y., Bezrodnyi V.V., Mikhtaniuk S.E., Fatullaev E.I., Darinskii A.A., Leermakers F.A.M., Supercomp. Frontiers and Innovations, 2018, 5, 60.
26. Popova E., Khamidova D., Neelov I., Komilov F., Chapter 3. "Lysine Dendrimers and Their Complexes with Therapeutic and Amyloid Peptides: Computer Simulation", in "Dendrimers Fundamentals and Applications"(IntechOpen), 2018, 29-45.
27. Neelov I.M., Adolf D.B., 2003, Macromolecules, 36, 6914.
28. Neelov I.M., Adolf D.B., 2004, J. Phys. Chem. B, 108, 7627.
29. Neelov I.M., Binder K., 1995, Macromolecular Theory and Simulations 4, 1063.
30. Shavykin O.V., Mikhailov I.V., Darinskii A.A., Neelov I.M., Leermakers F.A.M., Polymer, 2018,146, 256.
31. Okrugin B.M., Neelov I.M., Leermakers F.A.M., Borisov O.V., Polymer, 2017, 125, 292.
32. Shavykin O.V., Leermakers F.A.M., Neelov I.M., Darinskii A.A., Langmuir, 2018, 34, 1613.

Structural studies of 2-(2-(2-azido-5-chlorophenyl)-2-(5-methylfuran-2-yl)ethylidene)-1,1-dimethylhydrazine by heteronuclear two-dimensional NMR spectroscopy

Inna G. Borodkina[1], Gennady S. Borodkin[1], Alexandra A. Kolodina[1], Nadezhda S. Trofimova[1], Vladimir T. Abaev[2], Pavel B. Chepurnoy[1], Natalya V. Stankevich[1]

[1]Institute of Physical and Organic Chemistry at Southern Federal University, Rostov-on-Don, 344090 Stachki st., 194/2, Russian Federation
[2]Department of Chemistry, North-Ossetian State Uniersity, Vladikavkaz, 362025 Vatutina st., 46, Russian Federation
E-mail: nmr@ipoc.sfedu.ru
http://www.ipoc.rsu.ru

Introduction

2-(2-(2-Azido-5-chlorophenyl-)-2-(5-methylfuran-2-yl)ethylidene)-1,1-dimethyl-hydrazine was obtained. Analysis of heteroatomic HMBC and HSQC correlations allowed establishing full correspondence of ^{1}H and ^{13}C NMR signals of this compound.

Synthesis of 2-(2-(2-azido-5-chlorophenyl)-2-(5-methylfuran-2-yl)ethylidene)-1,1-dimethylhydrazine

Formaldehyde dimethylhydrazone is a useful one-carbon synthon introduced by spanish chemists as a neutral formyl-anion equivalent [1]. To take an advantage of its unusual reactivity to undergo electrophilic substitution at the methylene carbon atom as was reported earlier [2], we designed the three component condensation reaction aimed to obtain 2-azidobenzylfuran derivative **1** useful in further indole chemistry [3]. Unfortunately, under the action of iodine or bismuth triflate reaction invariably led to hydrazono transfer product **2** with small amount of difurylmethane **3** (scheme 1).

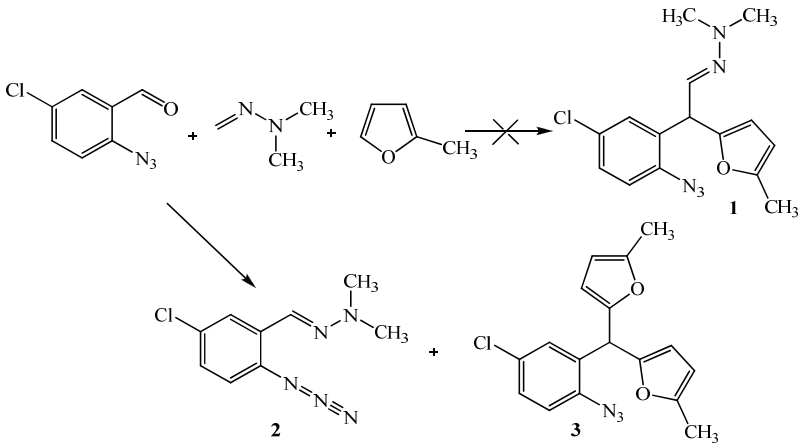

Scheme 1

Assignment of the ^{1}H and ^{13}C signals using the heteronuclear, two-dimensional NMR spectroscopy methods

In order to determine the structures of compound **2** assignment of the NMR ^{1}H spectra signals was performed on the basis of characteristic values of chemical shifts and cross-peak

analysis in the two-dimensional spectra of ^{1}H-^{13}C HSQC and HMBC correlations at temperature 30°C. Figure 1 shows the values of chemical shifts of protons, as well as key correlations observed in the HMBC spectrum.

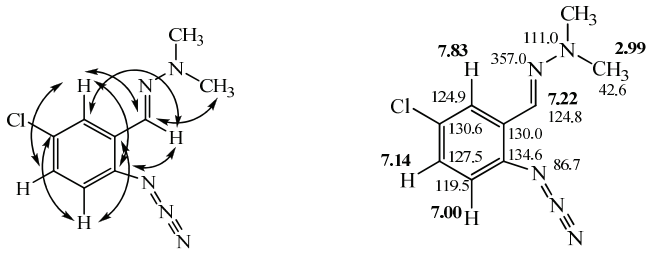

*Figure 1. The scheme of the main HMBC correlations (**A**) and correspondence of the ^{1}H and ^{13}C signals of compound **2** (**B**)*

Heteroatomic ^{1}H-^{13}C HSQC and HMBC correlations are given in the Table 1. Analysis of these data allowed performing complete assignment of signals of the NMR ^{1}H and ^{13}C spectra of compound **2** (Fig. 1).

*Table 1. Coordinates of cross-peaks in the HMBC and HSQC spectra of compound **2***

^{1}H, δ, ppm	**HMBC, ^{13}C, δ, ppm**	**HSQC, ^{13}C, δ, ppm**
7.84	124.8, 127.5, 130.0, 130.6, 134.6	124.9
7.22	124.9, 130.0, 134.6	124.8
7.14	119.5, 124.9, 130.6, 134.6	127.5
7.00	127.5, 130.0, 130.6, 134.6	119.5
2.99	124.8	42.6

Confirmation of the structure using the ^{1}H-^{15}N HMBC method

The cross-peaks of ^{1}H-^{15}N HMBC correlation spectrum of compound **2** (Fig. 2), obtained at 30°C, are given in the Table 2.

*Table 2. Coordinates of cross-peaks in the ^{1}H-^{15}N HMBC spectrum of compound **2***

^{1}H, δ, ppm	**HMBC, ^{15}N, δ, ppm**
2.98	111.0, 357.0
7.00	86.7
7.22	111.0, 357.0
7.84	86.7

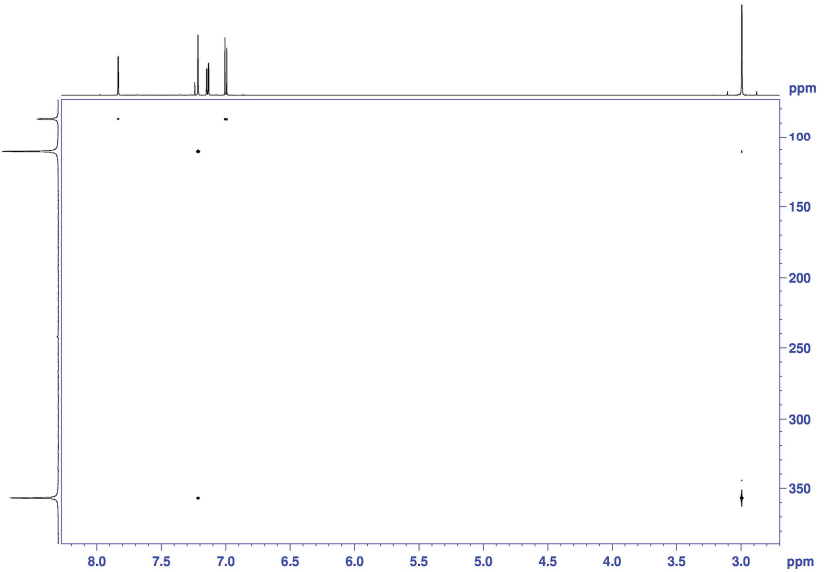

*Figure 2. The fragment of ^{1}H-^{15}N HMBC spectrum of compound **2** (30°C)*

References

1. J.-M. Lassaletta, R. Fernandez. - *Tetrahedron Lett.,* **33**, 3691-3694 (1992).
2. R. Fernández,.E. Martín-Zamora, C. Pareja, M. Alcarazo, J. Martín, J.-M. Lassaletta. – *Synlett,* **7**, 1158–1160 (2001).
3. V.T. Abaev, A.T. Plieva, P. N. Chalikidi, M. G. Uchuskin, I. V. Trushkov, A. V. Butin. - *Org. Lett*., **16**, 4150−4153 (2014).

Mini-protein denaturation at high temperatures

Ann Butyugina, Andrei V. Komolkin

Faculty of Physics, Saint Petersburg State University, St. Petersburg, 199034, Russia
E-mail: st068699@student.spbu.ru

Introduction

Proteins are high-molecular organic substances consisting of peptide-linked chains of amino acids. Despite the fact that in living organisms there are always compound complexes formed by several protein molecules in which every protein has its own function [1], these days close attention is also paid to mini-proteins [2,3] because they are considered as models of large systems.

The 1L2Y [4] protein was synthesized using standard F Solid-Phase Synthesis methods on an Applied Biosystems 433a Synthesizer at the university of Washington. As the smallest protein-like construct, Trp-cage miniproteins should provide a testing ground for both experimental studies and computational simulations of protein folding and unfolding pathways. For example, it was used to study the stability of proteins at high temperatures when dissolved in aqueous mixtures of amino acid-based ionic liquids [2]. This mini-protein was chosen because of its small size which means that it takes a small amount of time to model the system, but it does display secondary structural elements, such as α-helix and β-turn.

The purpose of this work is to investigate the stability of 1L2Y protein in an aqueous solution when heated to high temperatures by the molecular dynamics method. This method is one of the molecular systems modeling methods, successfully used to study the physicochemical properties of the condensed state of matter - isotropic liquids and solutions, liquid crystals [5].

Experimental section

In this paper, the task was set to repeat the experiment performed by the authors of the article [2], but using potentials OPLS-AA (Optimized potentials for liquid simulation— all atoms) [6] instead of CHARMM36 potentials. The atom coordinates were downloaded from wwpdb.org (Protein Data Bank) and, those coordinates being used, a model of a single 1L2Y molecule was created (in the freeware Jmol program) [7]. The simulation was carried out in the AKMD program. A system containing one 1L2Y protein molecule and 1989 SPC/E model water molecules was created and equilibrated. The resulting water solution was simulated for 10 ns at a temperature of 310 K, 14 ns at 390 K, and 135 ns at a temperature of 440 K in the NpT ensemble using equipment in the science park of St. Petersburg State University.

When processing the simulation results, the denaturation of the 1L2Y protein was of interest. The quantity of hydrogen bonds in the molecule was used as a numerical characteristic of the denaturation process. In the alpha helix, each amino acid is linked to the other, therefore, if the hydrogen bonds break due to the high temperature and their total number in the protein molecule decreases, the spiral unfolds and the protein is denatured.

The graph shows the dependence of the number of hydrogen bonds on the simulation time (Fig. 1.1). It can be seen that as the temperature increases from 310 K (from 0 to 9.8 ns) to 390 K (from 9.8 to 24 ns), the number of hydrogen bonds in the molecule increases by 10%, i.e. the molecule passes into a more beneficial conformation. However, the temperature of the system is still not enough to break the hydrogen bonds and the protein remains stable.

The system heated to a high temperature of 440 K and simulated for a long time (from 24 ns to 159 ns), the number of hydrogen bonds tends to decline significantly. By the end of the simulation, the number of hydrogen bonds in the protein molecule has dropped to two, which means that the protein has completely denatured. The value of the number of hydrogen bonds fluctuates, because some of them are unstable: they are broken and re-created occasionally. In

order to visually reduce sudden changes, the previous graph was smoothed using the moving average method.

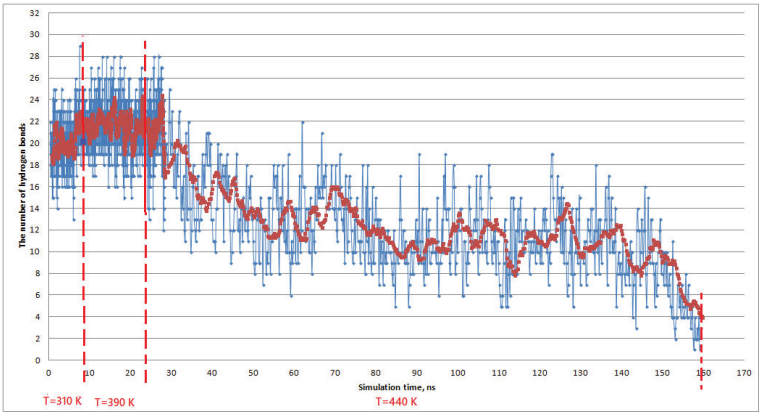

Figure 1. The dependence of the number of hydrogen bonds in the protein molecule on the simulation time (the smoothed line is highlighted in red)

Next, the structure of the alpha helix in the 1L2Y molecule at various temperatures was examined minutely. At 310 K, the hydrogen bonds, which are highlighted in red in the Fig. 2(a), connecting the turns of the alpha helix, were not destroyed and the protein remained stable. At 390 K, the system energy was still not enough to break intramolecular hydrogen bonds (Fig. 2(b)), and at a high temperature - 440 K - the hydrogen bonds in the helix broke and the protein completely denatured (Fig. 3).

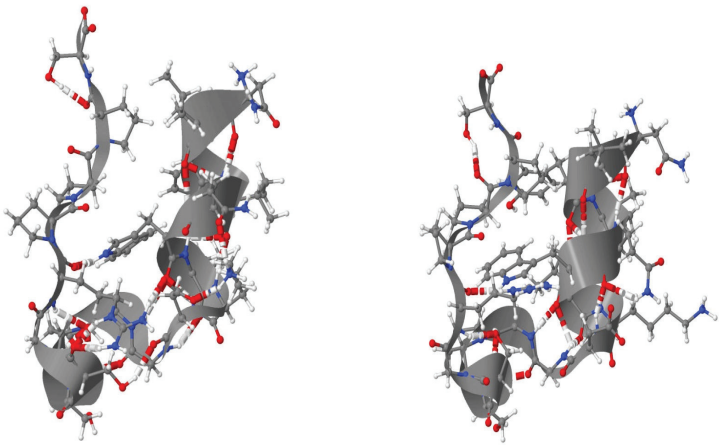

a) At the beginning of the simulation at 310 K (0.23 ns)

b) At the end of the simulation at 310 K (9.8 ns)

Figure 2. Alpha spiral structure at a temperature of 310 K

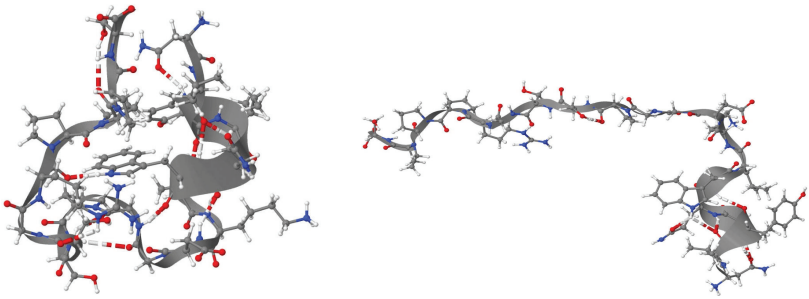

a) At the end of the simulation at 390 K (23.6 ns)

b) At the end of the simulation at 440 K (149.6 ns)

Figure 3. The structure of the alpha helix at a temperature of 390 K and 440 K

Acknowledgment

The authors thank the science park of St. Petersburg State University for providing the equipment for the experiment.

References

1. Жмуров А.А., Барсегов В.А. «Молекулярное моделирование с использованием графических процессоров», - Учебное пособие Москва – 2013, с 13. URL: https://hpc.mipt.ru/zhmurov/files/biomol/lectures.pdf (accessed 25.02.2019)
2. Guillaume Chevrot, Eudes Eterno Fileti, Vitaly V. Chaban .Protein remains stable at unusually high temperatures whensolvated in aqueous mixtures of amino acid based ionic liquids, J Mol Model (2016) 22: 258, DOI 10.1007/s00894-016-3123-9.
3. Gattin Z, Riniker S, Hore PJ, Mok KH, van Gunsteren WF (2009) Temperature and urea induced denaturation of the TRP-cage mini protein TC5b: a simulation study consistent with experimental observations. Protein Sci 18:2090–2099
4. wwpdb.org (accessed 22.02.2019)
5. Computer Simulation of Liquids / M. P. Allen, D. J. Tildesley, Clarendon Press, 1987. 385 c.
6. Jorgensen WL, Tirado-Rives J (1988). "The OPLS Force Field for Proteins. Energy Minimizations for Crystals of Cyclic Peptides and Crambin". J. Am. Chem. Soc. 110 (6): 1657–1666. DOI :10.1021/ja00214a001. PMID 27557051.
7. Jmol: an open-source browser-based HTML5 viewer and stand-alone Java viewer for chemical structures in 3D. URL: http://jmol.sourceforge.net/ (accessed 22.02.2019)

NOE application for ratio estimation of conformer populations in chromone-fused allylmorpholines

Nikita M. Chernov[1], Igor P. Yakovlev[1], Stanislav I. Selivanov[2]

[1]Saint Petersburg State Chemical Pharmaceutical Academy, Street Prof. Popova 14, 197376 Saint Petersburg, Russia
[2]Institute of Chemistry, State University of Saint-Petersburg, University prospect 26, 198504, Saint-Petersburg, Russia
E-mails: [1]nikita.chernov@pharminnotech.com; [2]nmr.group.spbu@gmaill.com

Introduction

During last years many problems of collection and processing of nuclear Overhauser effect (NOE) data and their correct analysis were analyzed and overcome. It lead to the possibility of accurate quantitative determination of interproton distances rij by 2D NOESY [1-3] or 1D NOE [4] experiments has appeared. As a result of the development of such methodology, a new term emerged - the exact nuclear Overhauser effect (eNOE), which is understood as a quantitative distance estimation with relative accuracy within ±5% of the actual value [5, 6].

Simultaneously, the same approach was used also in case of flexible molecules. Two main directions can be mentioned. Firstly, to determine the ratio of conformers under conditions of fast (in NMR time scale) conformational exchange. Secondly, to estimate most accurately (within 1%) the fraction of the minor conformer (in case when it`s less 5 %) in which two protons are situated much closer than in case of the dominant form [7, 8]. The second possibility of application NOE experiments is especially important for structural and conformational analysis of organic molecules in liquid when there are no other experimental methods for determining the ratio of conformers using, for example, measurements of averaged by fast exchange chemical shifts or scalar constants. It is possible due to non-linear character of cross-relaxation rate σ dependence on interprotone distance r_{ij}:

$$\sigma_{ij} \sim \tau_c (r_{ij})^{-6},$$

where τ_c is correlation time of overall rotating diffusion for rigid molecule in liquid. It means that in case two-position exchange A $\rightleftarrows$ B (Fig. 1a) averaged value of distance $\langle r_{ij} \rangle$ may be calculated on base relationship (Fig. 1b), in which P_A and P_B are populations of conformers A and B ($P_A + P_B = 1$). Their experimental values may be estimated from graphics $\langle r \rangle = f(P_A, P_B)$, which are needed to get for known (or calculated by molecular modeling program) values of distances r_A and r_B (Fig. 1c).

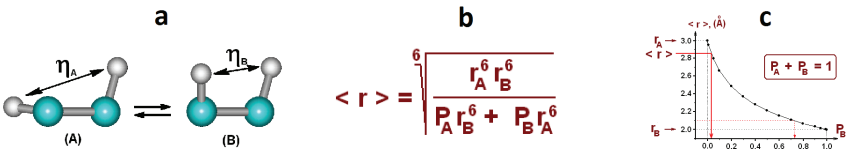

Figure 1 a) Process of NOE averaging at fast two-position conformational exchange, b) formula for averaged distance values $\langle r \rangle = f(P_A, P_B)$ and c) its graphic presentation at r_A = 3.0 Å and r_B = 2.0 Å

Comparison of experimental distance value $\langle r \rangle^{exp.}$ defined by NOE experiment with calculated ones and presented in the graphic form allows us to determine populations P_A and P_B (see red arrow in Fig. 1c). Recently, this simple graphical approach was very intensively used to prove conformational mobility in strychnine and other natural products [3, 6-11].

Experiments and results

This report presents the results of eNOE approach [12] to the quantitative estimation of the population ratio in liquid of two conformers associated with fast in NMR time scale restricted rotation of side substitutions around simple C_b-C_c bond in some chromone-fused allylmorpholines (Fig. 3). Synthesis of compounds under study was published in [13].

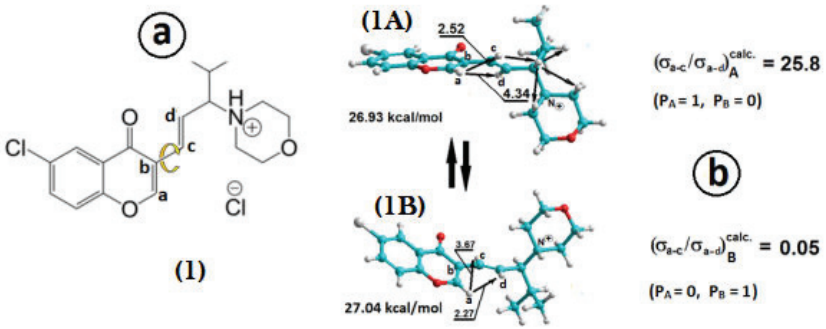

Figure 1. ***a)*** *Structure of in chromone-fused allylmorpholine* ***(1)*** *and two-position conformational exchange under study.*
b) *Calculated ratio of cross-relaxation rates on base calculated distances which were defined from conformer optimization data by MM2 method for each conformer. Distances are marked by arrows and their values (Å) are shown by figures*

To achieve this goal, the cross-relaxation rates for two pairs of protons H_a–H_c and H_a–H_d were measured with high accuracy using volume integration of the corresponding cross-peaks in the F.NOESY [14] spectra (Fig. 4a). These spectra were recorded for each compound at several mixing times in the interval 0.1 – 1.4 s and at least 64 scans for every t_1-increment were used to get exact values of cross-peak and diagonal volume integrals.

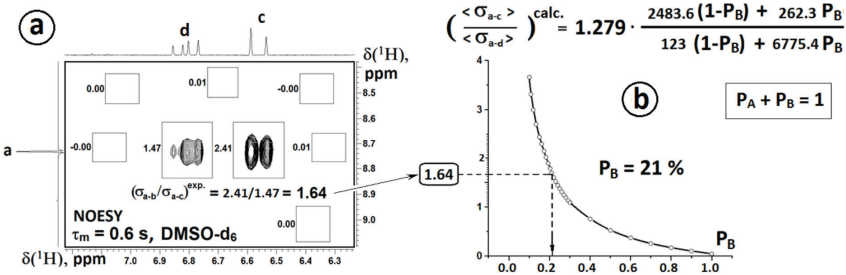

Figure 2. ***a)*** *Fragment of NOESY spectrum of adduct* ***(1)*** *in DMSO-d6 where volume integral values are given by figures (in % relatively diagonal signal of H_a) near corresponding rectangle.* ***b)*** *Graphic of calculated dependence of ratio cross-relaxation rates $<\sigma_{a-c}>/<\sigma_{a-d}>$ on population of minor conformer* ***(1B)***

While processing NOESY spectra the greatest attention was paid to eliminating phase distortions in the vicinity of integrated cross- and diagonal peaks, as well as to aligning the base plane [1, 15]. The reliability of the values of relative integral intensities when using the PANIC approach [16, 17] was ensured by repeating experiments with the same set of acquisition and

processing parameters, as well as by variation the relaxation delay D1. This was led to high reproducibility of the results of measuring the value of ratio $<\sigma_{a-c}>/<\sigma_{a-d}>$ which did not depend on mixing time τ_m.

Conclusion

NMR **a**nalysis of **m**olecular **f**lexibility **i**n **s**olution (so-called NAMFIS approach) **e**xact **N**uclear **O**verhauser **e**ffect (eNOE) data and **f**ast two-dimensional **NOE-s**pectroscop**y** (F.NOESY) were intensively used during study of chromone-fused allylmorpholine (**1**) in DMSO-d_6. Effectiveness of this methodology for quantitative estimation of conformer population ratio was checked at structural elucidation and conformational analysis of this compound. Because of molecular flexibility only averaged NMR parameters are accessible and spatial structure determination on base NOEs is more complicated. Nevertheless. comparison of the NOE data for chromone-fused allylmorpholine (**1**) obtained for only two selected proton pairs with their calculated values led to a quantitative evaluation of the minor form with high accuracy: population value in DMSO-d_6 is 21% with an error less ±2%.

Acknowledgments

NMR experiments were performed on spectrometer DPX-300 (Bruker) in the Resource Center "Magnetic Resonance Research Centre" of the Saint-Petersburg State University. The study was carried out under the financial support of the Russian Foundation for Basic Research (grant no. 17-74-10117).

References

1. N.H. Andersen, H.L. Eaton, X. Lai. Magn. Reson. Chem. 1989, 27(6), 515–528.
2. D. Neuhaus, M.P. Williamson . "The Nuclear Overhauser Effect in Structural and Conformational Analysis" (2nd ed.) // Wiley-VCH, New York, 2000. 619 P.
3. S.I. Selivanov, A.G. Shavva. Russ. J. Bioorg. Chem., 2002, 28(3), 194–208.
4. K. Stott, J. Keeler, Q.N. Van, A.J. Shaka. J. Magn. Reson., 1997,125 (2), 302–324.
5. B. Vögeli, Prog. Nucl. Magn. Reson. Spectrosc., 2014, 78, 1–46.
6. C.P. Butts, C.R. Jones, E.C. Towers et al. Org. Biomol. Chem., 2011, 9 (1), 177–184.
7. A. Kolmer, L.J. Edwards, I. Kuprov, C.M. Thiele. J. Magn. Reson., 2015, 261, 101–109.
8. C.R. Jones, M.D. Greenhalgh, J.R. Bame et al. Chem. Commun., 2016, 52, 2920 – 2923.
9. S. Schmidt et al. Eur. J. Org. Chem., 2014, № 6, 1147-1150.
10. J. Bame, C. Hoeck et al. Phys. Chem. Chem. Phys., 2018, 20(11), 7523-7531.
11. S.I. Selivanov, A.Yu. Solov`ev et al. Russ. J. Bioorg. Chem., 2007, 33(3), 302–309.
12. B. Vögeli, S. Olsson, R. Riek, P. Güntert . J. Struct. Biojlogy 1915, 191(3) 306–317.
13. N.M. Chernov, R.V. Shutov, O.I. Barygin, M.Y. Dron, G.L. Starova, N. N. Kuz'mich,I.P. Yakovlev. Eur. J. Org. Chem. 2018, 6304–6313.
14. Th. Geppert, M. Köck, M. Reggelin et al. Magn. Reson. Ser. B. 1995, 107(1) 91–93.
15. S.I. Selivanov, S.N. Morozkina et al. Chem. Het. Compounds 2008, 44(6), 654-665.
16. E. Esposito, A. Pastore. J. Magn. Reson. 1988, 76(2), 331–336.
17. S. Macura, B.T. Farmer II, L.R. Brown. J. Magn. Reson., 1986, 70(3), 493–499.

Porphyrins: proton spectra

Nina Djapic

University of Novi Sad, Technical Faculty "Mihajlo Pupin", Zrenjanin, Serbia
E-mail: nidjapic@gmail.com

Introduction

In the porphyrin proton spectrum, from the chemical shifts (δ) and scalar couplings (*J*), obtained can be the values for the elucidation of the: vinyl-, ethyl- and propionyl- side chain groups. The methyl- and methoxy- protons can be assigned after applying the relaxation phenomenon – nuclear Overhauser effect (NOE). The two-dimensional (2D) NMR techniques can provide the data for the complete porphyrin structural determination.

Porphyrin proton spectra

The pheophorbide *a* proton spectrum is depicted in Fig. 1.

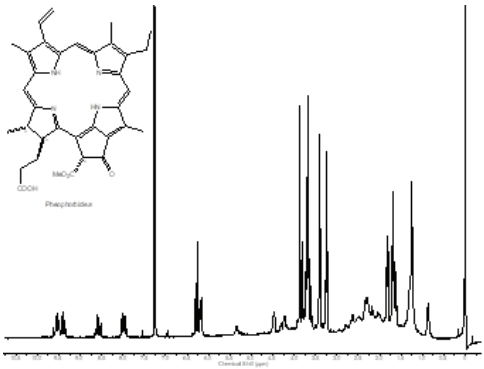

Figure 1. Pheophorbide a proton spectrum

The methylpheophorbide *a* proton spectrum is depicted in Fig. 2.

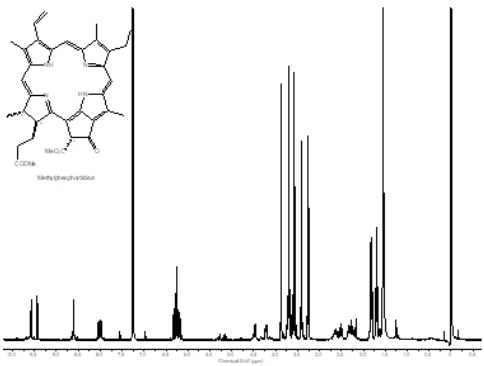

Figure 2. Methylpheophorbide a proton spectrum

The methylpyropheophorbide *a* proton spectrum is depicted in Fig. 3.

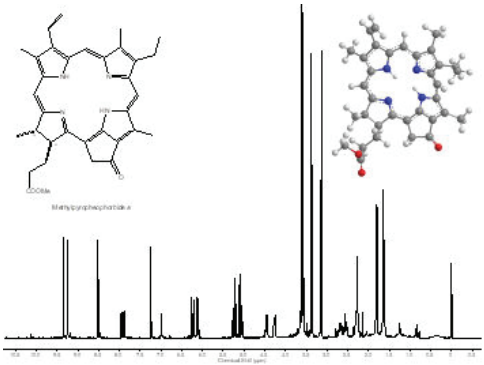

Figure 3. Methylpyropheophorbide a proton spectrum

The proton spectrum depicted in Fig. 4 is a derivate of one of the previously depicted porphyrins. Realize that the find out proton spectrum cannot turn one into a living Buridan's donkey. Contemplate a solution which is, more than, infinitesimally closer to the right one.

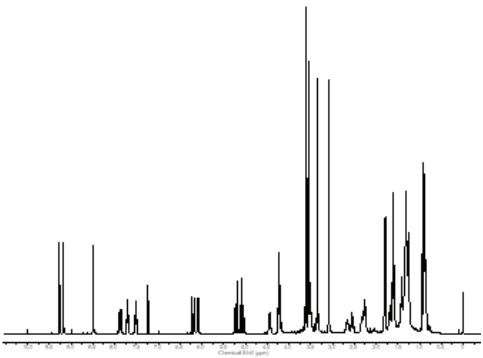

Figure 4. Find out proton spectrum

Acknowledgements

Theirs the merit for accuracy, mine is the fault for inaccuracy.

^{1}H-NMR evaluation of the LDH-A inhibitor Oxamate on the metastatic breast cancer cell lines MDA-MB-231 and MCF-7

Anaïs Draguet, Corentin Schepkens, Vanessa Tagliatti, Jean-Marie Colet

Department of Human Biology and toxicology at the university of Mons
E-mail: Anaïs.Draguet@student.umons.ac.be

Background

Breast cancer is the major cause of cancer death in women. Several existing treatments are associated with critical adverse effects, usually due to the exposure of undesired cells. New targeted therapies are in development or in clinical trial. These therapies could reduce the adverse effects.

Cancerous cells have a particular lactate metabolism. In terms of environment conditions, they could use this one as an energy source. Thus, one can anticipate that the inhibition of lactate metabolism could slow down the tumor development. For example, oxamate is an inhibitor of the lactate dehydrogenase A which converts pyruvate in lactate. The structural analogy with pyruvate allows a non-competitive inhibition. The action of this inhibitor was already studied in our lab on different cell lines as melanoma with encouraging results.

Experimental approach

The purpose of the present study was to evaluate the oxamate effect on metastatic breast cancer cell lines MCF-7 and MDA-MB-231. The evaluation was based on H-NMR analyses of the extracellular fluid as well as MCW cellular extracts. The NMR measurements were performed on a 600 MHz spectrometer (Avance, Bruker). In parallel, cell viability and proliferation were also performed at different oxamate concentrations and different exposure times. Following the lactate metabolism disruption, a decrease of cell viability and proliferation is observed.

References

1. Brooks A. George, « The science and translation of lactate shuttle theory », Cell Metabolism, 2018
2. Richard Vincent *et al.* , « Does the ^{1}H-NMR plasma metabolome reflect the host-tumor interactions in human breast cancer? », Oncotarget, 2017
3. Xintaropoulou Chrysi *et al.* , « A comparative analysis of inhibitors of the glycolysis pathway in breast and ovarian cancer cell line models », Oncotarget, 2015
4. Schepkens Corentin *et al.* , « A new classification method of metastatic cancers using a ^{1}H-NMR-based approach : a study case of melanoma, beast, and prostate cancer cell lines », Metabolites, 2019

Application of high-frequency EPR spectroscopy for the identification and separation positions of electrically active impurities of nitrogen, boron and vanadium in silicon carbide crystals and heterostructures

E. V. Edinach

Ioffe Institute, 194021 St. Petersburg, Russia
E-mail: elena.edinach@mail.ioffe.ru

Introduction

Silicon carbide (SiC) is a promising wide-gap semiconductor for applications in high-frequency, high-temperature, and high-power electronic devices. For this purpose *n*- and *p*-type SiC is grown by including donor (such as N) or acceptor (such as B, Al, and Ga) impurities. The further development of SiC-based semiconductor devices requires a good understanding of the electronic structure of donor and acceptor centers and their sites in the lattice.

In the 6H-SiC polytype structure, three nonequivalent crystallographic positions: one hexagonal (*h*) and two quasi-cubic (*k*1, *k*2) sites, are distinguished. The SiC crystal consists of tetrahedra with four bonds per atom, two of which are in the (11-20) plane; along the c axis, the ladder structure is formed.

SiC doping with vanadium is one of the main methods for fabricating semi-insulating substrates required for high-power microwave devices [1, 2]. If the vanadium concentration is higher than the uncompensated boron concentration, electrons from the vanadium donor level occupy all boron acceptor levels. Similar processes also occur in the case of nitrogen donor compensation: if the vanadium concentration is higher than the uncompensated nitrogen concentration, electrons from nitrogen donor levels occupy vanadium acceptor levels.

Experimental

Several series of 6H-SiC silicon-carbide polytype samples were grown by the sublimation sandwich method [3]. The samples under study are as follows: (i) Crystals with low nitrogen concentrations, $N_d - N_a \approx 1 \times 10^{17}$ cm^{-3}, where N_d and N_a are the donor and acceptor concentrations, were grown in vacuum at temperatures of 1700–1750ºC. (ii) Structures consisting of a semi-insulating 6H-SiC crystal substrate with a vanadium impurity and n-type 6H-SiC silicon-carbide layer grown on the substrate with a rather high uncompensated nitrogen concentration $N_d - N_a \approx 1 \times 10^{18}$ cm^{-3}. (iii) Structures according to item (ii) with a completely removed semi-insulating substrate.

Measurements are performed using the EPR/ESE spectroscopic complex, which was developed in the Ioffe Institute operating in the continuous wave and pulsed modes at frequencies of 94 and 130 GHz in a wide range of magnetic fields (–7÷ +7 T) and temperatures (1.5–300 K). A magneto-optical closed-cycle cryogenic system, highly stable generators (94 and 130 GHz), and a cavity-free system for supplying microwave power to the sample are used.

Results and discussion

Fig. 1 (left panel) shows the EPR spectra of shallow nitrogen N donors in the 6H-SiC crystal, measured in the continuous-wave (cw) mode in three ranges (X, W, and D) for two edge magnetic-field orientations in the crystal, B || c and B ⊥ c. The inset schematically shows the 6H-SiC crystal structure. The EPR spectra of nitrogen donors are described by the spin Hamiltonian (1) with the spin S = 1/2 and axial symmetry (eliminating the term describing the fine interaction),

$$H = g_{||}\mu_B B_z S_z + g_{\perp}\mu_B\left(B_x S_x + B_y S_y\right) + A_{||} S_z I_z + A_{\perp}\left(S_x I_x + S_y I_y\right). \quad (1)$$

The hyperfine structure in the EPR spectra is caused by interaction with the nitrogen ^{14}N nucleus, $I = 1$, the natural content of this isotope is 99.63%. Fig. 1 (left panel) clearly shows not only the increasing resolution of EPR spectral lines with increasing measurement frequency, but also the g-factor anisotropy.

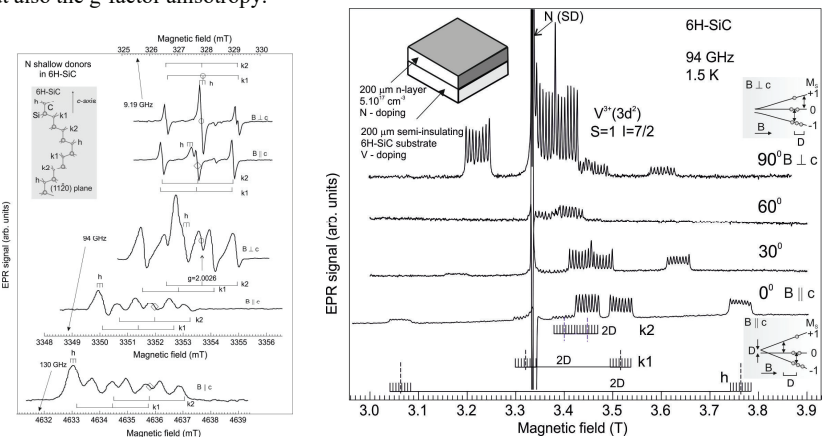

Figure 1. Left panel - EPR spectra of shallow nitrogen N donors in the 6H-SiC crystal. Right panel - EPR spectra of V^{3+} ions in the 6H-SiC crystal.

Fig. 1 (right panel) shows the EPR spectra of V^{3+} ions ($3d^2$ electronic configuration) substituting silicon in the 6H-SiC crystal. The spectra were measured at a frequency of 94 GHz at 1.5 K for four magnetic field orientations with respect to the hexagonal *c* axis. Three sets of spectra with a characteristic hyperfine structure caused by hyperfine interaction with the nuclear spin I = 7/2 of the dominant (99.75%) isotope ^{51}V are visible. The EPR spectra are described by the standard spin Hamiltonian (1) with axial symmetry and spin S = 1,

$$H = g_{||}\mu_B B_z S_z + g_{\perp}\mu_B\left(B_x S_x + B_y S_y\right) + D\left(S_z^2 - \frac{1}{3}S(S+1)\right) + A_{||}S_z I_z + A_{\perp}\left(S_x I_x + S_y I_y\right). \quad (2)$$

Two groups of 2I + 1 = 8 lines for each vanadium site in the 6H-SiC crystal are shown. It is also seen that the sign of the fine structure parameter D is positive for all vanadium V^{3+} sites [4]. In earlier works, only the magnitude D was measured. The inset in Fig. 1 (right panel) shows the energy levels for two edge magnetic-field orientations B || c and B ⊥ c; the circles indicate the Boltzmann distribution of the triplet- level population in the approximation of strong magnetic fields and low temperatures; three different vanadium sites in the crystal, i.e., the hexagonal (*h*) and two quasi-cubic (*k*1, *k*2), are indicated.

Fig. 2 shows the experimental and calculated orientation dependences of the EPR lines of the shallow boron acceptor in 6H-SiC without taking into account the hyperfine interaction. Solid blue lines are calculated curves for hexagonal (*h*) center, broken and dotted lines for two quasi-cubic (*k*1, *k*2) centers. The parameters used in the calculation are given in [5].

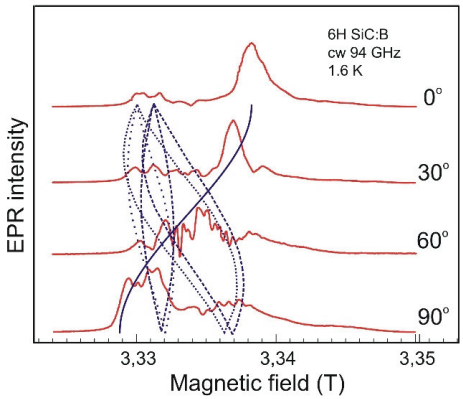

Figure 2. The experimental (red lines) and simulated (blue lines) EPR spectra of 6H-SiC:B for different orientations of the magnetic field

Summary

The high spectral resolution of high-frequency EPR spectroscopy makes it possible to identify impurities, to separate and distinguish nitrogen donor, deep compensating vanadium impurity site types and boron in silicon-carbide crystals and heterostructures and to uniquely determine the energy-level diagram. The measurements were performed using equipment developed at the Ioffe Institute, which allows operation in a wide range of magnetic fields from –7 to 7 T and temperatures from 1.5 to 300 K and requiring no infrastructure for producing cryogenic liquids.

Acknowledgements

This work has been supported by the Russian Foundation for Basic Research under Grant No. 19-52-12058, Deutsche Forschungsgemeinschaft (DFG) within the framework of the ICRC project TRR 160 and the Russian Academy of Sciences.

References

1. M. Yoganathan, A. Gupta, et al. Mater. Res. Soc. Symp. Proc. 815, J5.9 (2004).
2. M. Bickermann, R. Weingärtner, A. Winnacher, J. Cryst. Growth 254, 390 (2003).
3. E. Radovanova, R. Verenchikova, Yu. Vodakov, Sov. Phys. Semicond. 17, 640 (1983).
4. E. V. Edinach, A. D. Krivoruchko, et al., Semiconductors 54, 1, 150–156 (2020).
5. T. Matsumoto, O. Poluektov, J. Schmidt, et. al., Phys. Rev. B 55, 4, 2219 (1997).

Methylpyrazole as a molecular probe for the investigation of the acid-base properties of silica surface: computational ^{15}N NMR study

Alexandra A. Efimova

Faculty of Physics, St. Petersburg State University, Russian Federation
E-mail: sashaefimova15@yandex.ru
Scientific supervisor: Prof. Dr. Tolstoy P.M., Department of Physical Chemistry Institute of Chemistry, Saint-Petersburg State University

Introduction

Mesoporous materials have attracted high interest due to their potential applications in many fields such as controlled drug delivery, catalysis, adsorption and separation [1]. The usefulness of these materials lies in several structural properties, like facile functionalization, tunable pore size and large surface area [2]. Because of the small pore diameter, the physical behavior of the guest molecules in these materials is sensitive to the competition between host-guest and guest-guest attractive interactions. Proton-donating and proton-accepting properties of mesoporous silica surface, which are determined by the presence and spatial distribution of silanol groups (SiOH) (see schematic representation of a small area of such surface in Fig. 1), are often studied by using acids and bases as guest molecules [3]. Molecules of pyrazoles exhibit both basic and acidic properties, so they can form self-associates as well as various hydrogen-bonded complexes on the surface of mesoporous silica. One of the critical parameters that is sensitive to the structure and geometric properties of such hydrogen bonds is ^{15}N NMR chemical shift, which changes by ca. 100 ppm upon full protonation/deprotonation of pyrazole. It is interesting to study the possibility of predicting the types of complexes formed between pyrazoles and silanol groups on the silica surface by ^{15}N NMR spectroscopy, namely, by examining the average values of ^{15}N chemical shifts.

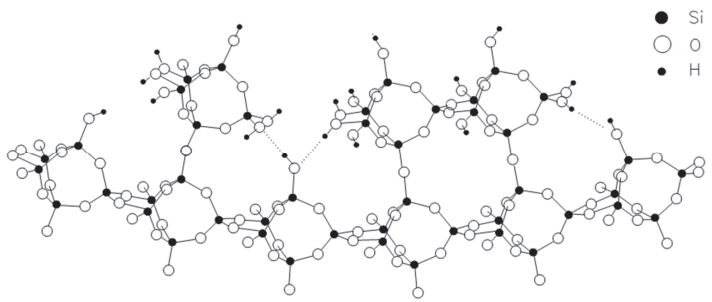

Figure 1. Schematic model of the mesoporous silica surface [4]

Aims and methods

For this study we chose 17 systems including methylpyrazole (**1**), its self-associates (cyclic dimer **2** and cyclic trimer **3**), molecules modelling SiOH groups of silica surface (**4** and **9**) and several mixed complexes, such as species **5**, **10** and others. The schematic structures of these systems are shown in Fig. 2.

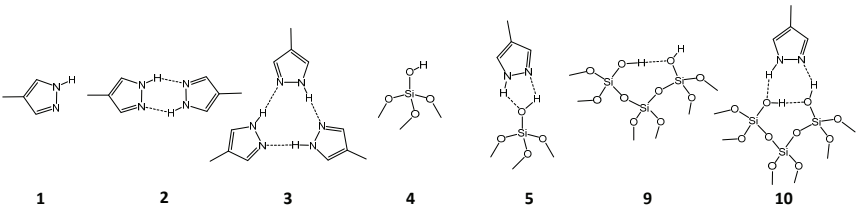

Figure 2. Schematic structures of some of the investigated systems

Geometry optimization and NMR chemical shifts were calculated using Gaussian09 at B3LYP/6-311++G(d,p) level of theory for each complex, and electron density topological analysis was performed using QTAIM (Quantum Theory of Atoms in Molecules) methodology.

Results

As an example of the results obtained in this work, in Fig. 3 is shown the correlation dependence between the energy of N–H···N, O–H···N and N–H···O hydrogen bonds and the values of corresponding isotropic ^{15}N NMR chemical shifts.

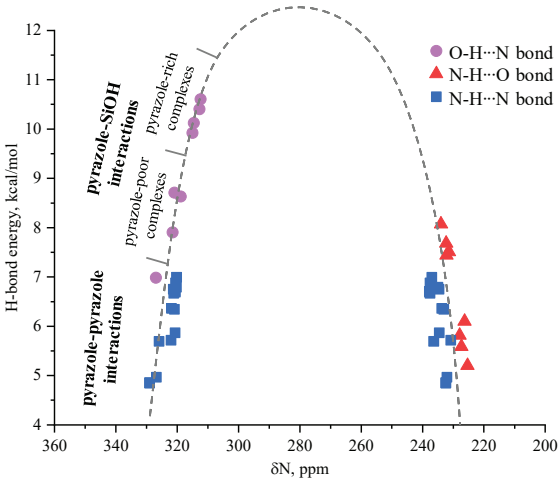

Figure 3. Dependence between hydrogen bond energies of N–H···N, O–H···N and N–H···O bonds and corresponding ^{15}N chemical shifts

Along the chemical shift axis there is a significant overlap of regions corresponding to different types of complexes, though it is possible to distinguish regions of data points associated with pyrazole-pyrazole contacts (N–H…N bonds) and contacts between SiOH groups and pyrazoles as proton acceptors (O–H…N bonds). In this work the obtained results are compared with the previously published experimental data [5].

References

1. Ide M., El-Roz M., De Canck E., Vicente A., Planckaert T., Bogaerts T., Van Driessche I., Lynen F., Van Speybroeck V., Thybault-Starzyk F., Van Der Voort P., *Phys. Chem. Chem. Phys.*, **2013**, *15 (2)*, 642–650

2. Meynen V., Cool P., Vansant E.F., *Microporous and Mesoporous Mater.*, **2009**, *125 (3)*, 170–223
3. Buntkowsky G., Breitzke H., Adamczyk A., Roelofs F., Emmler T., Gedat E., Grünberg B., Xu Y., Limbach H.-H., Shenderovich I., Vyalikh A., Findenegg G., *Phys. Chem. Chem. Phys.*, **2007**, *9 (35)*, 4843–4853
4. Shenderovich I.G., Mauder D., Akcakayiran D., Buntkowsky G., Limbach H.-H., Findenegg G.H., *J. Phys. Chem. B*, **2007**, *111 (42)*, 12088–12096
5. Torres Barthelemy V., *NMR Studies of the H-transfer and Dynamics of 1H-pyrazoles in the Crystalline State and Confined in Mesoporous Silica Materials, dissertation*, Free University of Berlin, **2010**

Peculiarities of water arrangement around nitrate-anion in aqueous solution. A computer simulation study

Maria I. Egorova, Andrei V. Egorov, Vladimir I. Chizhik, A. Laaksonen

Faculty of Physics, Saint-Petersburg State University, Russia
E-mail: maryaverina@gmail.com

Nitrate ion is involved in numerous chemical and biological processes in the fields of biochemistry, surface and environmental chemistry. Therefore, the understanding of nitrate solvation behavior is essential for explaining mechanisms of processes occurring in aqueous solutions. To study nitrate hydration an ab initio Car-Parrinello molecular dynamics (CPMD) simulations [1] were carried out. The study is focused on the mechanisms of water rearrangement in the vicinity of the anion.

CPMD simulations of a dilute aqueous solution of NO_3^- were carried out in canonical ensemble at 300 K. The model system contains one ion and 48 water molecules in the cubic periodic cell and its density was set to be equal to 1.000 g/cm^3 (corresponding cell size 11.56 Å). The initial configuration was taken from 1 ns classical simulation performed at 300 K using SPC-F water model [2]. The model nitrate anion was treated as a 4-site planar structure with a central nitrogen atom and three oxygen atoms at a distance of 1.22 Å with all O-N-O angles of 120^o [3]. Intermolecular interactions were described as the sum of Coulomb and Lennard-Jones potentials with parameters taken from [4]. DFT calculations were performed using the exchange functional proposed by Becke and the correlation energy expression by Lee, Yang, and Parr [5]. The valent-core interaction for all atoms was described by norm-conserving Troullier–Martins pseudopotentials [6]. The valence electron wave function was expanded in plan waves with an energy cut off of 90 Ry. The fictitious electron mass was set to 500 au and the time step to 0.1 fs. Nose thermostat was used to maintain the temperature. The model system was equilibrated during the 30 ps simulation. The production run was 140 ps long.

Molecular motion in nitrate-anion aqueous solution were described using the following characteristics: the self-diffusion coefficients for the anion and water molecules, the residence time of water in the hydration shell of the anion, and the times of reorientational motion for water molecules and NO_3^-. A special attention was given to the investigation of molecular origin of the electric field gradients experienced by nitrate ion.

References

1. Car, R.; Parrinello, M. – *Phys. Rev. Lett.*, 55, 2471-2474 (1985).
2. Toukan, K.; Rahman, A. – *Phys. Rev. B*, 31, 2643-2648 (1985).
3. Ebner, Ch.; Sonsone, R.; Hengrasmee S.; Probst, M. – *Int. J. Quant. Chem.*, 28, 805-814 (1999).
4. Megyes, T.; Bálint, S.; Peter, E.; Grósz, T.; Bakó, I.; Krienke, H.; Bellissent-Funel, M. – *J. Phys. Chem. B*, 113, 4054-4064 (2009).
5. Becke, A. D. – *Phys. Rev. A*, 38, 3098-3100 (1988); Lee, C.; Yang, W.; Parr, R. G. – *Phys. Rev. B*, 37, 785-789 (1988).
6. Troullier, N.; Martins, J. L. – *Phys. Rev. B*, 43, 1993-2006 (1991).

Nicotinamide riboside as a potential cardioprotective agent for counteracting doxorubicin-induced cardiotoxicity in H9C2 cells

Sophie Fourez, Matthieu Dallons, Vanessa Tagliatti

Department of Human Biology and toxicology at the university of Mons
E-mail: Sophie.Fourez@student.umons.ac.be

Introduction

Doxorubicin is the most used anticancer drug when no targeted therapy is available. This anthracycline drug presents a satisfying efficacy, however it also causes dose dependent and cumulative toxic effects, especially on the heart. Several researches were led to investigate the cardiotoxicity caused by doxorubicin in cancer treatment. It is now accepted that the mode of action of doxorubicin comes from the increase of ROS which causes an oxidative stress in cardiac cells. This can lead to severe heart diseases. The enzyme responsible for this is the NADH oxidase which is initially used in the mitochondrial phase of cellular respiration.

Doxorubicin can be reduced in semiquinone by eNOS and NADH oxidase. This semiquinone can activate oxygen into ROS which generate oxidative stress. This leads to the formation of a redox cycle which generates a lot of free radicals. We observed in previous results obtained by ^{1}H-NMR-based metabonomics that doxorubicin causes a energy metabolic switch from the Kreb's cycle to glycolysis. This leads to a lack in NAD^{+} for the Kreb's cycle supply. The redox cycle undergone by doxorubicin for the free radicals generation is suspected to be responsible for this lack of NAD^{+}.

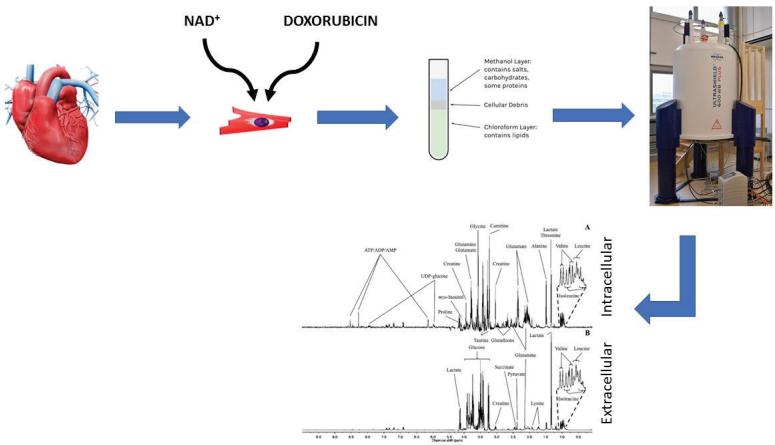

Figure 1. Procedure

Experimental strategy

In the present work, we will try to re-establish the availability in NAD^{+} in the Krebs cycle. For this purpose, nicotinamide riboside will be used as a cell culture medium supplement to restore the NAD^{+} intake. The cardiomyoblasts H9C2 cells will exposed to both supplement and doxorubicin to possibly restore the Kreb's cycle activity in order to prevent doxorubicin-induced toxicity. The supplement will also be used in complement with dexrazoxane, the current

approved cardioprotective drug, on doxorubicin-treated H9C2 cells. The potential effects of the supplement on the metabolic pathways in H9C2 cells will be investigated by ^{1}H-NMR-based metabonomics approach.

References

1. Maria A. Mitry and John G. Edwards, «Doxorubicin induced heart failure: Phenotype and molecular mechanisms», IJC Heart and Vasculature, 2016
2. Eun Hye Choi *et al*., «Cytoprotective effect of anthocyanins against doxorubicin-induced toxicity in H9c2 cardiomyocytes in relation to their antioxidant activities», Food and Chemical Toxicology, 2007
3. Elena Katsyuba *et al*., «De novo NAD+ synthesis enhances mitochondrial function and improves health», Nature, 2018

Nuclear spin-lattice relaxation in antiferromagnetic thermoelectric $CuFeS_2$

Stanislav O. Garkavyi[1], Ecaterina V. Schmidt[1], Vadim L. Matukhin[1], Georgy V. Mozzhukhin[2]

[1]Kazan State Power Engineering University, Kazan, 420066, Russia
[2]Department of Physics, Gebze Technical University, 41400 Gebze/Kocaeli, Turkey
E-mail: ololoiev77@mail.ru

Introduction

In recent years, thermoelectric properties of a well-known semiconductor mineral chalcopyrite $CuFeS_2$ attracted a lot of attention. This n-type semiconductor has a significant Seebeck coefficient at room temperature ($S \approx -500$ μV·K^{-1}), but relatively good thermal conductivity ($k \approx 10$ W·m^{-1}K^{-1}), which leads to a small value of thermoelectric figure of merit ZT = 0.008. Several directions of successful optimization of the electronic parameters of $CuFeS_2$ appeared [1-3]. As a result of the studies, it was possible to increase the value of thermoelectric figure of merit by more than two orders of magnitude up to values of ZT = 0.2-0.3 at 700 K. Work on doping the compound with various elements (Zn, Mn, Co, Ni, Pd) led to further improvement of its thermoelectric properties [4-6]. It is known that chalcopyrite is an antiferromagnetic with a Néel temperature of T_N = 823 K and it has been suggested that magnetic interaction can cause a large effective mass of charge carriers and, accordingly, a relatively high power factor in doped $CuFeS_2$ compounds. However, up to the present time, the magnetic reason for the increase in thermoelectric figure of merit has not been fully established. In this regard, it is of interest to study the spin-lattice relaxation of nuclear spins in chalcopyrite, since nuclear relaxation in semiconductor compounds is due to hyperfine interactions between nuclear spins and charge carriers [6, 7]. Previously, ^{63,65}Cu NMR method in a local field was used to study nuclear quadrupole interactions [8–10].

Methods

Samples from two mineral deposits “Talnakh” and “Sibai” were investigated. The nuclear magnetic resonance spectra in the local field and spin-lattice relaxation times of the Cu nuclei were measured with a Tecmag-Redstone multipulse NQR/NMR spectrometer. The ^{63,65}Cu spectra were obtained using the standard spin-echo sequence π/2-τ-π-echo. The time of nuclear spin-lattice relaxation by ^{63}Cu NMR in a local field was measured in the temperature range 77 - 300 K in sample of the $CuFeS_2$ from “Sibai” deposit, and at 77 K and 300 K in sample from “Talnakh” deposit, to obtain information about the features of the strong relationship between the electron and spin subsystems of this compound. The spin-lattice relaxation time T_1 was measured by the inversion recovery method of nuclear magnetization.

Results

Spin-lattice relaxation in electrically conductive materials, first of all, arises as a result of hyperfine interaction between the nucleus and free charge carriers and depends on their concentration [11]. In chalcopyrites, the dependence is pronounced - the higher the concentration of free carriers, the higher the spin-lattice relaxation rate and shorter than T_1. In fig. 1. a graph of the temperature dependence of the spin-lattice relaxation rate in the temperature range 77–300 K is presented. The graph shows an exponential decrease in the spin-lattice relaxation rate with decreasing temperature. It is seen that the temperature dependence is monotonic. Analyzing the nature of the temperature dependence of the spin-lattice relaxation rate according to the formula [12]

$$\frac{1}{T_1} \propto exp[-E_a/k_B T]$$

the activation energy, E_a = 17 meV in sample from “Sibai” deposit and E_a = 32 meV in sample from “Talnakh” deposit, can be obtained.

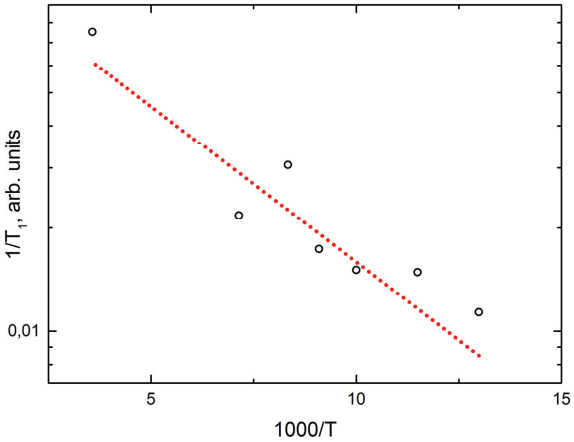

Figure 1. ^{63}Cu spin-lattice relaxation rate $1/T_1$ of $CuFeS_2$ sample from "Sibai" mineral deposit. The dashed line shows dependence obtained from the formula above

Conclusions

Results demonstrate a lower spin-lattice relaxation rate for the Sibai sample. Among the various mechanisms of spin-lattice relaxation in antiferromagnetics, the most effective is the Raman scattering of two and three magnons. The theory indicates a power-law temperature dependence of $1/T_1$ and a strong dependence of $1/T_1$ on the anisotropy J'/J of the spin system [13]. Analysis of the behavior of the spin-lattice relaxation rates and activation energy in $CuFeS_2$ samples showed that the spin-lattice relaxation rate is determined not by magnetization fluctuations, but by mechanisms related to electron diffusion.

References

1. Y. Li, T. Zhang, Y. Qin, T. Day, G. J. Snyder, X. Shi, L. Chen, J. Appl. Phys. 2014, 116, 203705.
2. N. Tsujii, J. Electron. Mater. 2013, 42, 1974–1977.
3. J. Li, Q. Tian, J.-F. Li, J. Alloys Compd. 2013, 551, 143–149.
4. W. D. Carr, D. T. Morelli, J. Electron. Mater. 2016, 45, 1346–1350.
5. H. Xie, X. Su, G. Zheng, Y. Yan, W. Liu, H. Tang, M. G. Kanatzidis, C. Uher, X. Tang, J. Phys. Chem. C 2016, 120, 27895–27902.
6. N. Tsujii, T. Mori, Appl. Phys. Express 2013, 6, 043001.
7. Handbook of Mineralogy (Eds.: J. W. Anthony, R. A. Bideaux, K. W. Bladh, M. C. Nichols), Mineralogical Society of America, Chantilly, VA 20151–1110, USA, 2003
8. Ogloblichev V.V., Sevastyanov I.G., Gavrilenko A.N., Matukhin V.L., Arapova I.J., Medvedev E.J., Garkavyi S.O., Schmidt E.V., J. App. Spectr., 2016, 83, 731.
9. Matukhin V.L., Pogoreltsev A. I., Gavrilenko A.N., Garkavyi S.O., Schmidt E.V., Babaeva S.F., Sukhanova A.A., Terukov E.I., Semiconductors, 2017, Vol 51, No. 1. pp. 4–7.
10. Matukhin V.L., Pogoreltsev A. I., Gavrilenko A.N., Garkavyi S.O., Schmidt E.V., Babaeva S.F., Sukhanova A.A., Terukov E.I., Semiconductors, 2018, Vol. 52, No. 8, pp. 969–972.

11. E. M. Levin, Phys. Rev. 2016, B 93, 245202.
12. A. A. Sirusi, J. H. Ross Jr., Annual Reports on NMR Spectroscopy, 2017, Vol. 92, pp. 137–198.
13. F. Raffa, M. Mali, J. Roos, D. Brinkmann, Physical review B, 1998, Vol. 58, pp. 2724–2729.

Proposal for the method for measuring ^{57}Fe NMR spectra of compounds based on $BiFeO_3$ unification

Natalia E. Gervits[1], Alexey V. Tkachev[1], Sergey V. Zhurenko[1,2], Anton V. Gunbin[1], Andrey A. Gippius[1,2], Vjacheslav S. Pokatilov[3]

[1]Lebedev Physical Institute, Russian Academy of Sciences, 119991, Moscow, Russia
[2]Moscow State University, Physical Department, 119992, Moscow, Russia
[3]Moscow State Technical University of Radio Engineering, Electronics, and Automation, 119454, Moscow, Russia
E-mail: ngervits@gmail.com

Introduction

For the first time, cycloid-type spacial spin-modulated structure (SSMS) was detected in $BiFeO_3$ (BFO) using neutrons [1]. Later, Zalessky observed a two-horned ^{57}Fe NMR spectrum and proposed a theoretical approach to describing it [2]. The search for cycloid destruction methods proved to be an essential task on the way to the practical application of BFO-based materials.

One of the fundamental parameters characterizing a cycloid is *m*, the anharmonicity parameter. In the literature, the value of this parameter even measured using a single method (zero-field NMR spectroscopy) varies from 0 to almost 1. This reasons for such a scatter need to be clarified. In this paper, we present our observations made during the study of several series of BFO-based samples, which can explain the ambiguity of determining the anharmonicity parameter by various scientific groups and propose a measurement technique that will allow us to unify and compare the results.

In this paper, we propose methods for working with a bismuth background, which interferes with the analysis of the ^{57}Fe spectrum, and also analyzed a possible reason for the discrepancy between the values of the anharmonicity parameter in the literature. We make several proposals for the unification of measurements. All proposals relate to the direct measurement phase, which helps to avoid further complication of the model and processing of spectra to determine the parameters of the SSMS.

Methods

The NMR spectroscopy allows one to obtain a direct field distribution. Although there are some complicating factors, such as a complex dependence of the signal intensity on the RF pulses amplitude, various relaxation processes, and superposition of signals from various nuclei. In this paper, we discuss ways to minimize the effects of these factors.

Acknowledgements

The reported study was funded by RFBR according to the research project № 17-52-80036.

References

1. I. Sosnowska, T. P. Neumaier, and E. Steichele, “Spiral magnetic ordering in bismuth ferrite,” *J. Phys. C Solid State Phys.*, vol. 15, no. 23, pp. 4835–4846, 1982.
2. A. V. Zalessky, A. A. Frolov, T. A. Khimich, A. A. Bush, V. S. Pokatilov, and A. K. Zvezdin, “57Fe NMR study of spin-modulated magnetic structure in BiFeO3,” *Europhys. Lett.*, vol. 50, no. 4, pp. 547–551, May 2000.

Investigation of the primary echo signal in polymers with three-spin groups

Irina Yu. Golubeva[1], Grigorii E. Karnaukh, Tatiana P. Kulagina[2]

[1]Facultyof fundamental physicalandchemicalengineering, Moscowstate University, Moscow, Russia,
[2]Institute ofproblemsofchemicalphysics RAS, 142432, Chernogolovka, Russia
E-mail: tan@icp.ac.ru

Introduction

The paper proposes a theory of primary echo signals (SE) in linear polymers with isolated groups of three spins ½ with arbitrary dipole-dipole coupling constants (DDI). A new method is proposed for calculating the SE signals $A_3(t,\tau)$ after exposure to two RF pulses [1], analytical calculations of the SE signal from an isolated group of three spins and numerical calculations are performed.

The method of calculating the signal

The proposed theory allows us to characterize the primary echo $A(t,\tau)$and the shape of the line $F(\omega)$in polymers containing selected three-spin groups

FID in linear polymers without meshes are calculated in the Anderson-Weight model with corresponding correlation functions of molecular motions$k_i(\tau)$:

$$G_i(t) = exp\left(-\omega_{loc}^2 \int_0^t (t-\tau)k_i(\tau)d\tau\right), i = 1{,}2$$

whereω_{loc} - the average local field created on any spin by both the spins belonging to the selected segment and all other spins in the chain.
For chains with free ends with FID has the form [2]:

$$G_r(t) = G_1(t)G_2(t)$$

In a linear polymer containing isolated three-spin groups, FID is expressed by the following formula:

$$G(t) = G_3(t)G_r(t)$$

where $G_3(t)$ –FIDi n the three-spin system ½ [1].
The SE expression looks similar for the entire spin system:

$$A(t,\tau) = A_3(t,\tau)A_r(t,\tau)$$

where$A_r(t,\tau)$- the primary echo signal in polymers [2], which is associated with the free induction decay$G_r(t)$:

$$A_r(t,\tau) = \frac{G_r(t)^2 G_r(\tau)^2}{G_r(t+\tau)}$$

Results and discussion

In the course of this work, the primary echo formula was obtained in linear polymers containing isolated three-spin groups, and the free-induction decay and solid-echo signals were modeled in linear polymers with a three-spin group½.

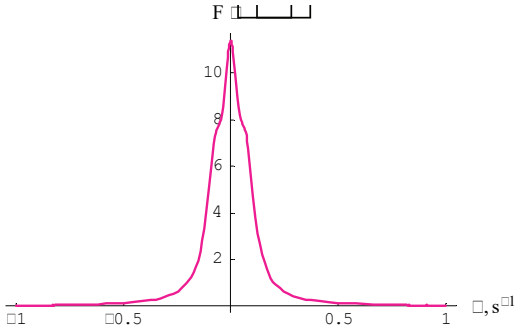

Figure 1. The line shape with the same constants DDI (weak influence)
$N_0 = 20, \alpha = 0{,}05, \omega_{loc} = 0.01c^{-1}, \tau_c = 0{,}04c, b = 5 \cdot 10^{-4}c$

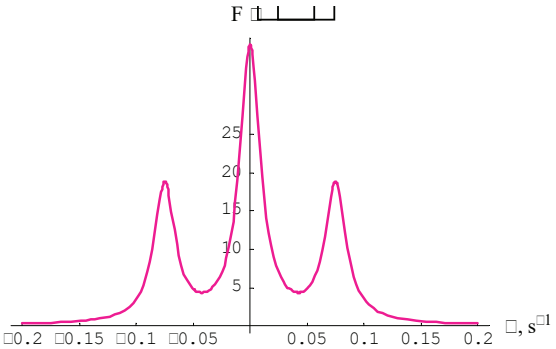

Figure1. The line shape with the same constants DDI (strong influence)
$N_0 = 20, \alpha = 0{,}05, \omega_{loc} = 0.01c^{-1}, \tau_c = 0{,}01c, b = 5 \cdot 10^{-4}c$

Acknowlegment

The work was carried out on the topic of the state assignment of the Ministry of Science and Higher Education No. 0089-2014-0021.

References

1. GolubevaI.Yu, Karnaukh G.E., Kulagina T. P. // Proceedings International Sch00l-Conference Magnetic Resonance and its Applications. 2019. P. 170.
2. Kulagina T. P., Karnaukh G. E., Kuzina A. N., Smirnov L. P. // *Russian Journal of Phys. Chem. B.* **7,** 170-176 (2013).

Numerical simulation of the nonlinear frequency shift of a ferromagnetic film resonator

Roman V. Haponchik, Alexey B. Ustinov

Department of Physical Electronics and Technology, St.Petersburg Electrotechnical University, St.Petersburg, -197376 Russia
E-mail: ferumno33@gmail.com

Introduction

The spin-wave resonator is a plane rectangular sample of a ferromagnetic film. The dimensions of the resonator, its shape, magnetic parameters of the film and a value of the bias magnetic field determine the resonant frequency spectrum. Practically, resonators based on an yttrium iron garnet (YIG) film are used usually because this material has the lowest parameter of relaxation of magnetization oscillations. It is known that with an increase in the microwave signal power exciting oscillations in a ferromagnetic film resonator, various nonlinear effects could be emerged. The effect of bistability [1] is observed and well enough studied in normally magnetized resonators. In the case of in-plane magnetized resonators, a nonlinear frequency shift and nonlinear damping of magnetization oscillations take place [2,3]. The purpose of this work is theoretical investigation of the nonlinear effects emerged in tangentially magnetized ferromagnetic film resonators.

Experimental prototype

The resonator represented an YIG film sample with a thickness of 7 μm and lateral dimensions $a = b = 1$ mm, which was grown epitaxially on a 0.5 mm thick gallium gadolinium garnet (GGG) substrate. The film had saturation magnetization of 1800 Oe. The resonator was magnetized in its plane. Magnetization oscillations were excited in the resonator by a microstrip antenna with a width of 50 μm and a length of 2 mm, one end of which was connected to a standard microstrip transmission line with a characteristic impedance of 50 Ω, and the other end was grounded. The resonator was positioned immediately on the microstrip antenna as is shown in Fig. 1. The microstrip structure with the resonator was placed between poles of a permanent magnet.

The nonlinear properties of the resonator were studied with measurements of the microwave absorption spectra at various input power levels of the applied microwave signal.

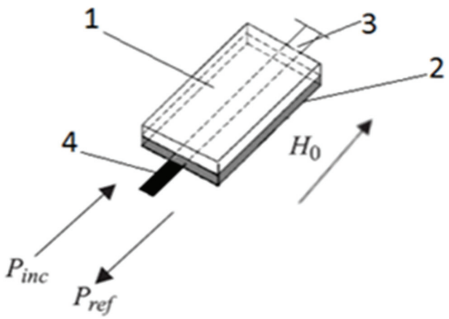

Figure 1. Schematic diagram of the resonator: 1 – GGG substrate, 2 – YIG film resonator, 3 – short circuit, 4 – microstrip antenna

Experimental results

Figure 2(a) shows a fragment of the resonator reflection spectrum corresponding to a main mode of the resonator measured for different input power levels. This characteristic was measured as $S_{11}(f) = 10\lg\left(\frac{P_{ref}(f)}{P_{inc}(f)}\right)$, where f is the microwave frequency and $P_{inc}(f)$ is the incident microwave power, and $P_{ref}(f)$ is the reflected signal power. The magnetic field H_0 was 1800 Oe, for which the resonant frequency was about 5.265 GHz. As is seen from the measured dependences, an increase in the power level leads to a change in resonant frequency due to the effect of a nonlinear frequency shift. Moreover, it leads to an increase in the width of the resonance curve due to the nonlinear damping of spin waves. Figure 2(b) shows the microwave absorption curves demonstrating their broadening with power increasing. Here $\overline{P}_{abs} = \frac{P_{abs}}{P_{abs\,max}}$.

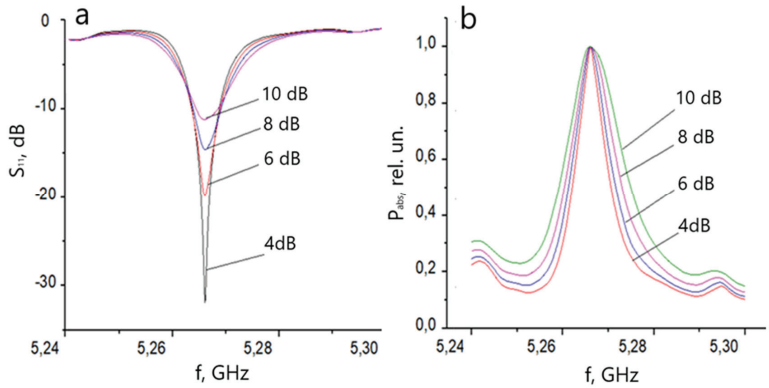

Figure 2. Resonator reflection spectrum corresponding to a main mode of the resonator measured for different input power levels (a) and a family of resonance curves (b) that shows increasing in the width of resonance curves

Figure 3 shows by points the experimental dependences of relaxation frequency ω_r and resonance frequency f_0(fig. 3b) from the absorbed power P_{abs}.

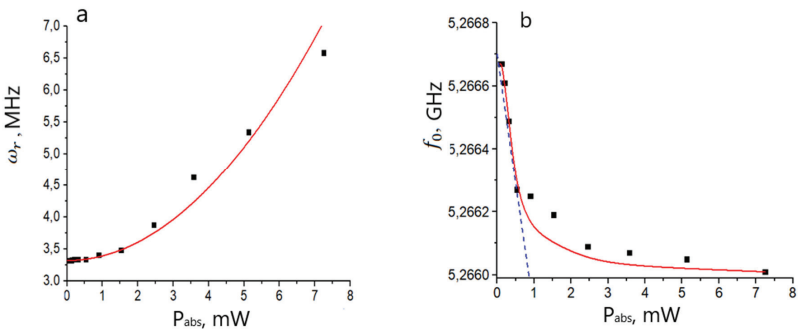

Figure 3. The relaxation frequency (a) and resonance frequency (b) versus absorbed microwave power. Points are experimental data, and curves are the results of calculations

Theoretical results

Behavior of the resonance frequency is typical for the ferromagnetic film resonators. It can be readily explained by considering a model of magnetization precession. For the lower resonance oscillation mode the equation has the following form:

$$\omega^2 = [(\omega_H + \omega_{M0}(1 - |U|^2)\left(\frac{1-e^{-kL}}{kL}\right)] * [(\omega_H + \omega_{M0}(1 - |U|^2)\left(\frac{k_y}{k}\right)\left(1 - \frac{1-e^{-kL}}{kL}\right)] \quad (1)$$

where $\omega_H = 2\pi|\gamma|H_i$, $\omega_M = 2\pi|\gamma|M_0$, $k = \sqrt{k_y^2 + k_z^2}$, $k_y = \frac{\pi}{b}$, and $k_z = \frac{\pi}{a}$, U – amplitude of the spin waves.

The experimental results were described in terms of a nonlinear oscillator:

$$\ddot{x} + 2\delta(\dot{x} + \alpha\dot{x}^2 + \beta\dot{x}^3) + \omega_0^2(x + \gamma x^3) = P\cos(pt) \quad (2)$$

where δ is attenuation decrement, α and β are nonlinear components of the attenuation decrement, γ is nonlinear coefficient of the frequency shift, ω_0 is resonance frequency, P is incident power, p is frequency of incident power.

Using this equation, we obtain relaxation frequency in the following way:

$$\omega_r = 2\delta(1 + \beta\omega_0^2|U|^2) \quad (3)$$

where $2\delta = 6{,}64$ MHz, $\beta = 3{,}7\times 10^{-15}\,\frac{1}{\mathrm{Hz}^2}$.

In order to describe the dependence of the resonance frequency on the absorbed microwave power, we used the following approach. As can be seen from the experimental data in Fig. 3, the resonance curves possess nearly Lorentzian shapes. For this reason, the normalized amplitude of magnetization oscillations was represented by a standard expression for the amplitude of induced oscillations on the absorbed power $\bar{P}_{abs}$:

$$U = \frac{\sqrt{\frac{P_{abs}}{B}}}{\sqrt{\left(\omega_0^2 - \omega^2\right)^2 + (2\omega_r\omega^2)^2}} \quad (4)$$

where B is coupling coefficient between the absorbed power of spin waves and the amplitude of oscillations of a ferrite resonator ($P_{abs} = B|U|^2$).

Using this expression and the known values of power, we calculate the amplitude of magnetization oscillations at the resonance frequency. And use it to find the coefficient $B = 2185$. The results of the numerical simulations are shown in Fig. 3 by solid curves. As is seen they describes experimental data in a good agreement.

Conclusion

Result of our investigation showed that our theory describes well the experimental data. One can use it to describe different nonlinear effects of the ferrite resonators.

Acknowledgements

The work was supported in part by the Ministry of Science and Higher Education of Russia.

References

1. Y.K. Fetisov, C.E. Patton, V.T. Synogach. IEEE Trans. Mag., **6**, 4511-4521 (1999).
2. H. Yan, Q. Wang and I. Awai. Electron. Lett. **32**, 1787-1789 (1996).
3. A.V. Drozdovskii, A.B.Ustinov. Tech. Phys. Lett. **36**, 834 (2010).

Ionic liquid of N-methylpyrrolidoneacetate as an extract agent in the process of selective cleaning of oil fractions

M. D. Ibragimova, S. A. Seidova

Y. H. Mammadaliyev Institute of Petrochemical Processes of Azerbaijan National Academy of Sciences, Az 1025, Baku, 30 Khojaly ave
E-mail: minaver-ibrahimova@rambler.ru
Key words: extraction purification, raffinate, extractant, ionic liquid, extract

The development of effective environmentally friendly methods for the production of base oils, as well as fuels that meet the ever-growing requirements of the standards for a set of physical- mechanical and operational properties is an urgent task for oil refining. In this aspect, the use of ionic liquids as a selective solvent in the processes of dearomatization and desulfurization and the creation of purification technologies that meet the requirements of "green chemistry" is very promising.

This report presents the results of studies of the selective purification of the distillate of hydraulic fluid AMG-10, diesel distillates of various compositions, as well as the kerosene fraction by extraction using the ionic liquid N-methylpyrrolidoneacetate synthesized on the basis of acetic acid and N-methylpyrrolidone as a selective solvent.

The effectiveness of the use of ionic liquids synthesized based on formic and acetic acids and various amines is shown by the results of studies conducted in the Institute of Petrochemical Processes of ANAS [1-2].

Using N-methylpyrrolidoneacetate as an extractant shows the possibility of:

- obtaining the basis of the hydraulic fluid AMG-10 that meets the requirements of TU 0253-021-46693-103-2006 by the method of extraction of the distillate with a temperature of start of boil 234 ° C and end of boil 306 ° C, as well as distillate with start of boil 222, end of boil 313 ° C obtained by compounding ten-degree fractions of oil from the Balakhany and Neft Dashlary deposits, isolated by distillation in an APH-2 laboratory unit. The conditions for the complete dearomatization of the hydraulic distillate by ion-liquid extraction were determined [3];

- dearomatization and desulfurization of straight-run diesel fraction (SDF) of primary oil refining, as well as a mixture of SDF with medium distillate fractions of secondary oil refining (SOR), in particular light catalytic cracking gas oil and light coking gas oil, with a volume ratio of SDF: SOR-70:30.

Depending on the conditions of extraction purification, the degree of dearomatization of the mixture of diesel distillates ranges from 60-80% wt., The degree of desulfurization 72.3-84.4% wt. The cetane number of diesel fuels obtained by the method of ion-liquid extraction purification increases and amounts to 50,4-54,6 depending on the composition of the initial diesel distillate, as well as on the implementation of extraction purification in one stage or in stages [4].

In the case of the combined method, in particular, extraction purification of hydrotreated distillate, almost complete dearomatization of the fuel was observed and the degree of desulfurization is 58,2% mass.

- extraction purification of kerosene fractions with a boiling point of 136-240, 145-250 and 185-250°C, differing in the content of aromatic hydrocarbons – 13,22; 19,2 and 17,3% mass respectively. According to the results of UV spectral analysis, when using a double excess of ion-liquid extractant with respect to the kerosene fraction, the residual content of aromatic hydrocarbons in the purified kerosene was 0,62-1,0% mass.

- the conditions for the regeneration of ionic liquid from extract solutions with repeated use without reducing efficiency have been established [5].

Thus, the results obtained indicate the effectiveness of the use of ionic liquids as a selective solvent in the creation of environmentally friendly technologies for the extraction purification of oil fractions.

References

1. А.Г.Азизов, М.Д.Ибрагимова, Ф.И.Самедова, В.А.Нагиев, Р.Б. Мамедов. Перспективность применения ионных жидкостей в процессах селективной очистки нефтяных фракций / Перспективные направления исследований в области нефтепереработки и нефтехимии (Сборник обзорных статей ИНХП НАНА) Баку "Элм", 2013, 462 с, с.86-121.
2. Л.М.Мирзоева, М.Д.Ибрагимова, В.А.Нагиев, С.Г.Юнусов, Н.К.Андрющенко, Г.Д. Гусейнов. Применение ионных жидкостей для обессеривания бензиновых фракций // Химия и технология топлив и масел, 2018, № 4 (608), 28-32.
3. V.M. Abbasov, S.Q. Aliyeva, V.A. Nagiyev, A.B.Xalilov, A.E. Alizadeh, H.J.Huseinov. Investigation of hydrocarbon group composition of hydraulic liquid AMG-10 prepared from oil rocks // International Journal of Scientific Engineering and Applied Science (IJSEAS) – Volume-3, Issue-10, October, 2017, p. 29-31.
4. М.Д. Ибрагимова, С.А. Сеидова, Г.Дж. Гусейнов, В.М. Аббасов и др. Исследование структурно-группового состава рафината и экстракта, полученных деароматизацией смеси прямогонной дизельной фракции с продуктами вторичной переработки нефти // Нефтепереработка и Нефтехимия, 2018, № 8, с. 14-20.
5. М.Д. Ибрагимова, В.М. Аббасов, С.Г. Алиева, А.Б.Халилов, В.А. Нагиев и др. Исследование процесса регенерации ионно-жидкостного состава N-метилпирролидонацетата из экстрактного раствора селективной очистки дистиллята, выделенного из Балаханской нефти // Нефтепереработка и Нефтехимия, 2017,№ 12, с.41-45.

Upscaling towards applications – water transport in C-S-H agglomerates studied by MRI measurements

Magdalena Janota, Peter J. McDonald, David A. Faux, Agata Gajewicz-Jaromin

Department of Physics, University of Surrey, UK

Understanding the transport properties of water in cementitious materials is crucial in predicting the service life of the material - durability. The transport properties depend on the cement pore microstructure and on the degree of saturation. However, it is now known that the microstructure depends on the sorption history. Therefore, there is a complex interplay between microstructure, sorption and transport. Traditional techniques such as gravimetry or permeability testing to measure sorption are limited. They do not provide spatially resolved information about the water saturation profile nor about the water-filled pore size distribution. Magnetic resonance imaging (MRI) is a powerful non-destructive method not only to visualise where water is within a sample but also, through spin relaxation time contrast, to provide information on the locally filled pore size distribution. In this study, we use 1D SPRITE MRI methods sensitive to short relaxation times to separate and resolve with circa 1.5 mm resolution water in hydrate interlayer, gel (nanometre) and capillary (micron) sized pores during repeated (1^{st}, 2^{nd} and 3^{rd}) wetting and drying cycles. The experiments are made using cylindrical white cement paste samples 60 mm long with water to cement ratio 0.5 and cured in a calcium hydroxide solution for 3 months. Samples dried to a different degree of saturation are compared. The study aims to explore the extent to which time-dependent microstructural changes occurring in response to water saturation changes cause anomalous sorption behaviour. A series of water distribution maps will be shown along with preliminary analysis using a new transport model under development.

Application of ^{1}H-NMR spectroscopy to highlight the metabolic plasticity of human melanoma cells upon glutamine depletion and glutaminase inhibition

Jérôme Jeandriens

Department of Human Biology and toxicology at the university of Mons

Melanoma is a malignant type of skin cancer involving an extensive metabolic reprogramming such as the activation of glycolysis under aerobic conditions, known as the Warburg effect, and the 'addiction' to glutamine. Here, we investigated the metabolic plasticity of melanoma cells upon glutamine deprivation. To this end, 451-Lu metastatic melanoma cells were cultured either with or without glutamine in the extracellular medium as well as in the absence or presence of CB-839, a glutaminase inhibitor. To reveal the metabolic alterations between the experimental groups, ^{1}H-NMR spectroscopy was performed on the extracellular fluid and on the intracellular compartment. The spectral data were then analysed and compared using a multivariate approach to reveal metabolic changes separating the different treatment groups. Our results indicated that glutamine depletion impacts the glycolytic activity and slows down melanoma growth. These findings reinforced the hypothesis that glutamine metabolism is a potential target for treatment of melanoma. Moreover, ^{1}H-NMR spectroscopy appears to be a relevant tool to extend our insights into the metabolic reprogramming of melanoma cells under environmental stressors such as glutamine depletion.

Absence of the signal after solid-echo pulse sequence in the system of three spins

Grigorii E. Karnaukh

Institute of the problems of the Chemical Physics RAS
Moscow reg., Chernogolovka, pr. Semenov, 1.
E-mail: karnaukh@icp.ac.ru

Introduction

In the system of three spins ½, two different sets of dipole-dipole coupling constants (DDI) were found for which there is no signal immediately after the action of the solid-echo pulse sequence. The reason is the formation of a density matrix, which commutes with the secular part of the Hamiltonian with any DDI constants, and does not contribute to the magnetization

Signal calculation after echo sequence

A system of three spins ½ with the interaction Hamiltonian is considered

$$H_d^z = b_{12}\left(2S_1^zS_2^z - S_1^xS_2^x - S_1^yS_2^y\right) + b_{13}\left(2S_1^zS_3^z - S_1^xS_3^x - S_1^yS_3^y\right) + b_{23}\left(2S_2^zS_3^z - S_2^xS_3^x - S_2^yS_3^y\right)$$

under the action of the pulse sequence $\left(\frac{\pi}{2}\right)_y - \tau - \left(\frac{\pi}{2}\right)_x - t -$, used to monitor solid echo.

Notation used: $\sigma_1 = b_{12} + b_{13} + b_{23}$, $\sigma_2 = b_{12}b_{13} + b_{12}b_{23} + b_{13}b_{23}$, $\omega = \frac{\sqrt{-6\sigma_2}}{2}$,

$G(\tau)$ – the signal of Free Induction decay, $A(\tau,\tau)$ – the signal of primary echo, $A(\tau,t)$ – the signal after the second pulse [1, 2].

In two cases a) $b_{12} = b_{13} = b_{23} = b$ and b) $\sigma_1 = 0$ it is proved that at some times the signal after the second pulse is absent, that is $A(\tau,t) = 0$. It follows from the continuity that at the moment of the second pulse $G(\tau) = A(\tau,\tau) = 0$.

It is proved that after the second pulse in both cases the same density matrix is formed, commuting with the Hamiltonian H_d^z with any set of dipole-dipole coupling constants (b_{12}, b_{13}, b_{23}) and not contributing to the magnetization.

Case a):

$$G(\tau) = 1 - \sin^2\frac{3b\tau}{2},\ A(\tau,\tau) = 1 - \sin^4\frac{3b\tau}{2},$$

$$A(\tau,t) = \frac{1}{4} + \frac{3}{8}\cos 3b(\tau - t) + \frac{1}{4}(\cos 3b\tau + \cos 3bt) - \frac{1}{8}\cos 3b(\tau + t)$$

From $G(\tau) = A(\tau,\tau) = 0$ it follows that $\sin^2\frac{3b\tau}{2} = 1$ and $3b\tau = \pi + 2k\pi$

Whence follows $A\left(\frac{\pi + 2k\pi}{3b}, t\right) = 0$. Therefore, after the second pulse there is no signal.

Case b):

$$G(\tau)=1-4\sin^2\frac{\omega\tau}{2}+3\sin^4\frac{\omega\tau}{2},A(\tau,\tau)=1-4\sin^4\frac{\omega\tau}{2}+3\sin^8\frac{\omega\tau}{2},$$

$$A(\tau,t)=\frac{7}{64}+\frac{27}{128}\cos 2\omega(\tau-t)+\frac{1}{4}cos\omega(\tau+t)+\frac{3}{128}\cos 2\omega(\tau+t)+$$

$$+\frac{1}{16}(cos\omega\tau+\cos\omega t)-\frac{3}{64}(\cos 2\omega\tau+\cos 2\omega t)-$$

$$-\frac{3}{32}(\cos\omega(2\tau+t)+\cos\omega(\tau+2t))+\frac{9}{32}(\cos\omega(2\tau-t)+\cos(\tau-2t))$$

From $G(\tau)=A(\tau,\tau)=0$ it follows that $\sin^2\frac{\omega\tau}{2}=1\Rightarrow\omega\tau=\pi+2k\pi$ and $A\left(\frac{\pi+2k\pi}{\omega},t\right)=0$.

We calculate this density matrix using evolution after the first pulse based on the work [3].

Case a) $3b\tau=\pi\,(\mathrm{mod}\,2\pi)$

$$S^x\left(\frac{\pi+3k\pi}{3b}\right)=\exp\left[-iH_d^z\frac{\pi+2k\pi}{3b}\right]S^x\exp\left[iH_d^z\frac{\pi+2k\pi}{3b}\right]=$$

$$=S_1^x\left(S_2^z-S_3^z\right)^2+S_2^x\left(S_3^z-S_1^z\right)^2+S_1^x\left(S_1^z-S_2^z\right)^2-$$

$$-\left[S_1^x\left(S_2^z+S_3^z\right)^2+S_2^x\left(S_3^z+S_1^z\right)^2+S_1^x\left(S_1^z+S_2^z\right)^2\right]=$$

$$=-4\left(S_1^xS_2^zS_3^z+S_2^xS_1^zS_3^z+S_3^xS_1^zS_2^z\right)$$

Case b) $\omega\tau=\pi\,(\mathrm{mod}\,2\pi)$

$$S^x\left(\frac{\pi}{\omega}\right)=S_1^x\left(\frac{1}{2}\left(1-\frac{3b_{31}b_{12}}{2\sigma_2}\right)\left(S_2^z-S_3^z\right)^2+\left(\frac{3b_{31}b_{12}}{2\sigma_2}-\frac{1}{2}\right)\left(S_2^xS_3^x+S_2^yS_3^y\right)\right)+$$

$$+S_2^x\left(\frac{1}{2}\left(1-\frac{3b_{12}b_{23}}{2\sigma_2}\right)\left(S_3^z-S_1^z\right)^2+2\left(\frac{3b_{12}b_{23}}{2\sigma_2}-\frac{1}{2}\right)\left(S_3^xS_1^x+S_3^yS_1^y\right)\right)+$$

$$+S_3^x\left(\frac{1}{2}\left(1-\frac{3b_{23}b_{31}}{2\sigma_2}\right)\left(S_1^z-S_2^z\right)^2+\left(\frac{3b_{23}b_{31}}{2\sigma_2}-\frac{1}{2}\right)\left(S_1^xS_2^x+S_1^yS_2^y\right)\right)+$$

$$\left[\begin{array}{l}\hat{S}_1^x\left(\frac{1}{2}\left(1+\frac{3b_{31}b_{12}}{2\sigma_2}\right)\left(S_2^z-S_3^z\right)^2+\left(\frac{1}{2}-\frac{3b_{31}b_{12}}{2\sigma_2}\right)\left(S_2^xS_3^x+S_2^yS_3^y\right)\right)+\\+S_2^x\left(\frac{1}{2}\left(1+\frac{3b_{12}b_{23}}{2\sigma_2}\right)\left(S_3^z-S_1^z\right)^2+\left(\frac{1}{2}-\frac{3b_{12}b_{23}}{2\sigma_2}\right)\left(S_3^xS_1^x+S_3^yS_1^y\right)\right)+\\+S_3^x\left(\frac{1}{2}\left(1+\frac{3b_{23}b_{31}}{2\sigma_2}\right)\left(S_1^z-S_2^z\right)^2+\left(\frac{1}{2}-\frac{3b_{23}b_{31}}{2\sigma_2}\right)\left(S_1^xS_2^x+S_1^yS_2^y\right)\right)\end{array}\right]-$$

$$-\left[S_1^x\left(S_2^z+S_3^z\right)^2+S_2^x\left(S_3^z+S_1^z\right)^2+S_3^x\left(S_1^z+S_2^z\right)^2\right]=$$

$$=-4\left(S_1^xS_2^zS_3^z+S_2^xS_1^zS_3^z+S_3^xS_1^zS_2^z\right)$$

In both cases, the same density matrix is formed before the second pulse.

After the second $\left(\frac{\pi}{2}\right)_x$ pulse we get the density matrix

$$-4\left(S_1^x S_2^y S_3^y + S_2^x S_3^y S_1^y + S_3^x S_1^y S_2^y\right)$$

We write the resulting density matrix and the Hamiltonian $\hat{H}_d^z$ with any DDI constants on a symmetric basis:

$$\left\{\begin{array}{c}\frac{\uparrow\uparrow\uparrow+\downarrow\downarrow\downarrow}{\sqrt{2}},\frac{\downarrow\uparrow\uparrow+\uparrow\downarrow\downarrow}{\sqrt{2}},\frac{\uparrow\downarrow\uparrow+\downarrow\uparrow\downarrow}{\sqrt{2}},\frac{\uparrow\uparrow\downarrow+\downarrow\downarrow\uparrow}{\sqrt{2}},\\ \frac{\uparrow\uparrow\downarrow-\downarrow\downarrow\uparrow}{\sqrt{2}},\frac{\uparrow\downarrow\uparrow-\downarrow\uparrow\downarrow}{\sqrt{2}},\frac{\downarrow\uparrow\uparrow-\uparrow\downarrow\downarrow}{\sqrt{2}},\frac{\uparrow\uparrow\uparrow-\downarrow\downarrow\downarrow}{\sqrt{2}},\end{array}\right\}$$

$$-4\left(S_1^x S_2^y S_3^y + S_2^x S_1^y S_3^y + S_3^x S_1^y S_2^y\right)=\frac{1}{2}\begin{pmatrix}3&0&0&0&0&0&0&0\\0&-1&0&0&0&0&0&0\\0&0&-1&0&0&0&0&0\\0&0&0&-1&0&0&0&0\\0&0&0&0&1&0&0&0\\0&0&0&0&0&1&0&0\\0&0&0&0&0&0&1&0\\0&0&0&0&0&0&0&-3\end{pmatrix}$$

$$H_d^z=\frac{1}{2}\begin{pmatrix}b_{12}+b_{23}+b_{31}&0&0&0&0&0&0&0\\0&-b_{12}+b_{23}-b_{31}&-b_{12}&-b_{31}&0&0&0&0\\0&-b_{12}&-b_{12}-b_{23}+b_{31}&-b_{23}&0&0&0&0\\0&-b_{31}&-b_{23}&b_{12}-b_{23}-b_{31}&0&0&0&0\\0&0&0&0&b_{12}-b_{23}-b_{31}&-b_{23}&-b_{31}&0\\0&0&0&0&-b_{23}&-b_{12}-b_{23}+b_{31}&-b_{12}&0\\0&0&0&0&-b_{31}&-b_{12}&-b_{12}+b_{23}-b_{31}&0\\0&0&0&0&0&0&0&b_{12}+b_{23}+b_{31}\end{pmatrix}$$

It is seen that the operators of the found density matrix and the interaction Hamiltonian commute. $\left[H_d^z, S_1^x S_2^y S_3^y + S_2^x S_1^y S_3^y + S_3^x S_1^y S_2^y\right]=0$. Besides,

$Tr\left(S_1^x S_2^y S_3^y + S_2^x S_1^y S_3^y + S_3^x S_1^y S_2^y\right)\left(S_1^\alpha + S_2^\alpha + S_3^\alpha\right)=0;\left(\alpha=x,y,z\right)$.

Therefore there is no contribution to magnetization.

Acknowledgements

This work was performed in accordance with the state task, state registration No. 0089-2019-0002.

References

1. T. P. Kulagina, G. E. Karnaukh, S. A. Andrianov. *Butlerov messages*, **35**, 1-9 (2013).
2. I.Yu Golubeva, G.E. Karnaukh, T. P. Kulagina, *Proceedings International Sch00l-Conference Magnetic Resonance and its Applications*, 170-172 (2019).
3. G. E. Karnaukh, T. P. Kulagina. *Proceedings XXIV Russian conference* "*Structure and dynamics of molecular systems*", 119-124 (2017).

Reorientational motion of water molecules in mixtures of imidazolium-based ionic liquids with water. A molecular dynamic simulation study

V. A. Konovalov, A. V. Egorov, V. I. Chizhik

Department of Nuclear-Physics Research Methods, Faculty of Physics, Saint-Petersburg State University
E-mail: konovalov.phys@gmail.com

Introduction

Mixtures of imidazolium-based ionic liquids (ILs) with water have been widely studied in the recent years for both fundamental and technological reasons. However, a clear understanding of mixture components dynamics on molecular level is still largely missing. In the present study molecular dynamics simulations were employed to investigate the water reorientational motion in water mixtures with 1-butyl-3-methylimidazolium nitrate, tetrafluoroborate and iodide.

Simulation details and results

For each system six concentrations (11, 20, 33, 40, 50 and 95 mol% of IL) were considered. Simulations were carried out in NPT ensemble at 298 K and 1 atm using the MDynaMix package [1]. Water was modeled with TIP5P [2] and SPC/E [3] models. ILs was simulated using the potentials described in [4-7]. The normalized reorientational autocorrelation functions for three vectors (vector connecting H atoms of water molecule, water dipole vector, and vector orthogonal to the plane of the molecule) were calculated and the corresponding values of correlation times were estimated (see, for instance, Fig. 1).

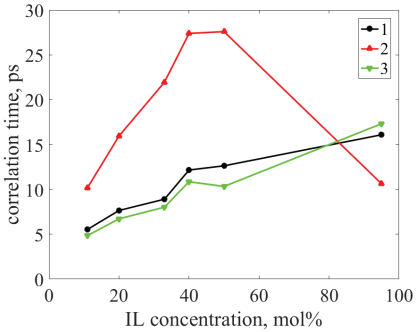

Figure 1. Concentration dependence of reorientational correlation times of TIP5P water in mixture with 1-butyl-3-methylimidazolium BF_4 at 298 K and 1 atm (1 – H-H vector, 2 – water dipole vector, 3 – vector orthogonal to the plane of the molecule)

References

1. A. P. Lyubartsev, A. Laaksonen. – *Comp. Phys. Comm.*, 128, 565 (2000).
2. W. Mahoney, W. L. Jorgensen – *J. Chem. Phys.*, 112, 8910 (2000).
3. H.J.C. Berendsen, J.R. Grigera, T.P. Straatsma – *J. Phys. Chem.*, 91, 6269 (1987).
4. J. N. C. Lopes, J. Deschamps, A. A. H. Padua – *J. Phys. Chem. B*, 108, 2038 (2004).
5. J.-C. Soetens, C. Millot, B. Maigret – *Phys. Chem. A*, 102, 1055 (1998).
6. T. Megyes, S. Balint, E. Peter, T. Grosz, I. Bako, H. Krienke, M.-C. Bellissent-Funel – *J. Phys. Chem. B*, 113, 4054 (2009).
7. K. Heinzinger – *Physica B*, 131, 196 (1985).

The study of intermolecular interactions involving models of modern volatile anesthetics by quantum-chemistry calculations

Mikhail Kostin[1], Peter Tolstoy[2], Sona Melikova[1]

[1]Faculty of Physics, Saint-Petersburg State University
[2]Institute of Chemistry, Saint-Petersburg State University
E-mail: kostin-micha@mail.ru

Introduction

One of the safest and most effective general anesthetics are halothane, enflurane, isoflurane, desflurane (Fig. 1), which are used to induct or maintain anesthesia. All these compounds are volatile, therefore applied as inhalation agents. Anesthetic effects are based on binding of these molecules to protein targets. The most common target of these general anesthetics is the gamma-aminobutyric acid receptor ($GABA_A$), activation of which suppresses neurons excitability. However, physicochemical process of binding to target molecules is still poorly understood [1]. The structure of volatile anesthetics contains at least one CH group, which can act as a proton donor in hydrogen bond formation. The occurrence of a group with halogen atoms (fluorine, chlorine, bromine), with general formula C-Hal, suggests the possibility of halogen bonding (C-Hal group as halogen donor and electron acceptor along the C-Hal bond) or hydrogen bonding (C-Hal group as electron density donor in directions roughly perpendicular to the C-Hal bond). The formation of halogen bonds is possible due to sigma-hole formation in electron density distribution [2]. Therefore, non-covalent interactions determine the features of selective binding for anesthetics molecules.

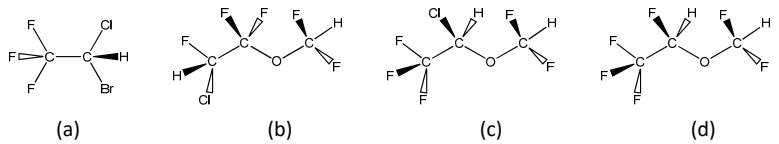

Figure 1. Structural formulas of fluorotan (a), enflurane (b), isoflurane (c), desflurane (d)

Aims

The overall goal of this work is to determine and study characteristics of non-covalent interactions that appear between models of anesthetic molecules and models of their targets. Here we report the results of the first part of this work, in which we have investigated the set of compounds (Fig. 2) containing C-Hal groups, which are able to mimic hydrogen and halogen bonds present in complexes formed by halothane. As hydrogen and halogen donors we have considered simple molecules, such as HX and XY, where X and Y are halogens.

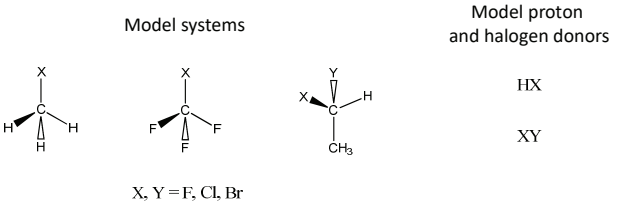

Figure 2. The set of model molecules that contain functional group of anesthetic

Results

As an example of the results of this study we present in Fig. 3 a series of compelxes formed by chloromethane with proton donor molecules (H-bond, Fig. 3a) or halogen donor molecules (X-bond, Fig. 3b). We have demonstrated that chloromethane molecule can serve an effective electron donor for up to three partner molecules, for H-bond and X-bond alike. Studying spectroscopic markers (chemical shifts) and complexation energies we observed significant anticooperativity effects on these parameters. We shown that the directionality of non-covalent bond in all studied cases is determined by the anisotropy of electron density distribution around the central chlorine atom and by further changes of this anisotropy upon subsequent formation of one, two or three H-bonds or X-bonds.

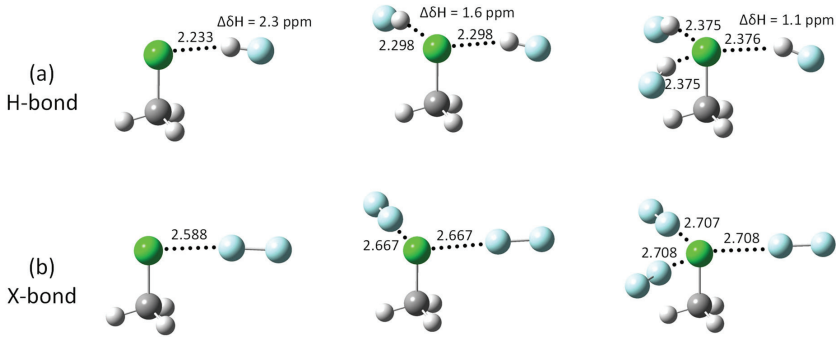

Figure 3. Anticooperative binding of HF molecules (a) or FF molecules (b) to CH_3Cl

Acknowledgements

This work was supported by RFBR grant 20-03-00536.

References

1. S.M. Melikova, K.S. Rutkowski, M. Rospenk, Spectrochim. Acta A, **2019**, 223, 117363
2. E.Yu. Tupikina, G.S. Denisov, P.M. Tolstoy, J. Comput. Chem., **2019**, 40, 2858-2867

Influence of the Si/AL ratio to the local structure of H-Mordenites

Ekaterina A. Krylova, Marina G. Shelyapina

Saint Petersburg State University, 7/9 Universitetskaya nab., St. Petersburg, Russia 199034
E-mail: krylovaea2803@mail.ru

Introduction

Many factors influence to the catalytic properties of zeolites, which depend on the method of preparation and the initial form of zeolite [1-2]. The proton form of mordenite, which has stronger acid sites, is usually obtained from the ammonia form by calcination at 300°C. It is well known that this procedure leads to significant degradation of the mordenite framework [3]. Such local damage cannot be detected by X-ray diffraction. The best choice for detection and analysis deformations is nuclear magnetic resonance (NMR) methods, which are sensitive to the local structure.

Results

In this paper, we study two series of mordenite samples H-MOR-X (X = 10, 20, 24, 128) and H-MOR-Y (Y = 9.9, 15.0, 15.2, 15.7, 15.8, 18.7, 19.8) with different Si/Al ratio. The ICP and EDS analysis were carried out to determine the actual composition. The real ratios were about 10% less than the declared ones according to the results of experiments.

The size and morphology of the samples were estimated using a scanning electron microscope and XRD analysis. All samples are small elongated crystals (about 200 nm long) and combined into larger agglomerates (up to several micrometers).

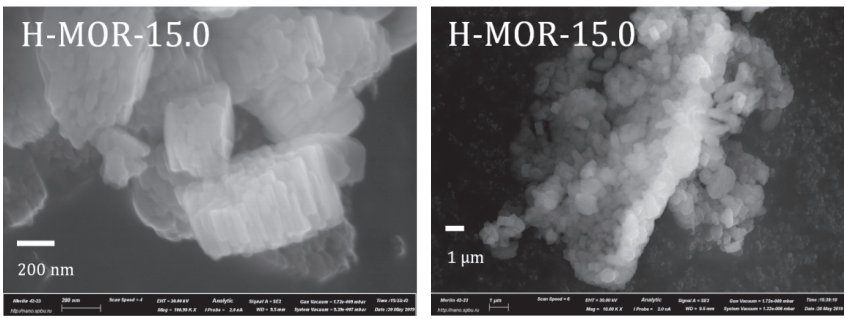

Figure 1. H-MOR-15.0 images at various scales taken by scanning electron microscope

Results of TGA studies show several stages of thermal degradation associated with desorption of water. For all samples, weight loss occurs in at least two steps. Step-I can be attributed to the loss of physisorbed water located on the outer surface and ‘free’ water in the main mordenite channel. Step-II could be associated with the release of water molecules located in the vicinity of cations. But for samples H-MOR-9.9, H-MOR-15.0, H-MOR-19.8 there is at least 1 more step of weight loss.

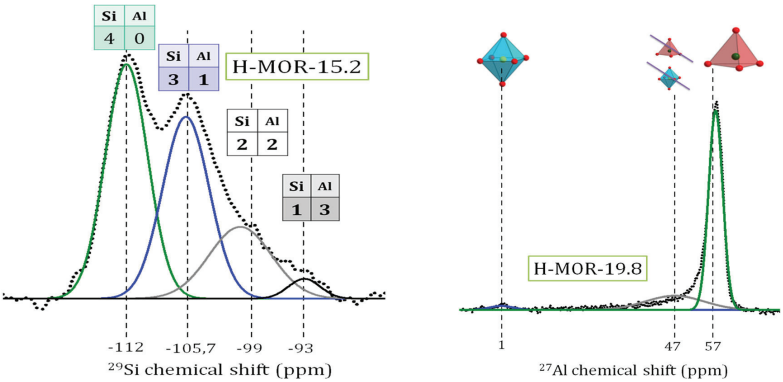

Figure 2. ^{29}Si MAS NMR (H-MOR-15.2 sample) and ^{27}Al MAS NMR (H-MOR-19.8 sample) spectra respectively

The results of ^{27}Al and ^{29}Si MAS NMR experiments (Fig.2) indicate partial destruction of the framework. Moreover, these defects are more insignificant with increasing of the Si/Al ratio. The main part of the frame is combinations (Si 4 | 0 Al) and (Si 3 | 1 Al). Positions (Si 2 | 2 Al) are less common, and only (Si 1 | 3 Al) is found in only one sample. Most of the aluminum nuclei are in a four-coordinated position (tetrahedron). Less than 40% of the atoms are in a six-coordinated position (octahedron). In addition, extra structural aluminum, conventionally called “five-coordinated”, is found in two samples.

Acknowledgements

The studies were carried out on the basis of the research park of St. Petersburg State University (Centre for microscopy and microanalysis, Centre for physical methods of surface investigation, Centre for x-ray diffraction studies, Magnetic resonance research centre, Thermogravimetric and calorimetric research centre) with the support of the grant No. 18-53-34004.

References

1. Schoonheydt R.A. – *Catal. Rev. Sci. Eng.* **35**, 129–168 (1993).
2. Vanelderen P. et al. – *Coord. Chem. Rev.* **257,** 483–494 (2013).
3. Zhukov Yuri M. et al. – *Int. J. Nanotechnol.* **13,** 136–146 (2016).
4. Zhukov Yuri M. et al. – *Int. J. Nanotechnol.* **13,** 136–146 (2016).

The significance of 3D modeling in assessment resectability of cancer of the pancreatic head

Aleksandra Sergeevna Kudashkina, Vladimir Maksimovich Cheremisin, Konstantin Vadimovich Paveletz, Dmitriy Sergeevich Rusanov, Viktoria Vladimirovna Pritz

Mariinstkiy State Hospital

Purpose of the research work: improving the results of surgical treatment of pancreatic head cancer due to increased accuracy of radiation diagnosis with 3D reconstructions of the pancreaticoduodenal zone, and their roles in the surgery planning algorithm.

Materials and methods: 25 patients with clinical patterns of mechanical jaundice and suspected space-occupying lesion in the pancreatic head region (according to ultrasound examination of the abdominal cavity organs) without secondary abnormalities were examined. During the preoperative stage, all patients underwent magnetic resonance imaging.

The resectability was evaluated based on the resectability criteria for non-metastatic pancreatic cancer according to M. D. Anderson, including the degree of spread to the superior mesenteric artery, superior mesenteric vein, celiac trunk and portal vein. The MRI signs of lesions in the major vessels included the adherence of the tumor to the vessel with the presence of tumor infiltration of perivascular tissue; circular contact between the tumor and the vessel by more than ½ circumference and its invasion into the vessel wall; the passage of the vessel through the tumor mass, its deformation along one of the walls with a length of more than 2 cm, or its occlusion during tumor germination

For the patients with relative resectability data, 3D models were constructed based on the MRI findings.

All patients with resectable and borderline-resectable forms underwent surgery. Pancreaticoduodenal resection with extended lymphadenectomy was performed. It was followed by the comparative analysis of 3D models with intraoperative imaging.

Results: in 22 patients (88%), the pancreatic head cancer diagnosis was confirmed after the standard MRI examination. In 2 patients (8%), choledocholithiasis was found. Stricture in the terminal part of the common bile duct with developing biliary hypertension and acute pancreatitis was detected in 1 patient (4%). In 5 patients (20%), the tumor was recognized as unresectable, it was resectable in 8 patients (32%). 9 patients (36%) showed signs of relative resectability of the existing mass.

Three-dimensional modeling of the pancreaticoduodenal zone was performed for the last group of the patients. As the preoperative three-dimensional images were compared with the actual intraoperative pattern, 8 patients (88.9%) got the diagnosis precision of 100%, and 1 patient (11.1%) showed data discrepancy – the actual mass dimensions of the mass had been smaller on the model.

Conclusions: it is currently advisable to use MRI at the primary stage of diagnosing pancreatic head cancer to determine the presence of a tumor and to evaluate its spread. When the standard MR imaging is supplemented with three-dimensional modeling, the precision in the evaluation of vascular invasion increases, which directly affects the preoperative staging of the oncological process and the choice of a treatment method for a patient.

Development and study of novel green membranes based on sodium alginate modified by MOFs

Anna I. Kuzminova, Anastasia V. Penkova

St. Petersburg State University, St. Petersburg, 199034 Russia
E-mail: ai.kuzminova@mail.ru

Introduction

One of the most popular membrane processes for the separation of low molecular weight components is the pervaporation, which allows the separation of azeotropic mixtures, mixtures of isomers and thermally unstable mixtures. Nowadays, the essential improvement of the transport properties of pervaporation membranes can be achieved by the modification of an polymer matrix by an inorganic filler that yields in developing the mixed – matrix membranes (MMMs). The introduction of inorganic filler in the polymer matrix of the membrane allows getting tailoring properties. MMMs combine the simplicity of processing polymer membranes with the superior transport properties of inorganic particles.

In the present work the novel membranes based on sodium alginate (SA) were prepared by introducing the metal-organic framework UiO-66(NH_2)-EDTA into the SA matrix. The improvement of the transport properties of polymer membranes occurs due to the porous structure of the metal-organic frameworks. The study of the physicochemical properties of the membranes was carried out by NMR spectroscopy, IR spectroscopy, scanning electron microscopy and thermogravimetric analysis. Contact angle was using for study of the surface properties of the membranes, the degree of swelling was study by the gravimetric method. The transport properties of the developed membranes were studied by pervaporation separation of the azeotropic mixture of isopropanol - water (88/12 wt.%). All developed membranes were highly selective for water (more than 95 wt.% water in the permeate). The introduction of UiO-66(NH_2)-EDTA into the SA matrix leads to significant changes in properties of membranes based on odium alginate.

Acknowledgements

This work was supported by Russian Foundation for Basic Research [grant No. 19-38-90008]. The experimental work was facilitated by equipments from Interdisciplinary Resource Centre for Nanotechnology, Magnetic Resonance Research Centre, Thermogravimetric and Calorimetric Research Centre, Centre for X-ray Diffraction Studies, Chemical Analysis and Materials Research Centre, Nanophotonics Centre and Centre for Geo-Environmental Research and Modelling at St. Petersburg State University.

Development of novel membranes based of PVA with MOFs for pervaporation separation of water/isopropanol mixture

A. I. Kuzminova, V. A. Surkova, A. V. Penkova, M. E. Dmitrenko, S. S. Ermakov

Saint Petersburg State University, Saint Petersburg, Russia
E-mail: viktoriasurkovaspu@gmail.com

Pervaporation is one of the fastest growing methods of membrane technology, which has great potential for the separation of liquid mixtures in the petrochemical, bioprocessing, and pharmaceutical industries. The advantages of pervaporation are efficiency and the ability to separate azeotropic mixtures. To get membranes with tailored transport properties, nowadays, are widely used mixed-matrix membranes (MMMs) obtained by introducing a filler to a polymer matrix.

In the present work the effect of introduction of metal-organic frameworks (MOFs) such as FeBTC and UiO-66(NH_2)-EDTA to polyvinyl alcohol was studied. The novel polymer membranes were prepared by bulk modification. The improvement of the transport properties of polymer membranes occurs due to the porous structure of the metal-organic frameworks.

The study of the physicochemical properties of the membranes was carried out by scanning electron microscopy, IR spectroscopy, NMR spectroscopy and thermogravimetric analysis. Contact angle was using for study of the surface properties of the membranes, the degree of swelling was study by the gravimetric method.

The transport properties of the developed membranes were studied in pervaporation separation of the azeotropic isopropanol - water (88/12 wt.%) mixture. All developed membranes were highly selective to water (more than 95 wt.% water in the permeate). It was shown that the introduction of MOFs (FeBTC and UiO-66(NH_2)-EDTA) into the PVA matrix leads to significant changes in the physicochemical and transport properties of pervaporation membranes.

Acknowledgements

This work was supported by the Russian Science Foundation (project No 17-73-20060). The experimental work was facilitated by equipments from Interdisciplinary Resource Centre for Nanotechnology, Chemistry Educational Centre, Centre for Diagnostics of Functional Materials for Medicine, Pharmacology and Nanoelectronics, Magnetic Resonance Research Centre, Thermogravimetric and Calorimetric Research Centre, Centre for X-ray Diffraction Studies, Chemical Analysis and Materials Research Centre, Nanophotonics Centre and Centre for Geo-Environmental Research and Modelling (GEOMODEL) at St. Petersburg State University.

Numerical simulation of the nonlinear spin-wave phase shift in magnetic films

Nikolai A. Kuznetsov[1,2], Erkki Lähderanta[2], Alexey B. Ustinov[1]

[1]Department of Physical Electronics and Technology, St.Petersburg Electrotechnical University, St.Petersburg, 197376 Russia
[2]LUT University, P.O.Box 20, FIN-53851 Lappeenranta, Finland
E-mail: kuzkolja@gmail.com, ustinov_rus@yahoo.com

Introduction

In recent years, spin waves (SWs) in magnetic films and nanostructures attract significant attention of scientists in connection with the existence of various nonlinear phenomena and possibilities for signal processing. In the new generation of magnonic logic devices, the information is encoded in the amplitude or phase of propagating SWs. Therefore, the phase shift control is of interest for all-magnon computing [1].

An emergence of a nonlinear phase shift for propagating SWs could be qualitatively explained using a precession model of the magnetization vector (Fig. 1 a). The motion of magnetization vector is described by Landau-Lifshitz equation, where the total magnetization vector $\boldsymbol{M}$ consists of the static magnetization $\boldsymbol{M_0}$ and dynamic magnetization $\boldsymbol{m}$ which is called SW amplitude. As follows from the Landau-Lifshitz equation, the length of the vector $\boldsymbol{M}$ is conserved. Therefore, as is seen from Fig. 1 a, an increase in SW amplitude $\boldsymbol{m}$ leads to a decrease in the static magnetization and to the shift of the dispersion curve, as is shown in Fig. 1 b. It should be noted that the SW amplitude is proportional to the square root of the microwave signal power transmitted by the SWs. Therefore, at a particular frequency of excitation spectrum the SW wave number changes with an increase in the input signal power. The change in the wave number leads to the nonlinear phase shift $\Delta\varphi_{NL}$ of the operating SW propagating in the stable nonlinear regime.

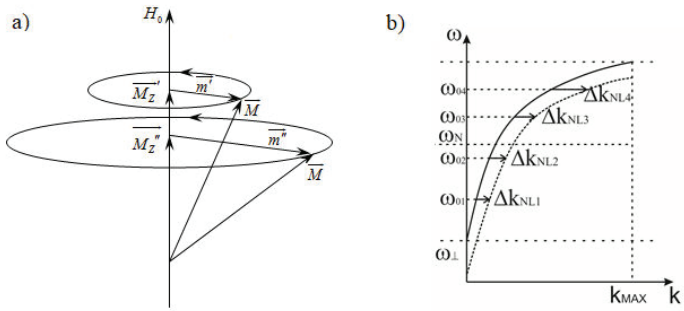

Figure 1. a) Precession magnetization model.
b) The nonlinear shift of the dispersion curve for the surface SWs

One of the promising phenomena for novel logic devices is a power-dependent nonlinear phase shift [2-4]. Thus, a work [5] describes the nonlinear logic gate which comprises the nonlinear phase shifter [4].

In spite of the aforementioned works, to our knowledge, there have been no investigations of the phase shift of two nonlinearly coupled spin waves propagating in one magnetic film. Therefore, the purpose of this work is to simulate the induced nonlinear phase shift of spin waves.

Simulation results

For a theoretical description and simulation of the induced nonlinear phase shift the envelope method was used. For this method a system of the two nonlinearly coupled Landau-Ginzburg (LG) equations was obtained. The solutions of such system are the functions which describe the SW amplitude and phase evolution. Using these solutions, the induced nonlinear phase shift of the operating SW $\Delta\varphi_{NL1}$ was numerically simulated.

The results shown in Fig 2 illustrates the computed dependences of $\Delta\varphi_{NL1}$ versus $|U_{02}|^2$, where $|U_{02}|^2$ is the amplitude of the pumping SW. The following parameters were used in simulation: frequency of the operating SW $f_0 = 5.665$ GHz, frequency of the pumping SW $f_N = 5.575$ GHz, external magnetic field $H_e = 1158$ Oe, SWs propagation distance $d = 5$ mm, saturation magnetization $4\pi M_0$=1750 G, film thickness $L = 13.6$ μm, ferromagnetic resonance linewidth $\Delta H = 0.5$ Oe, cubic and quintic nonlinear damping coefficients ν_{13}, ν_{15} and ν_{23}, ν_{25} of the operating and pumping wave respectively.

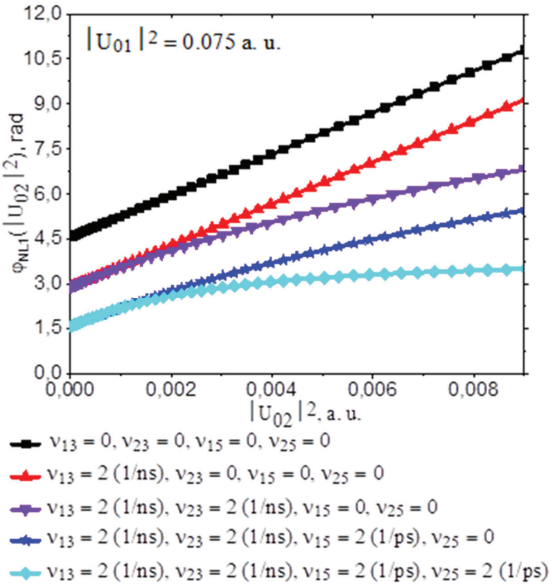

Figure 2. Induced nonlinear phase shift $\Delta\varphi_{NL1}$ as a function of the initial amplitude of the pumping wave for the surface SW configuration

On the Fig. 2, the solid lines with symbols show computed curves for different cubic and quintic nonlinear damping coefficients of both SWs. In case of $|U_{02}|^2 = 0$ there is a non-zero self nonlinear phase shift of the operating wave, which decreases when the higher damping coefficients of this wave are taken into account. Further, a growth of the dependences with increasing initial pumping wave amplitude illustrates that the induced nonlinear phase shift is added to the self-nonlinear phase shift. The linear response is obtained, when there is only linear damping of both waves is taken into account. The rounded but nonsaturated curves show a

typical computed response for non-zero $\nu_{13}, \nu_{15}, \nu_{23}$ and zero ν_{25}. The saturated curve shows the result with all non-zero damping parameters.

Conclusions

The induced nonlinear phase shift of spin waves in ferromagnetic film has been studied. A phenomenological model was developed, based on the assumption that the SW nonlinear dispersion relation depend on both operating and pumping power. The obtained results could be fundamental for all-magnon devices and logic circuits.

References

1. A.V. Chumak, “Fundamentals of magnon-based computing,” arXiv:1901.08934, 2019
2. A.B. Ustinov, B.A. Kalinikos, “Nonlinear microwave spin wave interferometer”, Tech. Phys. Lett., vol. 27, 2001
3. A.B. Ustinov, B.A. Kalinikos, “The power-dependent switching of microwave signals in a ferrite-film nonlinear directional coupler”, Appl. Phys. Lett., vol. 89, 2006
4. A.B. Ustinov, B.A. Kalinikos, “A microwave nonlinear phase shifter”, Appl. Phys. Lett., vol. 93, 2008
5. A.B. Ustinov, E. Lähderanta, M. Inoue, B.A. Kalinikos, “Nonlinear Spin-Wave Logic Gates”, IEEE Magn. Lett., vol. 10, 2019

Electronic paramagnetic resonance of Ehrlich ascites carcinoma cells cultured with magnetic nanoparticles

N. V. Latyshev[1], O. V. Kryukova[2], R. N. Yaroslavtsev[2], V. F. Pyankov[2], S. V. Stolyar[1,2]

[1]Siberian Federal University, Krasnoyarsk, Russia
[2]Krasnoyarsk Scientific Center, Federal Research Center KSC SB RAS Krasnoyarsk, Russia
E-mail: latnick@mail.ru

The effect of magnetic nanoparticles (MNPs) of iron oxide coated with arabinogalactan on the viability of Ehrlich ascites carcinoma (EAC) was studied. Suspension of EAC with MNPs was studied by electron paramagnetic resonance (EPR). A correlation was established between the proportion of cells dead in suspension EAC and the intensity of the EPR signal. This result could be accounted by the presence of nitric oxide (NO) molecules in the studied systems.

Introduction

Iron plays a huge role in processes in living organisms. Due to the biological compatibility of iron, nanoparticles of oxides (oxyhydroxides) based on it are used in various biomedical applications: preparations for iron deficiency anemia, contrast agents for magnetic resonance imaging, drug delivery. Currently, researchers are focusing on magnetic nanoparticles in tumor immunotherapy. Polysaccharide-coated magnetite nanoparticles (ferumoxytol) have shown a promising antitumor effect by activating tumor-related macrophages from a tumor growth-promoting phenotype to a tumor-suppressing phenotype [1]. MNPs can affect the phagocytic activity of macrophages, the yield of NO and reactive oxygen species [2]. Nitric oxide is capable of both stimulating the growth of tumor cells and exerting a cytotoxic effect [3]. NO in cells and tissues can form paramagnetic dinitrosyl iron complexes (DNIC), which are reliably recorded by EPR [4].

The purpose of this work is to determine the electron paramagnetic resonance of Ehrlich ascites carcinoma cells cultured with magnetic nanoparticles and to assess the relationship between the viability of tumor cells and the intensity of the EPR signal due to the presence of NO molecules.

Experiment

A suspension of EAC tumor cells and macrophage was extracted from the peritoneal cavity of laboratory animals on the 10th day after tumor transplantation. Suspension was cultivated together with magnetic nanoparticles for 60 min at a temperature of 37 °C. Nanoparticles coated with arabinogalactan, 50 nm in size, were prepared by chemical precipitation. Arabinogalactan-coated nanoparticles were characterized by transmission electron microscopy, Mössbauer spectroscopy, and IR spectroscopy.

To assess the viability of EAC cells, we stained with a 1% trypan blue solution using equipment included in the unique scientific facility “Complex of Equipment for Guided Cultivation of Isolated Organs”.

EPR spectra were recorded in the X-band range at a temperature of 85 K on a spectrometer Elexsys E580 (Bruker) of the Krasnoyarsk Regional Center for Collective Use of the Federal Research Center of the Siberian Branch of the Russian Academy of Sciences, Krasnoyarsk.

Results

Figure 1 (a) shows a characteristic curve of the resonant absorption of an EAC suspension. Absorption due to transferrin, cytochrome molecules, ceruloplasmin, and also Mo^{2+}-containing molecules are observed. Absorbances with a g-factor of 2.01-2.04, indicated

in the figure by 4, are reliably recorded. These absorption peaks are due to the presence of paramagnetic dinitrosyl iron complexes (DNIC), which include endogenous Fe and thiol (sulfur-containing) groups [5]. In these low-spin complexes, an unpaired electron is localized on the d_z^2 orbital of the iron atom. The geometric structure of the complexes is an octahedron or a square with a cis-arrangement of ligands in the plane of the square. The iron atom is in the Fe^+ state (electronic configuration d7), and the NO ligands are in the NO^+ state [5].

Figure 1 (b) shows the high-field sections of three resonance curves: isolated tumor (control), EAC cells cultured with used nanoparticles (MNPs) and plasma obtained after centrifugation of the EAC suspension.

A comparison of these curves indicates that ceruloplasmin (and transferrin) are exclusively in the plasma, and the presence of dinitrosyl iron complexes is associated with tumor cells and peritoneal macrophages present in the EAC suspension. Figure 1 (b) shows that the cultivation of a suspension of AKE with nanoparticles leads to a noticeable decrease in the signal from ceruloplasmin and an increase in the signal from dinitrosyl complexes.

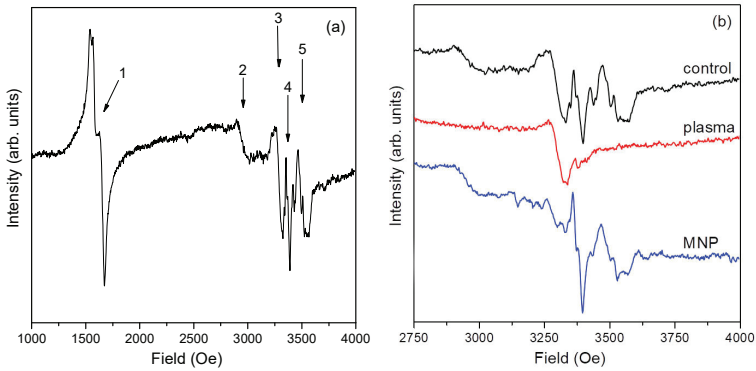

Figure 1. (a) EPR spectrum of the EAC. Peaks: 1- transferrin; 2- cytochromes; 3- ceruloplasmin; 4-DNIC; 5-Mo^{2+}-containing molecules. (b) EPR spectra of samples - control of the EAC, plasma, and EAC + MNP

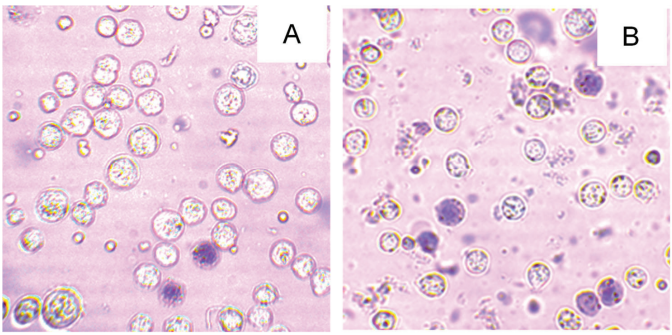

Figure 2. The number of dead cells in a suspension of Ehrlich ascites carcinoma. A - control; B - after cultivation with magnetic nanoparticles.

Figure 2 shows a control image of a suspension of cells EAC (a) and EAC after cultivation with magnetic nanoparticles (b) obtained using a light microscope. These images

indicate an increase in the number of dead cells after cultivation. The proportion of dead cells increases from 3-5% (control) to 20-30% (MNP).

Discussion

Our experiments demonstrate a correlation between the intensity of resonance absorption caused by the presence of paramagnetic dinitrosyl complexes (DNIC) and the number of killed EAC cells after culturing tumor cells with magnetic nanoparticles. With the increasing intensity of the DNIC signal, the proportion of dead cells increases. In other words, the death of EAC tumor cells in our experiments is associated with an increase in the concentration of NO. A unique feature of EAC cells is that they are capable of producing nitric oxide (see Fig. 1 (b)), which is associated with their defense mechanisms from the immune system [6, 7]. NO can stimulate the synthesis of some agents: interleukin-10 (IL-10), growth factors TGF p and TGF pi, prostaglandin E2 (PGE 2), which inhibit the protective activity of macrophages and increase the permeability of capillaries of the abdominal cavity for nutrient transport, which has a positive effect on the growth of tumor cells [3, 8-9].

We believe that in our experiments, macrophages are the main source of NO that regulates the number of tumor cells. The cultivation of EAC with magnetic particles increases the yield of nitric oxide NO (see Fig. 1 (b)) [2, 3]. Higher concentrations of NO and, consequently, reactive nitrogen species (RNS), lead to reactions that cause DNA damage [9], activation of various transcription factors [10, 11], due to which expression of p53 protein can increase, for example causing apoptosis of cells and their death.

References

1. S. Zanganeh. Iron oxide nanoparticles inhibit tumour growth by inducing pro-inflammatory macrophage polarization in tumour tissues / Zanganeh, S.; Hutter, G.; Spitler, R.; Lenkov, O.; Mahmoudi, M.; Shaw, A.; Pajarinen, J. S.; Nejadnik, H.; Goodman, S.; Moseley, M.; Coussens, L. M.; Daldrup-Link, H. E. // Nat. Nanotechnol. 2016. pp. 986–994.
2. Guo Zhaoming. CD47-targeted bismuth selenide nanoparticles actualize improved photothermal therapy by increasing macrophage phagocytosis of cancer cells. Zhaoming Guo, Ye Liu, Hao Zhou, Kun Zheng, Dong Wang, Mingli Jia, Pengcheng Xu, Kun Ma, Changhao Cui, Li Wang. 2019. pp.1–36.
3. A.F. Vanin. Paramagnetic nitrosyl complexes of heme and non-heme iron / Vanin A.F., Chetverikov A.G. // Biophysics. 1968. p. 608-615.
4. T.A. Raevskaya. Nitric oxide donors as modulators of drug resistance of tumors / dissertation. 2006.
5. A.F. Vanin Nitric oxide and its detection in biosystems by electron paramagnetic resonance / Uspekhi fizicheskikh nauk. 2000.V. 170. pp. 455–458.
6. Yu.P. Belsky. Ehrlich tumor cells stimulate the production of interferon by T cells and are not sensitive to autocrine nitric oxide / Belsky Yu. P., Belskaya N.V., Danilets MG and others // Issues. onkol. 2004.V.50, No. 6. p. 689–692.
7. VK. Patrushev. The role of nitric oxide in the immunosuppressive and antitumor activities of natural suppressor cells / Abstract. dis. - Tomsk. 2004. p. 1-22.
8. J. Bustamante. Sequential NO production by mitochondria and endoplasmic reticulum during induced apoptosis / Bustamante J, Bersier G, Badin RA, Cymeryng C, Parodi A, Boveris A. // Nitric Oxide. 2002. Vol 6. № 3 pp.333–341.
9. M. Jaiswal. Inflammatory cytokines induce DNA damage and inhibit DNA repair in cholangiocarcinoma cells by a nitric oxide-dependent mechanism. / Jaiswal M, LaRusso NF, Burgart LJ, Gores GJ // Cancer Res. 2000. pp.184–190.
10. Y. Li. 2,3,7,8-Tetrachlorodibenzo-p-dioxin (TCDD) induces microglial nitric oxide production and subsequent rat primary cortical neuron apoptosis through p38/JNK

MAPK pathway / Li Y., Chen G., Zhao J., Nie X., Wan C., Liu J., Duan Z., Xu G. // Toxicology. 2013. pp. 132–141.
11. J. Green. Transcriptional regulation of bacterial virulence gene expression by molecular oxygen and nitric oxide / Green J., Rolfe M.D., L.J. Smith // Virulence, 5 (2014), pp. 794–809.

Introduction to diffusion tensor imaging and tractography: basic physics, anatomy and ROI-based reconstruction of the major white matter bundles

Anna Y. Lavrova[1], M. A. Zubkov[2], V. M. Cheremisin[1]

[1]Faculty of General Medicine, Department of oncology with a course of Radiation diagnostics and Radiotherapy, Saint Petersburg State University, Saint Petersburg, Russia
[2]Department of Physics and Engineering, Saint Petersburg National Research University of Information Technologies, Mechanics and Optics, Saint Petersburg, Russia
E-mail: lavrova.anya@gmail.com

Introduction

Since its early introduction in 1988 diffusion tensor imaging (DTI) has become one of the most popular advanced MRI techniques with a plethora of clinical applications and quite an irreplaceable tool for in-vivo white matter fiber tracking. Nowadays there is already a multitude of software options for processing DTI data as well as schemes such data can be acquired. In our report, we present the anatomy, functions of the intra-brain connections and basic techniques for searching and reconstructing of main white matter fiber tracts.

Diffusion is a process of mass transport due to random thermal molecular motion. MRI focuses on self-diffusion, i.e. the diffusion of particles of a substance among other particles of the same substance. The speed (technically, the average displacement over time) of this motion is described by the self-diffusion coefficient D.

A lot of tissues have internal structure, where molecular motion in at least one direction is favored among others (i.e., they represent anisotropic medium). In this case, diffusion cannot be described by a single self-diffusion coefficient anymore. Self-diffusion tensor is then used to better describe diffusion in such a medium.

MRI pulse sequences can be made sensitive to diffusion by using diffusion-weighing gradient pulses. In order to speed up acquisition SE-SPI or TSE pulse sequences are usually used for acquiring diffusion-weighted images.

To reconstruct diffusion tensor from diffusion-weighted images, diffusion needs to be probed in at least 6 directions; the intensity of weighting is determined by the *b*-value; A $b=0$ is also often required; probing diffusion in more directions or at more *b*-values increases reconstruction robustness, but requires more scanning time.

Diffusion tensor, as is, is not too convenient to use in clinical practice; a few practical metrics are usually calculated from the reconstructed diffusion tensor: FA (fractional anisotropy), MD (mean diffusivity, AD (axial diffusivity), RD (radial diffusivity). Also, the principal diffusion direction can be determined from the tensor. Then, following this direction until it disappears (i.e., FA too low), one can track the path of an anisotropic fiber (e.g., a nerve) through 3D space. This way the nerve bundles can be tracked and visualized.

White matter fiber tracts

White matter tracts have 3 types of fibers, which interconnect different areas of the human central nervous system and have a variety of functions. There are an association, commissural and projection connections.

Association fibers connect cortical areas in each hemisphere and are represented by cingulum, superior and inferior occipitofrontal fasciculi, uncinate fasciculus, superior and inferior longitudinal fasciculi.

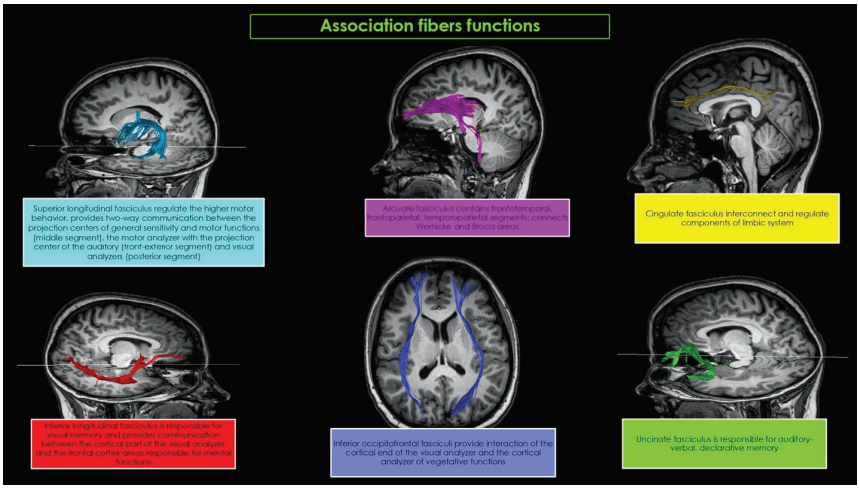

Figure 1. Association fibers functions

Commissural fibers interconnect similar cortical areas between opposite hemispheres and are represented by corpus callosum and commissures anterior and posterior.

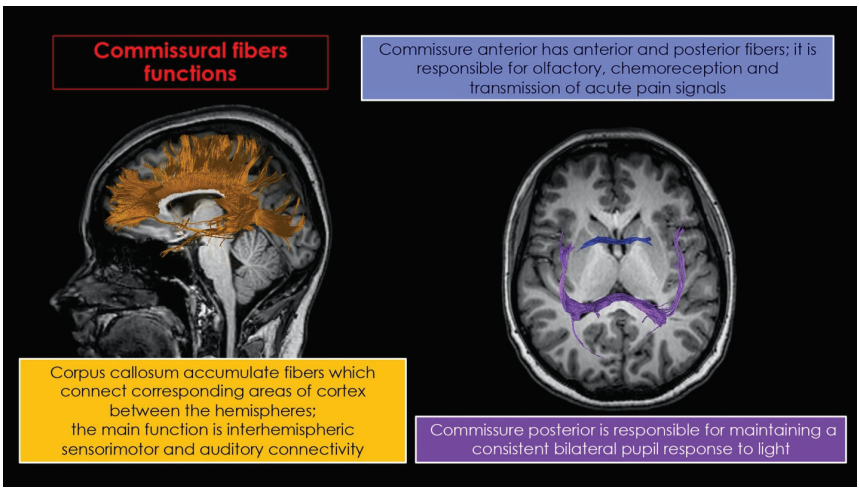

Figure 2. Commissural fibers functions

Projection fibers connect cortical areas with deep nuclei, brainstem, cerebellum, and spinal cord and are represented by corona radiata, which combine fibers from the internal capsule, including corticospinal, corticobulbar, corticopontine, corticothalamic tracts. One of the projection fibers is optic radiation, which is a part of the visual analyzer and connects the lateral geniculate body and occipital cortex.

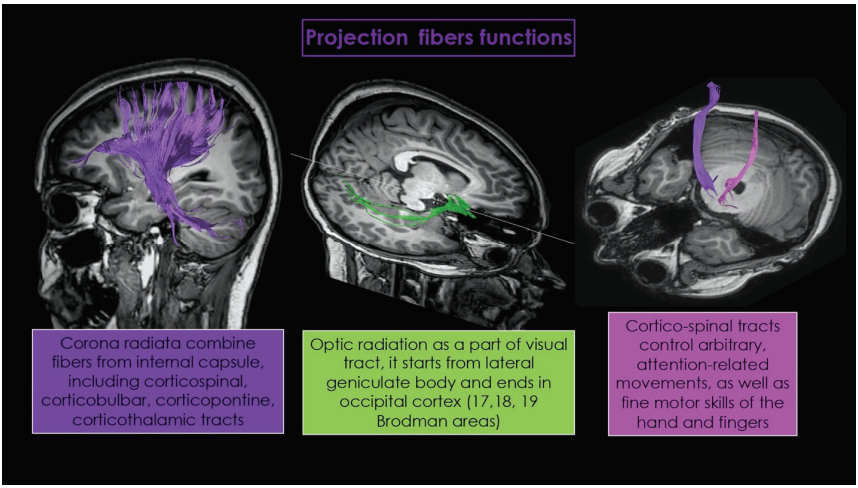

Figure 3. Projection fibers functions

Conclusion

The current DTI applications show the potential prospects to improve our knowledge about human brain connectivity and understanding of damage and recovery in diseases of the human nervous system. Tractography is a useful tool for the diagnosis and management of patients, particularly for surgery planning and outcome prediction. DTI is important for neuronavigation systems that enable intraoperative tractography-based guidance. Combined with functional MRI techniques it is become possible to access the relation between function and structure in healthy and diseased brains and assess whether fMRI measured cortical activity correlates with indices of the structural integrity of the subserving white matter tracts.

References

1. Borden, N. M., Forseen, S. E., & Stefan, C. (2015). Imaging Anatomy of the Human Brain: A Comprehensive Atlas Including Adjacent Structures. Springer Publishing Company.
2. White Matter Tracts (DTI), Lubdha M. Shahn, MD, retrieved from statdx.com.
3. White Matter Tracts, Karen L. Salzman, MD, retrieved from statdx.com.
4. Webb, W., & Adler, R. K. (2016). Neurology for the Speech-Language Pathologist-E-Book. Elsevier health sciences.

Development and study of novel pervaporation membranes based on sodium alginate modified by fullerene derivatives

Vladislav P. Liamin, Mariia E. Dmitrenko, Anastasia V. Penkova, Sergey S. Ermakov

Institute of Chemistry, St. Petersburg State University, St. Petersburg, Russia
E-mail: lyamin.vlad.322@gmail.com

Introduction

Nowadays, development of novel green highly effective membranes and enhancement its physicochemical and transport properties is very promising area due to high demand and relevance of membrane technologies. Membrane requirements are constantly increasing, leading to the need of the improvement the quality of membranes. It can be achieved by the development of mixed matrix membranes mixing of organic material (for example, polymer) as matrix and inorganic particles as filler. It allows combining of the best properties and advantages of both polymer and inorganic structures.

Membrane investigation

In the present research water soluble biopolymer sodium alginate (SA) was used as a matrix for further modifications by water soluble fullerene derivative – fullerenol. The optimal conditions for preparation and cross-linking of membranes based on SA-fullerenol composites were developed. Structural and physicochemical characteristics of developed membranes were studied by various physical and chemical methods of investigation (IR and NMR spectroscopies, scanning electron and atomic force microscopies, sorption experiments, contact angle measurements, etc.). The obtained membranes were tested in pervaporation dehydration of water-organic mixtures.

Results

It was shown that membrane based on SA-fullerenol (5%) composite possessed improved transport properties due to the changes of structure, morphology and surface properties.

Acknowledgements

This work is supported by Russian Science Foundation [project No 19-73-00105]. The experimental work was facilitated by equipment from Resource Centres for Nanotechnology, Magnetic Resonance, X-ray Diffraction Studies, Thermogravimetric and Calorimetric Research Centre, Chemical Analysis and Materials Research Centre and Centre "Nanofabrication of Photoactive Materials (Nanophotonics)" at St. Petersburg State University.

Development and characterization of novel pervaporation membranes based on polyphenylene isophtalamide modified by various fullerene derivatives

Vladislav P. Liamin, Mariia E. Dmitrenko, Andrey A. Zolotarev, Anastasia V. Penkova

St. Petersburg State University, 7/9 Universitetskaya nab., St. Petersburg 199034, Russia
E-mail: lyamin.vlad.322@gmail.com

Introduction

Currently, the development of membrane process – pervaporation for separation of liquid mixtures has become extremely relevant. This membrane method can be a good alternative method to traditional separation processes (e.g. distillation or extraction). One of the key factors for the effective pervaporation separation is the proper choice of a membrane. In this regard, the development of novel polymeric membranes with improved transport properties is required. One of the ways to solve this problem is the modification of known polymers by carbon nanoparticles and the preparation of mixed matrix membranes (MMMs) based on these composites. It allows combining of the advantages of both polymer and inorganic structures. Among the inorganic particles fullerene and its derivatives take an important place due to their unique structure. In the present work polyphenylene isophtalamide (PA) was used as the polymeric matrix for mixed matrix membranes preparation, while fullerene and water soluble fullerene derivatives (fullerenol, carboxyfullerene and fullerene derivative with L-arginine) were used as modifiers for PA.

Membrane investigation

The aims of the work were to prepare and characterize the structure of novel mixed matrix membranes based on polyphenylene isophtalamide (PA) modified by fullerene and its derivatives (fullerenol, carboxyfullerene and fullerene derivative with L-arginine) and to test them in pervaporation. Structural properties of the developed membranes were studied by various investigation methods (spectroscopic methods (NMR, FTIR), X-ray diffraction analysis, scanning electron and atomic force microscopies). The evaluation of changes in surface characteristics and physicochemical properties of modified membranes was carried out by contact angle measurements and sorption experiments. The transport properties of membranes were studied in pervaporation separation of industrially important methanol-toluene mixture.

Results

It was shown that the transport characteristics of mixed matrix PA membranes modified by fullerene derivatives were essentially improved as compared to membranes based on pristine PA and composite PA-fullerene due to the significant changes of structure and morphology of the polymeric membranes.

Acknowledgements

This work was supported by Russian Science Foundation [grant No. 17-73-20060]. The experimental work was facilitated by equipment from the Interdisciplinary Resource Centre for Nanotechnology, Magnetic Resonance Research Centre, Thermogravimetric and Calorimetric Research Centre, Centre for X-ray Diffraction Studies, Chemical Analysis and Materials Research Centre, Nanophotonics Centre, Centre for Diagnostics of Functional Materials for Medicine, Pharmacology and Nanoelectronics, and Centre for Geo-Environmental Research and Modelling at St. Petersburg State University.

Computer model and experimental investigation of ionic liquid-diesel fuel systems

Kenan Mammadhasanov[1*], Minaver D. Ibragimova[2], Sabina A. Seidova[2**], Andrei V. Komolkin[1]

[1]Faculty of Physics, Saint Petersburg State University, Saint Petersburg, 199034, Russia
[2]Y. H. Mammadaliyev Institute of Petrochemical Processes of Azerbaijan National Academy of Sciences, AZ 1025, Baku, 30 Khojaly ave., Azerbaijan
*E-mail: mammadhasanov@yandex.ru
**E-mail: sabina.seidova.ai@mail.ru

Introduction

With the growing environmental problem, the requirements for the content of aromatic and sulfur compounds in fuel are being tightened. In order to improve the environmental properties of diesel fuel and the productivity of its engine, it is necessary to develop more and more effective methods for extracting unwanted components from the composition of the diesel fraction. Despite the large-scale application in the industry of hydrotreating processes that allow obtaining high-quality diesel fuel, their existing shortcomings contribute to the development of alternative treatment methods.

Experimental methods

We investigated the extraction purification of the diesel distillate containing 16,5% mass of aromatic hydrocarbons and 960 ppm of sulfur compounds using anilinium formate as a selective extractant.

It was shown that with an equal mass amount of extractant and diesel distillate at a temperature of 40°C and a component contact time of 1 hour, the residual content of aromatic and sulfur compounds in the raffinate is 10,5% mass and 350 ppm, respectively. The yield of raffinate was 87,5% mass.

Computer simulation

Computer simulation of the process of refining of model components of petroleum was performed to study the interaction of ionic liquids with different types of components: alkanes, aromatics, thiophenes, and water. Molecular dynamics method provided information on diffusion, phase separation, selective interactions of components.

Simulations were started from the true solution (random mixture) of all compounds: model petroleum components and ionic liquid anilinium acetate (acetate was simulated instead of formate).

In the mixtures of ionic liquid with aliphatic and aromatic compounds, naphtha compounds aggregated in small droplets inside ionic liquid (Fig. 1). Ionic liquid after 21 ns of simulation organized porous system resembling zeolite structure. Diffusion coefficient of naphtha compounds was similar to the coefficient of that compounds in bulk phase (of order of 10^{-9} m^2/s), but diffusion coefficient of anilinium acetate was equal to 6×10^{-12} m^2/s at 65°C and it was much slower at room temperature (~2×10^{-12} m^2/s). Such slow motion require longer simulation of the process of phase separation and selective dissolution of naphtha components in ionic liquid.

Process of separation of water and petroleum components are fast to simulate within a few nanoseconds (Fig. 2) because of fast motion of both water (the diffusion coefficient is ~2.4×10^{-9} m^2/s at room temperature) and petroleum components.

Conclusions

Thus, based on the results obtained, the prospects of using anilinium formate ionic liquid in the process of extracting undesirable components from the composition of diesel distillate are established. Computer simulation allows one to study selective interactions of ionic liquids with different components and to predict their prospects for fuel refining.

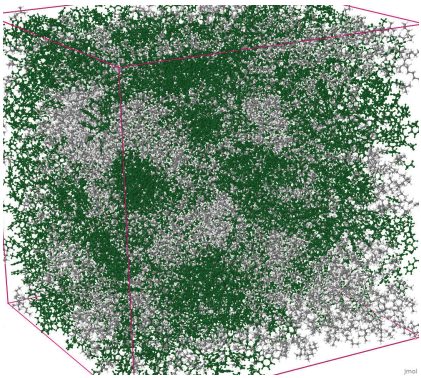

Figure 1. Phase separation of isooctane+ hexane mixture (gray) with anilinium acetate (green) after 21 ns of simulation

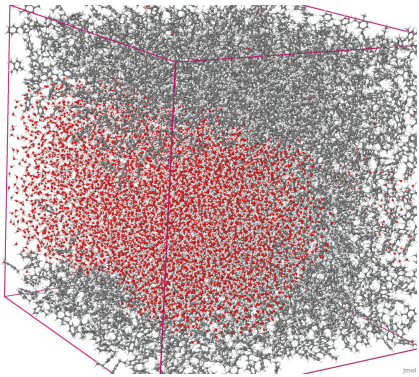

Figure 2. Phase separation in mixture of water and aromatic compounds (pseudocumene and ethylbenzene) after 5 ns of simulation

References

1. M. J. Ibrahimova, S. A. Seyidova, H. J. Huseynov, *et al*. Comparative results of selective cleaning of diesel fuel with ionic liquids based on formic and acetic acids. // Processes of petrochemicals and oil refining, 2019, № 1, p. 29-33 (in Russian)

Computer simulation of interaction of lysine dendrimer with molecules of Gly-Glu-Asp peptide

S. E. Miktaniuk, V. V. Bezrodniy, E. I. Fatullaev, I. M. Neelov

St. Petersburg National Research University of Information Technologies, Mechanics and Optics (ITMO University), Kronverkskiy pr.49, St.Petersburg, 197101, Russia
E-mail: i.neelov@mail.ru

Introduction

Dendrimers are repeatedly branched molecules with branches emanating from central core [1]. Dendrimers are used in wide range of biomedical applications including drug and gene delivery [2]. Lysine dendrimers are special type of dendrimers on the base of only one type (lysine) aminoacid residues which are enriched with positively charged amine groups [3]. They could be used as antiviral, antibacterial and antiamyloid agents and could form complexes with oppositely charged molecules for example DNA, polysaccharides and peptides.

Using molecular dynamic (MD) simulation we test in present paper could short regulatory Gly-Glu-Asp peptide [4-5] make complex with lysine dendrimer. Our MD calculations were performed using the GROMACS software and AMBER_99SB-ildn force fields. Simulation approach used here was described elsewhere for simulation of charged linear polymers and peptides [6-18] as well as for dendrimers [19-32]. Some properties of branched polymer structures were obtained by us earlier using numerical variant of self consistent field approach [33-36] and NMR experiments [22-24, 37-39]. In this paper we studied the system consisting of one dendrimer and 8 Gly-Glu-Asp peptides in water with explicit counterions. We used NPT ensemble (at temperature 300 K and pressure 1 ATM) and PME algorithm for calculation of electrostatic interactions.

Results and discussion

To characterize the size of the subsystems consisting of dendrimer or dendrimer and peptide molecules during the equilibration the mean squared gyration radius Rg(t) was used. This function was calculated using g_gyrate function of GROMACS software. The time dependence of gyration radius Rg at the beginning of calculation describes the process of compaction of subsystem consisting of dendrimer and peptide molecules during formation of complex (see Fig. 1a).

Fig 1a demonstrates time dependence for size of complex Rg. At the beginning (at time t=0) the size of complex is large, because the peptides are far enough from dendrimer. The size decrease with time for about 40 ns due to attractive interactions between dendrimer and peptide molecules. After this time the complex size (radius of gyration Rg) fluctuate but its average size did not change with time. Another quantity that can characterize the rate of complex formation is the total number of hydrogen bonds between dendrimer and each of 8 peptide molecules (Fig.1b). This function increases during first 30-40ns and after that fluctuates until the end simulation. Therefore, we can assume from all these results the complex forms during first 40ns and become close to equilibrium state after this time.

It was obtained that the size of the complex after 40 ns consisting of G2 dendrimer and 8 molecules of GED peptides (see Table 1) is about 1.5 time greater than size of dendrimer itself. The shape of the complex can be characterized by principal components of inertia tensor (see Table 1) where Rg11 is minimal and Rg33 is maximal eigenvalue of inertia tensor.

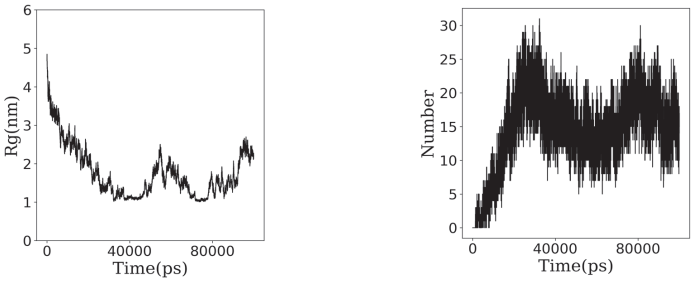

a *b*

Figure 1. Time dependence of size Rg(t) of subsystems consisting of G2 and 8 peptides (a), and number of hydrogen bonds between them (b).

The value of size Rg of complex and dendrimer in equilibrium state are evaluated by inertia radius averaged through the time t after equilibration of the system (see table 1).

Table 1. Size R_g, main components of inertia tensor Rg^{11}, Rg^{22} and Rg^{33} and axial ratio Rg^{11}/Rg^{33}

System	R_g^{11}, (nm)	R_g^{22}, (nm)	R_g^{33}, (nm)	R_g, (nm)	R_g^{33}/R_g^{11}
G2+8 peptides	1.08	1.51	1.65	1.76	1.54
G2	0.59	0,91	0,96	1.02	1.64

The rough evaluation of anisotropy of shape of dendrimer and complex could be done using axial ratio Rg^{33}/Rg^{11}. This ratio is equal 1,54 for dendrimer. Complex of dendrimer and peptides has similar axial ratio Rg^{33}/Rg^{11}=1,64.

In this paper we demonstrated the formation of dendrimer-peptide complex between lysine dendrimer and eight Gly-Glu-Asp peptide molecules. We also obtained its equilibrium size and shapeof complex.

Acknowledgements

This work was partly supported by grant 08-08 of Government of RF and RFBR grant 19-03-00715. The research is carried out using the equipment of the shared research facilities of HPC computing resources at Lomonosov Moscow State University.

References

1. Frechet J.M.J.,Tomalia D.A., 2001, Dendrimers and Other Dendriric Polymers, (West Sussex: John Wiley&Sons Ltd.)
2. Mendes L.P., Pan J., Torchilin V.P., 2017, Molecules, 22, 1401
3. Denkewalter R.G., Kolc J., Lukasavage W.J., Macromolecular Highly Branched Homogeneous Compound, 1983, US Patent № 4410688.
4. Kozina L.S., 2008, Antioxidant action of geroprotective peptide bioregulators, dissertation for a doctoral (Dr.Sci) degree, St.Petersburg
5. Anisimov V.N., Khavinson V.K., 2009, Biogerontology, 11, 139
6. Ennari J., Neelov I., Sundholm F., Polymer, 2001, 42, 8043
7. Ennari J., Neelov I., Sundholm F., Polymer, 2000, 41, 4057
8. Ennari J., Elomaa M., Neelov I., Sundholm F., 2000, Polymer, 41, 985
9. Ennari J., Neelov I., Sundholm F., Comput Theor Polym Sci, 2000, 10, 403

10. Ennari J., Neelov I., Sundholm F., Polymer, 2000, 41, 2149
11. Ennari J., Neelov I., Sundholm F., Polymer, 2004, 45, 4171
12. Darinskii A., Gotlib Yu., Lukyanov M., Lyulin A., Neelov I., Progress in Colloid & Polymer Science, 1993, 91, 13
13. Neelov I.M., Adolf D.B., McLeish T.C.B., Paci E., Biophysical Journal, 2006, 91, 3579
14. Gowdy,J.,Batchelor, M, Neelov, I, Paci, Journal of Physical Chemistry B, 2017, 121, 9518
15. Darinskii A., Gotlib Yu., Lyulin A., Neelov I., Vysokomolek. Soed.. Ser,A 1991, 33, 1211 (translation to English: Polymer Science, 33,1116)
16. Darinskii A., Lyulin A., Neelov I., Makromolekulare Chemie - Theory and Simulations (Macromolecular Theory and Simulations), 1993, 2, 523
17. Darinsky A., Gotlib Y., Lukyanov M., Lyulin A., Neelov I., Progress in Colloid and Polymer Science, 1993, 91, 13
18. Neelov I.M., Adolf D.B., Lyulin AV., Davies G.R., J. Chem. Phys., 2002, 117, 4030
19. Mazo M.A., Shamaev M.Y., Balabaev N.K., Darinskii A.A., Neelov I.M., Physical Chemistry Chemical Physics, 2004, 1285-1289
20. Neelov, I. M.; Janaszewska, A.; Klajnert, B, Bryszewska M., Makova N., Hicks D., Pearson N., Vlasov G.P., Ilyash M.Y., Vasilev D.S., Dubrovskaya N.L., Zhuravin I.A., Turner A.J., Nalivaeva N.N., Current Medical Chemistry, 2013, 20, 134
21. Falkovich S.G., Markelov D., Neelov I., Darinskii A., J. Chem. Phys., 2013, 139, 064903
22. Neelov, I. M., Markelov D.A, Falkovich S.G., Ilyash M.Y., Okrugin B.M., Darinskii A.A., Polymer Science, 2013, 55, 154
23. Neelov, I., Markelov D., Falkovich S.G.,, Paci E., Darinskii A., Tenhu H., Molecular Dynamics of Lysine Dendrimers in Computer Simulation and NMR. Dendrimers in Biomedical Applications, (London: RSC) 2013, 99-114
24. Markelov D.A., Falkovich S.G.,, Neelov, I. M., Ilyash M.Y., Matveev V.V., Lahderanta E., Ingman, P., Darinskii A.A., Physical Chemistry and Chemical Physics, 2015, 17, 3214
25. Okrugin B., Ilyash M., Markelov D., Neelov I., Pharmaceutics, 2018, 10, 129 (2018)
26. Neelov, I. M., O.V. Shavykin, Ilyash M.Y., Bezrodnyi V.V., Mikhtaniuk S.E., Fatullaev E.I., Darinskii A.A., Leermakers F.A.M., Supercomp. Frontiers and Innovations, 2018, 5, 60
27. Popova E., Khamidova D., Neelov I., Komilov F., Chapter 3. “Lysine Dendrimers and Their Complexes with Therapeutic and Amyloid Peptides: Computer Simulation”, in “Dendrimers Fundamentals and Applications”, (IntechOpen), 2018, 29-45.
28. Neelov I.M., Adolf D.B., 2003, Macromolecules, 36, 6914
29. Neelov I.M., Adolf D.B., 2004, J. Phys. Chem. B, 108, 7627
30. Neelov I.M., Binder K., 1995, Macromolecular Theory and Simulations 4, 1063
31. Shavykin O.V., Neelov, I. M., Darinskii A.A., Phys. Chem. Chem. Phys., 2016, 18, 24307
32. Shavykin O.V., Mikhailov I.V., Darinskii A.A., Neelov I.M., Leermakers F.A.M., Polymer, 2018,146, 256.
33. Okrugin B.M., Neelov I.M., Leermakers F.A.M., Borisov O.V., Polymer, 2017, 125, 292
34. Shavykin O.V., Leermakers F.A.M., Neelov I.M., Darinskii A.A., Langmuir, 2018, 34, 1613
35. B.M. Okrugin, R.P.Richter, F.A.M.Leermakers, I.M.Neelov, O.V.Borisov, E.B.Zhulina, Soft Matter, 2018, 14, 6230

36. Zhulina E.B., Neelov I.M., Sheiko S.S., Borisov O.V., Polymer Science, Series C, 2018, 60, 76.
37. Sheveleva N.N., Markelov D.A., Vovk M.A., Tarasenko I.I., Neelov I.M., Lahderanta E., Scientific Reports, 2018, 8, 8916
38. Sheveleva N.N., Markelov D.A., Vovk M.A., Tarasenko I.I, Neelov I.M., E.Lähderanta, 2019, RSC Adv. 9, 18018
39. Sheveleva N.N., Markelov D.A., Vovk M.A., Tarasenko I.I, Mikhailova M.E., Neelov I.M., 2019, Molecules, 24, 2481

Computer simulation of orientational dynamics in the peptide dendrimers with different excluded volume interactions

Sofia E. Miktaniuk[1], Valerii V. Bezrodniy[1,2], Oleg V. Shavykin[1,2], Igor M. Neelov[1,2]

[1]St. Petersburg National Research University of Information Technologies, Mechanics and Optics (ITMO University), Kronverkskiy pr.49, St.Petersburg, 197101, Russia
[2]St.Petersburg State University (SPbSU), 7/9 Universitetskaya nab., St.Petersburg, 199034,Russia
E-mail: kupala-89@mail.ru

Introduction

The peptide-based dendrimers have a wide range of uses, and biomedicine is one of the important ones. The poly-L-lisine dendrimers that containing only lysine residues in the repeating fragments (spacers) were considered earlier in many works [1-3]. In present paper we studied two lysine based dendrimers Lys2Gly and Lys2Lys where two additional aminoacide residues (2Gly or 2Lys) were inserted between each pair of neighboring branching points of usual lysine dendrimer.The glycine residues don't have a massive side groups as lysine [3]. It means that dendrimer with double glycine in spacers have a smaller excluded volume interactions than dendrimer with double lysine residues. 2Gly spacer also does not contain a charges as 2Lys spacer which has charge -2 in each repeat unit. These differences in chemical structure and charges of Lys2Gly and Lys2Lys dendrimers affect their properties [3]. We performed the molecular dynamics (MD) simulation of orientational mobility in these two new peptide denerimers of 2nd generation in water solvent with explicit account of counterions at temperature T=300K and pressure P=1atm using the program package Gromacs with AMBER99SB-ildn force field. The details of MD simulations were reported earlier for linear [7-19] and branched polymers [20-34].

The local structure

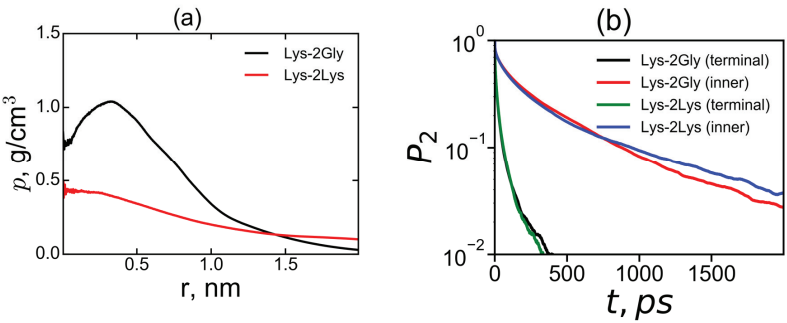

Figure 1. (a) The radial distribution of density of dendrimer's atom and (b)the second order autocorrelation functions (ACFs) for CH_2 of ε-amino group in inner and terminal lysine. Both dendrimers with double lysine and double glycine were considered

The radial distribution functions for densitiy $\rho(r)$ is characteristic of local structure of dendrimer relatively its center of mass and can be obtained from next formulae

$$\rho(r) = \frac{1}{M}\sum_i m_i \delta(r - r_i),$$

where m_i – molecular mass of the i-th atom and M, r_{com} mass of dendrimer as a whole and position of its center of mass, correspondingly. The radial distribution functions for densities

$\rho(r)$ of Lys-2Lys and Lys-2Gly dendrimers are shown on Figure 1a. It was found that Lys-2Gly dendrimer has a density profile, that comparable with density profile for usual lysine dendrimer studied in the work [1-3]. At the same time Lys-2Lys dendrimer has a lower density distribution due to the strong electrostatic repulsion of the charged spacers of the dendrimer from each other.

The manifestation of excluded volume interactions on the orientational dynamics

We estimated also mobility of the vector $\boldsymbol{d}$ between two hydrogens in the hydrocarbon CH_2 group near ε-amino group using the dependence of second order autocorrelation function (ACF) $P_2(t)$ on time t

$$P_2(t) = \frac{3}{2}\langle\frac{(\boldsymbol{d}(t),\boldsymbol{d}(0))^2}{|\boldsymbol{d}(t)|^2|\boldsymbol{d}(0)|^2}\rangle - \frac{1}{2}$$

The time dependence of $P_2(t)$ for both dendrimers are shown in Fig. 1b. It is easy to see that behavior of H-H vectors in terminal and inner lysines are different. I.e. terminal vectors rotate essentially faster, than inner for both dendrimers. At the same time the dependences of P2(t) for similar vectors of both dendrimers are close to each other (see Fig.1b).

Thus the presence of additional massive charged groups in Lys2Lys dendrimer weakly affects the local mobility of internal and terminal lysines. This result is in agreement with NMR experiment [3] and coarse-graining simulation [4].

Acknowledgements

This work was partly supported by grant 08-08 of Government of RF and RFBR grants 19-03-00715. The research is carried out using the equipment of the shared research facilities of HPC computing resources at Lomonosov Moscow State University supported by the project RFMEFI62117X0011.

References

1. S. Falkovich, D. Markelov, I. Neelov, and A. Darinskii. J. Chem. Phys. 2013, 139, 064903.
2. Markelov D.A, Falkovich S.G., Neelov I.M., Ilyash M.Yu, Matveev V.V., Lahderanta E., Ingman P., Darinskii A.A. Physical Chemistry and Chemical Physics. 2015, 17, 3214.
3. N.N.Sheveleva, D.A. Markelov, M.A. Vovk, M.E. Mikhailova, I.I.Tarasenko, I.M. Neelov, E. Lähderanta. Scientific Reports, 2018, 8, 8916.
4. Sheveleva N.N., Markelov D.A., Vovk M.A., Tarasenko I.I, Neelov I.M., E.Lähderanta, 2019, RSC Adv. 9, 18018.
5. Sheveleva N.N., Markelov D.A., Vovk M.A., Tarasenko I.I, Mikhailova M.E., Neelov I.M., 2019, Molecules, 24, 2481.
6. O.V.Shavykin, I.M.Neelov, A.A.Darinskii. Phys.Chem.Chem.Phys., 2016, 18, 24307.
7. Darinskii A., Gotlib Yu., Lukyanov M., Lyulin A., Neelov I., Progress in Colloid & Polymer Science, 1993, 91, 13.
8. Darinskii A., Gotlib Yu., Lyulin A., Neelov I., Vysokomolek. Soed.. Ser,A 1991, 33, 1211 (translation to English: Polymer Science, 33,1116).
9. Darinskii A., Lyulin A., Neelov I., Makromolekulare Chemie - Theory and Simulations (Macromolecular Theory and Simulations), 1993, 2, 523.
10. Darinsky A., Gotlib Y., Lukyanov M., Lyulin A., Neelov I., Progress in Colloid and Polymer Science, 1993, 91, 13.
11. Ennari J., Neelov I., Sundholm F., Polymer, 2001, 42, 8043.
12. Ennari J., Neelov I., Sundholm F., Polymer, 2000, 41, 4057.
13. Ennari J., Elomaa M., Neelov I., Sundholm F., 2000, Polymer, 41, 985.

14. Ennari J., Neelov I., Sundholm F., Comput Theor Polym Sci, 2000, 10, 403.
15. Ennari J., Neelov I., Sundholm F., Polymer, 2000, 41, 2149.
16. Ennari J., Neelov I., Sundholm F., Polymer, 2004, 45, 4171.
17. Neelov I.M., Adolf D.B., McLeish T.C.B., Paci E., Biophysical Journal, 2006, 91, 3579/
18. Gowdy,J.,Batchelor, M, Neelov, I, Paci, Journal of Physical Chemistry B, 2017, 121, 9518.
19. Neelov I.M., Adolf D.B., Lyulin AV., Davies G.R., J. Chem. Phys., 2002, 117, 4030.
20. Mazo M.A., Shamaev M.Y., Balabaev N.K., Darinskii A.A., Neelov I.M.,Physical Chemistry Chemical Physics, 2004, 1285.
21. Neelov, I. M.; Janaszewska, A.; Klajnert, B, Bryszewska M., Makova N., Hicks D., Pearson N., Vlasov G.P., Ilyash M.Y., Vasilev D.S., Dubrovskaya N.L., Zhuravin I.A., Turner A.J., Nalivaeva N.N., Current Medical Chemistry, 2013, 20, 134.
22. Falkovich S.G., Markelov D., Neelov I., Darinskii A., J. Chem. Phys., 2013, 139, 064903.
23. Neelov, I. M., Markelov D.A, Falkovich S.G., Ilyash M.Y., Okrugin B.M., Darinskii A.A., Polymer Science, 2013, 55, 154.
24. Neelov, I., Markelov D., Falkovich S.G.,, Paci E., Darinskii A., Tenhu H., Molecular Dynamics of Lysine Dendrimers‖ in Computer Simulation and NMR. Dendrimers in Biomedical Applications, (London: RSC) 2013, 99-114
25. Markelov D.A., Falkovich S.G.,, Neelov, I. M., Ilyash M.Y., Matveev V.V., Lahderanta E., Ingman, P., Darinskii A.A., Physical Chemistry and Chemical Physics, 2015, 17, 3214.
26. Okrugin B., Ilyash M., Markelov D., Neelov I., Pharmaceutics, 2018, 10, 129.
27. Neelov, I.M., Shavykin, Ilyash M.Y., Bezrodnyi V.V., Mikhtaniuk S.E., Fatullaev E.I., Darinskii A.A., Leermakers F.A.M., Supercomp. Frontiers and Innovations, 2018, 5, 60.
28. Popova E., Khamidova D., Neelov I., Komilov F., Chapter 3. “Lysine Dendrimers and Their Complexes with Therapeutic and Amyloid Peptides: Computer Simulation”, in “Dendrimers Fundamentals and Applications”(IntechOpen), 2018, 29-45.
29. Neelov I.M., Adolf D.B., 2003, Macromolecules, 36, 6914.
30. Neelov I.M., Adolf D.B., 2004, J. Phys. Chem. B, 108, 7627.
31. Neelov I.M., Binder K., 1995, Macromolecular Theory and Simulations 4, 1063.
32. Shavykin O.V., Mikhailov I.V., Darinskii A.A., Neelov I.M., Leermakers F.A.M., Polymer, 2018,146, 256.
33. Okrugin B.M., Neelov I.M., Leermakers F.A.M., Borisov O.V., Polymer, 2017, 125, 292.
34. Shavykin O.V., Leermakers F.A.M., Neelov I.M., Darinskii A.A., Langmuir, 2018, 34, 1613.

Experimental application of alanine detectors for control of technological irradiations at the accelerator ILU-10 at INP RK

Zh. T. Mukan[1,2], A. B. Ruhin[1], T. A. Seredavina[1], N. S. Suchkova[1], Zh. Beksultanov[1], I. V. Danko[1], N. V. Gluchshenko[1]

[1]*Institute of Nuclear Physics, Almaty, Kazakhstan*
[2]*Gumilev ENU, Nur-Sultan, Kazakhstan*
E-mail: zhuldiz_mukan@mail.ru

At present, radiation technologies (RT) are becoming more demanded in various fields of human activities. Currently, medical products, food products, agricultural products are exposed to radiation treatment and this list is constantly expanding.

Dosimetric control during radiation sterilization of irradiated products is controlled by regulatory documents [1, 2].

The works in this sphere are performed at INP RK on the electron accelerator ILU-10.

The performed studies have confirmed the capabilities of using RT and tablet dosimeters (DT) on alanine in RT.

Among the methods of radiation dosimetry, a special place is occupied by electron paramagnetic resonance (EPR), based on resonant absorption of electromagnetic radiation by unpaired electrons appeared during irradiation of substances.

The aim of this work was the adaptation and application of the method of EPR dosimetry on alanine during technological radiation treatment of agricultural and food products under the action of bremsstrahlung in the dose range from 1 Gray to several kilo Gray.

Alanine is recommended by the IAEA and International Standards for control of technological exposures in the dose range used in radiation sterilization. The signal in the alanine dosimeter is linear over a wide range of doses and does not change over a long period of time. The subject of the study was the measured doses on alanine detectors, irradiated by bremsstrahlung on the accelerator ILU-10 within the dose range of 5.6-70.7 Gy, with average accelerated electron beam currents from 0.25 mA to 6.0 mA.

EPR data on DT were obtained on the basis of their exposure to γ - radiation of Cs 137 from the source. Further measurements and conversion of signals into a dose showed a linear dependence of the dose on the average accelerator current.

Thus, the research results confirm the feasibility and capabilities of using DT on the electron accelerator ILU-10.

References

1. GOST ISO 11137—2011. Sterilization of medical products. Radiation sterilization.
2. GOST 34155—2017. Guidelines for dosimetry in the study of the radiation effects on food and agricultural products.

Posterior reversible encephalopathy syndrome (PRES) in patients in the postpartum period

D. A. Narenkova[1], V. M. Cheremisin, I. G. Kamyshanskaya[1,2], P. I. Simeshchenko[2], V. V. Prits[2]

[1]St. Petersburg State University, Faculty of Medicine, Radiation Diagnostics and Radiotherapy Course, Department of Oncology, 199106, St. Petersburg, 21 line V.O., d. 8.
[2]SPb GBUZ "City Mariinsky Hospital", 194104, St. Petersburg, Liteiny pr., 56
E-mail: dashanarenkova@gmail.com

Relevance

Syndrome of posterior reversible encephalopathy is a clinical and radiological syndrome characterized by reversible vasogenic damage to the brain, usually posterior localization, as well as clinical symptoms in the form of headache, epileptic seizures and other neurological findings. This study presents 10 patients in the postpartum period with characteristic clinical manifestations and reversible discirculatory foci according to MRI, which confirms the PRES syndrome.

Purpose of the study

Study the features of the MR picture of PRES syndrome in patients in the postpartum period.

Material and methods

This study involved 20 people. All female patients in the postpartum period. The age of patients is from 21 to 35 years. These patients experienced a characteristic clinical picture in the form of headaches, visual impairment, confusion, and convulsions, which made it possible to suspect a PRES syndrome. The patients were referred for an MR study based on the St. Petersburg City Mariinsky Hospital. The study was conducted on a Philips Ingenia 3.0T high-field magnetic resonance imager and included a standard protocol: T1 and T2-VI in three projections, as well as TIRM, SWI, and a diffuse-weighted sequence. In 5 patients, the MRI protocol was supplemented by MR spectroscopy.

Results

An MR study of these patients revealed small bilateral, sometimes symmetrical, areas of the hyperintensive MR signal T2-VI and TIRM in the white and adjacent gray matter of the brain. Predominant localization is the frontal, parietal and occipital lobes of the brain. On diffusion-weighted images, signs of the presence of cytotoxic edema were not detected. MR spectroscopy did not reveal high Cho or Cr peaks characteristic of the neoplastic process. Normal NAA and minor changes in the Lip-Lac complex allowed to exclude inflammatory changes in the brain.

The revealed changes were reversible, since after the disappearance of clinical symptoms, during the control MR study, these zones were not determined (Fig 1).

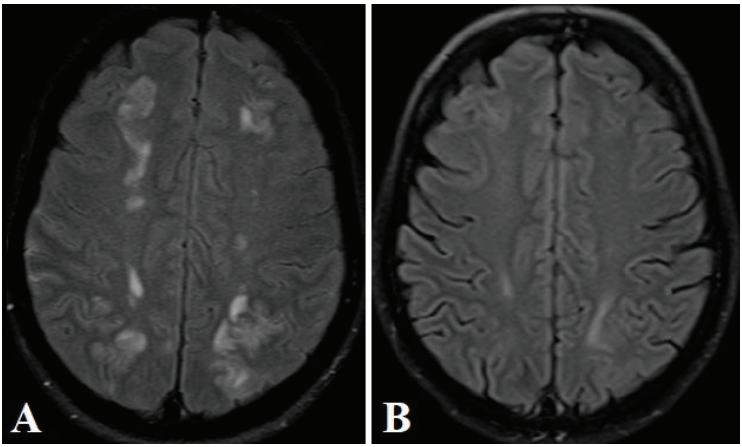

Figure 1. A - Changes in MRI detected 10 hours after the development of clinical manifestations. B - Almost complete regression of focal changes on MRI after 7 days

Findings

Changes detected in the syndrome of posterior reversible encephalopathy must be differentiated with progressive multifocal encephalopathy, multifocal ischemic stroke, venous sinus thrombosis. The radiation criteria of the PRES syndrome according to MRI are: bilateral (symmetrical) lesion at the border of white and gray substances with predominantly supratentorial and subconvexital localization, the absence of signs of cytotoxic edema according to DWI data and, as a rule, the absence of a contrast pattern. MR spectroscopy makes it possible to differentiate PRES syndrome with tumor and inflammatory lesions of the brain. After the start of appropriate therapy, against the background of a clinical improvement in the patient's condition, the detected changes completely regress.

References

1. Jharendra P. Rijal, Smith Giri, Suvash Dawadi, Khagendra V. Dahal. Posterior reversible encephalopathy syndrome (PRES) in a patient with late postpartum eclampsia. BMJ Case Rep. 2014 Published online 2014 Feb 27. doi:10.1136/bcr-2013-203162
2. Luiz Carlos Porcello Marrone, Giovani Gadonski, Luciano Passamani Diogo, et al. Posterior Reversible Encephalopathy Syndrome: Differences Between Pregnant and Non-Pregnant Patients. Neurol Int. 2014 Jan 17; 6(1): 5376.

Investigations and modeling of MRI contrast enhancement in the presence of magnetic nanoparticles

A. V. Nikitina, Yu. V. Bogachev, Ya. Yu. Marchenko, B. P. Nikolaev

Department of Physics, Saint-Petersburg Electrotechnical University "LETI"
5, prof. Popov st., Saint-Petersburg, 197376, Russia
E-mail: nastya_nikitina1996@mail.ru

Introduction

Magnetic resonance imaging (MRI) is a recognized method of modern non – invasive medical diagnostics. Thanks to this method, a new rapidly developing direction has appeared – magnetic resonance theranostics, in which modern diagnostic methods are combined with therapy [1]. For this purpose, MRI uses new multimodal contrast agents based on gadolinium or magnetic iron oxide nanoparticles. These theranostic nanoparticles must not only have high NMR relaxation efficiency, but also be stable, biocompatible, non-toxic, and have the ability to functionalize for interaction with certain biological objects.

To improve the information content and quality of magnetic resonance imaging in the presence of multimodal contrast agents, it is necessary to improve the contrast of MR images. Contrast can be controlled by changing the parameters of the pulse RF sequences of the MRI scanner [1-3]. Therefore, the simulation of magnetic resonance imaging, analysis and optimization of parameters of the applied pulse RF sequences is relevant for conducting MRI studies in the presence of new theranostic nanoparticles.

Method of research

To simulate magnetic resonance imaging in the presence of theranostic nanoparticles, NMR relaxation of protons in aqueous solutions of magnetic nanoparticles based on iron oxide was studied. Magnetic iron oxide nanoparticles in the dextran shell were synthesized as research objects. Iron oxide nanoparticles were prepared by coprecipitation of solutions of ferrous and trivalent iron salts with an excess of alkali in the presence of CsCl at 80 °C in the N_2 atmosphere according to the reaction scheme:

$$FeSO_4 \times 7H_2O + 2(FeCl_3 \times 6H_2O) + 8NH_4OH = Fe_3O_4\downarrow + 6NH_4Cl + (NH_4)_2SO_4 + 23H_2O.$$

Then a stabilizer was introduced to prevent aggregation of magnetic nanoparticles and to increase the dispersion stability. To stabilize the nanodispersed iron oxide, a 30% dextran solution (9-11 kDA) was used. Stabilization was achieved by ultrasound exposure.

The measurement of NMR relaxation times and recording of NMR spectra were performed using a high-resolution NMR spectrometer CXP-300 (Bruker, Germany) with a magnetic field of 7.1 T. Measurements were made at a temperature of 23 ± 2 °C.

Table 1. NMR relaxation characteristics of aqueous solutions in the presence of magnetic nanoparticles

C, mMol/ L	*T*1, ms	*T*2, ms	*T*2*, ms
0.1	1956	18.62	8.61
0.5	868	4.10	2.63
1	508	3.01	1.52
2	287	1.48	0.81
4	149	0.75	0.43
8	78	0.38	0.24
10	63	0.34	0.19

In order to optimize the contrast of MR images, the dependences of the MR signal intensity on the concentration of contrast agents were modeled and analyzed for three frequently used in MRI RF pulse sequences: *spin – echo,* inversion-recovery, FLASH.

Research result

To conduct a comparative analysis of the simulated MR tomograms, the values of the MR signal intensity for different concentrations of magnetic nanoparticles were determined at fixed parameters for the above three RF pulse sequences. The dependence of the MR signal intensity on the concentration of magnetic nanoparticles was constructed (Fig.1, a) for the *spin echo* pulse sequence. Similar dependencies were also defined for the inversion-recovery and FLASH sequences.

From the dependencies shown in Fig. 1 (a), it can be concluded that the studied magnetic nanoparticles significantly reduce the signal intensity on *T*2-weighted tomograms in the region of accumulation of contrasting agents. This decrease in signal intensity characterizes the magnetic nanoparticles under study as a good negative contrast agents.

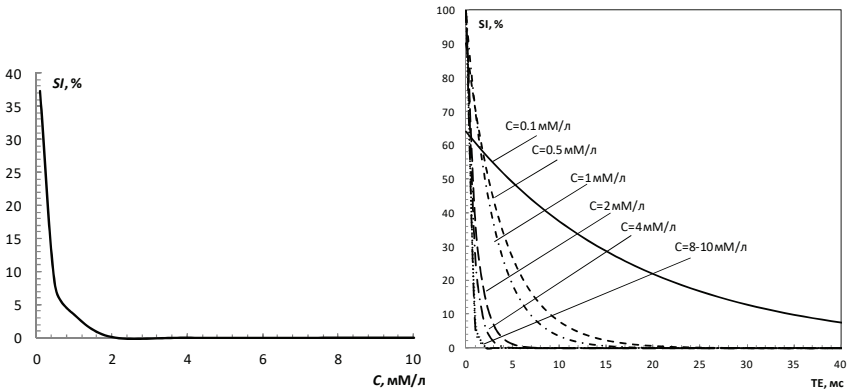

a b

Figure 1. The dependences of the MR signal intensity on the parameters of pulse RF sequences

For practical use of magnetic nanoparticles based on iron oxide as negative contrast agents, it is necessary to determine the optimal parameters of pulse sequences for different concentrations of these agents. The dependences of the MR signal intensity on the parameters of three pulse RF sequences were investigated and recommendations were formulated for choosing the optimal values of these parameters to achieve the best contrast of MR images in the presence of contrast agents. In Fig. 1 (b) the dependence of the MR signal intensity on the parameter *TE* (echo time) of the *spin echo* sequence for different concentrations of magnetic nanoparticles is presented.

By the dependencies shown in Fig. 1 (b), it can be concluded that at small values of the echo time, the magnetic nanoparticles under study will slightly weaken the signal at the place of their accumulation. At the same time, the higher the concentration of nanoparticles, the more they affect the signal intensity. From the graph in Fig. 1 (b) it can be seen that for significant suppression of the MR signal in the area of accumulation of the contrast agent, and therefore for better contrast of this area, it is necessary to select an echo time value of more than 40 ms.

Program to optimize parameters of pulse RF sequences

A program in the Delphi programming environment was developed to select the optimal parameters of pulse RF sequences during MRI studies in the presence of various contrast agents. This program clearly illustrates the change in the contrast of MR images for different concentrations of contrast agents. The working window of the program for conducting MRI

studies in the absence of any contrast agents is shown in Fig. 2. The window of this program displays the dependence of the MR signal intensity on various parameters of the selected sequence of RF pulses for different brain substances. It also presents simulated MR images showing the signal intensity on the "gray" scale. When the user changes the value of the sequence parameter, the dependence of the NMR signal intensity on this parameter is dynamically changed and the corresponding MR image is modeled. This allows the user to select the optimal contrast of the MR image needed in a specific MRI study.

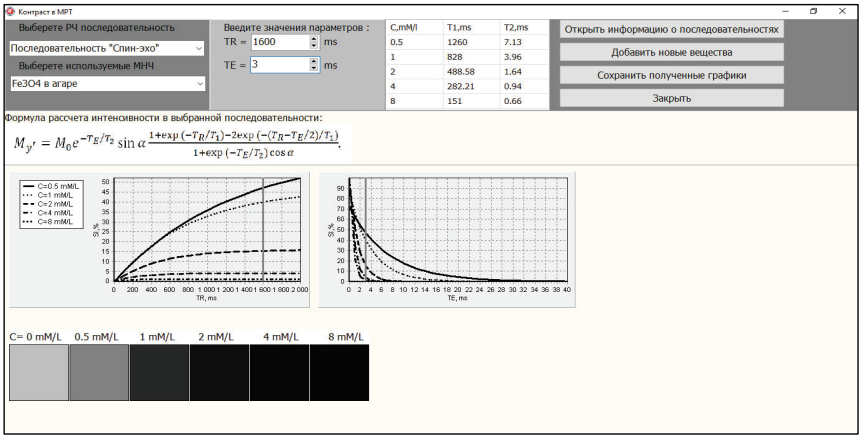

Figure 2. The working windows of the program

Results

Thus, the influence of parameters of pulse RF sequences often used in MRI (*spin echo*, *inversion-recovery, FLASH*) on the contrast of magnetic resonance images was studied. As a result, a program was developed for modeling magnetic resonance imaging and determining the optimal values of parameters of pulse RF sequences to achieve the best contrast of MR images. This program was tested in MRI studies using negative contrast agents based on magnetic iron oxide nanoparticles and positive contrast agents based on gadolinium. The effect of contrast agents on the NMR signal intensity at different concentrations of these agents is analyzed.

Using this program allows you to reduce the time of MRI studies, to evaluate the possibility of using different contrast agents for contrasting of MR images. The developed program for monitoring parameters of pulse RF sequences in MRI studies can also be used for training of students and medical staff.

References

1. Bogachev Y.V., Nikitina A.V., et al. NMR Relaxation Efficiency of Aqueous Solutions of Composite $MgZnFe_3{-}x{-}yO_4$ Nanoparticles // Applied Magnetic Resonance, 2017. V. 48. I. 7. P.715–722
2. Kuperman V. Magnetic resonance imaging physical principles and applications, University of Maryland College Park, Maryland, Academic Press, 2000. 197 p.
3. R. Thomas, In-Kyu Park, Yong Yeon Jeong. Magnetic Iron Oxide Nanoparticles for Multimodal Imaging and Therapy of Cancer. // Int. J. Mol. Sci. 2013, vol.14, pp.15910-15930.

Study of the structure of spiro-linked nitrocyclopropanecarboxylates by 1D and 2D NMR spectroscopy

V. V. Pelipko, R. I. Baichurin, S. V. Makarenko

Herzen State Pedagogical University of Russia, Department of Organic Chemistry, Center of collective use at the Faculty of Chemistry "Instrumental methods for the study of nitro compounds, coordination, biologically active substances and nanostructured substances" 48 Moyka River Embankment, Saint Petersburg 191186, Russia
E-mail: kohrgpu@yandex.ru
http://kohrgpu.ru, http://ckpo.herzen.spb.ru/?page=organic-chemistry

The interaction of alkyl 3-bromo-3-nitroacrylates with cyclic CH acids opens up the possibility of the synthesis of carbo- and heterocycles [1, 2]. We have obtained spiro-linked nitrocyclopropanecarboxylates **1, 2a, b** based on the reaction of methyl 3-bromo-3-nitroacrylate with cyclic CH acids – 2,2-dimethyl-1,3-dioxane-4,6-dione (Meldrum's acid) and 3-methyl-1-phenyl-1*H*-pyrazole-5(4*H*)-one [2].

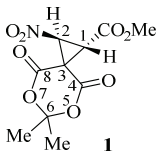

1

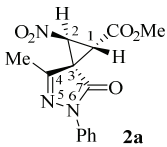

2a

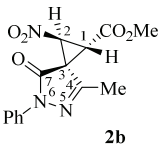

2b

The rigidly fixed structure of the spirocyclic molecules **1, 2a, b** makes them very attractive objects for studying by NMR spectroscopy, including using 2D experiments.

In the ^{13}C NMR spectra of compounds **1, 2a, b** the observed J-coupling constants of the H–C^1 (168.5-172.5 Hz) and H–C^2 (191.9-197.0 Hz) atoms (Fig. 1) are consistent with the literature data of the cyclopropane structures [3, 4] and testify in favor of the presence of a three-membered carbocyclic structure in the molecule.

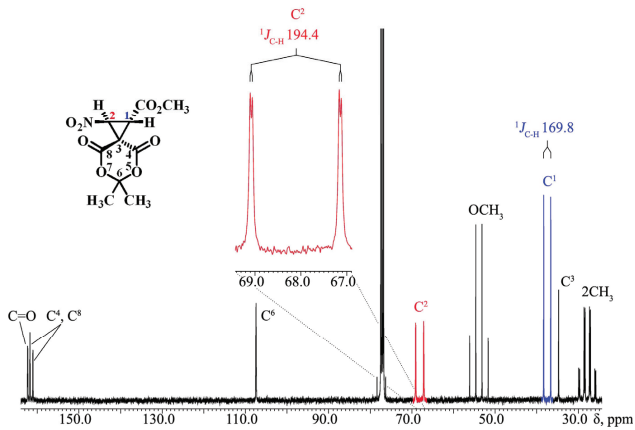

*Figure 1. ^{13}C NMR spectrum of compound **1** ($CDCl_3$)*

The study of the representatives of nitrocyclopropanecarboxylates **1, 2a** by the ^1H-^{15}N HMBC method ($CDCl_3$) showed that the signal of the nitrogen atom of the NO_2 group

corresponds to -15.2 and -12.1 ppm (Fig. 2, 3), respectively, which is consistent with the few published data for nitrocyclopropane structures [5]. Taking into account the closeness of the values of nitrogen chemical shift (NO_2) in nitroacrylates (δ_N -10.0 ÷ -11.18 ppm) [6], as well as in the nitrocyclopropanes **1, 2a** that we studied, it can be assumed that such a spectral pattern indicates effective electronic conductivity cyclopropane ring, indirectly indicating changes in the hybridization of formally sp3 hybrid carbon atoms.

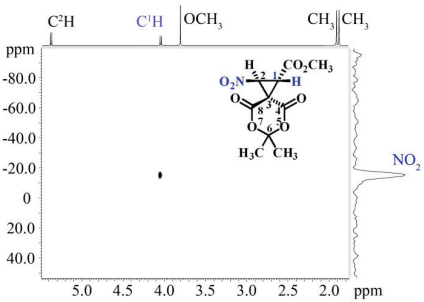

*Figure 2. ^1H–^{15}N HMBC NMR spectrum of compound **1** ($CDCl_3$)*

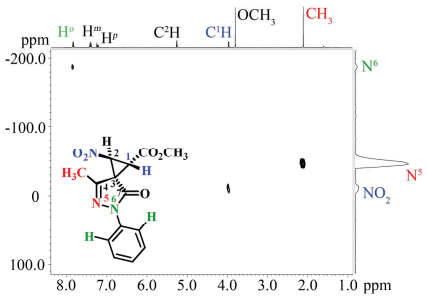

*Figure 3. ^1H–^{15}N HMBC NMR spectrum of compound **2a** ($CDCl_3$)*

In addition, the use of ^1H-^{15}N HMBC NMR spectroscopy using the example of compound **2a**, allowed not only to determine the chemical shifts of nitrogen atoms, but also to carry out their correct assignment.

Thus, the molecules of spiro-linked nitrocyclopropanecarboxylates turned out to be rather convenient objects for demonstrating the capabilities of 1D and 2D NMR spectroscopy methods for determining the structure of cyclic compounds.

The studies were carried out in the center of collective use at the Faculty of Chemistry of the Herzen State Pedagogical University of Russia on the Jeol ECX-400A spectrometer at 399.78 (^1H), 100.53 (^{13}C) and 40.52 (^{15}N) MHz with standard experimental settings. The residual signals of a non-deuterated solvent (for ^1H nuclei) or the signals of a deuterated solvent (for ^{13}C nuclei) were used as a standard. The chemical shifts of ^{15}N were determined with respect to CH_3NO_2.

References

1. A. I. Pekki, S. V. Makarenko, K. V. Altukhov, V. M. Berestovitskaya. – *Rus. J. Gen. Chem.*, 80, 1048-1049 (2010).
2. V. V. Pelipko, S. V. Makarenko – Sbornik trudov Vserossijskoj konferencii «Himiya nitrosoedinenij i rodstvennyh azot-kislorodnyh sistem» (AKS-2019). M. 23-25 oktyabrya 2019. S. 190-196.
3. A. J. Gordon, R. A. Ford. The Chemist's Companion. New York: Wiley, 1972.
4. E. Pretsch, P. Buehlmann, C. Affolter. Structure determination of organic compounds. Berlin: Springer-Verlag, 2000.
5. M. Achmatowicz, O. R. Thiel, G. Gorins et al. – *J. Org. Chem.* 73, 6793-6799 (2008).
6. V. V. Pelipko, S. V.Makarenko, R. I. Baichurin et al. – *Russ. J. Org. Chem.,* 53, 1799-1808 (2017).

The study of urinary stones by the method of electron paramagnetic resonance

Alina A. Pichugina, Larisa V. Tsyro

Institute of Natural and Technical Sciences, Surgut State University, Lenina avenue 1, Surgut, Russian Federation
E-mail: alina.com9@mail.ru
http://www.surgu.ru

Introduction

Urolithiasis, or urolithiasis, is a heterogeneous group of various pathological and metabolic cascades leading to the formation of stones present in the urinary tract [1].

Urinary or renal stones are solid crystals that are formed during the accumulation on the inner surface of the kidneys of an excess of uric acid, calcium, magnesium, ammonium salts, in the form of various phosphates, carbonates, oxalates [2, 3].

Basically, urinary stones are complex multiphase materials consisting of inorganic crystals surrounded by an organic matrix [2]. According to their composition, urinary stones are divided into the following types: oxalate, phosphate, urate and cystine [4, 5]. For example, oxalate-type urinary stones consist of calcium oxalate (CaC_2O_4), which can be present in the stone in three crystalline forms: calcium oxalate monohydrate - whewellite ($CaC_2O_4 \cdot H_2O$) – the most common form, calcium oxalate dihydrate - weddellite ($CaC_2O_4 \cdot 2H_2O$) – occurs 2 times less often and calcium oxalate trihydrate - caoxite ($CaC_2O_4 \cdot 3H_2O$), which is quite rare [6].

The difference in the pathological activity of whewellite and weddellite is associated with the adhesive nature of their crystalline faces [7, 8]. Thus, the formation of urinary stones formed by whealellite-type calcium oxalate is caused by hyperoxaluria, while the other crystalline form, weddellite, is caused by hypercalciuria [9].

Phosphate urinary stones include minerals such as hydroxyapatite ($Ca_5(PO_4)_3(OH)$), struvite ($MgNH_4PO_4 \cdot 6H_2O$), brushite ($Ca(HPO_4)_2 \cdot 2H_2O$) and vitlocite ($Ca_9Mg(HPO_4)(PO4)_6$).

The main components of urate urinary stones are uricite ($C_5H_4N_4O_3$) and uric acid dihydrate ($C_5H_4N_4O_3 \cdot 2H_2O$). Cystine urinary stones are formed by cystine ($C_6H_{12}N_2O_4S_2$) [4-6].

The formation of various forms of urinary stones is associated with various factors occurring in the human body [5]. There are many assumptions about the mechanisms of their formation [10–12]. However, this issue is still debatable. Therefore, in this work, we examined urinary stones by electron paramagnetic resonance, because This method allows you to evaluate the presence of certain radical particles present in urinary stones. And as you know, in the human body, most biological processes are radical in nature.

Results

The samples were studied by ESR on a JEOL JES-FA200 spectrometer. Spectrum conditions: t = 25 °C, microwave frequency ~ 9.4 GHz, modulation frequency 100 kHz, sensitivity $7 \cdot 10^9$ spin/0.1 mT, maximum magnetic field scan 500 mT, modulation width 1. The sample was placed in a quartz ampoule with a diameter of 5 mm.

According to the EPR results presented in Fig. 1, it can be seen that, despite the type of urinary stone, the presence of paramagnetic centers is observed in all samples, the total number of which is about 10^{17}–10^{18} spin/g.

In all the EPR spectra of the samples under study, a narrow line is observed in the region of the g factor ~ 2, which refers to organic matter. The main components that form organic matter in uroliths are proteins, glycoproteins and mucopolysaccharides. Also, in addition to the

narrow line in all spectra, a wide line is observed in the region of the g-factor of ~ 2.3, the interpretation of which is difficult due to the fact that, in addition to the main components, urinary stones contain various organic compounds that form the so-called matrix around the nucleation center of urinary stone. In samples of urinary stones b and c, a weak signal with a g factor of ~ 4.0 - 4.2 is observed. This signal can be assigned to paramagnetic centers Fe^{3+} or Cu^{2+}.

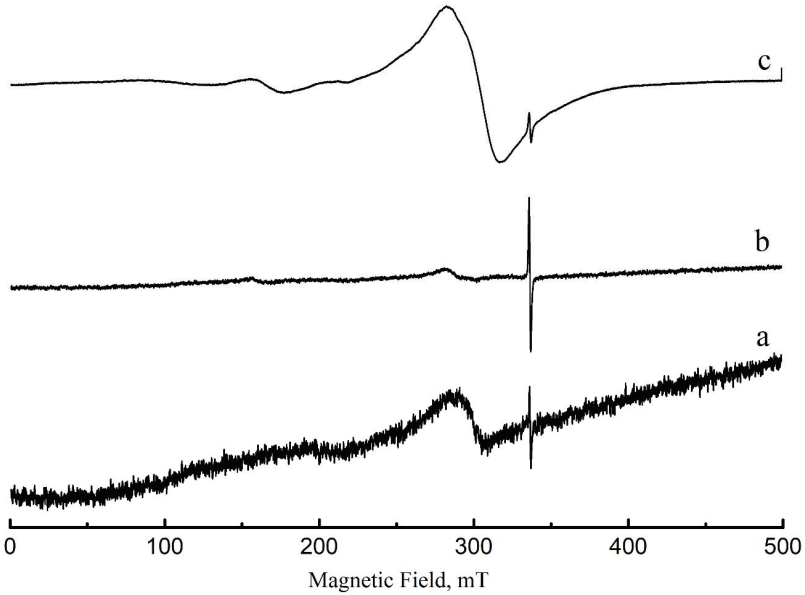

Figure 1. ESR-spectra of urinary stones: a – oxalate stone; b – phosphate stone;c – urine stone

Despite the fact that the set of lines in the EPR spectra of the studied samples of urinary stones is almost the same, they differ in the number of spin centers (Table 1). This suggests that with the formation of urinary stones in the body, various radical processes occur, leading to the formation of pathogenic neoplasms.

Table 1. Urinary stones paramagnetic resonance data

Sample	$C_{general}$, spin/g	Peak I		Peak II		Peak III	
		g	C_I, spin/g	g	C_{II}, spin/g	g	C_{III}, spin/g
a	$9 \cdot 10^{17}$			2,259	$4{,}73 \cdot 10^{15}$	2,005	$1{,}30 \cdot 10^{13}$
b	$9{,}23 \cdot 10^{17}$	4,250	$4{,}75 \cdot 10^{17}$	2,352	$3{,}38 \cdot 10^{15}$	2,005	$4{,}42 \cdot 10^{14}$
c	$2{,}45 \cdot 10^{18}$	4,068	$3{,}97 \cdot 10^{16}$	2,226	$1{,}46 \cdot 10^{16}$	2,004	$2{,}71 \cdot 10^{14}$

Phosphate stones, like oxalate, and urate can be single-core and multi-core. The latter indicates the presence of multiple initiating centers. Paramagnetic centers — the nuclei of associates – act as initiating centers. Such centers must either be removed from the body (for example, during metabolism), or localized at some spatial point so that its activity is "quenched" (for example, by "enclosing" the radical in an impenetrable "bag"). If the process of the appearance of foreign radicals becomes more frequent, then the mass of material of the "bag" can become very large, and negative macro processes will begin in the body. Such processes are associated not with the formation of molecular associates, but with the formation of stones.

Thus, the study showed that paramagnetic particles are contained in urinary stones of various origins. The total number of paramagnetic particles is $10^{17} – 10^{18}$ spin/g, which indicates the direct participation of such particles in the formation of urinary stones. Paramagnetic particles act as centers - nuclei of associates.

References

1. S. Tamosaityle, V. Hendrixson, A. Zelvys, R. Tyla, Z.A. Kucinsliene, F. Jankevicius, M. Pucctaive, V. Jablonskiene, V. Sablinskas. – *Journal of Biomedical Optics*, 18, 2, 0270011-1-0270011-7 (2013).
2. A.M. Ali, N.A.N. Raj, S. Kalainathan, P. Palanichamy. – *Materials Letters*, 62, 2351-2354 (2008).
3. E.V. Wilson, M.J. Bushiri, V.K. Vaidyan. – *Spectrochimica Acta Part A*, 77, 442-445 (2010).
4. M.A. Childs, L.A. Mynderse, L.J. Rangel, T.M. Wilson, J.E. Lingeman, A.E. Krambeck. – *Journal of Urology*, 189, 1347-1351 (2013).
5. I.A. Abboud. – *Environmental Geochemistry and Health*, 30, 445-463 (2008).
6. M. Microvic, A. Dosen, S. Eric, P. Vuily, B. Matovie, A. Rosie. – *Microchemical Journal*, 152, 1-6 (2020).
7. X. Sheng, M.D. Ward, J.A. Wesson. – *Journal of the American Society of Nephrology*, 16, 1904-1908 (2005).
8. F. Grases, A. Costa-Bauza, L. Garcia-Ferragut. – *Advances in Colloid and Interface Science*, 74, 169-194 (1998).
9. D. Bazin, C. Leray, F. Ticlens, C. Bonhomme, L. Bonhomme-Coury, F. Damay, D. Le Denmat, J. Sadoine, J. Rode, V. Frochot, E. Letavernier, J.-P. Haymann, M. Daudon. – *Comptes Reduc Chimie*, 19, 1492-1503 (2019).
10. S. Ghosh, S. Basu, S. Chakraborty, A.K. Mukherjee. – *Applied Cristallography*, 42, 629-635 (2009).
11. M. Khullar, S.K. Sharma, S.K. Singh, P. Bajwa, F.A. Sheikh, V. Relan, M. Sharma. – *Urological Research*, 32, 190-195 (2004).

Using composite excitation pulses for T2 relaxation measurements with the inverse integral transformation

Daria Poltorabatko, Vitalii Salnikov, Kuprian Beliychenko, Ivan Mershiev, Galina S. Kupriyanova

Immanuel Kant Baltic Federal University, Institute of Physics, Mathematics and Information Technology, 236016, Kaliningrad, Russia
E-mail: IMershiev@kantiana.ru

Nuclear magnetic resonance relaxometry is widely used for the analysis of multicomponent mixtures in chemical, petroleum and food industries [1]. T_2 relaxation time measurements are usually made using Carr-Purcell-Meiboom-Gill sequences, which is series of refocusing 180° radio frequency pulses following an exciting 90° radio frequency pulse. To correct the errors in the calibration of radio frequency pulses and to rid of the unwanted components of the residual magnetization, EXORCYCLE phase cycling are usually used. For several steps of phase cycling for the exciting and refocusing pulses, one can get rid of the decay signals of free induction and partially compensate the presence of a magnetic field gradient [3]. Moreover, the magnetic field gradient has a large effect on the relaxation rate, which makes it difficult to identify individual relaxation components for the complex samples.

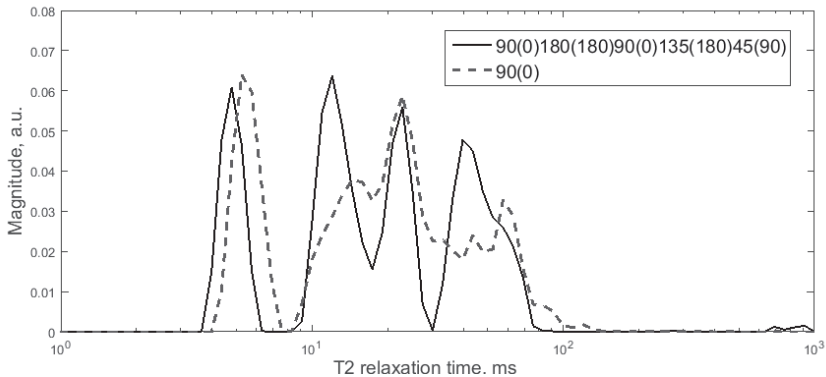

Figure 1. Comparison of relaxation times distrubutions

Comparison of measurement results using inverse integral conversion for a sample of soy lecithin. The experiments were performed using the CPMG method with a conventional 90° excitation pulse and a $90_0180_{180}90_0135_{180}45_{90}$ composite pulse [3]. Experimental result shows that compensation of magnetic field inhomogeneity with the composite pulse allows increasing the resolution of individual components of relaxation times distribution.

References

1. D. Capitani, A. P. Sobolev, V. Di Tullio, L. Mannina, and N. Proietti, “Portable NMR in food analysis”, *Chem. Biol. Technol. Agric.*, vol. 4, no. 1, pp. 1–14, 2017.
2. N. N. Jarenwattananon and L. S. Bouchard, “Breakdown of Carr-Purcell Meiboom-Gill spin echoes in inhomogeneous fields”, *J. Chem. Phys.*, vol. 149, no. 8, 2018.
3. M. H. Levitt, “Composite pulses”, *Prog. Nucl. Magn. Reson. Spectrosc.*, vol. 18, no. 2, pp. 61–122, 1986.

^{1}H and ^{13}C NMR investigation of SLAS in mixtures and SiO_2 dispersions

Maria V. Popova, Viktoria V. Vasinovich, Elizaveta A. Andronova

Department of Nuclear-Physics Research Methods,
198504, St. Petersburg, Uljanovskaja, d. 1, Russia
E-mail: m.v.popova@spbu.ru

Introduction

We use ^{1}H and ^{13}C spectroscopy for the investigation of mixed-surfactant systems and surfactant in SiO_2 aqueous dispersion. The aggregation and interfacial behavior of aqueous solution and binary mixtures of anionic (sodium lauroyl sarcosinate, SLAS) and cationic (dodecylammonium bromide, DTAB) surfactants were investigated. SLAS has unique physical and chemical properties, such as low toxicity, dermatology softness, hydrolysis resistance, high efficiency in hard water, and, most important, the fast biodegradability.

One of the most important attributes of sarcosinate amphiphiles is their good compatibility with other surfactants. It is well known that in the practical application of surfactants generally amphiphilic mixtures are used. This situation is caused by the lower cost of mixtures compared to the individual surfactants. The other reason is the fact that in many cases the mixtures have properties, which are practically more important than in case of the individual components. Thus, it is of great interest both for application and for basic research to predict physical and chemical properties of sarcosinates in mixtures with co-surfactant and SiO_2 particles for information about the micelle morphology.

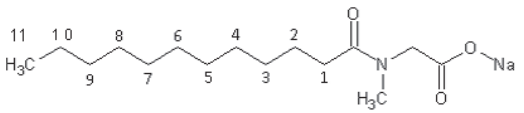

Figure 1(a). The molecular structure of SLAS

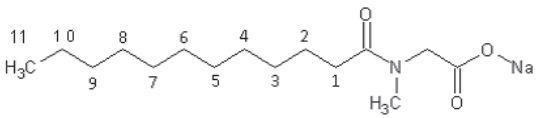

Figure 1(b). The molecular structure of DTAB

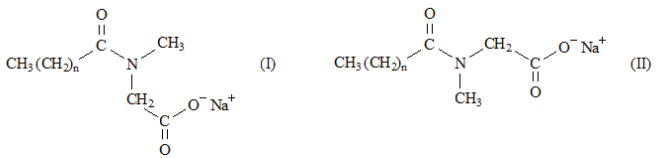

Figure 2. Two conformers of SLS: (I) cis- and (II) trans-configurations

Materials and methods

SLAS and DTAB (see Fig. 1) were acquired from Sigma-Aldrich and used without additional purification. We studied the NMR parameters of SLAS in mixtures with DTAB at different molar fractions of both surfactants from 0.5 CMC to 3 CMC and in silica dispersions at different concentration of SLAS.

All ^{1}H and ^{13}C NMR experiments were performed using a Bruker AVANCE 500 (Center for Magnetic Resonance of St. Petersburg State University), with Larmor frequencies 500 MHz for the proton spins, and of 125 MHz for the^{13}C nuclear spins, respectively.

Results and discussion

In surfactant molecules with the amide bond the energy barrier for the rotation about this bond was sufficiently high (because of the partially double character of the amide bond), and therefore two different relatively stable conformers (cis- and trans-conformers) exist in such molecules (see Fig. 2). Since the isomerization rate is slow in the NMR time-scale and the N-alkyl groups of the SLAS cis- and trans-molecules are chemically (and magnetically) inequivalent, a splitting of the resonance lines for the N-alkyl groups in the ^{1}H and ^{13}C NMR spectra has been registered [1-3].

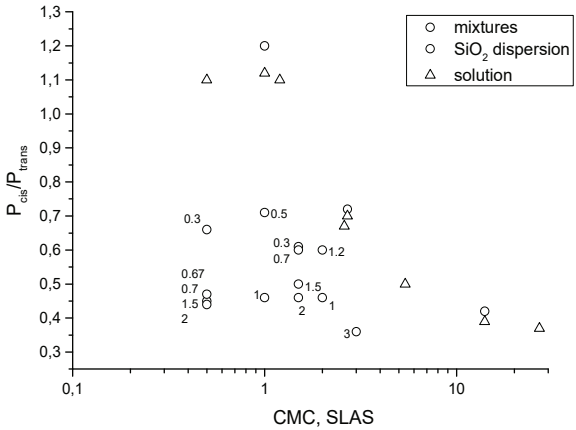

Figure 3. The relative fractions of the SLAS molecules in the cis-form (pcis) and trans-form (ptrans), determined via proton spectra of the N-CH_2, N-CH_3 and 1CH_2 groups at different concentrations; T = 273 K

When the ^{1}H spectral lines are well-resolved for both conformers, the relative concentrations (fractions) of the cis- and trans-forms can be estimated from the integral intensities of lines. The relative fractions of the cis-form (p_{cis}) and the trans-form (p_{trans}) are plotted in Fig. 3 as functions of the SLAS concentration and different DTAB concentration (both concentration are in CMC value), herewith $p_{cis} + p_{trans} = 1$.

The transition from one conformation to another upon reaching CMC is due to the more favorable of the trans-conformers, because this conformation is more preferable in the micellar state. The fraction of the cis-conformers in mixtures is noticeably lower than in solutions and dispersion at similar SLAS concentrations in the whole concentration region (see Fig. 3). It can be argued that micelles in mixtures are already formed at concentration lower CMC of SLAS.

Moreover, an increase of the concentration of co-surfactant, DTAB, from 0.3 CMC to 0.7 CMC causes the decrease of cis-conformers in 1.5 times. When the SLAS concentration is equal to CMC, an increase of the DTAB concentration from 0.5 CMC to 1 CMC also causes the decrease of cis-conformers fraction in 1.5 times.

The spectral separation of the ^{13}C resonance lines $\delta^{internal}$ for the trans- and cis-conformers, which is called as "internal chemical shift" was almost independent of surfactant concentration as in the case of solutions. But the distance between the COO and CON-lines for trans-conformers was noticeably smaller than in solutions. These peaks are almost merged into one single line in two cases: 1) when the concentration of both surfactants is less than CMC and 2) when the concentration of SLAS equals to 2 CMC and DTAB concentration equals to 1 KKM.

^{13}C spectral line of the $11CH_3$-group is characterized by a single line, i. e. the cis- and trans-conformations have no direct reflections in this spectral fragment in the monomer state. However, these spectra consist of more lines in some concentration region (remember that ^{13}C spectra are registered using the proton decoupling and, therefore, there is no spectrum splitting due to interactions with protons). This effect observed when: 1) concentrations are higher than CMC: of 1.5, 2, and 3 CMC of SLAS and 2) when the concentrations of both surfactants are lower than CMC values. The signal of $11CH_3$-groups was consist of three lines in this case. One line refers to CH_3-group of the DTAB molecule and two lines refer to the $11CH_3$-group of the SLAS molecule. In solutions with c < CMC and c = 1.5 CMC, the line from $11CH_3$ was single peak. A similar effect was observed by us in SLAS solutions [1, 2].

References

1. Popova, M. V., Chernyshev, Y. S., Michel, D. & Chizhik, V. I.,^{1}H and ^{13}C NMR investigation of conformational and aggregation behavior of sodium N-lauroyl sarcosinate, Journal of Molecular Liquids. 280 (2019) 40-48. https://doi.org/10.1016/j.molliq.2019.02.029.
2. M.V. Popova, D. Michel, Behavior of sodium Lauroyl Sarcosinate in solution and binary mixtures by means NMR, Appl. Magn. Reson. 45 (2014) 353-364. https://doi.org/ 0.1007/s00723-014-0531-9.
3. E. Oshimura, Y. Yamashita, K. Sakamoto, Conformational Behavior of N-Acylamino Acid Oil and N-Acylamino Acid Surfactant in Aqueous Solution, J. Oleo Sci. 56, 115 (2007) 115-121. https://doi.org/10.5650/jos.56.115.

Correlations of internal magnetic field due to grains in microfluids

Mikhail G. Rudavets

Institute of Problems of Chemical Physics, RAS, Chernogolovka, Moscow region, 142432, Russia
E-mail: rudavets@gmail.com

1. Introduction

Effect of confinement from the micrometer size [1-4] down to a distance scale of the nanometer size [5, 6] received large attention in the NMR over the past two decades. The ultimate goal in these studies is the pore characterization and the development of more robust NMR imagination techniques. For this purpose, new approaches that distinguish the spatial heterogeneity of the pore interior have been attempted. Specifically, to control the heterogeneity in the proton-carrying microfluidic pores with the injected paramagnetic grains, ^{1}H-spin echo techniques was developed [1-4] that measure directly the correlations of IMF. In these studies, the inhomogeneity of IMF is generated due to the susceptibility contrast between the paramagnetic grains and the surrounding fluid. Without the external magnetic field, the paramagnetic grains are not magnetic. When the magnetic field is applied, the induced magnetization of the grains is aligned with the direction of the external magnetic field. IMF generated by the magnetic grains is random to the extent of the spatial randomness of the grains themselves. The correlations of IMF, which is probed by ^{1}H-NMR [1-3], are driven by the grains' correlation, assuming that magnetic interactions between the grains exceed the thermal energy [7].

Magnetization of the grains in the microfluids has attracted considerable interest since they have been employed in a variety of the microfluidic devises operating due to the influence of the magnetophoretic and magnetohydrodynamic forces. Examples of the application include the manipulation with the grains' flow by the lab-on-a-chip systems, drag delivery, magnetic separators and stirring, studying the chain-like pattern formation, etc. Along with the aggregation of the (para) diamagnetic grains having the size of few tens microns, the aggregation arises in the dispersions of the nanoscale ferromagnetic particles. In ferrofluids, however, the effect of the thermal fluctuations is significant, destroying the self-organization.

Spins of the protons respond to the field of the grains in the microfluid and are used for studying of the latter [1-3]. Due to the chain-like structure of the grains, the protons that are in the immediate neighborhood of the chain belong to the quasi-one dimensional structure or the channel. Their IMF correlators show non-zero initial slope. This is contrasted with vanishing initial slope of IMF correlator in the bulk. The reason for the difference in the IMF correlators lies in the difference of the grains' correlators. They have a finite slope when the grains are in the channel, and the slope vanishes when the grains belong to the bulk fluid. In the present study, we employ the simplest correlator of the grains, i.e. OZ approximation, what is supposed to be reasonable under the clusterization [8]. The purpose of the paper is to consider implications of OZ approximation for the characterization the geometry of the pores.

For the typical NMR conditions [1-3], the subsystem of the grains' magnetic moments is independent of the protons' subsystem. This decoupling of the magnetic subsystems allows us to analyze the NMR response of the protons in the magnetic field generated by the grains disregarding the interactions between the protons themselves. In the static external magnetic field B_0, the (para) diamagnetic grains become magnetized. The dipolar force on the grain $\#2$ due to the grain $\#1$, whose magnetic moments $\vec{\mu}_i = m\hat{z}$, $i = 1, 2$ are aligned along the z-direction of the external magnetic field [9],

$$\vec{F}_{dip} = \frac{3\mu_0}{4\pi}\frac{m^2}{r^4}\left(\hat{r}\cdot\left(1-3\cos^2\theta\right)-\hat{\theta}\cdot\sin 2\theta\right), \tag{1.1}$$

where μ_0 is the permeability of free space (SI units), r stands for the spacing between the centers of the spherical grains, θ denotes the angle between the $\hat{z}$-axis and the radius vector from the position of $\vec{\mu}_1$ to $\vec{\mu}_2$, $\hat{r}$ and $\hat{\theta}$ refer to the orthonormal unit vectors in the direction of increasing r and θ. By Eq. (1.1), the north magnetic pole of a grain is attracted to the south pole of the nearest neighbour grain providing the chain-like clusterization. The dipolar energy between the magnetic grains at contact and at $\theta = 0$ reads,

$$U_{dip} = -\frac{\pi R^3 \chi_{eff}^2 B_0^2}{9\mu_0}, \tag{1.2}$$

where R stand for the radius of the spherical grains, χ_{eff} refer to the volume magnetic susceptibility difference between the grain and the fluid. Putting in Eq. (1.2) the typical experimental parameters [1], i.e. $B_0 = 2$ T, $R = 25$ μm, $\chi_{eff} = -10^{-5}$ (for diamagnet silicon dioxide in a nonmagnetic fluid) gives the dipolar energy $U_{dip} = -10$ eV. We also estimate the induced magnetic moment of a grain, $m = (4\pi/3)R^3\chi_{eff}B_0/\mu_0 = -10^{11}\mu_B$, with μ_B being the Bohr magneton. The magnetic moment of a grain generates the magnetic field at its proximity, $B_z^{(i)} = \mu_0/(2\pi)m/R^3 = -\frac{2}{3}\chi_{eff}B_0 = -1.3\times10^{-5}$ T. Compare this field with the internal field within a slender ellipsoid of the close packed grains, $B_z^{(i)} = \mu_0/(4\pi)(2\pi/3)M_z = -0.3\times10^{-5}$ T where $M_z = m/(4\pi R^3/3)$ is the magnetic moment density that is supposed to be homogeneous within the ellipsoid, with $(2\pi/3)$ being the so called shape factor [5].

2. IMF correlators

When the grains undergo the movement in the fluid, the velocity relaxation processes is supposed to contribute to the grains' density and the IMF correlators. The expression for the IMF correlator for the motionless grains was derived in [1]. The result can be conveniently represented in the form that accounts for the grains' movement, namely

$$c_{\vec{k}}^{BB}(t) = b_{z\vec{k}}^2 S_{\vec{k}}^{\rho\rho}(t) \tag{2.1}$$

where the r.-h.-side is the Fourier transform of the IMF correlation function, $c_{\vec{k}}^{BB}(t) = \int d^3r\, e^{i\vec{k}\vec{r}}\left\langle B_z^{(i)}(\vec{0},0)B_z^{(i)}(\vec{r},t)\right\rangle$, since the convolution property of the IMF correlator of [1] permits its reduction by the Fourier transform, $b_{z\vec{k}}$ stands for the Fourier transform of the z-component of the magnetic field due to the magnetic moment of a grain, the z-component of the internal magnetic field instantaneously depends on the grains distribution, $B_{z\vec{k}}^{(i)}(t) = b_{z\vec{k}}\rho_{\vec{k}}(t)$, $S_{\vec{k}}^{\rho\rho}(t) = \left\langle \rho_{\vec{k}}^*(0)\rho_{\vec{k}}(t)\right\rangle$ is the dynamical structure function of the grains. The duration of the NMR spin echo sequence in the data [1] is about milliseconds, what is compatible to the velocity relaxation time of the grains in the water. The simplest model that accounts for the relationship between the correlators of IMF and the particle correlators is provided by the model that studies the light scattering by the density fluctuations in the fluids. By making use the similarity between the formalisms of the light scattering and the present

system, we restrict the analysis with the situation when the microfluid is the motionless background, and the grains are affected by the magnetic field gradients and the hydrodynamic viscous drag force. The set of the kinetic equations for the correlators of the IMF and the grains gives the structure function

$$S_{\vec{k}}^{\rho\rho}(t) = e^{i\omega_D t} S_{\vec{k}}^{\rho\rho}, \tag{2.2}$$

where $\omega_D = \vec{\upsilon}\vec{k}$ is the Doppler frequency and $S_{\vec{k}}^{\rho\rho}$ is the static equilibrium structure function. Eq. (2.2) gives the spin echo attenuation $E = (1 - \cos\omega_D t) S_{\vec{k}}^{\rho\rho}$. Obviously the grains' movement reduces the IMF correlator. If the grains are immobile or the NMR time scale is short compared to the inverse Doppler frequency, i.e. for grains with $\vec{\upsilon} \perp \vec{k}$, then $E = S_{\vec{k}}^{\rho\rho}$. Using OZ approximation for $S_{\vec{k}}^{\rho\rho}$ and carrying out the integrals required in [1], we give the IMF correlator in the channel $c^{BB}(z) = (8\pi/3)^2 \xi_0^{-2} \xi \exp(-|z|/\xi)$, which resembles OZ correlator of the grains. In the bulk, the initial slope of the IMF correlator is calculated to be zero, $\partial_z c^{BB}(z)|_{z=0} = 0$.

Acknowledgements

The work is supported in part by the program # 008920190002.

References

1. H. Cho and Y.-Q. Song, Phys. Rev. Lett. **100,** 025501 (2008).
2. B. Audoly, P.N. Sen, S. Ryu, and Y. Q. Song, J. Magn. Reson. **164**, 154 (2003).
3. Y.-Q. Song, S. Ryu, and P. N. Sen, Nature (London) **406**,178 (2000).
4. R.L. Kleinberg, in: P.-Z. Wong (Ed.), Methods in the Physics of Porous Media, Academic Press, London, 1999, p. 337.
5. J. Baugh, A. Kleinhammes, D. Han, Q. Wang, Y. Wu, Science 294 (2001) 1505.
6. W.S. Warren, Science 294 (2001) 1475.
7. H. M. Jaeger, S. R. Nagel, and R. P. Behringer, Rev. Mod. Phys. 68, 1259 (1996).
8. J.M. Ziman, Models of Disorder, CUP, Cambridge, UK, 1979, p.131
9. E. Furlani, Permanent Magnet and Electromechanical Devices**,** Academic Press, San Diego, 2001, p.140.

Model of ions in concentrated solutions of ionic surfactants for the molecular dynamics method

A. M. Ryzhkov, A. V. Komolkin

Faculty of physics, Saint Petersburg State University, 7-9 Universitetskaya embankment, Saint Petersburg 199034, Russia
E-mail: st054892@student.spbu.ru

Nowadays Molecular dynamics method is the main way to research solutions in liquid phase. Various force fields are used for modeling different molecules and their surroundings to achieve better results. In this work some parameters of ions in ionic surfactant solution were analyzed in order to determine the most accurate ones. In the previous work [1] charges on ion's atoms were calculated by using quantum chemistry methods and simulation with different parameters of the Coulomb potential was carried out. The Lennard-Jones potential, meanwhile, remained unchanged. By this time systems with bigger size and various concentration were studied to obtain better statistics.

The following parameters were used in the simulation: 1000 ions of Heptanoic acid, 1000 sodium ions and 28212 water molecules. We used SPC/E [2] model of water and took sodium ion model from Dang's paper [3]. Interaction parameters of other atoms were taken from widely used force field file OPLS-AA. Concentration of salt was 1.567 M, which is approximately equal to 4 CMC. Ensemble of simulation was NpT, thermostat and barostat were Nose-Hoover with following parameters 700 fs and 2000 fs respectively. Temperature was 298 K, density of solution was 1.048 ±0.001. Another system was: 330 ions of Heptanoic acid, 330 sodium ions and 31446 water molecules. Simulation conditions were the same. Concentration was 0.514 M, which is approximately equal to 1.5 CMC.

Time of the simulation was a few nanoseconds. During the simulation aggregates formed (figure 1). They are connected through hydrophilic parts and sodium ions. As a result we analyzed radial distribution functions (RDF) for sodium ions, water molecules and salt ions (figure 2), RDF between the center of the micell and COO groups, sodium ions and water molecules and numbers of aggregation.

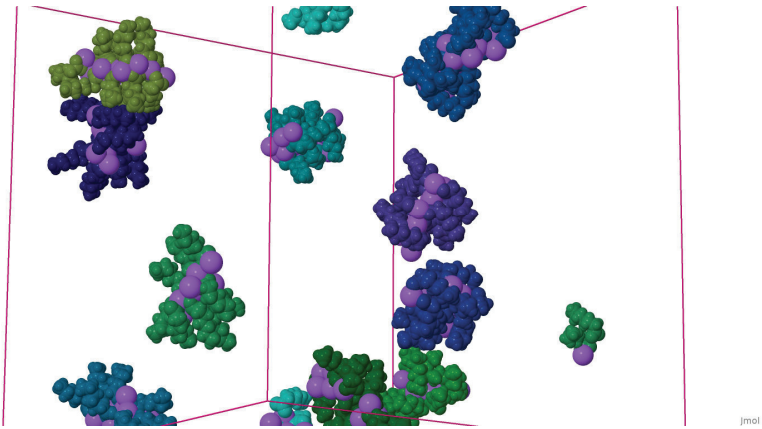

Figure 1. Snapshot of the system during simulation. Purple atoms are sodium ions

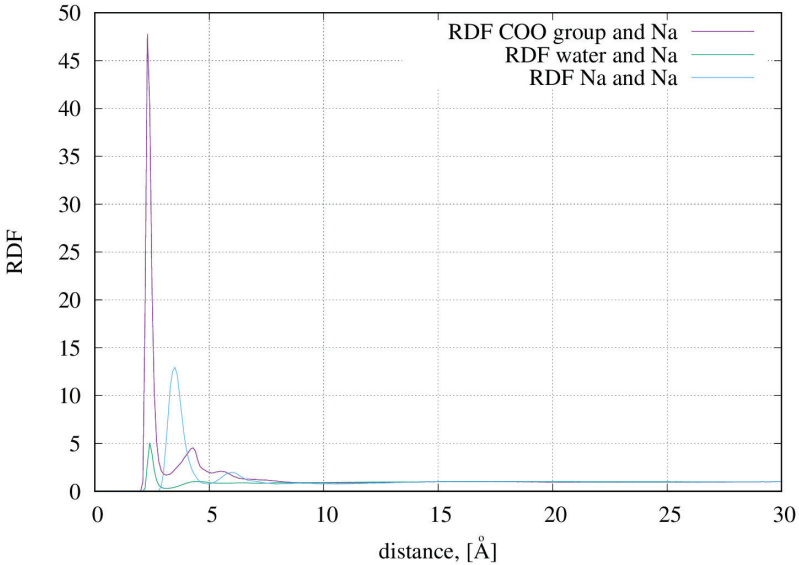

Figure 2. Radial distribution functions

Acknowledgements

Research was carried out using computational resources provided by Resource Center "Computer Center of SPbU" (http://cc.spbu.ru).

References

1. Ryzhkov A.M., Antonova N.A., Komolkin A.V. Analyzing the parameters of atom-atom interactions for Molecular dynamics simulations of micelle formation // Magnetic resonance and its applications: Proceedings 16th International School-Conference, Saint Petersburg, March 31-April 5, 2019. - Saint Petersburg: publishing house VVM Ltd., 2019. - pages 237-240
2. H. J. C. Berendsen, J. R. Grigera, T. P. Straatsma. The missing term in effective pair potentials. – *J. Phys. Chem.*, 1987, 91 (24), pp 6269–6271
3. L. X. Dang. Mechanism and thermodynamics of ion selectivity in aqueous solutions of 18-crown-6 ether: a molecular dynamics study. – *J. Am. Chem. Soc.*, 117, 6954-6960 (1995)

Molecular dynamics modeling of ionic liquid [BMIM][SCN]

A. A. Selivanov, A. V. Ievlev

Department of Nuclear Physics Research Methods, Saint Petersburg State University, 199034, 7/9 Universitetskaya nab., Saint Petersburg, Russia
E-mail: st068986@student.spbu.ru

Introduction

Recently, ionic liquids (IL) have been increasingly used as components of polymer electrolytes for new current sources. They have several advantages, such as low flammability, low vapor pressure, wide space of thermal, chemical and electrochemical stability, which make it possible to produce more environmentally friendly current sources the based on IL.

One of the newest methods of studying IL is Molecular Dynamics Modelling (MDM). This method belongs to a class of computer experiments. It allows observing the behavior of molecules of a substance in liquid phases, their displacements, relative position, conformations, etc. MDM also allows to determine the physical-chemical properties of the investigated substances, which can afterwards be compared with a real experiment.

The goal of this work is to study IL [BMIM][SCN] with the MDM. This IL was selected, because of an experimental work was provided to study its physical-chemical properties [1]. The simulation is carried out in GROMACS 2019.4 software package.

Experimental section

To solve this problem models of $BMIM^+$ and SCN^- ions should be built with Jmol software package.

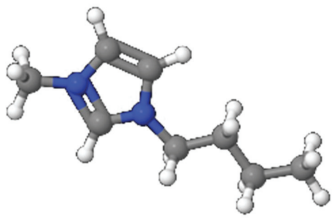

Figure 1. Cation $[BMIM]^+$

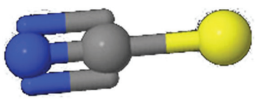

Figure 2. Anion $[SCN]^-$

Then, using the Automated Topology Builder (ATB) service, individual topology files (.itp) were obtained.

For the MDM calculation of our system, the following parameters were selected:

- 300 molecules of ionic liquid
- Simulation time - 150 ns
- Simulation step - 1 fs
- Simulation Method: Leap-frog
- NVT ensemble
- Thermostat: V-rescale
- Temperature - 298 K, Initial pressure - 1 atm.
- Force Field - Gromos-54A7

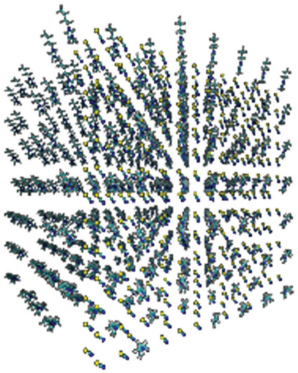

Figure 3. Initial system configuration

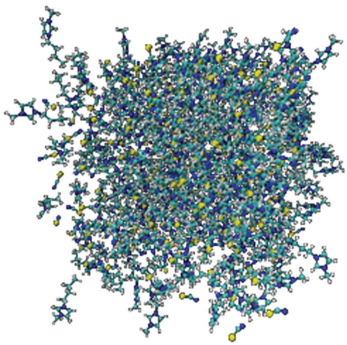

Figure 4. System configuration after 300 ns simulation

Further, the first 50 nanoseconds were calculated in the NpT ensemble with speed generation according to Maxwell distribution. The Berendesen's thermostat and barostat also has been used. The purpose of this calculation is to get our system "mixed up" and to achieve a certain state of equilibrium from which we could make a "productive" calculation.

After the initial simulation, calculation continued in the NpT ensemble without speed generation. 150 ns were calculated so that the system came to a state of equilibrium.

After that, the NVT ensemble was set up and next 150 ns were calculated. NVT ensemble makes it possible to determine dynamic characteristics more accurate, e.g. diffusion coefficient. As a result, the following system was obtained (Fig.4).

Density of a box is one of parameters which can prove that the simulation has been provided correctly. It can be obtained by command *gmx density*. The graph may be plotted based on this data (Fig.5). This figure shows that average density of the system is $\rho_{av} = 1079 \pm 9 \frac{kg}{m^3}$. This value is quite close to the experimentally obtained one, which, according to [4], is 1069.7 $\frac{kg}{m^3}$ under normal conditions.

To discuss the mobility of molecules, the one should determine Mean Square Displacement (MSD) for each ion. The command *gmx msd* can provide it (See Fig.6).

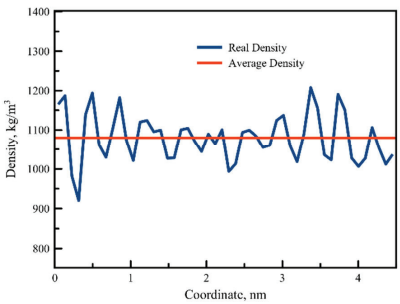

Figure 5. Dependence of the system density on the coordinate

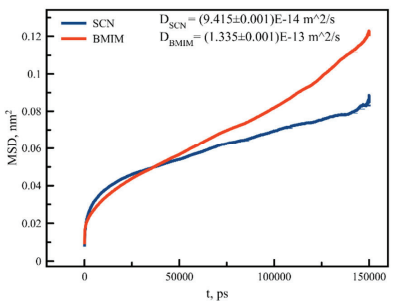

Figure 6. Dependence of the MSD on the time t

Using the Einstein's equality $\lim_{t\to\infty}\langle\|\boldsymbol{r}_i(t)-\boldsymbol{r}_i(0)\|^2\rangle = 6D_i t$ diffusion coefficients for $BMIM^+$ cation and SCN^- anion can be obtained:

$$D_{BMIM} = (1{,}335 \pm 0{,}001) * 10^{-13}\ \frac{m^2}{s}$$

$$D_{SCN} = (9{,}415 \pm 0{,}001) * 10^{-14}\ \frac{m^2}{s}$$

As one can see, anion's mobility is lower than cation's mobility. This suggests, that there is a mistake in the simulation. It will be corrected in the subsequent simulation.

Comparing obtained coefficients with similar ones, which were obtained by NMR-diffometry experiment, one can see that these coefficients differ by 150-250 times:

$$D_{BMIM} = 2{,}032 * 10^{-11}\ \frac{m^2}{s}$$

$$D_{SCN} = 2{,}426 * 10^{-11}\frac{m^2}{s}$$

Acknowledgment

Scientific research were performed at the «Computing Centre» of Research park of St.Petersburg State University.

References:

1. O. Cabeza et al, Synthesis, Microstructure and Volumetry of Novel Metal Thiocyanate Ionic Liquids with BMIM Cation. J. Mol. Liq. 283 (2019) 638-651.
2. Комолкин А.В., Шеляпина М.Г. Метод молекулярной динамики: Учеб.-метод. пособие — Спб.: Изд-во «Соло», 2007. - 72с., ил.
3. Неелов И.М. «Введение в молекулярное моделирование биополимеров», - учебное пособие, Санкт-Петербург 2014.
4. Density and Viscosity of Binary Mixtures of Thiocyanate Ionic Liquids + Water as a Function of Temperature, U.Domanska and M.Krolikowska, J Solution Chem. 2012 Sep; 41(8) 1422-1445

Precise proton-proton distance estimation on base eNOE-data in Ir(III) complex at slow (in NMR time scale) exchange condition

Julia R. Shakirova, Sergey P. Tunik, Stanislav I. Selivanov

Institute of Chemistry, Saint-Petersburg State University, University prospect 26, 198504, Saint-Petersburg, Russia
E-mails: degget2006@gmail.com; nmr.group.spbu@gmaill.com

Introduction

Iridium complexes of the $[Ir(N^C)_2(N^N)]^+$ type are well-known luminescent compounds [1] which found numerous applications as emitting components of *o*rganic *l*ight *e*mitting *d*iode (OLED) devices [2], sensors [3], probes in bioimaging [4] and nonlinear optical materials [5]. These compounds display extremely versatile photophysical behavior determined by delicate balance between energy of frontier orbitals taking part in photoexcitation processes and their relative contribution into emissive excited states. Among preferable physical methods for structural and conformational analysis of these complexes NMR spectroscopy, X-ray data and DFT calculations are most informative sources of their spatial structures and comparison of results obtained on base these experimental (in liquid and solid states) and calculating methods usually applied to prove conformational stiffness or intramolecular mobility of the studied compounds.

In this report *n*uclear *O*verhauser *e*ffect (NOE) was used to get the set of extremely correct interproton distances r_{ij} in iridium-(III) complex (I) dissolved in acetone (Fig. 1) and to compare these distances with corresponded X-ray data in solid state which were published earlier [6]. This approach allows to detect and analyze the main sources and causes of discrepancies between NMR and X-ray examinations including internal flexibility of molecular fragments.

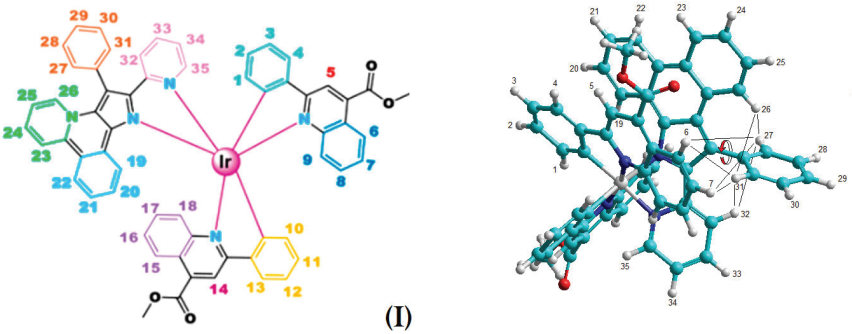

Figure 1. Iridium-(III) complex (I) and its spatial structure (on right). Through-space interactions with protons of mobile phenyl ring are shown by lines

Owing to the development of experimental techniques [7] and methods for the correct processing of NOE data [8-11], it has become possible even for small molecules in extreme narrowing limit ($\omega_o\tau_c << 1$) to measure accurately interproton distances r_{ij} with errors which do not exceed 5% of the measured value. Such precise measurements based on NOE analysis were incorporated into a separate group of experiments and since 2015 have received the name "*e*xact NOE" and the abbreviation "eNOE" [12].

Experiments and results

NOESY spectra of iridium-(III) complex (**I**) were recorded at 20° C on spectrometer DPX-300 (300 MHz) with different mixing times 0.1, 0.2, 0.3, 0.4, 0.6, 0.8, 1.0, 1.2, 1.4 s and to check experimental accuracy NOESY spectrum at $\tau_m = 0.6$ was recorded twice. Number of scans for one t_1-increment was 128 and number of such increments for two-dimension spectrum was 256. To decrease input of relaxation factor on accuracy at Fast NOESY condition [9] we saved the sum of mixing time τ_m and relaxation delay D1 for any value of τ_m: $D1 + \tau_m = 3.2$ s [8]. After phase correction in F2- and F1-directions of all (these) phase-sensitive NOESY spectra about 90 cross-peaks S_{ij} and S_{ji} were identified and integrated together with diagonal ones S_{ii} and S_{jj} for each value τ_m by using "MestReC" program and PANIC (***p***eak ***a***mplitude ***n***ormalization for ***i***mproved ***c***ross-relaxation) approach [12]. It allowed us to calculate corresponded related values S_{ij}/S_{ii}, S_{ji}/S_{jj} and determine 89 cross-relaxation rates σ_{ij} and σ_{ji}, respectively (Fig. 2a). These initial data were used for calculation of distances r_{ij} by well-known calibrate method in approximation of isotropic diffusion motion: $r_{ij} = r^{ref.}(\sigma^{ref.}/\sigma_{ij})^{-6}$. NMR distances r_{ij} ($r^{ref.} = r_{18\text{-}17} = 2.45$ Å) in comparison with X-ray data are presented in Fig. 2b.

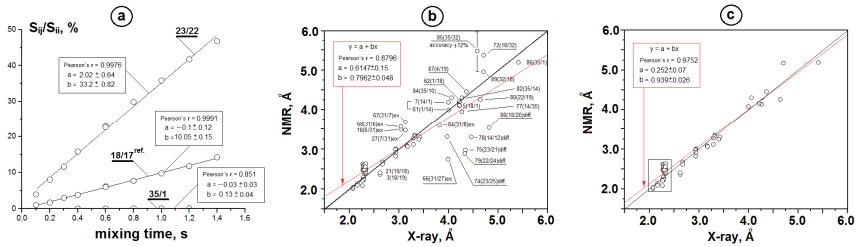

Figure 2. ***a)*** *– Dependence of relative integral intensities of cross-peaks for reference distance $r_{18\text{-}17}$ and two most short and long distances in Iridium-(III) complex* ***(I)*** *on mixing time τ_m.* ***b)*** *– Correlation between NMR and X-ray distances for full set and* ***c)*** *– for smoothed set of NMR data*

The sources of discrepancies between NMR and X-ray distance values include spin-diffusion effects ($r_{14\text{-}12}$, $r_{23\text{-}21}$, $r_{22\text{-}24}$, $r_{23\text{-}25}$ and $r_{18\text{-}20}$), influence of slow (in NMR time scale) rotation of phenyl ring at five-member circle. In this case all NOE`s of *ortho*- (H^{27}, H^{31}) and *meta*-protons (H^{28}, H^{30}) with nearest protons in other rings may be averaged by this internal motion. That is why, all data associated with spin diffusion and exchange processes were removed from the initial correlation (Fig. 2b), as well as data with low accuracy in determining the cross-relaxation rates σ_{ij} in the case of an error of more than 34% of the measured value. For example, in case of distance $r_{35\text{-}32}$ the error in determining $\sigma_{35\text{-}32}$ is 100%, which led to a related error in the distance of 12%. As a result of such data smoothing, a significant improvement in the correlation parameters is observed (Fig. 2c).

The other reason of discrepancies is different values of C-H distances which are usually applied to solid state (0.98 Å) and liquid state (~1.05 Å) descriptions of aromatic systems: $r_{C\text{-}H}^{(X\text{-}ray)} = 0.98$ Å and $r_{C\text{-}H}^{(MM2)} = 1.05$ Å. It leads to an increase in the interproton distance between vicinal protons in the liquid state by approximately 0.15 angstroms compared with X-ray diffraction data (Fig. 3a) and simultaneously to degrease of distance between nearest *ortho*-protons located in adjustment rigid rings of ligands. This is clearly seen in the NMR/X-ray correlation in the range 2.0 - 2.5 angstroms which is indicated by a rectangle in Fig. 2c and is presented in detail in Fig. 3a. Correlation between NOE and X-ray data in Fig. 3b shows the result of an increase of 0.15 angstroms of all distances between vicinal protons which gives additional improvement in correlation parameters. Slow (in NMR time scale) rotation of phenyl

ring leads to underestimation of averaged NOE-values for distance $<r_{6\text{-}31}>$ and $<r_{7\text{-}31}>$ because protons 6 and 7 are situated closely (~3 Å) from the nearest proton 31 only half time.

During of the second half time they are very far (~7 Å) from the same proton due to exchange 31 ⇄ 27 (Fig. 3c, red points). These exchange effects are not observed in the case of dipole-dipole interactions of protons 26 and 32 with protons 27 and 31, since the distances between them remain almost unchanged as a result of the exchange 27 ⇄ 31 (Fig. 3c, black points).

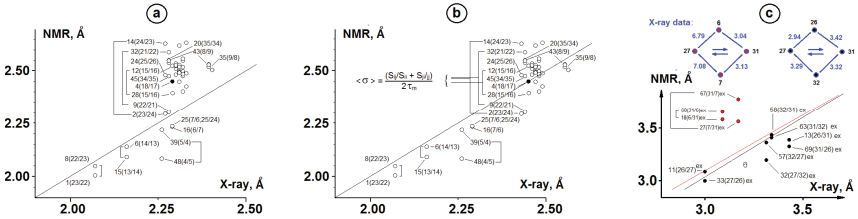

Figure 3. ***a)*** *– Short distance region of NMR/X-ray correlation for Iridium-(III) complex (**I**) in case of solid state C-H distance values and* ***b)*** *– in case of liquid state C-H distance values.* ***c)*** *– Effects of the distance average by slow (in NMR time scale) rotation of phenyl ring*

Moreover, to improve the correlation between NMR and X-ray distances the average values of the cross relaxation rates were applied using relationship: $<\sigma_{ij}> = (S_{ij}/S_{ii} + S_{ji}/S_{jj})/2\tau_m$, In addition, the spin-lattice relaxation times of protons were measured and they turned out to be from 0.5 to 1.5 s. This made it possible to solve the problem of integrating overlapping diagonal peaks by using their average value. Finally, the effects of the diffusion anisotropy on the accuracy of distance estimation on base eNOE are also discussed in this work.

Conclusion

Application of the best fit control method for distance estimation in iridium-(III) complex (**I**) allowed us to improve successfully accuracy of NOE results in liquid in comparison with X-ray data. This approach was useful for perception and understanding of different type discrepancies between NMR and roentgen distance values. It simultaneously allowed to get the independent evidence of slow in NMR time scale mobility of phenyl ring.

Acknowledgments

Spectral NMR investigations were performed in the Resource Centers "Magnetic Resonance Research Centre" and X-ray diffraction data were received due to resource center "X-Ray Structural Analysis" of the Saint-Petersburg State University. This research has been supported by grant of the Russian Science Foundation (grant 19-13-00132).

References

1. H. Xu, R. Chen, Q. Sun, W. Lai, Q. Su et al, Chem. Soc. Rev., 2014, 43, 3259−3302.
2. P. Tao, W.-L. Li, J. Zhang, S. Guo, Q. Zhao, H. Wang, B. Wei, S.-J. Liu, X.-H. Zhou, Q. Yu, B.-S. Xu, W. Huang, Adv. Funct. Mater., 2016, 26, 881−894.
3. Q. Zhao, F. Li, C. Huang,. Chem. Soc. Rev., 2010, 39, 3007−3030.
4. Y. Liu, P. Zhang, X. Fang, G. Wu, S. Chen et al, Dalton Trans., 2017, 46, 4777−4785.
5. C. Dragonetti, S. Righetto, D. Roberto, R. Ugo et al, Chem. Commun. 2007, 4116−4118.
6. J.R. Shakirova, O.A. Tomashenko, E.E. Galenko, A.F. Khlebnikov, P. Hirva, G.L. Starova, Sh.-H. Su, P.-T. Chou, S.P. Tunik, Inorg. Chem., 2018, 57, 6853−6864.

7. D. Neuhaus, M.P. Williamson, “The Nuclear Overhauser Effect in Structural and Conformational Analysis” (2nd ed.), Wiley-VCH, New York, 2000. 619 P.
8. N.H. Andersen, H.L. Eaton, X. Lai, Magn. Reson. Chem., 1989, 27(6), 515–528.
9. Th. Geppert, M. Köck, M. Reggelin et al, J. Magn. Reson., Ser. B, 1995, 107(1), 91–93.
10. S.B. Landy, B.D.N. Rao, J. Magn. Reson., 1989, 83(1), 29–43.
11. S.I. Selivanov, A.G. Shavva, Russ. J. Bioorg. Chem., 2002, 28(3), 194–208.
12. B. Vögeli, S. Olsson, R. Riek, P. Güntert . J. Struct. Biojlogy 1915, 191(3) 306–317.

Obtaining MR images of nuclei other than a hydrogen nucleus by an indirect method using double nuclear magnetic resonance

S. A. Shubin, V. V. Frolov, K. V. Tyutyukin

St. Petersburg State University, 1, Ulyanovskaya str., St. Petersburg, 198504, Russian Federation
E-mail: shubinsa1@gmail.com

Introduction

The technique described in this work is based on the spin echo double resonance (DRSE) technique [1, 2] and can be used to obtain MR images from nuclei other than the hydrogen nucleus, connected by spin-spin interaction with the latter and being part of biologically significant molecules involved in important biological processes inside living organisms. The development of methods in this direction is of paramount importance, in view of the participation of such substances in energy metabolism in the body. What can allow obtaining MR images weighted by energy parameters - mapping with the determination of areas of living tissues with increased or decreased energy consumption.

Experimental results

In this work, as an experimental substance, a phosphorus-containing compound trimethyl phosphate was used. To obtain NMR images of phosphorus-containing components, we used the pulse sequence shown in Fig. 1.

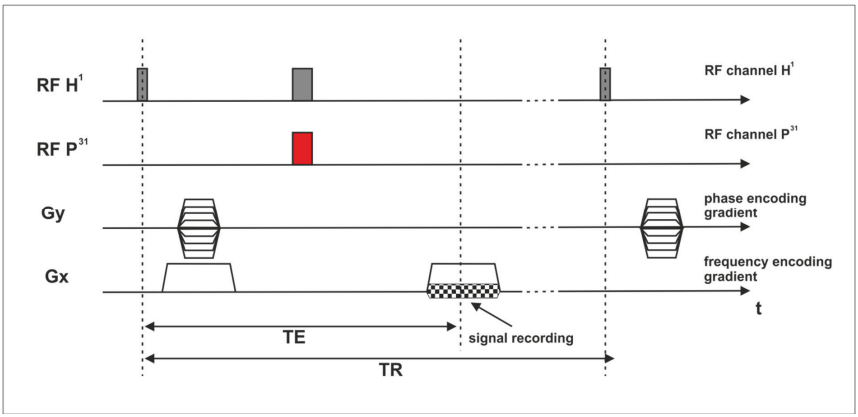

Figure 1. Full pulse sequence

By acting on the protons with a pulse sequence of 90^0-τ-180^0-τ-echo and turning on another 180^0 pulse at the frequency ω_0^H at the same time as 180^0 pulses at the frequency ω_0^P, we can obtain an MR image from ^{1}H not coupled by spin-spin interaction with ^{31}P [3]. Thus, the spatial distribution of ^{31}P is displayed indirectly as attenuation of the proton signal intensity. However, if we subtract the MR image mentioned above from the MR image obtained from all protons in the sample, then as a result we get the MR image of ^{1}H nuclei bonded to ^{31}P nuclei. In other words, we will get a true image of the distribution of ^{31}P nuclei, but many times more intense than obtained directly from phosphorus nuclei.

Image subtraction was performed using the OpenCV Python module [4]. To do this, it was necessary to carry out pixel-by-pixel analysis with the introduction of threshold values of allowable pixel intensities, to discard background pixels and noise. In Fig. 2. the results of subtraction, MR images obtained from all protons in the sample, and MR images from ^{1}H not associated with ^{31}P spin-spin interaction are presented. The maximum contrast in phosphorus is achieved at $\tau = 22.5$ms.

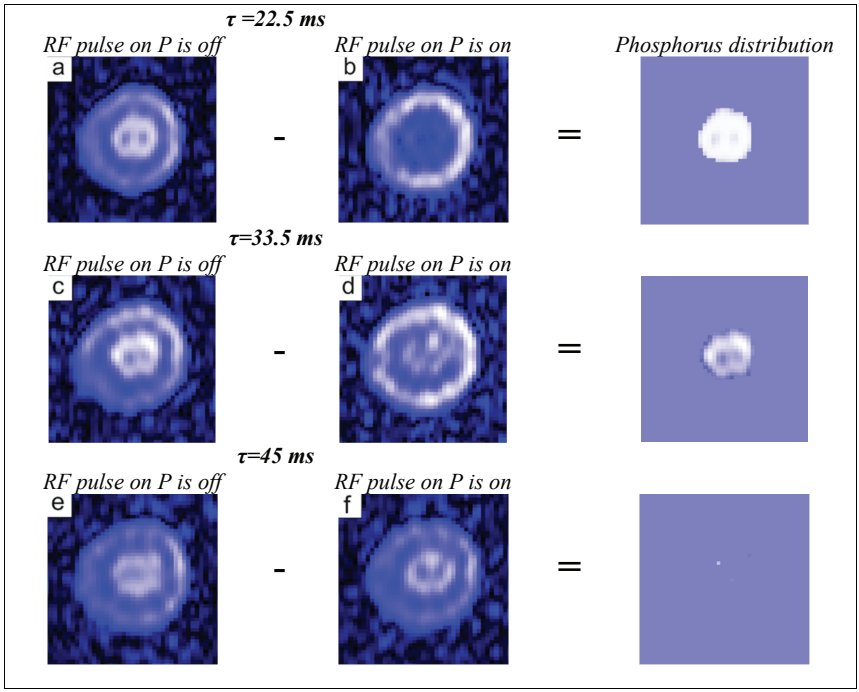

Figure 2. Substrate

Summary

Using this technique and taking the NMR signal only from protons, we obtain the distribution of phosphorus-containing components in the sample. Considering the fact that the ^{1}H gyromagnetic ratio is 2.5 times greater than the ^{31}P gyromagnetic ratio, the sensitivity to ^{31}P is almost 16 times less, all other things being equal, because in the general case, the intensity of NMR signals of nuclei with a gyromagnetic ratio γ is proportional to γ^3. It becomes very advisable to obtain MR images of ^{1}H spins associated with ^{31}P by means of a scalar spin-spin interaction, indirectly, obtaining the distribution of ^{31}P in the sample. This is especially important in the case of a weak field, where the sensitivity problem is very acute. On the other hand, it is in a weak field that internuclear scalar interactions manifest themselves most strongly, since the splitting caused by them does not depend on the field level.

References

1. A. G. Webb, S.C.R. Williams, and L. D. Hall. Generation of Coupled Spin-Only Images Using Multiple-Echo Acquisition. Journal of Magnetic Resonance 84 p.159-165 (1989).

2. Malcolm H. Levitt, Spin Dynamics Basic of Nuclear Magnetic Resonance 2nd ed.
3. Shubin, S., Frolov, V., Tyutyukin K. Display of Phosphorus-Containing Components on Low-Frequency Magnetic Resonance Images Using Double Magnetic Resonance. *Appl Magn Reson* (2019).
4. Practice OpenCV 2.4-image processing and analysis (2013).

Interaction of DNA with azobenzene-containing surfactant

Irina A. Silanteva, Veronika V. Mamontova, Andrei V. Komolkin

Faculty of Physics, Saint Petersburg University, 199034, 7-9 Universitetskaya embankment, Saint Petersburg, Russia
E-mail: i.silanteva@spbu.ru

Introduction

Substances containing an azobenzene group are interesting because they can transform from trans- to a cis-isomer under the influence of UV radiation. The transition to a new conformation is accompanied by a change of their properties. This phenomenon can be used for creating various photosensitive nano-objects [1] and, in particular, for the reversible light-controlled DNA compaction. The DNA compaction is needed to create gene vectors.

In this work, the cationic surfactant C_4-Azo-OC_6TMACl is considered, the Cl^- anion was added for modeling instead of Br^- used in experimental works. Cation C_4-Azo-OC_6TMA^+ (hereinafter named Azo, Fig. 1) contains an azobenzene fragment in its hydrophobic tail, which is connected by a short alkyl chain to a charged head group. The charge of the head group is localized on hydrogen atoms. The cis-isomer is Γ-shaped and it is more hydrophilic compared to trans-isomer.

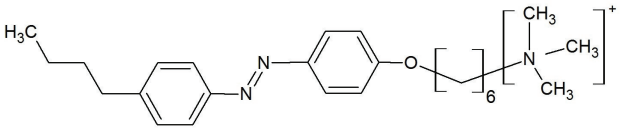

Figure 1. Chemical structure of C_4-Azo-OC_6TMA^+ cation

Experimental studies show that the interaction of C_4-Azo-OC_6TMAB with DNA [2-6] is very sensitive to the ionic strength of the solution (NaCl concentration). It is known that the trans-isomer compacts DNA better than the cis-isomer. The properties of the cis-isomer is still not well studied unlike the properties of the trans-isomer, which has been studied in sufficient detail. The followed questions are to be solved. How does the structure of surfactants' aggregates depend on ionic strength? What is the difference in the structure of the formed aggregates between the trans- and the cis-isomers of Azo? What is the difference between the trans- and the cis-isomers of Azo at interaction with DNA?

In this work the interaction of Azo cations with a fragment of double-stranded DNA with the length of 18 base pairs d(GCCCAGCATTTCACCCAG) and with a total charge –34*e* was considered.

Simulation was carried out by molecular dynamics in AKMD program [7] using AMBER force field and SPC/E model for water.

Results

Initially the systems consisting of 18 cis- Azo cations with 18 Cl^- counterions in aqueous solution and in saline were examined. The sizes of the boxes were 90Å. In both systems, Azo cations are assembled into aggregates; due to the shape of the cations, they are obtained spherically symmetric, rather than ordered, as in the case of the trans-isomer. Distribution function over the distance to the center of mass shows that the charged heads of Azo are located on the micelle periphery and the opposite ends are located in the center, see Fig. 2. The presence of the salt in the solution promotes the adhesion of Azo cations, larger micelles are formed in saline.

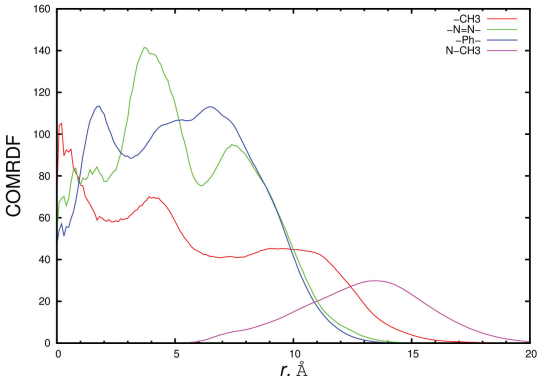

Figure 2. Distribution function over the distance to the center of mass for atoms of cis-Azo cation in aggregate in a saltless solution. Red is H of -CH_3, green is N of -N=N-, blue is C of benzene, crimson is H of -$N(CH_3)_3$

As a next step a system of 17 trans-isomers of Azo, a fragment of dsDNA, 17 Na^+ ions in aqueous solution is introduced. After 32 ns, an aggregate of 11 Azo cations attached to DNA is formed in the system, see Fig. 3a. The orientation of Azo cations in an aggregate is close to parallel or antiparallel. Starting from this state, gradually changing the angle between the bonds, in 1.1 nanoseconds, Azo was transferred from the trans- to the cis-isomer. Azo cations in the aggregate have lost their orientation, the aggregate continues to be attached to DNA, Fig. 3b. The addition of NaCl salt in physiological concentration to the system with the already cis-isomer Azo configuration also did not lead to detaching of an aggregate. Finally only in a system with a double physiological salt concentration (0.298 M) did the aggregate separate from DNA into solution.

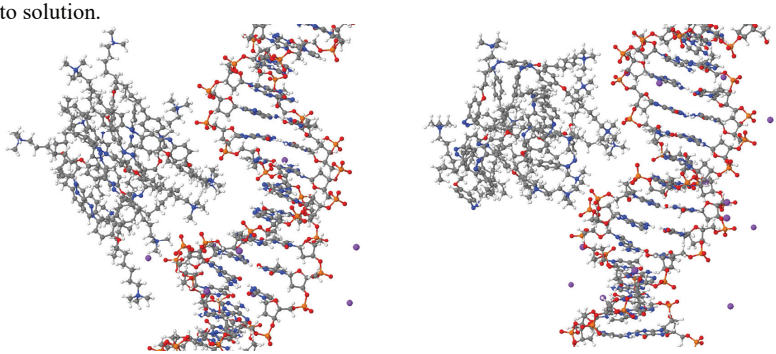

a *b*

Figure 3. Aggregate of Azo in trans- (a) and in cis- (b) configurations on DNA in a saltless solution

Acknowledgements

This research was carried out using computational resources provided by the Resource Center "Computer Center of SPbU" (http://www.cc.spbu.ru/en), ID: 42365282.

References

1. S. Santer. Remote control of soft nano-objects by light using azobenzene containing surfactants. *J. Phys. D:* Appl. *Phys.*, 51(1), 013002 (2018)
2. N. Kasyanenko, L. Lysyakova, R. Ramazanov, A. Nesterenko, I. Yaroshevich, E. Titov, G. Alexeev, A. Lezov, I. Unksov Conformational and phase transitions in DNA – photosensitive surfactant solutions: Experiment and modeling. *Biopolymers,* 103(2), 109-122 (2015).
3. Y. Zakrevskyy, A. Kopyshev, N. Lomadze, E. Morozova, L. Lysyakova, N. Kasyanenko, S. Santer. DNA compaction by azobenzene-containing surfactant. *Physical Review E - Statistical, Nonlinear, and Soft Matter Physics*, *84*(2), 021909_1-9 (2011).
4. N. Kasyanenko, I. Unksov, V. Bakulev, S. Santer DNA Interaction with Head-to-Tail Associates of Cationic Surfactants Prevents Formation of Compact Particles. *Molecules*, 23, 1576 (2018).
5. Y. Zakrevskyy, E. Titov, N. Lomadze, and S. Santer. Phase diagrams of DNA–photosensitive surfactant complexes: Effect of ionic strength and surfactant structure. *J. Chem. Phys.*, 141, 164904 (2014).
6. Y. Zakrevskyy, J. Roxlau, G. Brezesinski, N. Lomadze, S. Santer Photosensitive surfactants: Micellization and interaction with DNA. *J. Chem. Phys.,* 140, 044906 (2014).
7. A. V. Komolkin and A. Laaksonen and A. Maliniak. Molecular dynamics simulation of a nematic liquid crystal. *J. Chem. Phys.*, 101, 4103-4116 (1994).

Possible spatial spin modulation in europium orthoferrites

Anastasia Sklyarova[1], Vadim I. Popkov[2], Ivan V. Pleshakov[2], Vladimir V. Matveev[3]

[1]Faculty of Mathematics and Physics, Charles University, 18000 Prague 8, Czech Republic
[2]Ioffe Institute, 26 Polytekhnicheskaya Str., 194021 St. Petersburg, Russian Federation
[3]St. Petersburg State University, 7/9 Universitetskaya nab., 199034 St. Petersburg, Russian Federation
E-mail: asklyaro@gmail.com

In this project we study one of the co-called rare-earth elements (REE) ferrites: europium orthoferrite. Although $EuFeO_3$ is known already quite a long time and this bulk material itself has been well studied, science the beginning of nanomaterials era the interest to this substance renews due to the potential application of its nanocrystals [1, 2]. From literature data it is known that properties of ferrites (for example $YFeO_3$) may depend on the preparation route which was used for the material obtaining [3]. Here we study the europium orthoferrite polycrystalline samples with different crystalline size, which have been obtained using a combustion method. We focus on the local properties study using ^{57}Fe NMR method. Obtained at 4.2 K NMR spectrum of sample with a particle size of several microns shows a complex structure and can be explained by several hypothesis, one of them is a possible spatial distribution of iron spins in our sample.

Acknowledgements

This research is partially supported by OP RDE project No. CZ.02.2.69/0.0/0.0/16_027/0008495, International Mobility of Researchers at Charles University.

References

1. X. Niu, H. Li, and G. Liu, J. Mol. Cat. A 2005, 232, 89.
2. Y. Dwivedi and S. C. Zilio, J. Nanosci. Nanotechnol. 2014, 14, 1.
3. M. Shang, Ch. Zhang, T. Zhang, L. Yuan, L. Ge, H. Yuan, and Sh. Feng, Appl. Phys. Let. 2013, 102, 062903.
4. X. Niu, H. Li, and G. Liu, J. Mol. Cat. A 2005, 232, 89.

1H NMR study of soybean oils

Mark Smirnov, Ivan Mershiev, Alexsander Musaenko, Galina Kupriyanova

Instutute of Physics-Mathematical Sciences, Immanuel Kant Baltic Federal University, Kaliningrad, 236041 Russian Federation
E-mail:galkupr@yandex.ru
http://kantiana.ru

Introduction

In recent years, much attention has been paid to the study of vegetable oils, which is associated with an increase in the growth of cases of falsification of high-quality oils. Various methods are used to study the quality of vegetable oils, determine their authenticity and detect possible fraud, such as chromatographic in combination with mass spectroscopic (MS), ultraviolet (UV) and magnetic resonance (NMR) methods [1,2]. For the analysis of oils, typical target compounds are fatty acids, triacylglycerol, sterols, volatiles, phenolic compounds, phospholipids and trace elements [2]. Metabolic profiling requires the identification and quantification of a number of isolated metabolites belonging to different classes of compounds. This method is usually based on a spectrum that can be considered a "fingerprint" of the product. Methods of infrared spectroscopy (FTIR) and NMR can be applied in this case. Important results have been achieved in the study of the characteristics of olive oils [1-5].

Techniques based on high resolution 1H NMR are used as a powerful tool for quickly quantifying the composition of fatty acids in vegetable oils without the need for any sample processing. However, high resolution NMR is an expensive method that requires significant costs to maintain the stable operation of the superconducting magnet, as well as the costs of using deuterated solvents.

Along with high-resolution NMR methods, methods of relaxation spectroscopy in a low magnetic field and magnetic resonance imaging are being developed to determine the quality of food products and their composition [4]. The use of Halbach stationary magnets with a magnetic field of up to 1 Tesla contributed to the creation of relatively cheap compact NMR relaxometers [6]. 1H NMR relaxationometry methods were used to study various varieties of technical oils, polymer products from the point of view of their degradation [7]. The main advantage of this method is the low cost of research and portability of the equipment. From the point of view of solving the problem of identifying counterfeit products among high-quality oils, it is important to find identification features for various varieties of vegetable oils and their mixtures that would form the basis for determining their quality and degree of falsification.

The aim of this work was to study the possibility of using 1H NMR of the relaxation method to establish the dependence of relaxation parameters on the degree of processing of products from soybean, soybean oil. This paper presents the results of an experimental study by NMR in a weak magnetic field of samples of extraction and hydrated soybean oil. The results of measurements of the longitudinal and transverse relaxation times of soybean oils are compared with the data obtained for olive, linseed oils, etc. in order to study the possibility of distinguishing them.

Samples

Three samples of hydrated soybean oil and one sample of extraction soybean oil, differing in the content of phosphorus and sterol (Table 1) produced by the " Soybean Community" (Kaliningrad), were investigated. Three samples of olive oil (Sizma Zeytinyagi Natural) produced in Turkey and two samples (Extra virgin olive oil, Olive oil Iberia) of the highest category of olive oil produced in Spain, flaxseed oil, and bone oil (produced in Turkey) were investigated to compare their relaxation characteristics with the relaxation characteristics of soybean oils.

Research Methods

1H NMR relaxation experiments on measuring the spin-lattice times T 1 and spin spin relaxation T2 of vegetable oils were carried out on an NMR-NQR spectrometer Tecmag Apollo using the NT NMR Version 3 program. The magnetic field of the permanent magnet in the gap is B = 330 mT. The permanent magnet of the relaxometer consists of two permanent magnets having a size 60x80x100 mm, connected by a U-shaped magnetic circuit, with a gap of 25 mm. The inhomogeneity of the magnetic field at the location of the axis coil with the sample is 0.1 mT / cm. The size of the working coil of the sensor: D = 5.5 mm, L = 12 mm. The radio frequency circuit was tuned at a frequency of 13.648 MHz.. . The Carr-Purcell-Meiboom-Gill (CPMG) sequence was used for the transverse relaxation time T_2 measurements. The longitudinal relaxation times were measured by the inversion-recovery method. The durations of 90 and 180 pulses were determined for each sample during preliminary experiments. The duration of the 90-pulse is 8-10 μs, and 180 is 18- 20 μs. To process the experimental data, we used the modified RILT script [7, 8], executed in the MatLab environment. The regularized Laplace Inverse Transformation (RILT) algorithm is based on the fminsearch function of the MatLab package, which finds the minimum scalar function of several variables, starting with some initial estimate. The distribution function of relaxation times f (T_i) is the inverse integral transformation of the experimental data array y (t) . The function f (T_i) is calculated by the method of regularized least squares. To obtain smooth and regular output, the algorithm provides a choice of regularization parameter. The regularizer is represented as: $REG = \alpha^2 \Sigma (ri - Rijgj)^2$, where α is the regularization parameter, gj is the relaxation time distribution vector, ri is the second derivative of gj, Rij is the matrix that determines the shape of the regularizer .

Measurement results

Studies have shown that the distribution functions of the longitudinal and transverse relaxation times f (T1) and f(T2) of the oil samples are multicomponent, differing both in the relative intensities of the peaks and the width of the distribution lines. Peak values of transverse T2 and longitudinal relaxation times T1, as well as data on the phosphorus and sterol content in the studied soybean oil samples, which were provided by the soybean oil manufacturer, are presented in Table 1. From Table 1 it can be seen that relaxation times depend both on the degree and method of processing soybean oils, and on the content of phosphorus and stearin. However, we did not find a correlation between phosphorus content and relaxation times. It can be seen that hydrated sample No. 2 has longer transverse relaxation times T_{21} and T_{22} and narrower distribution lines of relaxation times than extraction oil. However, in hydrated samples with a reduced phosphorus content, we observed a tendency to decrease the relaxation time T_{21}. The results of relaxation measurements of some types of olive oils are given in Table 1. The comparative diagram of T_{21} and T_{22} relaxation times is presented in Fig 1.

Table 1. Relaxation characteristics of soybean oils

№ soybean oil	phosphorus content (mg/kg)	stearin	T_{11}, ms	T_{12}, ms	T_{21}, ms	T_{22}, ms
1 extraction	596	1,52	1259	138	182	60,2
2 hydrated	223	0,57	1259 724	158	195	64,6
3 hydrated	153	0,39	724	138	182	69,2
4 hydrated	6,6	0,02	955	138	182	64,6

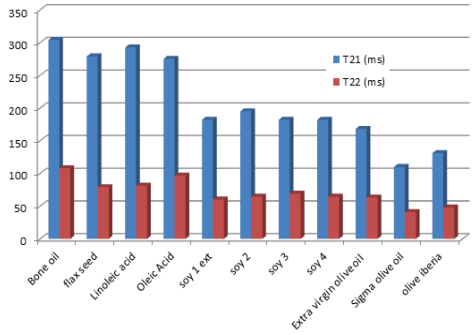

№ масло соевое	T_{21},ms	T_{22}, ms
Extra virgin olive oil	63	168
Sigma Zeytinyagi Nanural olive oil	41	110
flax seed	79	279
Bone oil	108	304
Olive oil Iberia	47,86	131,8

Figure 1. The comparative diagram of relaxation times T2 some types of olive oil produced in Spain, flaxseed oil, and bone oil

Conclusion

The paper presents the results of an experimental study of the relaxation times of 4 soybean oil varieties of varying degrees of processing, manufactured at the Soya Commonwealth enterprise. Despite the difference in relaxation characteristics of the studied samples, the correlation dependence of T2 and T1 on the content of phosphorus and stearin is not observed. However, it can be seen that data on the distribution of relaxation times can be used to distinguish soybean oil from other varieties studied, such as flax seed oil, bone oil, olive oil.

References

1. Manninaa L.and Sobolev A. P. Special Issue Review Magn. Reson. Chem. 2011, 49, S3–S11
2. Hidalgo F.J., Zamora, R. Trends Food Sci. Technol. 14 (2003) 499
3. Simoneau C., McCarthy M.J., J.B. German, Food Res. Int. 26 (1993) 387
4. Pauli G. F., Gödecke T., Jaki B. U., and Lankin D. C. Quantitative 1H NMR: Development and Potential of an Analytical Method – an Update. J. Nat. Prod. 2012 April 27; 75(4): 834–851. doi:10.1021/np200993k
5. Lamanna R., Imparato G., Tano P., Braca A., D'Ercole M. and Ghianni G. Territorial origin of olive oil: representing georeferenced maps of olive oils by NMR profiling. Magnetic Resonance in Chemistry, 2017, 55, 639-647
6. Blümich B., Haber-Pohlmeier S., & Zia W. Compact NMR. Berlin.Boston, Walter de Gruyter GmbH, 2014. 276 p
7. Sinyavsky N.Ya., Mershiev I.G., Kupriyanova G.S. New approaches to identification and quality assessment of oils. Marine intelligent technology. Electronic network (ISSN 2588-0233) and print (ISSN No. 2073-7173) publications. VI International Baltic Marine Forum. 4 (42) T. 3 2018
8. Marino I.-G. http://www.mathworks.com/matlabcentral/fileexchange/6523-rilt/content/rilt.m

Spectral characteristics of metal complexes of tetrapeptide with metal ions in solutions determined by NMR spectroscopy

Artyom S. Tarasov, Ilfat Z. Rakhmatullin, Dmitry S. Blokhin, Vladimir V. Klochkov

Institute of Physics, Kazan Federal University, Kazan, Kremlevskaya Str., 18, Russian Federation
E-mail: tarasov_as2010@mail.ru

Introduction

Alzheimer's disease (also senile dementia of the Alzheimer's type) is an incurable neurodegenerative disease characterized by the accumulation of β-amyloid plaques and neurofibrillary tangles in the brain tissue. Plaques are composed of fibrils formed as a result of aggregation of small peptides with a length of 39-43 amino acid residues called amyloid Aβ peptides [1-3]. These peptides are the product of enzymatic cleavage of a larger precursor protein - APP (amyloid precursor protein). This transmembrane protein plays an important role in neuron growth, its survival and recovery from damage. Oligomers of cytotoxic protegrin peptides are capable of causing the death of certain cells by the formation of transmembrane pores [4-6]. These antimicrobial peptides have a wide spectrum of action and can be used as new drugs.

Metal ions such as Zn^{2+}, Co^{2+}, Cu^{2+}, Mn^{2+} and Gd^{3+} are possible pathogenic agents in Alzheimer's disease due to the accumulation of these metals in amyloid deposits. A possible mechanism for the aggregation of the Aβ peptide caused by these ions was proposed by the formation of a metal-peptide monomer complex, which causes strong conformational changes, which facilitates the interaction of various peptides of the molecule. It is also assumed that antimicrobial protegrins peptides exhibit high activity as a result of interaction with transition metal ions. To study the effect of metal ions on peptides, we will consider the following oligopeptides: tetrapeptide N-AC-Ser-Phe-Val-Gly-OMe, Aβ-peptides ($Aβ_{13-23}$, $Aβ_{16-22}$, $Aβ_{10-35}$, $Aβ_{1-40c}$, $Aβ_{1-42}$) and antimicrobial peptides (PG-1, PG-3, PG-5), which are believed to contain a peptide aggregation center.

One of the important directions of modern biomedicine is the study of the interaction of bioorganic compounds, and the scientific interest is focused both on the features of the spatial structure of molecules in complexes and on the spatial structure of the resulting complexes. Investigation of the spatial structure and interaction mechanisms of amyloid Aβ peptides and antimicrobial protegrins peptides with complexes of metal ions will make it possible to understand how the action of these ions on peptides is related to the peculiarities of their structure, which, in turn, will open up the possibility of modeling and creating drugs based on such models.

We carried out our preliminary studies of the interaction of Co^{2+} and Mn^{2+} ions and $Aβ_{13-23}$ peptide in [7-8].

The gradual addition of a manganese salt to $Aβ_{13-23}$ peptide causes selective and progressive broadening of the lines of NMR signals, as well as an increase in the proton relaxation time, which allows displaying residues that have a non-vanishing dipolar or scalar interaction with the electron spin of the Mn^{2+} ion. The most noticeable disappearance of signals in spectra, at high concentrations of Mn^{2+} ions, was observed in the NH area of aspartate (D23NH). This may be due to the shielding of aspartate by a manganese ion due to the close proximity of the ion and aspartate to each other.

Now we obtained new data for study the interaction of Gd^{3+} ions and NAc-Ser-Phe-Val-Gly-OMe tetrapeptide (Fig. 1).

The study of the formation of NAc-Ser-Phe-Val-Gly-OMe tetrapeptide complex with gadolinium salt $GdCl_3$ is also an interesting task. This tetrapeptide is a model compound for

high resolution NMR spectroscopy of biomolecules, where it is possible to work out new techniques before moving on to longer oligopeptides [9]. Gadolinium ion has special nuclear-physical and magnetic properties that can give specifically effect when interacting with various amino acid residues.

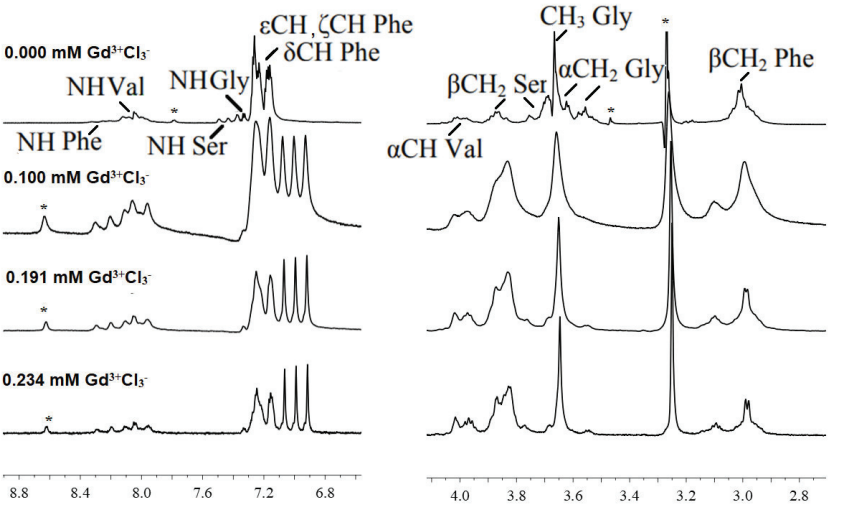

Figure 1. Fragments of ^{1}H NMR spectra set of the NAc-Ser-Phe-Val-Gly-OMe tetrapeptide with different concentrations of gadolinium (III) chloride in phosphate buffer solution (90% H2O + 10% D2O, 500 µl), - impurity and solvent signals*

Acknowledgements

This work has been performed according to the Russian Government Program of Competitive Growth of Kazan Federal University.

References

1. K. S. Usachev, S. V. Efimov, A. R. Yulmetov, A. V. Filippov, O. N. Antzutkin, S. Afonin, V. V. Klochkov – *Magn. Reson. Chem.*, 50, 784-792 (2012)
2. K. S. Usachev, A. V. Filippov, E. A. Filippova, O. N. Antzutkin, V. V. Klochkov – *J. Mol. Struct.*, 1049, 436-440 (2013)
3. K. S. Usachev, A. V. Filippov, O. N. Antzutkin, V. V. Klochkov – *Eur. Biophys. J.*, 42, 803-810 (2013)
4. K. S. Usachev, S. V. Efimov, O. A. Kolosova, A. V. Filippov, V. V. Klochkov – *J. Biomol. NMR*, 61, 227-234 (2015)
5. K. S. Usachev, S. V. Efimov, O. A. Kolosova, E. A. Klochkova, A. V. Aganov, V. V. Klochkov – *J. Biomol. NMR*, 62, 71-79 (2015)
6. O. A. Kolosova, K. S. Usachev, A. V. Aganov, V. V. Klochkov – *BioNanoScience*, 6, 317-319 (2016)
7. R. J. Abdrakhmanov, D. S. Blokhin, K. S. Usachev, F. Kh. Karataeva, V. V. Klochkov – *BioNanoScience*, 7, 204-206 (2017).
8. R. J. Abdrakhmanov, D. S. Blokhin, K. S. Usachev, V. V. Klochkov – *BioNanoScience*, 8, 423-427 (2018).
9. D. S. Blokhin, S. Berger, V. V. Klochkov – *MRSej*, 15, 13202 (2013).

Evolution of the magnetic structure of a binary helimagnet FeP in an external field by ^{31}P NMR

Aleksei V. Tkachev[1], Andrei A. Gippius[1,2], Sergei V. Zhurenko[1,2], Norbert Büttgen[3], Martina Schädler[3], Igor V. Morozov[4], Ivan O. Chernyavskii[4], Alexander S. Moskvin[5]

[1]*P.N. Lebedev Physics Institute of the RAS, Moscow, Russia*
[2]*Faculty of Physics, M.V. Lomonosov Moscow State University, Moscow, Russia*
[3]*Institut für Physik, Augsburg University, Augsburg, Germany*
[4]*Faculty of Chemistry, M.V. Lomonosov Moscow State University, Moscow, Russia*
[5]*Institute of Natural Sciences and Mathematics, Ural Federal University, Ekaterinburg, Russia*
E-mail: tkachevav@lebedev.ru
https://sites.lebedev.ru/ru/sites/nmr/3975.html

Introduction

The scientific interest in iron phosphide FeP is related mainly to its complex helicoidal magnetic structure, the details and origin of which are still under discussion [1-3]. The recent discovery of superconductivity in isostructural MnP and CrAs under high pressure provided an additional impetus to the study of these compounds. Neutronography studies reveal the incommensurate magnetic structure with constant pitch angle of iron magnetic moment along *c* axis. However, Mössbauer spectroscopy reveals a clear sign of cycloid anharmonicity up to $m \approx 0.96$ along with significant anisotropy [2, 4].

Applying ^{31}P NMR

Nuclear magnetic resonance on ^{31}P may provide a rich information about magnetic structure of the studied compound due to huge variety of possible approaches: powder NMR in zero field and in different applied fields, single crystal NMR in different fields and orientations. Despite some indirectness of these methods (studying local fields on the nuclei of non-magnetic atoms) NMR avoids solving the inverse task and the influence of additional factors, such as quadrupole splitting and isomer shift, characteristic of Mössbauer spectroscopy.

FeP magnetic structure

Field dependence

Powder NMR clearly demonstrates evolution of the FeP magnetic structure with field. Already zero field measurements provide information about local fields inhomogeneity and its distribution. Low field spectra demonstrate typical powder-like picture revealing the significant binding of the magnetic structure to the crystal axes. Increasing field causes gradual transition to the oriented phase with clearly seen coexistence of two phases in moderate fields (Fig. 1).

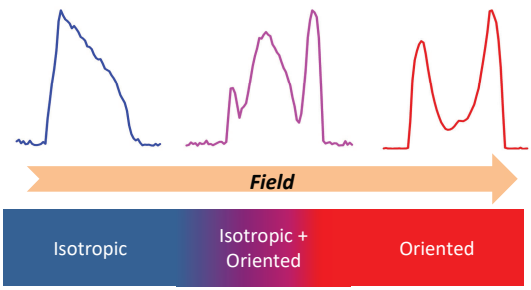

Figure 1. Powder spectrum field dependence

Single crystal measurements

The rotation of the single crystal around (010) axis gives a picture of spatial distribution of local fields. For instance, measurements at a resonant frequency of 33 MHz characterize a purely isotropic (non-oriented) phase, since the entire spectrum lies below 3 T. Observed spectra demonstrate a superposition of two two-horn structures, typical to cycloid (Fig. 2). Each of them reaches a maximum range of ≈ 1.7 T, but at different sample orientations, which indicates the angle between the corresponding planes of cycloids being ≈ 47^0.

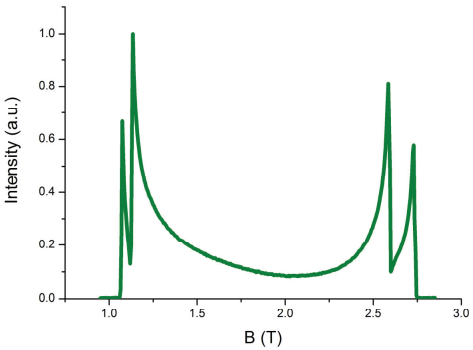

Figure 2. Typical single crystal spectrum in non-oriented phase

Acknowledgements

This work is supported by the RFBR grants #17-52-80036 and #18-33-01282 mol_a.

References

1. G.P. Felcher, et al., *Phys. Rev. B* **3**, 3046 (1971).
2. A.V. Sobolev, et al., *Journal of Alloys and Compounds* **675**, 277-285 (2016).
3. K. Motizuki, et al.. Electronic Structure and Magnetism of 3d-Transition Metal Pnictides. Springer, Berlin Heidelberg, 2010.
4. L. Häggström, et al., *J. Magn. Magn. Mater.* **30**, 249 (1982).

NMR-visualization of the structure of plants

Violet Traxel, Konstantin Tyutyukin, Yury Chernyshev, Viacheslav Frolov

St. Petersburg State University,1, Ulyanovskaya str.,
St. Petersburg, 198504, Russian Federation
E-mail: violet-2001@mail.ru

Introduction

Magnetic resonance imaging (MRI) is a standard method of medical diagnosis. However, the field of MRI applications is significantly wider. In particular, MRI can be used to investigate the structure of plant objects. It is not feasible to use industrial medical scanners for this purpose for economic reasons. The study presented has used a homebuilt NMR scanner for small objects operating in a field of 7 mT. Relaxation times and self-diffusion coefficients can be used as characteristic parameters that are displayed on magnetic resonance images of parts of plants.

Method

For the simplest two-pulse sequence rotating the nuclear magnetization by 90 and 180 degrees [1], respectively, with the interval τ, the dependence of the spin echo signal amplitude $A(\tau)$ on relaxation parameters (spin-spin relaxation time T2) and diffusion parameters (self-diffusion coefficient D) is as follows [2, 3]:

$$A(\tau) = A_0 \exp\left(-\frac{2\tau}{T_2}\right) \bullet \exp\left[-D\gamma^2 G^2 \delta^2 (\Delta - \frac{\delta}{3})\right]$$

Here γ is gyromagnetic ratio, δ and Δ see Figure 1.

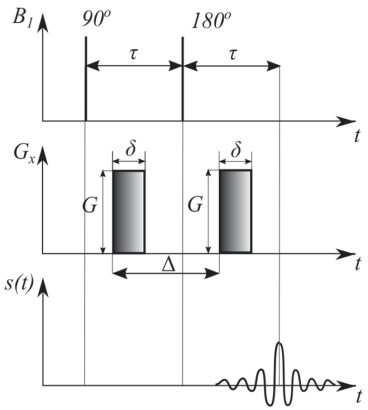

Figure 1. The pulse sequence for self-diffusion coefficient measurements

In biological objects, especially plants, the result of the D measurement depends on the direction of gradient **G**. However, Eq. (1) becomes incorrect if the free diffusion process is limited to some obstacles in the sample volume, for example in the case of a porous medium or in bioobjects with a cellular or fibrous structure. Generally the equation of attenuation of the echo signal (1) will be transformed to very difficult look depending on a form and the size of obstacles, and the measured coefficient of self-diffusion D is replaced with some effective D_{eff} value. In particular, for diffusion between two parallel planes divided by distance of a, $D_{\text{eff}} \approx D$

if $D\tau$ <<2a that corresponds to diffusion in the free environment. However in the case of $D\tau$>> 2a $D_{eff} \approx a^2/(12\tau)$. It follows that the apparent self-diffusion coefficient D_{eff} decreases with the increase in diffusion observation time 2τ, that corresponds to a decrease in the mean square amount of particle displacement.

In the limit, the D_{eff} value is simply the mean square displacement of the particle divided by the observation time (2τ).

Results

Examples of experimental dependencies of spin echo signals from plant stems showing self-diffusion anisotropy are given in Figures 2 and 3.

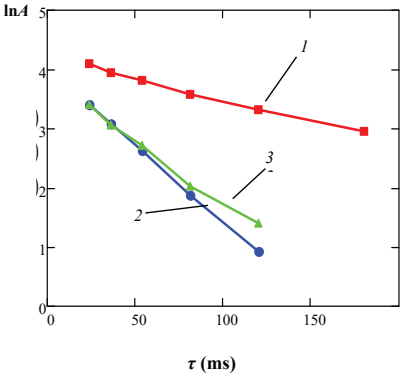

*Figure 2. The dependence on the logarithmic scale of the spin echo intensity (arbitrary units) on the interval τ in the absence of a gradient and in the gradient directed across the **Petroselinum crispum** stem and along the stem.*
*1 - G=0; 2 - **G** along the stem;*
*3 - **G** across the stem*

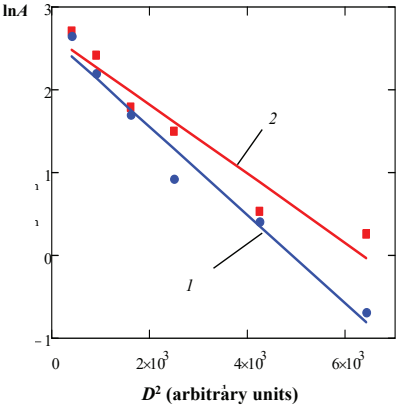

*Figure 3. The dependence of the intensity of the spin echo at t = 200 ms on the gradient square directed along and across the **Apium graveolens** stem.*
*1 - **G** along the stem;*
*2 - **G** across the stem*

Acknowledgments

Participation in the School-Conference of one of the authors(V. T.) is supported by the St. Petersburg State University Travel grant.

References

1. V. I. Chizhik, Y. S. Chernyshev, A. V. Donets, V. V. Frolov, A. V. Komolkin, M. G. Shelyapina. Magnetic Resonance and Its Applications**.** Springer Cham Heidelberg New York Dordrecht London. 2014, XX, 782 p. 234 illus. — ISBN 978-3-319-05298-4, ISBN 978-3-319-05299-1.
2. Богачев Ю.В., Грунин Л.Ю., Князев М.Н., Фролов В.В.,Чернышев Ю. С. Магнитный резонанс. Основы и применение. СПб.: Изд-во СПбГЭТУ «ЛЭТИ», 2014. 168 p. - ISBN 978-5-7629-1636-3.
3. S.V. Ievleva, N.V. Luzhetckaia, K.V. Tyutyukin, V.V. Frolov - *Appl. Magn. Reson*. **48**, 699–706 (2017)

Features of the study of bitumen compositions by electron paramagnetic resonance

Larisa V. Tsyro[1], Alina A. Pichugina[1], Felix G. Unger[2]

[1]Institute of Natural and Technical Sciences, Surgut State University, Lenina avenue 1, Surgut, Russian Federation
[2]Chemical Faculty, National Research Tomsk State University, Lenina avenue, 36, Tomsk, Russian Federation
E-mail: tsyro@xf.tsu.ru
http://www.surgu.ru

Introduction

The structure of bitumen is determined by chemical compounds, which are: 1) free radicals; 2) compounds with spin dipole moments; 3) compounds in which electronic orbitals are completely closed and do not give significant spin dipole moments. The first group includes compounds with at least one unpaired electron, the second group includes compounds (including heterocompounds) with π-orbitals, and the third group includes compounds with exclusively σ-bonds in the outer orbitals.

The structure of bitumen has a central spherical structure, the power center is represented by one or more paramagnetic molecules. The force properties of the center are compensated by layers of spin-polarized molecules possessing the properties of being attracted to the free radicals of the center. The colloidal particles thus formed are uniformly placed in the dispersion medium of molecules with σ-bonds. Obviously, the ratio of these molecules determines the size and strength of colloidal particles and the entire dispersed system as a whole.

The power center is a sufficiently active radical, the possibility of recombination of which is blocked by a thick protective layer of spin-polarized molecules. This explains the futility of attempts to model the structure of such colloidal particles by introducing individual stable radicals, whose molecules cannot fundamentally be force centers, but can only increase the solvate layers of existing associates. If they are absent, stable radicals are evenly distributed in the dispersion medium due to the spatial removal of the effective molecules of the medium from the geometric center of action of the unpaired electron of the free radical.

The durability of the structure of bitumen depends on the resistance of the power center of a dispersed particle. If the center is an active paramagnetic particle, the force parameters of which are compensated by strong solvate layers of spin-polarized molecules (as, for example, in compound residual bitumen), then such a colloidal particle provides a long unchanged state. f the center is a packet structure of a graphite-like crystallite, then despite the relatively good strength characteristics at the time of manufacture, this bitumen quickly ages and, as a result, rapid destruction of the road due to crystallite growth.

In compounded bitumens, the ratio of gut structures to amorphous is such that the best samples do not have the first ones at all, and as a rule, these cases correspond to bitumen obtained at low temperatures, that is, in a mode where coking elements are completely absent. Thus, it can be stated that two types of associative combination cores are found in bitumen and other oil-like systems, one of which exhibits amorphous properties, forming the basis of natural oils and non-oxidized bitumen, the stability of which is proved by millions of years of occurrence in oil traps. Another species has crystalline properties, rapidly grows in number under temperature influences, leads to a graphite-like material, the entire mass of the oil-like system and thus makes it unstable. The band theory of conductivity allows us to prove that the appearance of associates of graphite-like structures in a bitumen system with an amorphous paramagnetic power center is the primary act of a phase transition corresponding to the merging

of the Fermi zone and the valence band, which leads to the rapid transformation of the material into a graphite-like mass unsuitable for road surface.

This phenomenon is detected both by the method of X-ray diffraction analysis and by the ESR method, where the burst structures exhibit charge properties and give the line of absorption of conduction electrons (Dyson line). Unpaired electrons in such a structure are defined as spin power centers of mobile conduction electrons, due to which more and more molecules of solvate shells are drawn into the reaction of transition to the crystalline state.

The aim of this work was to analyze bitumen by the electron spin resonance method.

Research Methods

The electron spin resonance (ESR) method was used to analyze the cores. Preliminary preparation consisted of grinding a core sample in ball mills. The powder thus obtained was placed in an ampoule made of quartz glass, the ampoule was placed in the resonator of an ESR spectrometer. A spectrometer of the SE/X brand operating in the X-band was used. The device was tuned (the corresponding microwave modulation was selected), the spectrum was recorded. Conditions of spectrum shooting: a) field width 700 mT; b) sweep time 16 min; c) ν 9 GHz; d) the sensitivity was selected depending on the sample. Microwave modulation was selected in such a way that saturation would not occur for the sample.

Results

To assess the durability of bitumen and compositions based on them, it is not enough to use GOST standards that characterize the end products of the "oxidation" process without interpreting the "plate to plate" or "onion skin" structures. The first of them, unacceptable from the point of view of durability, but with completely acceptable GOST parameters for oxidized oil residues, are a consequence of the high-temperature process. The oxidizing method for producing bitumen almost everywhere leads to the emergence of pack structures that are not regulated by GOST. The high temperature of the oxidation process leads to an increase in the proportion of dehydrogenation reactions, which are accompanied by the release of a large amount of water and the acceleration and more active occurrence of homolytic processes. The proportion of reactions leading to oxygen accumulation decreases. This is accompanied by a decrease in the content of spin-polarized molecules (resins), which leads to the destruction of associates and the growth of crystallites of carbenes and carboids. This fact is reflected in the ESR spectra of the obtained products in the form of a Dyson line.

The more asymmetric the absorption line, the greater the number of buried structures present in the oxidized sample, therefore, the worse its quality in terms of stability over time.

In the table 1 shows the data of an ESR study of the quality assessment of oxidized samples. The ratio of the heights of the lower ($h_н$) and upper ($h_в$) half peaks of the peak of free radicals (g ~ 2), showing the degree of asymmetry of the peak, was used as an estimated characteristic.

Table 1. ESR spectroscopy data for assessing the quality of initial and oxidized samples

Sample	$h_н / h_в$
BND 40/60	0,09
BNK 45/190	0,98
tar atmospheric vacuum tube -3 (source)	0,32
tar atmospheric vacuum tube -3 (oxidized by air, 6 hours)	0,13
tar atmospheric vacuum tube -3 (oxidized with activated air, 6 hours)	0,29

tar atmospheric vacuum tube -3 (oxidized with activated air enriched with water vapor, 6 hours)	0,45
asphalt + tar (source)	0,55
asphalt + tar (oxidized by air, 3 hours)	0,11
asphalt + tar (oxidized with activated air, 3 hours)	0,14
asphalt + tar (oxidized with activated air enriched with water vapor, 3 hours)	0,21

The use of modifiers allows you to fix many of the negative qualities of asphalt concrete, but there is no universal modifier to fix all its technical characteristics.

ESR spectra of modified bitumen with polyolefins show a decrease in the intensity of the line of conduction electrons in oxidized bitumen and a general improvement in the mechanical properties of the residual. The best results on the reduction of conduction electrons were obtained using oxidized atactic polypropylene (APP), which, apparently, are the most promising modifiers for correcting the crystal structure of bitumen subjected to thermal overloads upon receipt.

In the table 2 for different samples of organic binders, data on the depth of penetration of the needle at 25 ° C and ESR spectroscopy are presented. The binders comply with the requirements of GOST in terms of needle penetration depth of 0.1 mm at 25 °C (the norm for grades 60-90), but at the same time they have low performance properties. The samples give the Dyson line, which characterizes the presence of pack structures.

Table 2. The penetration depth of the needle and the degree of asymmetry of the absorption peak of free radicals for various organic binders

Name of material (manufacturer, where the sample was taken from)	**The depth of penetration of the needle at 25 °C**	**$h_н/h_в$**
Bitumen BND 60/90 (Oil refinery Achinsk, road construction department - 3)	76	0,28
Bitumen BND 60/90 (Oil refinery Achinsk, road repair construction department Krivosheino)	77	0,57
Bitumen BND 60/90 (Oil refinery Achinsk, road repair construction department Chazhemto)	68	0,61
Bitumen BND 60/90 + 1,5 atactic polypropylene (Perm Oil Refinery)	56	0,70
Bitumen BND 60/90 + 2,5 atactic polypropylene (Perm Oil Refinery)	57	0,73

Asphalt concrete is a multi-parameter system, which is still being created by trial and error. The presented results of the work on the oxidation of oil facilities under conditions of activation of air components showed the possibility of changing and controlling the formation of pack structures in bitumen using the ESR method. The use of modifiers both for straight-run bitumen and for these materials is effective, however, the durability of the road being used, all other things being equal, depends on the stability of the binder.

Optimization of polar metabolite extraction from White Adipose Tissue for ^{1}H-NMR spectroscopy. Comparison with HR-MAS NMR on tissue section

Sophie Tumson[1,2], Manon Delcourt[1,2], Jean-Marie Colet[1]

[1]Department of Human Biology and toxicology at the university of Mons
[2]Department of Molecular and metabolic biochemistry at the university of Mons
E-mail: Sophie.TUMSON@student.umons.ac.be

Background

Nowadays, ^{1}H-NMR-based metabolomic appears as a powerful and efficient technic when it comes to study the complete metabolite networks of various biological samples (cells, tissues, biological fluids). In our laboratory, we focus on the metabolite signature of numerous tissues including the white adipose tissue in an obesity context. Actually classical ^{1}H-NMR analyses require some preliminary extraction steps to specifically isolate polar and no-polar metabolites. However, the traditional methanol-chloroform-water extraction protocol, previously validated on other tissues in our lab, requires some adjustments and improvements for its use regarding adipose tissue. Indeed, our preliminary results seem to indicate a poor polar metabolic extraction yield. This might be due to chemical and mechanical limits of the extraction method when applied on the highly lipophilic intracellular content of adipocytes.

In this proposed study, we will compare results obtained on tissue extracts analysis by liquid ^{1}H-NMR spectroscopy and the HR-MAS spectra from adipose tissue section. This latter technique combines the advantages of two highly successful NMR techniques: the “high resolution” for liquids and the “line narrowing” for solids [1, 2]. Furthermore, the HR-MAS technique does not require any metabolite extraction that may overwhelm previously discussed technical and methodological limits.

References

1. F. Desmoulin et al., “Etude critique de l’utilisation de la RMN HR-MAS pour l’analyse des tissues biologiques”, ScienceDirect, N°11, 2008.
2. C. Henoumont, S. Laurent, R. Muller, L. Vander Elst., “la spectroscopie HR-MAS : un nouvel outil pour la caractérisation des nanoparticules de fer”, Chimie nouvelle, N°118, 2015.

^{1}H NMR study of water in pillared mordenite and ZSM-5 zeolites

Anna S. Tyurtyaeva, Marina G. Shelyapina, Denis Yu. Nefedov, Anastasya O. Antonenko, Yurii S. Chernyshev

Saint Petersburg State University, 7/9 Universitetskaya nab., Saint Petersburg 199034, Russia;
E-mail: st064982student.spbu.ru

Introduction

Layered zeolites are used as precursor for mesoporous catalysts. For the successful development of these materials, knowledge on the structure and dynamics of both structural parts are highly required. In this contribution we report on the results of our studies of the local structure of the pillared mordenite and ZSM-5 zeolites, as well as the study of dynamics of water molecules inside the interlamellar space.

Experimental section

The samples were synthesized according to the procedure described in our previous work [1]. Pillaring of the obtained materials was done as proposed by Na et al. [2]. The preparation method included four steps: (i) preparing of lamellar zeolites by self-assembling method using cetyltrimethylammonium bromide (CTAB) and polyethylene glycol (PEG) as mesopore creating agents in a one-pot synthesis; (ii) introduction of TEOS molecules into the interlamellar space; (iii) hydrolysis and formation amorphous SiO_2; (iv) calcination (evacuation of organic molecules).

In this contribution we report on the results of our study of water molecules in a nanoconfinement: the space between 2D zeolite sheets.

^{1}H NMR experiments were done using a Bruker Avance IIITM 400 MHz solid-state NMR spectrometer (operating with Topspin version 3.2) using a double-resonance 4mm low temperature magic angle spinning (MAS) probe. The temperature was changed within a temperature range from 173 to 293 K and controlled with accuracy 0.5 K. In MAS experiment the rotation frequency was equal to 12 kHz. Spin-lattice relaxation times were measured using the so-called inversion-recovery method (180° – τ – 90°). To measure $T_{1\rho}$ relaxation times the spin-locking technics was applied. In our experiment the frequency of the locking pulse was chosen to be 40 kHz. In addition, T_1 relaxation times were measured at 90 MHz using Bruker SXP 4-100 spectrometer.

According to thermal gravimetric analysis, the water release in the both pillared zeolites occurs in one step. The mordenite sample exhibits both higher water content (14.3 and 10.1 mass % for the pillared mordenite (MOR-P) and ZSM-5 (MFI-P) samples, respectively) and higher temperature of water release (56 and 28 ºC for the MOR-P and MFI-P samples, respectively).

The ^{1}H MAS NMR spectra recorded within the temperature range from 173 to 293 K for MOR-P are shown in Fig. 1 (all the spectra are shown relative to TMS). They confirm that the majority of water molecules are situated inside the mesopores: at room temperature water molecules are bounded with the framework oxygen by hydrogen bonds (the signal at about 2.7 ppm). However, with temperature decreasing one observes disappearing of the water-framework hydrogen bonds due to formation of bulk water with further crystallization (the signal at about 6 ppm). The small signals at 0-1 ppm corresponds to hydroxyl groups.

For the both studied pillared zeolites the temperature dependences of ^{1}H spin-lattice relaxation times T_1 and $T_{1\rho}$ exhibit a rather complex behavior that reflects the phase transitions that nanoconfined water undergoes. The activation energy, as determined from the $T_{1\rho}(1/T)$

dependence using the Blombergen-Purcell-Pound (BPP) model, Fig. 2, was found equal to 25.9 and 30.7 kJ/mol for the MOR-P and MFI-P samples, respectively.

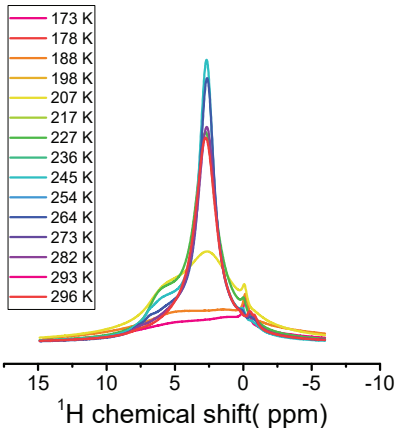

Figure 1. ^{1}H MAS NMR spectra (rotation frequency 12 kHz) recorded at various temperature for the MOR-P sample

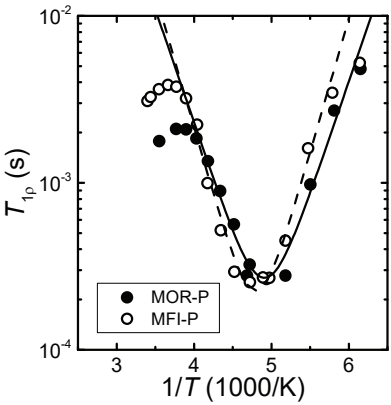

Figure 2. ^{1}H Relaxation times $T_{1\rho}$ versus inverse temperature in MOR-P (solid symbols) and MFI-P (open symbols); lines show the fit within the BPP model

Acknowledgements

The work was funded by the Russian Foundation for Basic Research (project No. 18-53-34004). The materials were synthesized by R.I. Yocupicio-Gaxiola. The studies were performed at the Research Park of Saint Petersburg State University (Centre for Diagnostics of Functional Materials for Medicine, Pharmacology and Nanoelectronics).

References

1. R.I. Yocupicio-Gaxiola, V. Petranovskii, J. Antúnez-García, S. Fuentes Moyado, Appl. Nanosci. 9 (2019) 557–565.
2. K. Na, M. Chol, W. Park, Y. Sakamoto, O. Terasakl, R. Ryoo, J. Am. Chem. Soc. 132 (2010) 4169–4177.

Rotational motion of ions in alkylammonium nitrate ionic liquids. A molecular dynamics simulation study

Milosh Ubovich, Vsevolod V. Beshanov, Andrei V. Egorov

Faculty of Physics, Saint-Petersburg State University, Russia
E-mail: ubovich.milosh@yandex.ru

Introduction

Alkylammonium nitrate protic ionic liquids (AN PILs) are considered as perspective electrolytes for advanced fuel cells. Although the structural characteristics of AN PILs are rather widely studied, a detailed analysis of the ions dynamics is still lacking. In the present study a subset of three alkylammonium nitrate PILs: ethyl-, propyl-, and butylammonium nitrates, was investigated using molecular dynamics computer simulation.

Simulation details and results

For each of three AN PILs a model system of 300 nitrate and 300 alkylammonium ions in cubic cell with periodic boundary conditions was simulated in the NPT ensemble at 298 K and atmospheric pressure using the MDynaMix package [1]. The alkylammonium cations were modeled using the potentials described in Refs. [2-4]. Model nitrate anion was treated as a 4-site planar structure with a central nitrogen atom and three oxygen atoms at a distance of 1.22 Å with all O-N-O angles of 120^o [5]. Intermolecular interactions were described as the sum of Coulomb and Lennard-Jones (6-12) potentials. Three different potential parameters sets, taken from Refs. [6-8], were considered.

To describe the reorientational motion of ions the normalized time autocorrelation functions of various intramolecular vectors were calculated. A special attention was given to the reorientational correlation time of the N-H molecular vectors of the alkylammonium cations. The effect of the alkyl chain length on the dynamical properties of alkylammonium nitrate PILs was studied in details.

References

1. A. P. Lyubartsev, A. Laaksonen. − Comp. Phys. Comm., 128, 565-589 (2000).
2. T. Mendez-Morales, J. Carrete, O. Cabeza, et al. – J. Phys. Chem. B, 118, 761-770 (2014).
3. V. Gomez-Gonzalez, B. Docampo-Alvarez, O. Cabeza, et al. – J. Chem. Phys., 143, 124507 (2015).
4. T. Mendez-Morales, J. Carrete, J. R. Rodriguez, et al. − Phys. Chem. Chem. Phys., 17, 5298-5307 (2015).
5. C. Ebner, R. Sansone, S. Hengrasmee, M. Probst. − Int. J. Quant. Chem., 75, 805-814 (1999).
6. T. Megyes, S. Balint. − J. Phys. Chem. B, 113, 4054-4064 (2009).
7. Y. Umebayashi, W.-L. Chung, T. Mitsugi, et al. – J.Comput. Chem. Jpn., 7, 125-134 (2008).
8. A. Laaksonen, H. Kovach. – Can. J. Chem., 72, 2278-2285 (1994).

Physicochemical characterisation of bovine and porcine gelatin based soft candies by Time Domain (TD) NMR Relaxometry

Sirvan Sultan Uguz[1], Emin Burcin Ozvural[2], Mecit Halil Oztop[1]

[1]Department of Food Engineering, Middle East Technical University, Ankara, Türkiye
[2]Department of Food Engineering, Çankırı, Karatekin University, Çankırı, Türkiye

Gelatin is a water-soluble protein derived from collagen and is non-toxic, inexpensive, commercially available and has great film-forming properties. It is produced by using the bones or skins of the animals. The difference between bovine and porcine gelatin comes from the differences on amino acid compositions. Gelatin is widely used in food industry a thickener, stabilizer and gelling agent. Porcine gelatin is not preferred by some people due to religious beliefs. In Turkey, use of porcine gelatin in food products is not allowed. However, since gelatin production does not occur at a level that satisfies the demand of the industry, most of the gelatin is imported from other countries. Since import increases the cost, there is tendency to adulterate the formulations by using porcine gelatin. In that regard there is an essential necessity for reliable and methods detect the source of commercial gelatin in food products. Polymerase chain reaction (PCR) based, chromatographic and spectroscopic techniques such as FTIR have been used for this purpose. In this study, the objective is to see whether relaxation times (T_1 and T_2) could be used as markers to detect the source of gelatin in different soft candy products. Candies prepared with PG, BG were tested using an NMR system operating at a frequency of 20.34 MHz. *CPMG* (for T_2) and *Saturation Recovery* (T_1) sequences were used to find the relaxation times. To complete the information obtained from NMR, water activity, total soluble solids (Brix^o) values were also measured. Results showed that despite the similar Brix^o values, a_w and T_2 relaxation times were different. Higher a_w was associated with longer T_2 values which could be an expected result. To show that gelatin type is causing the different relaxation behaviour, FTIR, titratable acidity and pH will be the next step for this study.

NMR studies of diisopropylammonium iodide embedded into opal

N. I. Uskova[1,2], E. V. Charnaya[1], D. Yu. Podorozhkin[1], S. V. Baryshnikov[3]

[1]St.Petersburg State University, St. Petersburg, 198504 Russia
[2]St.Petersburg State University of Aerospace Instrumentation, 190000 Russia
[3]Blagoveschensk State Pedagogical University, Blagoveschensk, 675002 Russia
E-mail: natalyauskova.spbu@gmail.com

Introduction

New organic ferroelectrics such as diisopropylammonium iodide (Curie temperature 415 K and spontaneous polarization 33 μC/cm^2) are an interesting object to study [1-5]. They exhibit all the basic physical properties observed in type $BaTiO_3$ inorganic ferroelectrics. In addition, organic ferroelectrics are generally simple and environmentally friendly in processing, have lightweight and can be mechanically flexible. NMR methods allow researches at the microscopic level and in contrast to many other methods, give immediate information on structural transitions.

In this work, the main attention was paid to the influence of size effects on the temperature of phase transitions in the diisopropylammonium iodide (DIPAI)

Samples and experiment

The sample under investigation was DIPAI embedded in opal matrices. The results were compared to the results obtained for the DIPAI crystal powder.

The measurements were performed using a pulse Bruker Avance 400 NMR spectrometer in the range from room temperature to 420 K. The pulse sequence used for acquiring the spectrum was a standard cross-polarization (from proton to 13C) MAS pulse sequence.

Results

The ^{13}C CP-MAS NMR spectrum of DIPAI ($C_6H_{16}NI$) at room temperature demonstrates six lines corresponding to 6 crystallographically non-equivalent carbon positions (Figure 1). Above 370 K, the spectrum changes, new 3 lines appear. These lines correspond to the signal from a new phase. With further heating, the intensity of the initial six lines decreases. At a temperature of 380 K, only three NMR lines are observed. The hysteresis of this structural transition was more than 10 K.

Similar patterns are observed for DIPAI embedded in opal (Figure 2). However, the temperature range of the phase transition becomes wider. When heated, the two phases coexist in the range from 347 to 380 K, and when cooled, in the range from 364 to 343 K.

The results demonstrate the emergence of the structural phase transition in bulk and nanostructured DIPAI. It is shown for DIPAI within opal that two different phases coexist in a wide temperature range and the temperature of the lower boundary of the phase transition decreases by about 23 K when heated and 15 K when cooled compared to the bulk sample.

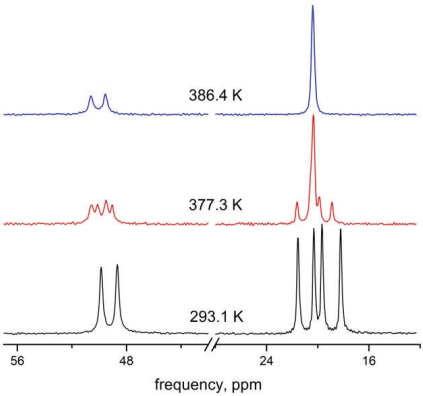

Figure 1. ^{13}C NMR CP-MAS spectra of DIPAI at different temperatures

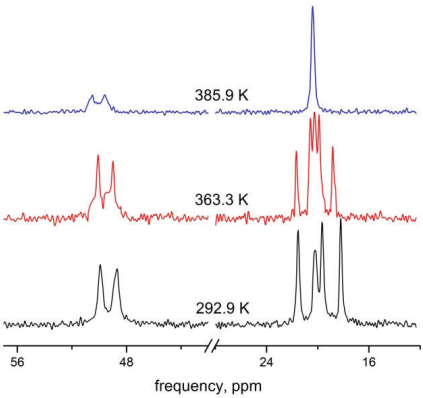

Figure 2. ^{13}C NMR CP-MAS spectra of DIPAI in opal at different temperatures

In conclusion, NMR methods allowed us to identify structural changes in bulk and nanostructured DIPAI and to show a more complex nature of the phase transitions than previously thought.

References

1. M. Owczarek, K. A. Hujsak, D. P. Ferris, et al. – *Nat Commun*, **7**, 1–10 (2016).
2. S. Horiuchi, Y. Tokura. – Nat Mater, **7**, 357–366 (2008).
3. R. K. Saripalli, D. Swain, S. Prasad, H. Nhalil, H. L. Bhat, T. N. Guru-Row, S. Elizabeth. – J. Appl. Phys., **121**, 114101 (2017).
4. C. Jiang, W.-Y. Tong, H. Lin, C. Luo, H. Peng,C.-G. Duan. – Phys. Status Solidi A, **214**, 1700029 (2017).
5. L. Louis, K. C. Pitike, A. Ghosh, S. Poddar, S. Ducharme, S. M. Nakhmanson. – J. Mater. Chem. C, **6**, 1143 (2018).

Hydrogen bond and proton transfer in homo-conjugated anions of phosphorous-containing acids. Effects in ^{1}H and ^{31}P NMR spectra

Daria O. Ustimchuk, Valeriia V. Mulloyarova, Peter M. Tolstoy

Institute of Chemistry, Saint Petersburg State University, Saint Petersburg, Russia
E-mail: ustimchuk.d@yandex.ru

Introduction

Phosphinic (R_2POOH), phosphoric ($(RO)_2POOH$) and phosphonic ($RPO(OH)_2$) acids in aprotic solutions can form complexes with strong hydrogen bonds (cyclic and chain-like dimers and trimers). Even stronger hydrogen bonds could be formed if when the proton-donating and proton-accepting abilities of interacting moieties are matched, as it happens in case of homo-conjugated anions [1], i.e. complexes formed between an acid and its anion (see examples in Figure 1).

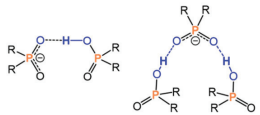

Figure 1. Homo-conjucated anionic complexes of phosphorous-containing acids with their anions in the ratio 1:1 and 2:1 (R = H-, Ph-, Me-, PhO-, MeO-)

While the neutral self-associated are fairly well studied [2,3,4], the complexation energy and the geometry of hydrogen bonds within homo-conjugates are largely unknown, though it might be expected that these structures would retain high conformational mobility and exhibit fast proton transfer processes similar to neutral self-associates [3].

Aims

The main goal of this work is to characterize the energetic, geometric and spectroscopic properties of several homo-conjugated anions of phosphinic and phosphoric acids using a combination of experimental ^{1}H and ^{31}P NMR spectroscopy and quantum-chemical calculations. The study of such complexes by NMR is hindered by the fast proton and molecular exchange processes, as well as conformational isomerism within each complex, which lead to averaging of NMR signals. To remedy this situation we have performed the experimental NMR measurements at temperatures as low as 100 K, using a mixture of liquefied deuterated freonic gases CDF_3/CDF_2Cl as a solvent. At these temperatures many dynamic processes are slowed down and signals of complexes of different stoichiometry could be observed separately. The quantum-chemical DFT calculations were done for homo-conjugated anions in vacuum conditions and within taking the counter-cation into account at the B3LYP/6-311++G(d,p) level of theory.

Results

In Fig. 2 the low-field part of the sample, containing a small amount of $(PhO)_2POOH$ acid in the presence of large excess of $TEA^{+}(PhO)_2POO^{-}$ salt is shown (TEA – tetraethylammonium). There are two signals of bridging protons in hydrogen-bonded complexes visible at 14 and 17.5 ppm. These signals were assigned to the cyclic trimer of $(PhO)_2POOH$ [2] and presumably to anionic complex 1:1 (further confirmation of the this assignment is pending). Interestingly, even the large excess of the $(PhO)_2POO^{-}$ anions in solution did not suppress the formation of neutral cyclic self-associates. Apparently, the enthalpy loss upon switching from three very strong hydrogen bonds in homo-conjugates to

three somewhat weaker hydrogen bonds in cyclic trimer was effectively compensated by the entropy gain due to the larger number of un-complexes anions in the latter case. An important role in this thermodynamic equilibrium is played by the conformational mobility of interacting moieties present in homo-conjugates. This mobility was studied by quantum-chemical calculations for a model acid H_2POOH and its complexes.

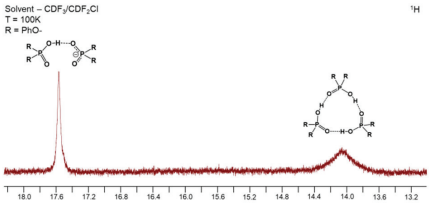

Figure 2. Low-field parts of NMR spectra of anionic complexes of $(PhO)_2POOH$

We have identified three possible conformers of homo-conjugated anions with 1:1 stoichiometry (Fig. 3), which interconvert by rotation around dihedral angles and by proton transfer within the OHO hydrogen bond. Pairs of structures (**1**&**4**, **2**&**5**, **3**&**6**) are energetically degenerate and chemically equivalent in the sense that they are mirrow images of each other and thus have the same set of NMR chemical shifts.

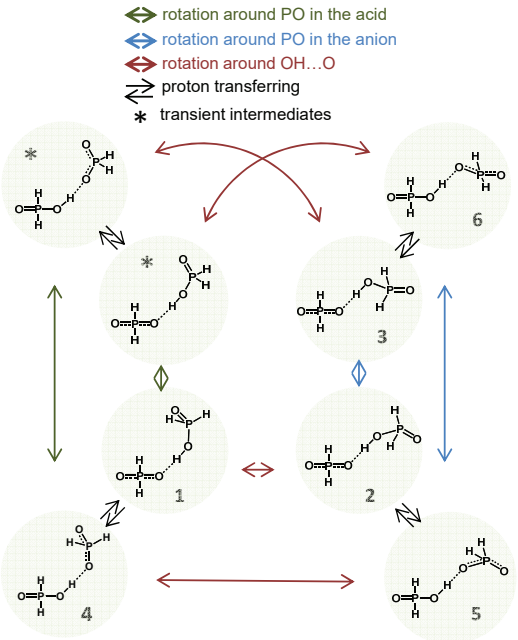

Figure 3. Calculated structures of various conformers of homo-conjugates anion of 1:1 stoichiometry of hypophosphorous acid in vacuum (the charges are omitted for simplicity)

For all conformers δ^1H of bridging proton is ~18 ppm, which agreed well with the experiment (Fig. 2). In all cases, $\delta^{31}P$ of anion and acid within a conformer differ by ~2 ppm.

Upon complexation the ^{31}P NMR chemical shift of H_2POOH changes by ~12 ppm (from ~–17 to ~–29 ppm) and that H_2POO^- anion changes by ~6 ppm (from ~–25 to ~–31 ppm). Preliminary calculations show that all energy barriers separating structures **1**–**6** are below 5 kcal/mol which would make transition between conformers fast in the NMR timescale, averaging $\delta^{31}P$ to a single value even at low temperature.

Acknowledgements

This work was supported by the Russian Science Foundation (project No 18-13-00050).

References

1. P. M. Tolstoy et.al. Characterization of Fluxional Hydrogen-Bonded Complexes of Acetic Acid and Acetate by NMR: Geometries and Isotope and Solvent Effects. - *J. Am. Chem. Soc*. **126**, **17**, **5621-5634** (2004)
2. V. V. Mulloyarova et.al. Cyclic trimers of phosphinic acids in polar aprotic solvent: symmetry, chirality and H/D isotope effects on NMR chemical shifts. - *Phys. Chem. Chem. Phys.* 20(7), 4901-4910 (2018)
3. V. V. Mulloyarova et al. Conformational Mobility and Proton Transfer in Hydrogen-Bonded Dimers and Trimers of Phosphinic and Phosphoric Acids - *J. Phys. Chem. A*. 123, 6761-6771 (2019)
4. R. E. Asfin et al. The infrared spectra and enthalpies of strongly bound dimers of phosphinic acids in the gas phase. $(CH_2Cl)_2POOH$ and $(C_6H_5)_2POOH$. - *J. Mol. Struct*. 608, 161–168 (2002)

NMR-based metabolomic evaluation of the toxicity threshold of 1,2-dichloroethane in an invertebrate model

Florent Valcke, Aude Devalckeneer

Department of Human Biology and toxicology at the university of Mons
E-mail: Florent.Valcke@student.umons.ac.be

Introduction

1,2-dichloroethane (DCE) is a halogenated hydrocarbon widely and mainly used for the manufacture of polyynyl chloride (PVC). Also used as solvent, DCE accumulates in ground and water area close to the industrial site. In ecotoxicology, this kind of molecule is worrying because it can affect several organs such as lungs, kidneys or liver and cause oxidative stress, and inflammation. DCE is metabolized by two metabolic pathways, the main one being the oxidation of DCE via CYP2E1 in chloroethanol resulting in oxidative stress [3]. If the main pathway is saturated, the other pathway consists of conjugation via glutathione and glutathione S-transferase (GST) leading to the formation of glutathione episulfonium ions able to form protein and DNA adducts [4]. Both pathways are respectively responsible for oxidative stress and genotoxicity. The toxicity assessment of DCE is ensured by a metabolomic approach based on nuclear magnetic resonance of the proton (^{1}H NMR) for the evaluation of toxicity biomarkers. The invertebrate model organism used is Helix aspersa, a snail living at the air-soil interface justifying its use as a good bioindicator.

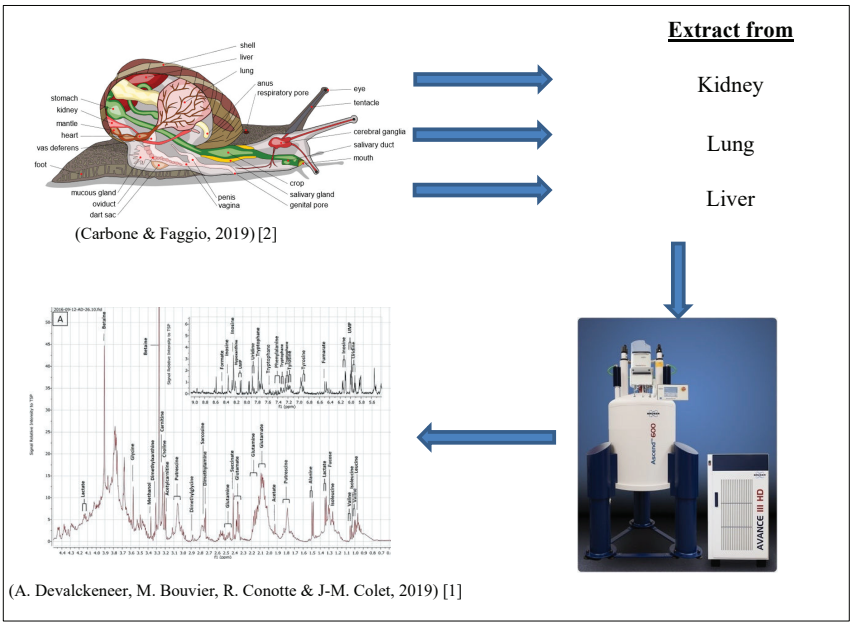

Figure 1. Experimental design

Bibliographie

1. A. Devalckeneer, M. Bouviez, R. Conotte, & J-M. Colet (2019). Proton Nuclear Magnetic Resonance (1H NMR)profiling of isolated organs in the snail Helix aspersa

maxima. *Ecological Indicators*, *105*(December 2018), 177–187. https://doi.org/10.1016/j.ecolind.2019.05.058

2. Carbone, D., & Faggio, C. (2019). *Helix aspersa* as sentinel of development damage for biomonitoring purpose: A validation study. *Molecular Reproduction and Development*. https://doi.org/10.1002/mrd.23117
3. Storer, Richard D., & Conolly, R. B. (1985). An investigation of the role of microsomal oxidative metabolism in the in vivo genotoxicity of 1,2-dichloroethane. *Toxicology and Applied Pharmacology*, *77*(1), 36–46. https://doi.org/10.1016/0041-008X(85)90265-0
4. Crespi, C. L., Seixas, G. M., Turner, T. R., Ryan, C. G., & Penman, B. W. (1985). Mutagenicity of 1,2-dichloroethane and 1,2-dibromoethane in two human lymphoblastoid cell lines. *Mutation Research Letters*, *142*(3), 133–140. https://doi.org/10.1016/0165-7992(85)90053-3

Flavonoid C-glycoside rotameric conformational analysis using NMR-spectroscopy

Andrei K. Whaley[1], *Vladimir G. Luzhanin*[1], *Stanislav I. Selivanov*[2]

[1]*Saint Petersburg State Chemical Pharmaceutical University, Street Prof. Popova 14, 197376 Saint Petersburg, Russia*
E-mail: 9968639@gmail.com
[2]*Institute of Chemistry, State University of Saint-Petersburg, University prospect 26, 198504, Saint-Petersburg, Russia*
E-mail: nmr.group.spbu@gmaill.com

Introduction

Flavonoids are a group of widely distributed plant polyphenol secondary metabolites fulfilling multiple roles throughout a plant's life [1]. Flavonoids are mainly flower pigments taking part in pollinator attraction, UV protection and chemical signaling. In nature flavonoids are usually found as conjugates with carbohydrate residues formed through O-glyosidic linkages with the anomeric hydroxyl group of the carbohydrate, but other types of glycoside linkages are known. For example, O-glycosyl flavones are known as one of the major components in the genus Iris, where they are contained in the leaves and flowers from which they have been mainly isolated [2].

Flavonoid C-glycosides are considered a rare occurrence in the plant kingdom contained in a restricted group of plant families, but as time goes flavonoid C-glycoside are being found in a rising number of plants and plant families [3]. There are only a few reports about C-glycosylflavonoids from the genus Iris. Their contribution to flower colour of the plant was recently described by Mizuno et al. [4]. C-Glycosylflavonoids are found to be minor constituent in plant extracts and their roles in plant physiology still needs further research. Inspection of their NMR data revealed signal duplication, indicating the presence of rotamers (Fig. 1).

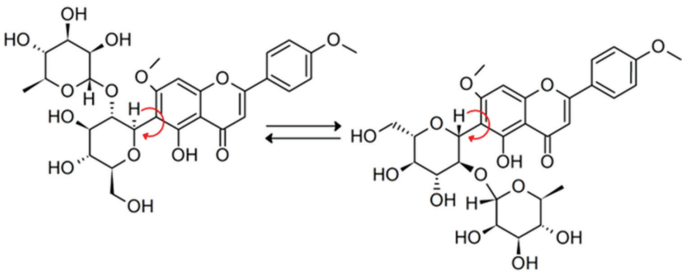

Figure 1. The structure of Embinin a C-Glycosylflavonoid and its conformational exchange due to hindered rotation around the C-glycosidic bond giving rise to two rotamers

Flavonoid C-glycosides NMR spectrum peeks are often doubled due to the hindered rotation between the anomeric glycoside carbon atom and the aromatic carbon atoms of ring A - C1″(sp3)-C6(sp2) or C1″(sp3)-C8(sp2) (see figure 2 for flavone numeration) giving rise to two rotameric conformations. It has been reported in the literature that the existence of flavonoid C-glycoside rotamers of the C1″(sp3)-C6(sp2) type is found mainly when next to the C-glycosidic linkage in ring A there is either an O-methoxy group or an O-glyosidic linkage at the C7 carbon atom. Likewise, it has been reported that flavonoid C-glycosides of the C1″(sp3)-C8(sp2) type almost exclusively give rise to two rotameric conformations due to the steric bulk of the flavonoid ring B. Also, the rotameric equilibrium between C-glycosides is strongly affected by the solvent used for NMR [5-7].

Currently NMR-spectroscopy is a powerful and diverse tool used for the analysis of molecular structures. Unlike most modern spectroscopic methods of structural analysis NMR can be considered a dynamic method of analysis capable of capturing and registering molecular change due to conformational, tautomeric and equilibrium processes happening with rate constants comparable to the "NMR time scale" which enables one to observe and quantify equilibrium processes in solution. NMR analysis of conformers most often is performed through the measurement of coupling constants, chemical shifts and peak intensities at room temperature or lower in different solvents to determine the relative populations of conformers in solution. Through varying of the temperature, it is possible to find conformational barriers and calculate the energy needed for conformer interconversion and equilibrium [8].

The goal of our research was to perform NMR-analysis of the structure and conformational equilibrium of the flavonoid C-glycosides that we managed to isolate from the leaves of *Rubus chamaemorus* using NMR spectroscopy.

Experiments and results

For the first time we were able to isolate six flavonoid C-glycosides from the leaves of the plant *Rubus chamaemorus* L. (the cloudberry) from the family *Rosaceae*. The isolated C-glycosides seem to be acylated derivatives of α-L-3″-O-rhamnopyranosyl-β-D-6-C-glucopyranosyl-7,4′-di-O-methylapigenin (Fig. 2) an isomer of the aforementioned C-glycoside Embinin (Fig. 1).

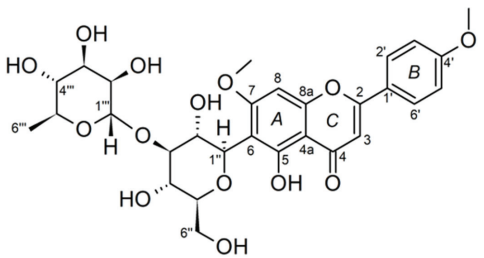

Figure 2. The structure and numeration of α-L-3''-O-rhamnopyranosyl-β-D-6-C-glucopyranosyl-7,4'-di-O-methylapigenin

The isolated C-glycosides showed doubled sets of rotamer signals in the NMR-spectra. Below (Fig. 3) the effects of variable-temperature experiments on the obtained L-rhamnose anomeric proton and methyl signals for a solution of a mixture of two flavonoid C-glycosides are shown.

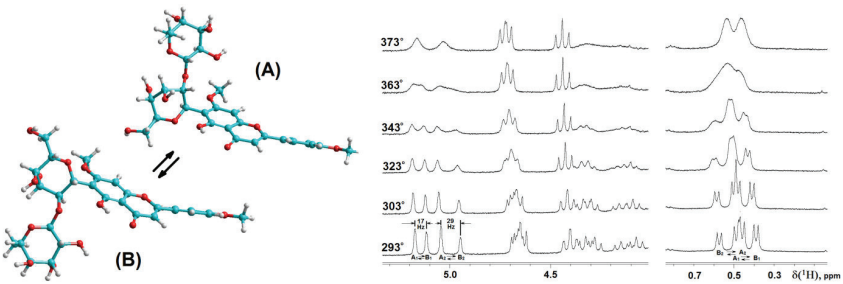

Figure 3. Dynamic effects of varying temperature on the signals in NMR ^1H spectra of the anomeric L-rhamnose and methyl protons of a solution containing a mixture of two flavone C-glycosides (DMSO-d_6, 300 MHz)

By varying the temperature, we were able to find the coalescence temperature T_c and calculate the energy barrier between the rotameric pairs due to relationship for two-position exchange [9]:

$$\Delta G_A^{\neq} = 4.57Tc[10.62 + \log(X/2\pi(1 - \Delta P)) + \log(Tc/\Delta\nu)],$$

$$\Delta G_B^{\neq} = 4.57Tc[10.62 + \log(X/2\pi(1 + \Delta P)) + \log(Tc/\Delta\nu)],$$

where T_c – coalescence temperature (in °K), $\Delta\nu$ – difference of chemical shifts (in Hz), $X = 2\pi\Delta\nu\tau$ ($1/\tau = 1/\tau_A + 1/\tau_B$), the value $\log(X/2\pi(1 - \Delta P)$ – is defined from graphic dependence on ΔP, $\log X = 2.3\ln X$, $\Delta P = P_A - P_B$ and $P_A + P_B = 1$. In the result free energies of activation $\Delta G_A^{\neq}$ and $\Delta G_B^{\neq}$ are defined in calories per mole.

For example, in our case (see Fig. 3) for the first rotameric pair: $\Delta\nu^{(1)} = 17$ Hz, $T_c^{(1)} = 365$ °K, $P_A^{(1)} = 0.52$, $P_B^{(1)} = 0.48$, $\Delta P = 0.04$. In the result it was calculated: $\Delta G_A^{\neq(1)} = 18.99$ kcal/mol and $\Delta G_B^{\neq(1)} = 18.90$ kcal/mol. For the second rotameric pair: $\Delta\nu^{(2)} = 29$ Hz, $T_c^{(2)} = 370$ °K, $P_A^{(2)} = 0.6$, $P_B^{(2)} = 0.4$, $\Delta P = 0.2$. Then: $\Delta G_A^{\neq(2)} = 19.12$ kcal/mol and $\Delta G_B^{\neq(2)} = 18.80$ kcal/mol. These calculated values of free energies of activation for both flavone C-glycosides (Fig. 3) are similar. This similarity proves the similarity of their structures and conformational flexibility.

Conclusion

Using NMR spectroscopy, we managed to establish the probable structure of six C-Glycosylflavonoids in DMSO-d_6 that were isolated earlier from the leaves of *Rubus chamaemorus*. Full signal identification in NMR ^{1}H spectra of these compounds were made on base of different correlation methods (COSY, NOESY, HSQC) and **v**ariable-**t**emperature (VT) NMR experiments. It allowed us to discover and examine conformational exchange connected with hindered rotation around the C-glycosidic bond in studied flavonoid C-glycosides and also to calculate free energies of activation by using coalescence temperature values.

Acknowledgments

Spectral investigations were performed in the Resource Centers "Magnetic Resonance Research Centre" of the Saint-Petersburg State University. The study was carried out under the financial support of the Russian Foundation for Basic Research (grant no. 18-33-00464).

References

1. A. N. Panche, A. D. Diwan, S. R. Chandra, Flavonoids: an overview // Journal of Nutritional Science, 2016, 5, e47, 1–15.
2. H. Wang, Y. Cui, C. Zhao, Mini-Rev. Med. Chem., 2010, 10, 643–661.
3. F.L. Courts, G. Williamson, The occurrence, fate and biological activities of C-glycosyl flavonoids in the human diet, Crit. Rev. Food Sci. Nutr., 2015, 10, 1352–1367.
4. T. Mizuno, T. Yabuya, J. Kitajima et al, Plant Physiol. Biochem., 2013, 72, 116–124.
5. S. Rayyan, T. Fossen, H. Solheim Nateland, Ø. M. Andersen, Isolation and identification of flavonoids, including flavone rotamers, from the herbal drug 'Crataegi folium cum flore' (hawthorn). Phytochemical analysis, 2005, 16(5), 334–341.
6. G. Zhou, R. Yan, X. Wang, S. Li et al, Phytochemistry Reviews, 2019, 18(2), 443–461.
7. A.K. Whaley, W. Ebrahima, M. El-Neketic, E.U. Ancheeva, F.C. Özkaya, N.I. Pryakhina, N.U. Sipkina, V.G. Luzhanin, Z. Liu, P. Proksch, New Acetylated Flavone C-Glycosides from Iris lacteal, Tetrahedron Letters, 2017, 58(22), 2171–2173.
8. C.F. Tormena, Conformational analysis of small molecules: NMR and quantum mechanics calculations, Prog. Nucl. Magn. Res. Sp-py., 2016, 96(8), 73–88.
9. H. Shanan-Atidi, K.H. Bar-Eli, J. Phys. Chem., 1970, 74 (4), 961–963.

Magnetic proximity effects in nanostructured $(SrFe_{12}O_{19})_X(CaCu_3Ti_4O_{12})_{1-X}$ composites

A. Yagfarova[1], I. Yatsyk[1,2], J. Deeva[3], I. Gilmutdinov[1], N. Lyadov[2], T. Chupakhina[3], R. Eremina[1,2], T. Gavrilova[2]

[1]Kazan (Volga Region) Federal University, Kazan, Russia
[2]Kazan E. K. Zavoisky Physical-Technical Institute of the RAS, Kazan, Russia
[3]Institute of Solid State Chemistry of the RAS (UB), Ekaterinburg, Russia
E-mail: adilyayagfarova@gmail.com

Introduction

Composite materials attract much attention due to the possibility to create the new structure combining the components with high values of the magnetic susceptibility and dielectric permittivity in different component proportions, because they can be used in variety of applications. Here we present the investigation of core-shell structured two-component composites, which physical properties differ from non-structured composite materials. One of the components of the composite material is $CaCu_3Ti_4O_{12}$ (CCTO), which dielectric behavior exhibits an extraordinarily high dielectric constant and shows good thermal stability in a wide temperature range (100–600K). As the second component of the composite material we chose the strontium hexaferrite $SrFe_{12}O_{19}$ (SFO) to modulate the magnetic properties of the composite.

Sample characterization

SFO_xCCTO_{1-x} composites (x = 0.01, 0.03, 0.07 and 0.1) were prepared by conventional solid-state synthesis route. Strontium hexaferrite was added to the stoichiometric amount of the oxides CaO, CuO and TiO to form the CCTO component around SFO nanoparticles. Depending of the synthesis conditions we can get a simple mixture of the two components or the nanostructured composite, when SFO microinclusions are inside CCTO matrix. In the case of nanostructured composite, the ESR spectra consist of one broad line. If the structure of composite is not form the ESR spectra consist of two clearly visible lines from each magnetic component of composite (SFO and CCTO) (Figure. 1a). Based on X-ray diffraction measurements we could find the limit concentration of the formation of a nanostructured sample. We did not observe the SFO reflections in the diffraction patterns of SFO_xCCTO_{1-x} (x = 0.03 and 0.07), therefore, it can be assumed that there was formed a nanostructured composite. SFO reflections in the diffraction patterns of the composite material were observed for x=0.01 and x=0.1. It follows that the concentration x=0.01 is too low and x=0.1 is too high to form the specific microstructure.

SFO_xCCTO_{1-x} (x = 0.03, 0.07) composites were carefully investigated by transmission electron microscope (TEM). The TEM study showed the shredded $SFO_{0.07}CCTO_{0.93}$ sample consisted from regions of the large CCTO single crystals without inclusions (Figure 2 a), as well as of CCTO regions with the nanocrystalline SFO inclusions were observed (Figure 2 b, c). The presence of SFO nanoinclusion is confirmed by the electron diffraction pattern (insert in Figure 2 b), where the rings from SFO crystallites are visible.

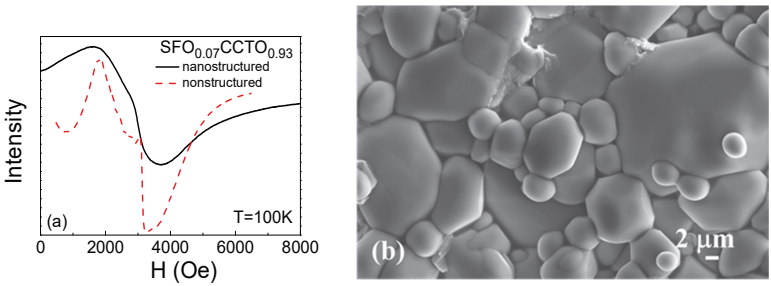

Figure 1. (a) ESR spectra of $SFO_{0.07}CCTO_{0.93}$: solid line corresponds to the nanostructured composited, dashed line - non-structured composite; (b) SEM images of $SFO_{0.03}CCTO_{0.97}$

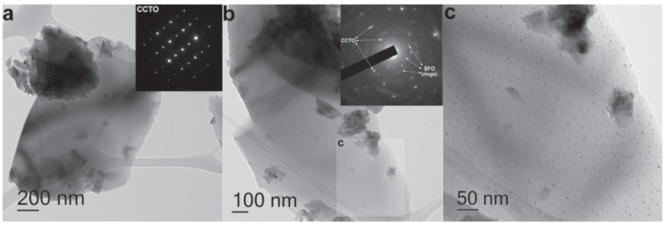

Figure 2. (a, b, c) TEM images SFOxCCTO1-x (x = 0.07) of different magnification

Magnetic properties

Electron spin resonance (ESR) spectra of SFO_xCCTO_{1-x} composite materials are presented in Figure. 3.

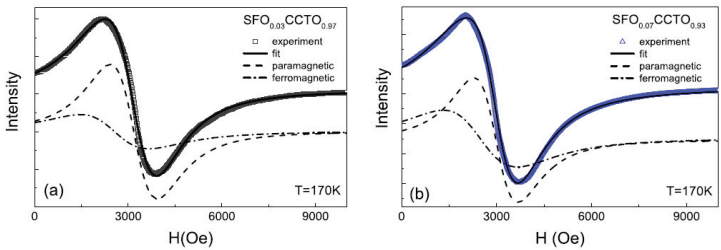

Figure 3. Decomposition of the ESR spectrum of SFO_xCCTO_{1-x} at T = 170 K in X-band: (a) x = 0.03, (b) x = 0.07

Based on the microanalysis we suggest that the broad ESR line for x = 0.03 and 0.07 corresponds to the case of the strong mutual influence of the composite components, that results to the one broad ESR line of the complex shape. Because of the presence SFO microinclusions in CCTO matrix confirmed by TEM analysis we suggest that the ESR spectrum for x = 0.03 and 0.07 consists of two lines: paramagnetic line from CCTO component with $H_{res}^{par} \approx 3200$ Oe and ferromagnetic line from SFO component with $H_{res}^{fer} < 3000$ Oe. The ferromagnetic line broadens with decreasing the temperature and makes the ESR spectra of composites asymmetric. The details of the decomposition of the ESR spectra for SFO_xCCTO_{1-x} as the sum of two Lorentz lines from ferromagnetic and paramagnetic phases at T = 170 K are given in Figure. 3a for x = 0.03 and in Figure. 3b for x = 0.07.

Temperature dependencies of resonance fields, linewidths and integral intensities of both ferromagnetic and paramagnetic lines are shown in Figure. 4 a, b,c respectively. We can see that the resonance field of paramagnetic resonance line for x = 0.03 have the same behavior and similar absolute values with pure CCTO phase with H_{res} = 3200 Oe due to Cu2+ S = 1/2, g-factor g = 2.15. From Figure. 4a we see that only for the concentration x = 0.07 the resonance fields of the paramagnetic line are lower than for pure CCTO and decrease with decreasing the temperature together with ferromagnetic line. The temperature behavior of the resonance fields for ferromagnetic line H_{res}^{fer} is closed to the pure SFO. The temperature dependence of the linewidth ΔH^{fer} is less than in pure SFO, while ΔH^{par} is mush sensitive to the presence of the ferromagnetic inclusions and increases in 6–7 times in respect to pure CCTO (Figure. 4b). Temperature dependence of the integral intensity of the paramagnetic line corresponds to the Curie-Weiss law in all temperature range only for pure CCTO. For x = 0.03 and x = 0.07 the integral intensity has the maximum at $T \sim 200$ K and than decreases with decreasing the temperature followed by the increasing of the integral intensity of the ferromagnetic line only for x = 0.07 (Figure. 4c). We suggest that below T < 200 K the influence of the ferromagnetic field of SFO-component dominates over thermal vibrations of magnetic moments in CCTO phase, thus SFO microinclusions "magnetizes" the paramagnetic CCTO leading to the decreasing of the integral intensity of the paramagnetic signal. The broadening of the paramagnetic line may occur due to an additional internal magnetic field from the ferromagnetic SFO component.

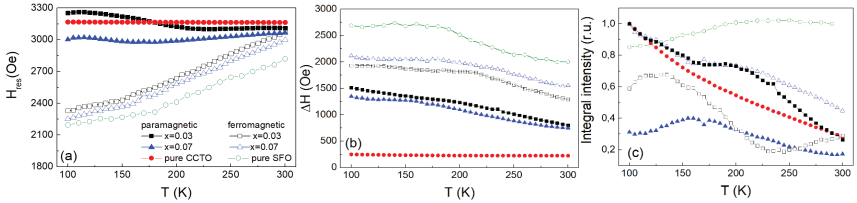

Figure 4. Temperature dependence of (a) resonance field, (b) linewidth, (c) integral intensity of the ferromagnetic and paramagnetic resonance lines in SFOxCCTO1-x (x =0, 0.03, 0.07,1). Open symbols correspond to the ferromagnetic line; full symbols correspond to the paramagnetic line

Conclusions

The magnetic properties of SFO_xCCTO_{1-x} nanostructured composites (x = 0.03, 0.07) demonstrated the strong mutual influence of two magnetic phases, manifested in the ESR lineshape and in the changing of the Weiss constant Θ and effective magnetic moment for paramagnetic phase in respect to the pure CCTO and in the decrease in the Curie temperature of the ferromagnetic phase TC in respect to the pure SFO (magnetization measurements data are presented in [1]). The observed mutual influence on the magnetic ordering temperatures of both components can be tentatively attributed to the magnetic proximity effect. SFO_xCCTO_{1-x} composites were subjected to mechanochemical treatment to study the size-effect on their magnetic properties.

References

1. T.P. Gavrilova, J.A. Deeva, I.V. Yatsyk, A.R. Yagfarova, I.F. Gilmutdinov, N.M. Lyadov, F.O. Milovich, T.I. Chupakhina, R.M. Eremina. – *Physica B: Condensed matter.*, V. 536, 303-309 (2018).

Structure and dynamics of [$CuCl_n$(1,2-diaminoethane)] complexes in aqueous solution by Quantum Chemistry and Molecular Dynamics methods

Irina Yefimova[1*], *Andrei V. Egorov*[1], *Enisa Selimović*[2], *Tanja Soldatović*[2], *Andrei V. Komolkin*[1]

[1]*Faculty of Physics, Saint Petersburg State University, St. Petersburg, 199034, Russia*
[2]*Department of Chemical-Technological Sciences, State University of Novi Pazar, Novi Pazar, Serbia*
[*]*E-mail: yefir2000@gmail.com*

Introduction

Over the past decades, transition metal complexes have attracted considerable attention in medicinal inorganic chemistry, especially as synthetic metallonucleases and metal-based anticancer drugs that are able to bind to DNA molecules under physiological conditions. The use of metal-based drugs presents the most important strategy in the development of new anticancer and antimicrobial agents [1].

The present study is focused on structure and dynamics of [$CuCl_n$(1,2-diaminoethane)] complexes (labeled henceforth as [$CuCl_n$(en)]) in aqueous solution using quantum chemistry calculations and molecular dynamics simulation.

Structure of [$CuCl_n$(en)] complexes in aqueous environment

A set of three complexes ([$CuCl_2$(en)], [$CuCl_1$(en)]$^{1+}$ and [Cu(en)]$^{2+}$) in aqueous environment was modeled by restricted Hartree-Fock method using GAMESS program [2]. The calculations were performed in the basis set CCT (cc-pVTZ [3]) with multiplicity 2.

Initial configuration of the isolated electrically neutral [$CuCl_2$(en)] complex was optimized *in vacuo*. Its optimized structure is shown in Fig. 1. The coordination of copper ion is tetrahedral. This configuration was taken as initial for the simulations of complexes with water.

Adding water molecules (up to 10) leads to 5-coordinated copper ion (see Fig. 2, only water molecules in the first hydration shell of copper ion are shown for clarity) independently on their initial positions and number. Dissociation of $CuCl_2$ was not observed.

Double charged system [Cu(en)]$^{2+}$ in aqueous environment tends to form 6-coordinated ion complex (Fig. 3). Single charged [CuCl(en)]$^{1+}$ in aqueous environment tends to build 6-coordinated ion complex in two ways (Fig. 4a, 4b). Results of quantum chemical calculations are summarized in Table.

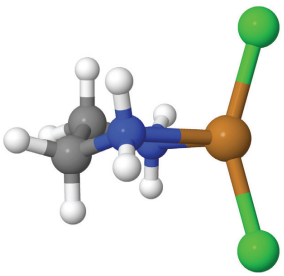

Figure 1. The optimized structure of [$CuCl_2$(en)] complex in vacuo

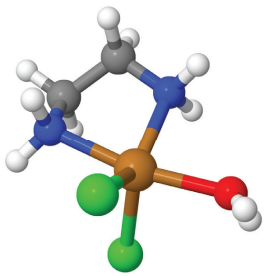

Figure 2. One of the optimized structures of [$CuCl_2$(en)] aqua complex

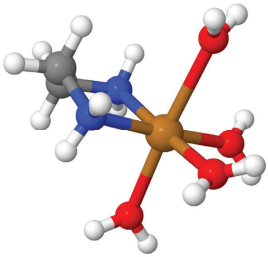

Figure 3. The optimized structure of $[Cu(en)]^{2+}$ aqua complex

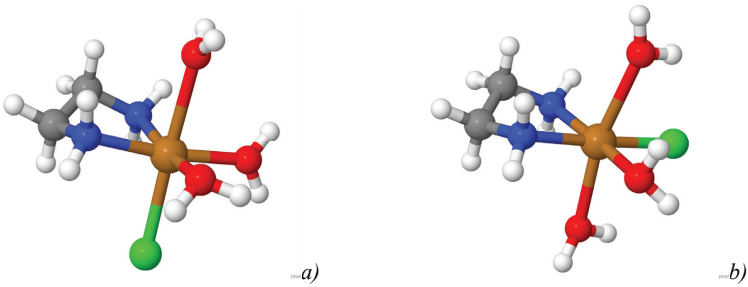

a) *b)*

Figure 4. Two (a and b) optimized structures of $[CuCl_1(en)]^{1+}$ aqua complexes

Table 1. Number of atoms in the first coordination shell of copper ion for the investigated aqua complexes

Complex	N	Cl	H_2O	Structure
$[Cu(en)]^{2+}$	2	–	4	octahedron
$[CuCl(en)]^{1+}$	2	1	3	octahedron
$[CuCl_2(en)]$	2	2	1	5-coordinated

Molecular dynamics modeling

The molecular dynamics simulations of infinitely dilute aqueous solution of 1,2-diaminoethane and $CuCl_2$ were carried out. Structural and dynamical characteristics (radial distribution functions, lifetime of water molecules in the hydration shell of the ion, coordination number of the ion, and other parameters) of the system were analyzed.

References

1. E. Selimović, A. V. Komolkin, A. V. Egorov, T. Soldatović. "Substitution behavior of square-planar and square-pyramidal Cu(II) complexes with bio-relevant nucleophyles" – *J. Coord. Chem.*, 71, 1003 (2018).
2. M. S. Gordon, M. W. Schmidt. In book: "Theory and Applications of Computational Chemistry, the first forty years". C. E. Dykstra, G. Frenking, K. S. Kim, G. E. Scuseria (editors). – Elsevier, Amsterdam, 2005. Pages 1167-1189.
3. N. B. Balabanov, K. A. Peterson. "Systematically convergent basis sets for transition metals. I. All-electron correlation consistent basis sets for the 3d elements Sc-Zn" – *J. Chem. Phys.*, 123, 064107 (2005).

Characterization of acid sites in zeolite Y by ^{31}P MAS NMR spectroscopy

Dmitry S. Zasukhin, Yury G. Kolyagin, Ivan A. Kasyanov

Faculty of Chemistry, Lomonosov Moscow State University, Leninskiye Gory 1, bld. 3, 119991 Moscow, Russia
E-mail: zasukhin@gmail.com

Introduction

Zeolites are crystalline aluminosilicates, which are widely used in industry as catalysts for oil refining processes because of their developed porous system and the presence of Brønsted (BAS) and Lewis (LAS) acid sites. Despite a large amount of experimental information about these materials being already published, there is no general, reproducible, and sufficiently accurate method for the qualitative and quantitative determination of the strength and localization of acid sites in zeolites and zeolite-based catalysts.

It is well-known in literature that application of ^{1}H NMR NMR spectroscopy allows one to determine the total amount of BAS in the studied zeolite [1]. However, this method does not make it possible to evaluate strength and amount of LAS or the location of any acid sites in pores and channels of the material.

Later it was proposed to apply ^{31}P MAS NMR spectroscopy of various phosphorus-containing probe molecules, such as trimethylphosphine (TMP) and trialkylphosphine oxides (TXPO) to characterize the acid sites of zeolites. Using such a technique, it became possible to observe and evaluate qualitatively the content of BAS and LAS of different strength in the structure of zeolites and other heterogeneous acid catalysts [2]. However, the technique suggested did not give any quantitative data on acid sites. In addition, only a few types of zeolites were studied, so the technique cannot be applied for all kinds of industrial zeolite catalysts.

Our work is aimed at creating an approach for the qualitative and quantitative determination of acid sites in various types of zeolites and zeolite-like catalysts based on ^{31}P MAS NMR spectroscopy of basic phosphorus-containing probe molecules different in size.

Experimental section

All NMR experiments were performed by using AVANCE-II 400WB Bruker NMR spectrometer with 4 mm double-channel MAS probe. For quantitative measurements 90-degree pulse (2.0 μs) with high-power ^{1}H decoupling and preliminary ^{31}P saturation was used.

In our study, we used oxides of various trialkylphosphines: trimethyl, triethyl, tri-n-butyl and tri-n-octylphosphines (TMPO, TEPO, TBPO, TOPO). As a model system, we used commercially available dealuminated zeolite Y (FAU) from the Zeolyst company (CBV-720). This zeolite has both BAS and LAS and both of them are involved in the reactions that occur while catalytic cracking of different hydrocarbons. Samples for NMR experiments were prepared by the addition of the required amount of probe molecules dissolved in dichloromethane to a zeolite calcined on a vacuum line.

Owing to the difficulties during sample preparation and a large number of possible error sources, it was necessary to introduce a reference for further quantitative assessment. We decided to use an internal standard, since it allows us to be sure that any changes in the recording conditions will not affect the spectra obtained, because we can use the ratio of integrals from reference and studied sample instead of using the absolute values of integrals.

To select an internal standard, the following requirements were imposed: 1) the standard should have a suitable chemical shift and not overlap either with the signals of the adsorbed probe molecules or with the side bands, 2) the standard should not interact with probe molecules or with the studied zeolite samples, 3) the standard should have a low specific surface area.

In our work, we attempted to introduce calcium phosphate ($Ca_3(PO_4)_2$), hydroxyapatites, and aluminium phosphate in the form of tridymite ($AlPO_4$-tridymite) as an internal standard. It was found out that $AlPO_4$-tridymite is the most suitable reference sample, since the chemical shift of its signal is located in the region of -30 ppm, which allows us to solve the problem of band overlapping from standard and the studied probe molecules with a slight decrease in the rotation speed.

Figure 1 shows the ^{31}P NMR spectrum of tri-n-butylphosphine oxide (TBPO) adsorbed on zeolite CBV-720 with $AlPO_4$-tridymite as an internal standard. The rectangles mark the regions corresponding to different acid sites: B – the Brønsted acid sites, B+L – the region with overlapping Brønsted and Lewis sites, L – Lewis acid sites, "Phys. Ads." – physically adsorbed TBPO. The signals recorded on the samples studied are consistent with those presented in literature regions characteristic for zeolites of various structure [3].

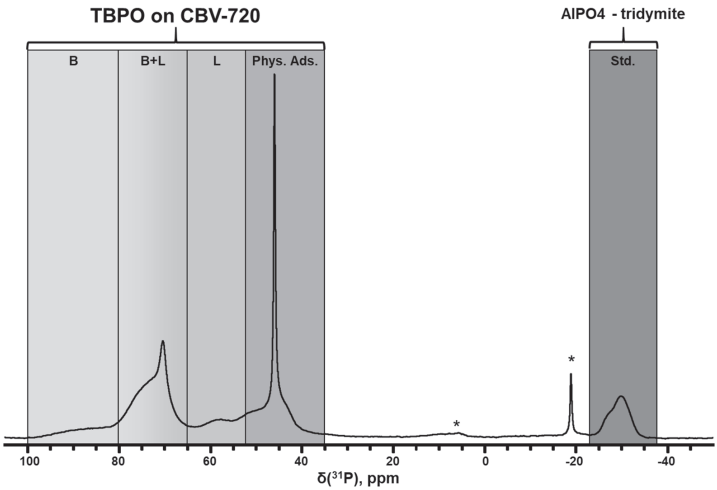

Figure 1. Typical ^{31}P MAS NMR spectrum of adsorbed TBPO on CBV-720 zeolite

The correlation of signal intensities between the corresponding ones to acid sites and an internal standard, the mass and amount of substances in the sample known in advance, has made it possible to quantify the content of BAS and LAS in a zeolite.

Furthermore, for the correct quantitative assessment of acid sites, it was necessary to optimize the conditions of spectra acquisition, as ^{31}P nuclei, depending on their location, can have different relaxation times. In fact, it turned out that $AlPO_4$-tridymite and some probe molecules have rather long relaxation times. It means that their intensity and integrals depend on time between the scans (Fig. 2). To solve this problem, we used high-power ^{1}H decoupling and preliminary ^{31}P saturation procedures, as application of these techniques allows to transform an accidental error into a constant deviation.

In addition, the use of probe molecules of different geometry makes it possible to separate active sites according to their accessibility: an increase in the size of alkyl substituents leads to diffusion limitations, which is observed when comparing small (TMPO, TEPO, TBPO) and large (TOPO) probe molecules. A comparison of this data resulted in estimation of both the total acidity of zeolites (when using TMPO, TEPO, TBPO) and the amount of acid sites on the outer surface (when using TOPO) of zeolite Y.

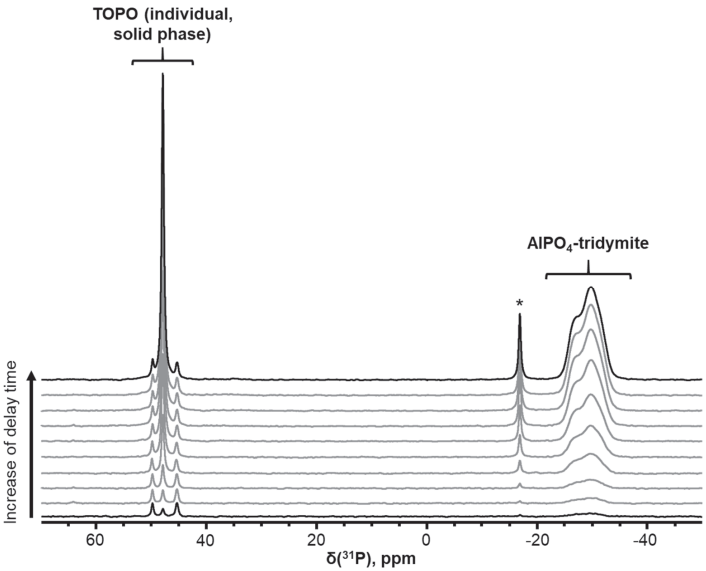

Figure 2. ^{31}P MAS NMR spectra of TOPO and $AlPO_4$-tridymite mixture

Also, conducting experiments in a controlled atmosphere allows us to evaluate not only the accessibility of various acid sites for substrates of different size, but also to evaluate the diffusion coefficients of these substrates within the porous structure of zeolites. The experimental results indicate that TBPO molecules completely penetrate the zeolite structure already at slight heating, while TOPO molecules seem to be too bulky to move into the zeolite pores.

***

Thus, a novel technique based on ^{31}P MAS NMR spectroscopy of adsorbed trialkylphosphine oxides as probe molecules for zeolite acid sites has been proposed. It has been shown that probe molecules of different size can differentiate BAS and LAS located in the pores and on the outer surface of zeolite Y. Introduction of AlPO4-tridymite as an internal reference has made it possible to estimate quantitatively BAS and LAS in zeolite.

Acknowledgements

The authors gratefully acknowledge Russian Science Foundation (project № 19-73-10160) for the financial support.

References

1. Freude D., Hunger M., Pfeifer H., Schwieger W. // Chem. Phys. Lett., 1986, 128., 62-66.
2. Zheng A., Huang S.-J., Liu, S.-B., Deng F. // Phys. Chem. Chem. Phys., 2011, 13, 14889-14901
3. Zhao Q., Chen W.-H., Huang S.-J., Wu Y.-C., Lee H.-K., Liu S.-B. // J. Phys. Chem. B, 2002, 106, 4462-4469

A magnetic resonance spectroscopy in complex differential diagnosis of nodular lesions of the thyroid gland

K. V. Zinkevich, V. M. Cheremisin, I. G. Kamyshanskaya

Mariinsky hospital, St. Petersburg

Magnetic resonance spectroscopy is used in the diagnosis of various oncological diseases, but information about its use in thyroid lesions is limited. We examined 15 patients with thyroid nodules larger than 1 cm3 that were surgically removed. 13 benign and 2 malignant tumors were identified. Peak choline was observed in all cases of carcinoma, and in 1 of the benign cases. The sensitivity was 100%, and the specificity was 92.3%.

Nodular formations of the thyroid gland occupy a leading place in the structure of all endocrinopathies. 4-12% of thyroid lesions are malignant. At present, there is no universal marker for preoperative identification of malignant changes in the thyroid gland. Magnetic resonance spectroscopy is a non-invasive method that measures chemicals or metabolites in the human body, which can help in assessing the malignancy of thyroid formations.

The aim of the study was to clarify the place of magnetic resonance spectroscopy in assessing the malignancy of thyroid nodules at the stage of preoperative examination.

Materials and methods

The study was conducted on the basis of the city's Mariinsky hospital in St. Petersburg from September 2018 to December 2019. The study included 15 patients with thyroid nodules larger than 1 cm^3 who were admitted to the hospital for surgical treatment of the thyroid gland. The average age of patients was 52.4 years, the interval was from 26 to 80 years. The ratio of women to men was 13:2. All patients underwent thyroid hormone measurements, ultrasound, fine needle aspiration biopsy under ultrasound control, and magnetic resonance spectroscopy (MRS). Subsequently, a (Hemi-) thyroidectomy was performed. Patients with previous thyroid surgery, known malignancy, and radiation exposure were not included in the study.

The studies were performed on a Phillips Ingenia MR tomograph with a magnetic field induction of 3.0 T. The neck Area was scanned in the sagittal, axial and coronal planes. After localization of the lesion and refinement of it in three planes, a voxel was placed on it. After the water suppression pulses were applied, data was collected. According to MR spectroscopy, the ratio of choline to creatine was estimated at 136 and 270 TE at each node. iron, with a known malignant disease and radiation exposure.

Research result

Magnetic resonance spectroscopy data from 15 patients were compared with the results of histological studies of postoperative material.. A total of 13 benign tumors (10 follicular adenomas and 3 colloidal goiter) and 2 malignant (papillary thyroid cancer) were detected. In 1 of 13 benign cases, a peak of choline was detected. In 2 malignant nodes of carcinomas, the peak of choline was also observed in MRS. The sensitivity of the MRS method was 100%, and the specificity was 92.3%.

Conclusion

The first experience of using magnetic resonance spectroscopy allows us to hope that this is a promising, not only non-invasive, but also sensitive and specific method in the differential diagnosis of thyroid nodules, which needs to improve the research methodology.

Literature

1. Gupta N, Goswami B, Chowdhury V, Ravishankar L, Kakar A. Evaluation of the role of magnetic resonance spectroscopy in the diagnosis of follicular malignancies of thyroid. Archives of surgery. 2011;146(2):179-82.
2. Aghaghazvini L, Pirouzi P, Sharifian H, Yazdani N, Kooraki S, Ghadiri A, Assadi M. 3T magnetic resonance spectroscopy as a powerful diagnostic modality for assessment of thyroid nodules. Archives of Endocrinology and Metabolism vol.62 no.5 São Paulo Oct. 2018.
3. Michele N Minuto, Laetitia Shintu, Stefano Caldarelli. Proteomics, and Metabolomics: Magnetic Resonance Spectroscopy for the Presurgical Screening of Thyroid Nodules. Curr Genomics. 2014 Jun; 15(3): 178–183.

Poems about School

* * *

Чижик-Spinus, где ты был?
– «Я сигнал за хвост ловил!
Сделал я ему “Фурье” –
Закружилось в голове!»

Цели «Spinus»’а просты:
Дать научные мосты!
Пусть у вас здесь будет шанс
Пообщаться «в резонанс»!

В Школе здесь научат всех
Сочетать с наукой смех,
Дискотеки с Э-Пе-эР,
Я-Ка-эР и Я-эМ-эР!

В Школе много новых лиц,
Будем превращать их в птиц:
Вдруг хотя б одной из ста
Дастся «Нобель-высота»!

2010

* * *

Spinus, Spinus, where you were?
Did you dive in the Resonance world?
– “Yes! I dived with my great joy –
Resonance is a pleasant toy!”

“Spinus” school invited you
To look for a knowledge clue.
We will show the signal birth
In the field of our Earth!

If you wish to have success,
At the School achieve progress!
We will teach you all to fly
In the scientific sky!

We desire you to get
Many victories-побед!
It will be a good surprise
If you catch the Nobel prize!

2010

Electrophoretic NMR assembly

Extending the capability of conventional NMR instruments

P&L Scientific

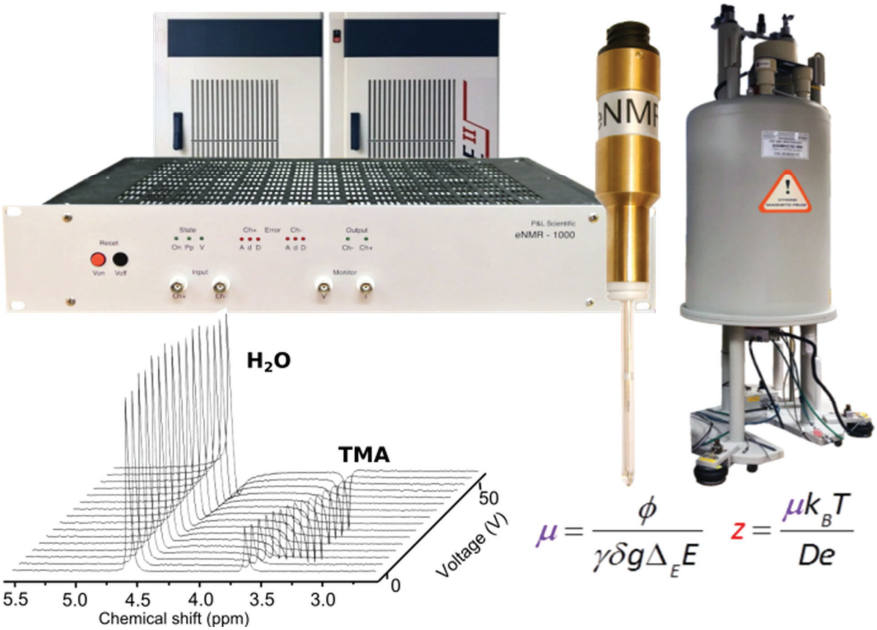

The electrophoretic mobility and the effective charge can be obtained by recording the variation of spectral phase by increasing electric field

Key features

- Well-established scientific background and proven technology
- Operates as add-on for any conventional NMR spectrometer and probe with gradient; requires no additional hardware or software
- Advanced sample cell and RF filter system
- Straightforward embedding of high voltage pulse generation in conventional NMR pulse programs
- Probe and user protection system

©P&L Scientific, 2020
info@plscientific.se

Specifications

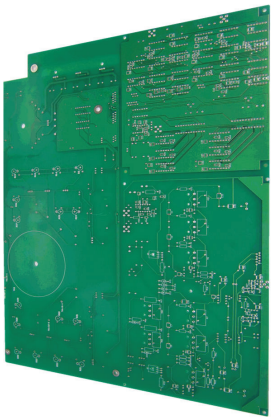

Output voltage:	0 to ±1000 V
Digital To Analogue converter size:	2×12 bit
Output current	
at ±1000 V:	0 to ±100 mA
at ±500 V:	0 to ±200 mA
Output power:	
Peak power	300 W
Mean power	30 W
Minimum/maximum pulse length:	500 µs / 1 s
Duty cycle:	30 %
Output pulse shapes:	Rectangular
Slew rate:	Greater then 25 V / µs
Settling time (to 2%):	Less than 200 µs for 2 kV step
Stability	
Drift with time	Less than 200 ppm/hr, noncumulative
Drift with temperature	Less than 300 ppm/°C
RF Filters	10 MHz low pass
Power consumption:	80 W for 220 V AC
Dimensions of the main unit:	430×340×90 (fits in standard 19'' rack); weight - 8 kg

Selected applications

Physical chemistry – ion pairing and association in simple and complex (polyelectrolytes) ionic mixtures.

Batteries and fuel cells - chemically selective measurement of ionic migration.

Biochemistry – biomolecular charge and association.

Analytical chemistry – electrophoretic analysis of complex ionic mixtures

Pharmaceutical chemistry – release and association of charged drugs

Metallorganic chemistry – the structure of supramolecular complexes from the observed charge

©P&L Scientific, 2020
info@plscientific.se

2D electrophoretic mobility spectroscopy (2D MOSY) based on eNMR

Extending the power of 2D NMR spectroscopy

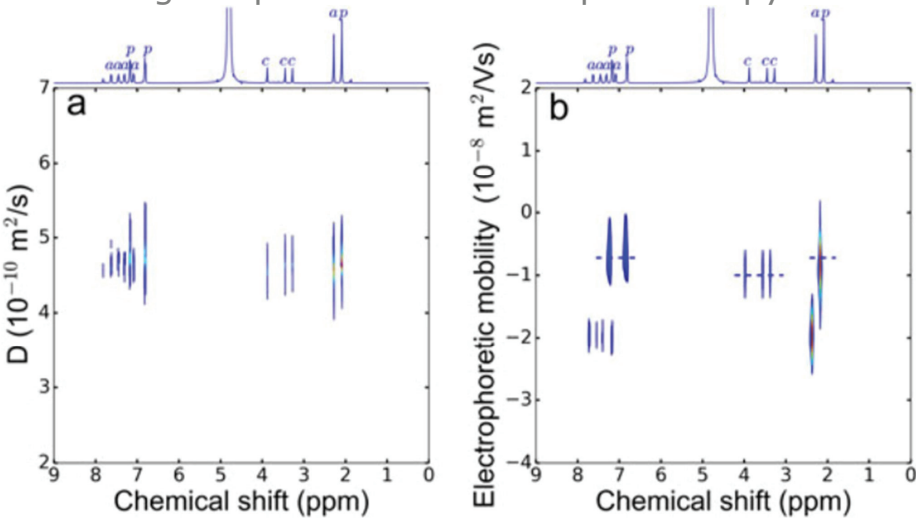

Direct comparison of 2D DOSY (a) and 2D MOSY (b) experiments for a dissolved Thomapyrin® tablet clearly illustrates the superior performance of the 2D MOSY in selection of the different species

Selected articles for eNMR applications

Y. Fang, P. V. Yushmanov, and I. Furó, Assessing 2D electrophoretic mobility spectroscopy (2D MOSY) for analytical applications, Magn. Reson. Chem. 55 DOI: 10.1002/mrc.4558 (2017).

E. Bialik, B. Stenqvist, Y. Fang, Å. Östlund, I. Furó, B. Lindman, M. Lund, and D. Bernin, Ionization of cellobiose in aqueous alkali and the mechanism of cellulose dissolution, J. Phys. Chem. Lett. 7 5044-5048 (2016).

M. Giesecke, F. Hallberg, Y. Fang, P. Stilbs, and I. Furó, Binding of monovalent and multivalent metal cations to polyethylene oxide in methanol probed by electrophoretic and diffusion NMR, J. Phys. Chem. B 120 10358−10366 (2016).

M. Bielejewski, M. Giesecke and I. Furó, On electrophoretic NMR. Exploring high conductivity samples, J. Magn. Reson. 243 17-24 (2014).

L. Patel, O. Mansour, M. Crossman, P. Griffiths, Electrophoretic NMR characterization of charged side chain cationic polyelectrolytes and their interaction with the anionic surfactant, sodium dodecyl sulfate, Langmuir 2019, 35, 28, 9233-9238

©P&L Scientific, 2020

info@plscientific.se

Our NMR services

Repair and modification of the NMR spectrometers and hardware components

- RF amplifiers
- Gradient units
- Synthesizer and SGU 400 - 1000 boards
- Power supplies and shim system
- Temperature and MAS controllers

Repair of the NMR probes:

- Solving arcing problems; bad sensitivity and RF tuning/matching
- Replacing broken glass and ceramics in the probe body
- Repairing certain gradient coils in diffusion and high-resolution probes
- Repair of MAS probes; arcing and spinning problem
- Repair of probe accessories for temperature control

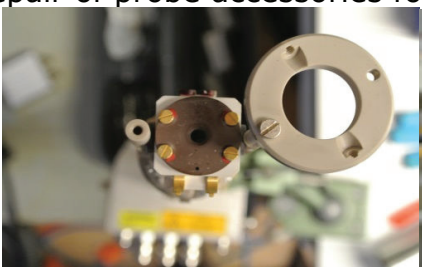

Modification of the NMR probes

- Adaptation of an existing NMR probe to a different spectrometer or NMR frequency.
- Change of RF coil position and configuration
- Adaptation of temperature control components and connectors
- Change of body geometry, dimensions and mounting
- Modification NMR inserts used in several diffusion NMR probes (like Bruker Diff30) to different frequency or double-tuned configuration

©P&L Scientific, 2020
info@plscientific.se

Author Index

Abaev, Vladimir T., 158
Afarideh, Hoseyn, 131
Aganov, Albert, 67
Ahokas, J., 134
Alakshin, E. M., 76
Alexandrova, Svetlana Ya., 147
Andronova, Elizaveta A., 236
Antonenko, Anastasiia O., 77, 271
Antonova, N. A., 150
Atta, Ramadan, 79
Avilova, I. A., 135
Baichurin, R. I., 230
Balevičius, V., 33
Baryshnikov, S. V., 275
Beksultanov, Zh., 224
Beliychenko, Kuprian, 235
Beshanov, Vsevolod V., 273
Bezrodniy, Valeriy V., 152, 155, 217, 221
Bikmullin, Aydar, 67
Blokhin, Dmitriy S., 67, 261
Bochkin, Georgii A., 80
Bogachev, Yu. V., 227
Boldyrev, K. L., 135
Bondareva, Valentina M., 125
Borodkin, Gennady S., 158
Borodkina, Inna G., 158
Bortolotti, Villiam, 96, 122
Brizi, Leonardo, 96, 122
Bunkov, Yu. M., 26
Büttgen, Norbert, 263
Butyugina, Ann, 161
Bystrov, Sergei S., 33, 83, 130
Cabal Mirabal, Carlos, 30, 88, 130
Chai Jong, Seo, 131
Charnaya, Elena V., 32, 77, 275
Chepurnoy, Pavel B., 158
Cheremisin, Vladimir M., 200, 210, 225, 293
Chernov, Nikita M., 164
Chernyak, A. V., 135
Chernyavskii, Ivan O., 263
Chernyshev, Yurii S., 33, 265, 271
Chizhik, Vladimir I., 33, 83, 88, 103, 130, 176, 195
Chupakhina, T., 285
Cifelli, M., 111
Colet, Jean-Marie, 35, 169, 270
Dai, Jing, 113
Dallons, Matthieu, 177
Danko, I. V., 224
Deeva, J., 285
Delcourt, Manon, 35, 270
Devalckeneer, Aude, 280
Djapic, Nina, 167
Dmitrenko, Mariia E., 79, 85, 110, 202, 213, 214
Dolgorukov, G. A., 76
Draguet, Anaïs, 169
Dvinskikh, Sergey V., 111, 113
Edinach, E. V., 170
Efimova, Alexandra A., 173
Egorov, Andrei V., 33, 83, 176, 195, 273, 288
Egorova, Maria I., 176
Ehrenberg, Helmut, 70
Eichhoff, Uwe, 41
Eremina, R., 285
Ermakov, Sergey S., 110, 202, 213
Fatkhullin, Bulat, 67
Fatullaev, Emil I., 152, 217
Faux, David A., 96, 190
Fazlizhanova, Dina I., 140
Fel'dman, Edward B., 80
Filkins, Max, 39
Fourez, Sophie, 177
Fraissard, Jacques, 36
Frolov, A., 56
Frolov, Viacheslav V., 37, 251, 265
Gabdulkhakov, Azat, 67
Gajewicz-Jaromin, Agata, 190
Galitskaya, Elena, 127
Garaeva, Natalia, 67
García Naranjo, J., 88
Garkavyi, Stanislav O., 179
Gavrilenko, Andrey N., 50
Gavrilova, T., 285

Gervits, Natalia E., 140, 182
Ghergherehchi, Mitra, 131
Giba, Ivan S., 64
Gilmutdinov, I., 285
Gippius, Andrei A., 140, 182, 263
Gluchshenko, N. V., 224
Golubev, Alexander, 67
Golubeva, Irina Yu., 100, 183
Grunin, Leonid Yu., 38, 86
Grunin, Yuriy B., 86
Gunbin, Anton V., 140, 182
Haase, J., 77
Haponchik, Roman V., 185
Harrison, Arthur, 39
Höfer, Peter, 41
Huseynov, G. J., 44
Ibragimova, Minaver D., 44, 188, 215
Ievlev, A. V., 89, 244
Indris, Sylvio, 70
Islamov, Daut, 67
Istok, Örs, 92
Ivanova, Maria S., 86
Janota, Magdalena, 190
Järvinen, J., 134
Jenczyk, Jacek, 45
Jurga, Stefan, 45
Kamyshanskaya, I. G., 225, 293
Karnaukh, Grigorii E., 100, 183, 192
Kasyanov, Ivan A., 290
Khabibulin, Dzhalil F., 125
Khalilov, A. B., 44
Khmelenko, V. V., 134
Khusainov, Iskander, 67
Khusnutdinova, Naira R., 93
Kirik, Sergei D., 125
Kitanin, D., 56
Klochkov, A. V., 76
Klochkov, Vladimir V., 67, 261
Klochkova, Evelina, 67
Kogon, Remi, 96, 122
Kolodina, Alexandra A., 158
Kolyagin, Yury G., 290
Komolkin, Andrei V., 113, 138, 150, 161, 215, 242, 254, 288
Kondratyeva, E. I., 76
Konovalov, V. A., 33, 195
Koptyug, Igor V., 46
Kostin, Mikhail A., 64, 196
Krylova, Ekaterina A., 198
Kryukova, O. V., 206
Kudashkina, Aleksandra S., 200
Kulagina, Tatiana P., 100, 183
Kuo, Chia Nung, 140
Kupriyanov, Pavel, 103
Kupriyanova, Galina S., 106, 115, 117, 235, 258
Kuzmin, V. V., 76, 108
Kuzminova, Anna I., 85, 110, 201, 202
Kuznetsov, Nikolai A., 203
Laaksonen, A., 176
Lähderanta, Erkki, 203
Lapina, Olga B., 48, 125
Latyshev, N. V., 206
Lauren, S., 88
Lavrova, Anna Y., 210
Lee, D. M., 134
Liamin, Vladislav P., 85, 213, 214
Lores Guevara, M., 88
Lue, Chin Shan, 140
Luzhanin, Vladimir G., 282
Lyadov, N., 285
Majhi, Debashis, 111, 113
Makarenko, S. V., 230
Mamadazizov, Sultonazar, 106, 115, 117
Mammadhasanov, Kenan, 215
Mamontova, Veronika V., 254
Maraşlı, A., 117
Marchenko, Ya. Yu., 227
Marchenkov, V. V., 77
Markelov, Denis A., 93, 138
Masas, Daria S., 86
Matukhin, Vadim L., 50, 179
Matveev, Vladimir V., 33, 257
McDonald, Peter J., 96, 190
Meersmann, Thomas, 39
Melikova, Sona, 196
Mershiev, Ivan, 235, 258
Michel, Dieter, 52
Miktaniuk, Sofia E., 155, 217, 221
Morozov, Igor V., 263
Moskvin, Alexander S., 263

Mozzhukhin, Georgy V., 106, 115, 117, 179
Mukan, Zh. T., 224
Muller, R. N., 88
Mulloyarova, Valeria V., 64, 120, 277
Musaenko, Alexsander, 258
Muzafarov, A. M., 135
Nagmutdinova, Anastasiia, 96, 122
Narenkova, D. A., 225
Navratil, Jiri, 50
Neelov, Igor M., 152, 155, 217, 221
Nefedov, Denis Yu., 32, 271
Nikitina, A. V., 227
Nikolaev, B. P., 227
Novak, Pavel, 50
Nurullina, Liliya, 67
Ostras', Alexei S., 64
Oztop, Mecit Halil, 274
Ozvural, Emin Burcin, 274
Papulovskiy, Evgeniy, 48, 125
Paveletz, Konstantin V., 200
Pavlovskaya, Galina E., 39
Pelipko, V. V., 230
Penkova, Anastasia V., 79, 85, 110, 201, 202, 213, 214
Pichugina, Alina A., 147, 232, 267
Pirogov, Yury A., 53
Pleshakov, Ivan V., 257
Plotnikova, Yu., 56
Podorozhkin, Dmitrii Yu., 32, 275
Pogoreltsev, A. I., 56
Pokatilov, Vjacheslav S., 182
Poltorabatko, Daria, 235
Popkov, Vadim I., 257
Popova, Maria V., 236
Pritz, Viktoria V., 200, 225
Privalov, A. F., 127
Pyankov, V. F., 206
Pylaeva, Svetlana A., 64
Rabdano, Sevastyan O., 130
Rakhmatullin, Ilfat Z., 261
Rameev, B. Z., 58, 115, 117
Rigby, Sean P., 39
Rudavets, Mikhail G., 239
Ruhin, A. B., 224
Rusanov, Dmitriy S., 200
Ryzhkov, A. M., 242
Safiullin, K. R., 76, 108
Salnikov, Vitalii, 235
Samoilo, Aleksandr S., 125
Schädler, Martina, 263
Schepkens, Corentin, 169
Schmidt, Ecaterina V., 50, 179
Seidova, Sabina A., 44, 188, 215
Selezneva, E. V., 135
Selimović, Enisa, 288
Selivanov, A. A., 244
Selivanov, Stanislav I., 164, 247, 282
Seredavina, T. A., 224
Sevastianov, Iliya G., 50
Shakirova, Julia R., 247
Sharifi, A. M. Saleh, 131
Shavykin, Oleg V., 152, 155, 221
Sheludiakov, S., 134
Shelyapina, Marina G., 198, 271
Shubin, Aleksandr A., 48, 125
Shubin, S. A., 251
Silanteva, Irina A., 254
Simeshchenko, P. I., 225
Sinitsyn, Vitaly, 127
Sklyarova, Anastasia, 257
Smirnov, Mark, 258
Soldatović, Tanja, 288
Stanislavovas, A. A., 76, 108
Stankevich, Natalya V., 158
Stolyar, S. V., 206
Suchkova, N. S., 224
Surkova, V. A., 202
Suryaprakash, N., 61, 62
Tagirov, M. S., 76, 108
Tagliatti, Vanessa, 35, 169, 177
Tarasov, Artyom S., 261
Tatarinova, E. A., 135
Tietz, Frank, 70
Tkachev, Aleksei V., 140, 182, 263
Tolstoy, Peter M., 64, 120, 196, 277
Traxel, Violet, 265
Trofimova, Nadezhda S., 158
Tsyro, Larisa V., 147, 232, 267
Tumson, Sophie, 270
Tunik, Sergey P., 247
Tyurtyaeva, Anna S., 271

Tyutyukin, Konstantin V., 37, 251, 265
Ubovich, Milosh, 273
Uguz, Sirvan Sultan, 274
Unger, Felix G., 267
Usachev, Konstantin, 67
Uskov, Andrei V., 32
Uskova, N. I., 275
Ustimchuk, Daria O., 277
Ustinov, Alexey B., 185, 203
Vafadar, M., 117
Valcke, Florent, 280
Validov, Shamil, 67
Vasil'ev, Sergey G., 80, 135
Vasiliev, S., 134
Vasinovich, Viktoria V., 236
Vogel, Michael, 127
Voronin, Aleksandr S., 138
Wang, Chengbo, 39
Wang, Xinpei, 39
Whaley, Andrei K., 282
Yagfarova, A., 285
Yakovlev, Igor P., 164
Yakovlev, Ilya V., 48
Yaroslavtsev, R. N., 206
Yatsyk, I., 285
Yefimova, Irina, 288
Yusupov, Marat, 67
Zasukhin, Dmitry S., 290
Zhurenko, Sergei V., 140, 182, 263
Zinkevich, K. V., 293
Zinkevich, Tatiana, 70
Zolotarev, Andrey A., 79, 110, 214
Zubkov, M. A., 210

Magnetic Resonance and its Applications

Proceedings

Saint Petersburg State University
March 29 — April 3, 2020

Подписано в печать 28.03.2020. Формат 60 × 84 $^{1}/_{16}$.
Бумага офсетная. Гарнитура Times. Печать цифровая.
Усл. печ.л. 17,78. Тираж 150 экз. Заказ № 1165.

Отпечатано в Издательстве ВВМ.
198095, Санкт-Петербург, ул. Швецова, 41.